

**The Synthesis of Organometallic Nanorods from Molybdenum and Tungsten
Diisonitrile Complexes and a New Method to Synthesize Air-Stable Sodium
Cyclopentadienide (NaCp)**

By

James B. Updegraff III

Submitted in Partial Fulfillment of the Requirements

for the Degree of

Master of Science

in the

Chemistry

Program

YOUNSTOWN STATE UNIVERSITY

August, 2004

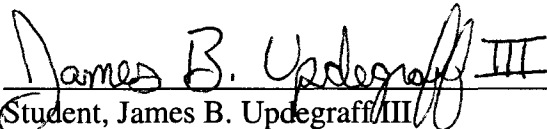
**The Synthesis of Organometallic Nanorods from Molybdenum and Tungsten
Diisonitrile Complexes and a New Method to Synthesize Air-Stable
Sodiumcyclopentadienide (NaCp)**

by

James B. Updegraff III

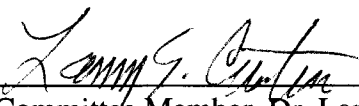
I hereby release this thesis to the public. I understand this thesis will be made available from the OhioLink ETD Center and the Maag Library Circulation Desk for public access. I also authorize the University or other individuals to make copies of this thesis as needed for scholarly research.

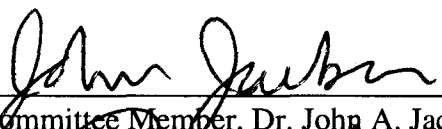
Signature:

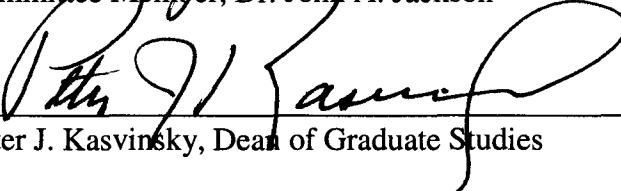
 7/27/04
Student, James B. Updegraff III Date

Approvals:

 7/17/04
Thesis Advisor, Dr. Allen D. Hunter Date

 7/26/04
Committee Member, Dr. Larry S. Curtin Date

 7/21/04
Committee Member, Dr. John A. Jackson Date

 7/28/04
Peter J. Kasvinsky, Dean of Graduate Studies Date

Abstract

Bis(diisonitrile) complexes were synthesized, characterized and are reported. The precursor to the bis(diisonitrile) complex, the bis(dinitrogen) complex, was synthesized by reducing the appropriate metal halide, MoCl_5 or WCl_6 , with magnesium metal in the presence of two equivalents of a bidentate phosphine under an inert nitrogen atmosphere in THF. The bis(diisonitrile) complex was then synthesized by reacting the appropriate dinitrogen metal complex with ten equivalents of 1,4-diisocyanobenzene or a derivative thereof. The solubility of these complexes was tuned *via* alkyl substituents on both the phosphine and the bis(diisonitrile) ligands although substitution on the phosphine had the greatest effect. The trimetallic isonitrile bridged complexes were then synthesized by combining the bis(diisonitrile) complex with two equivalents of *cis*-(cyclooctene)pentacarbonylchromium(0). The trimetallic complexes exhibited an iridescent color denoting the presence of a highly conjugated π -system. The presence of this highly conjugated system implies that these complexes may possess electrical conductivity properties.

A new, one-pot synthesis, of sodium cyclopentadienide, NaCp, is also reported. In this new method, dicyclopentadiene was cracked in a high-boiling, inert, non-polar solvent while sodium metal was being melted and finely divided in the same flask. The resulting CpH monomer then reacted with the finely divided sodium metal to produce NaCp, which precipitates out of the non-polar solvent. The NaCp that was produced shows remarkable stability towards air, is not pyrophoric like that produced by conventional

methods, and does in fact have Cp ring-transfer capabilities as shown by the successful synthesis of ferrocene using the NaCp produced by this new one-pot method.

Service crystallography of samples provided by Dr. Guy Crundwell of Central Connecticut State University is also reported.

Acknowledgements

I would first like to thank Dr. Allen D. Hunter for giving me the opportunity to pursue a Master's degree, as well as the support and guidance needed to fulfill this quest.

I would like to thank the rest of the Hunter group, especially Dr. Matt Zeller who made me into a better chemist than I could ever dream to be and Cindy Perrine whose undying and unwavering support has meant more to me than she will ever know.

I would like to thank the faculty of the YSU chemistry department, in particular, Dr. John Jackson for agreeing to sit on my committee and for the "hockey talks" and Dr. Larry "Bone" Curtin who not only listened to me whine but also gave me numerous words of wisdom and more importantly, was a friend.

Last, but certainly not least, I owe my undying gratitude to not only God, but to my family as well. Without the love and support of my parents, Jim and Cheryl, and my brother and sister, Shaun and Holly, nothing that I have done would have ever been possible.

Table of Contents

	Page
Abstract	iii
Acknowledgments	v
Table of Contents	vi
List of Equations	xi
List of Figures	xiv
List of Schemes	xvii
List of Tables	xviii
List of Abbreviations	xxiii
Chapter 1. Introduction	
1. Organometallic structure and bonding	1
2. Organometallic polymers and dendrimers	14
3. Organometallic nanomaterials	20
4. References	33
Chapter II. Experimental	
1. Reagents	36
2. Instrumentation	36
3. Synthesis of 1,2-bis(dimethoxyphosphoryl)benzene	37
4. Synthesis of 1,2-bis(phosphino)benzene	38
5. Synthesis of 1,2-bis(dichlorophosphino)benzene	39
6. Attempted synthesis of 1,2-bis(di(pentafluoro)phosphino)benzene	40
7. Synthesis of 1,2-bis[3,5-bis(trifluoromethyl)benzene]phosphino]benzene	41

8. Synthesis of 1,2-bis(di(<i>p</i> -anisole)phosphino)benzene	42
9. Synthesis of bis(di(<i>p</i> -tolyl)phosphino)ethane	43
10. Synthesis of bis(dinitrogen)bis(diphenylphosphinoethane)tungsten(0)	45
11. Synthesis of bis(dinitrogen)bis[1,2-bis(di(<i>p</i> -ethylbenzene)phosphino)benzene]molybdenum(0)	46
12. Synthesis of bis(dinitrogen)bis[1,2 bis (di(<i>p</i> -ethylbenzene)phosphino)benzene]tungsten(0)	48
13. Synthesis of <i>cis</i> -bis(1,4-diisocyanobenzene)bis[diphenylphosphinoethane]tungsten(0)	49
14. Synthesis of <i>cis</i> -bis(2,3,5,6-tetramethyl-1,4-diisocyanobenzene)bis[(diphenylphosphino)ethane]tungsten(0)	50
15. Synthesis of bis(2,3,5,6-tetramethyl-1,4-diisocyanobenzene)bis[1,2-bis(di(<i>p</i> -ethylbenzene)phosphino)benzene]molybdenum(0)	51
16. Synthesis of bis(2,3,5,6-tetramethyl-1,4-diisocyanobenzene)bis[1,2 bis (di(<i>p</i> -ethylbenzene)phosphino)benzene]tungsten(0)	52
17. Attempted synthesis of bis [1, 2-bis (di{ <i>p</i> -ethylbenzene})phosphinobenzene]dinitrogencarbonylmolybdenum(0)	54
18. Synthesis of bis(diphenylphosphinoethane)carbonyl(DMF) tungsten(0)	54
19. Synthesis of μ -C,C'-[bis[bis{di(<i>p</i> -ethylbenzene)phosphino}benzene]bis(<i>p</i> -diisocyanotetramethylbenzene)molybdenum(0)]bis(pentacarbonylchromium(0))	55
20. Synthesis of μ -C,C'-[bis[bis{di(<i>p</i> -ethylbenzene)phosphino}benzene]bis(<i>p</i> -diisocyanotetramethylbenzene)tungsten(0)]	

bis(pentacarbonylchromium(0))	57
21. Attempted synthesis of μ -C,C'-[bis[bis{di(<i>p</i> -ethylbenzene)phosphino}benzene]bis(<i>p</i> -diisocyanotetramethylbenzene)molybdenum(0)]bis(η^5 -cyclopentadienyl dicarbonylmanganese(0))	58
22. Attempted synthesis of μ -C,C'-[bis[bis{di(<i>p</i> -ethylbenzene)phosphino}benzene]bis(<i>p</i> -diisocyanotetramethylbenzene)molybdenum(0)]bis([bis(di(<i>p</i> -ethylbenzene)phosphino)ethane]carbonylmolybdenum(0))	59
References	61
Chapter III. Results and Discussion	
1. Phosphines	62
2. Dinitrogen complexes	69
3. Bis(diisonitrile) complexes	77
4. Capping reactions	84
References	94
Chapter IV. Conclusions	95
References	
Chapter V. Solid Sodium cyclopentadienide, NaCp	
1. Introduction	96
2. Experimental	102
A. Synthesis of sodium cyclopentadienide	102
B. Synthesis of sodium indenide	103

C. Synthesis of 1,2,3,4,5-pentamethylcyclopentadienylsodium	104
D. Synthesis of ferrocene	105
3. Results and Discussion	
1. Synthesis and physical properties of sodium cyclopentadienide	
107	
2. Synthesis and physical properties of pentamethylsodium cyclopentadienide	
110	
4. Conclusions	111
References	112
Chapter VI. Crystallography	
1. Introduction	114
6.1.1a. Crystal growth	114
6.1.1b Crystal selection	116
6.1.2. Diffraction	119
6.1.2a Components of a Diffractometer	119
A. X-ray generator	119
B. Detectors	120
C. Monochromator and Collimator	121
D. Goniometer and Goniometer heads	122
6.1.2b. Basic Principles of Diffraction	123
2. Experimental	125
1. 4-Bromothiophene-2-carboxaldehyde	125

2. Zinc di(pyridin-2-yl)methanone diiodide	128
3. Zinc di(pyridin-2-yl)methanone dibromide	132
4. N-(9 H-fluoren-9-ylidene)-N-(4-methoxyphenyl)amine	137
5. 2,3-bis(5-bromothiophen-2-yl)quinoxaline	142
6. 5,10,15,20-tetrakis(5'-methylthien-2'-yl)porphyrin	147
7. 1,2-bis(4-bromothiophen-2-yl)ethane-1,2-dione	153
8. 5-nitro-2-thiophenecarboxaldehyde	156
9. N-(9 H-fluoren-9-ylidene)-3,4-dimethylbenzenamine	159
10. Bis(2,3-di(5-bromothiophen-2-yl) quinoxaline) silver nitrate	164
11. Bis(2,3-di(thiophen-2-yl)quinoxaline) silver nitrate	171
12. Nitroanthracene	180
13. <i>o</i> -1-nitro-2-ethylbenzene and <i>p</i> -methylbenzensulfonate	184
14. Fluoren-9-ylidene-(4-nitrophenyl)amine	190
References	195
Appendix I. X-Ray data for 1,2-bis [3,5-bis ({trifluomethyl} benzene) phosphino] benzene	196
Appendix II. X-Ray data for <i>cis</i> -bis(2,3,5,6-tetramethyl-1,4-diisocyanobenzene) bis[diphenylphosphinoethane]tungsten(0)	206

List of Equations

Equation	Page
1.1.1 General synthesis for a bis(diisonitrile) complex	13
1.2.1 Methods to prepare polymers by step growth polymerization	16
1.2.2 Methods to prepare polymers by step growth polymerization	16
1.3.1 Synthetic methods for preparing isonitriles	24
1.3.2 Synthetic methods for preparing isonitriles	24
1.3.3 General synthesis for bis(isonitriles)	24
1.3.4 Synthetic route for the preparation of phosphines derived from dppe	25
1.3.5 Synthetic route to 1,2-bis(phosphino)benzene	26
1.3.6 Chlorination reaction of 1,2-bis(phosphino)benzene	27
1.3.7 Synthetic route for the preparation of dinitrogen complexes	28
1.3.8 Synthetic route for the preparation of bis(diisonitrile) complexes	28
1.3.9 Synthetic route for the preparation of a terminal metal complex	29
1.3.10 Synthetic pathway for the preparation of a carbonyl-terminated metal complex	29
1.3.11 General pathways for the preparation of metal-isonitrile complexes	30
1.3.12 General pathways for the preparation of metal-isonitrile complexes	30
3.1.1 Kyba's synthesis of 1,2-bis(phosphino)benzene	62
3.1.2 Synthesis of 1,2-bis(dichlorophosphino)benzene	64
3.1.3 Attempted synthesis of 1,2-bis(di(pentafluorobenzene)phosphino)benzene	65
3.1.4 Synthesis of 1,2-bis({3,5-bis(trifluoromethyl)benzene}phosphino)benzene	66

3.1.5	Synthesis of 1,2-bis(di(<i>p</i> -aniso)phosphino)benzene	68
3.2.1	Synthesis of bis(dinitrogen)bis[1,2-bis(<i>p</i> -ethylphenylphosphino)benzene] molybdenum(0) and the tetrahydride by-product	70
3.2.2	Synthesis of bis(dinitrogen)bis[1,2-bis(diphenylphosphino)ethane] tungsten(0)	70
3.2.3	Synthesis of bis(dinitrogen)bis[1,2-bis(<i>p</i> -ethylphenylphosphino)benzene] molybdenum(0)	72
3.2.4	Synthesis of bis(dinitrogen)bis[1,2-bis(<i>p</i> -ethylphenylphosphino)benzene] tungsten(0)	73
3.3.1	Synthesis of bis(1,4-diisocyanobenzene)bis((1,2-bis(diphenylphosphino) ethane)tungsten (0)	78
3.3.2	Synthesis of bis(2,3,5,6-tetramethyl-1,4-diisocyanobenzene)bis(1,2-bis (diphenylphosphino)ethane)tungsten(0)	79
3.3.3	Synthesis of bis(2,3,5,6-tetramethyl-1,4-diisocyanobenzene) bis(1,2-bis(di(<i>p</i> -ethylphenyl)phosphino)benzene)molybdenum(0)	81
3.3.4	Synthesis of bis(2,3,5,6-tetramethyl-1,4-diisocyanobenzene) bis(1,2-bis(di(<i>p</i> -ethylphenyl)phosphino)benzene)tungsten(0)	82
3.4.1	Attempted synthesis of bis(1,2-bis(di(<i>p</i> -ethylphenyl)phosphino)benzene) dinitrogencarbonylmolybdenum(0)	85
3.4.2	Synthesis of bis(1,2-bis(diphenylphosphino)ethane)carbonyl(DMF) tungsten(0)	88
3.4.3	Synthesis of μ -C,C'-[bis(<i>p</i> -diisocyanotetramethylbenzene)bis{1,2-bis {di(<i>p</i> -ethylphenyl)phosphino}benzene}]molybdenum(0)]	89

	bis(pentacarbonylchromium(0))	
3.4.4	Synthesis of μ -C,C'-[bis(<i>p</i> -diisocyanotetramethylbenzene)bis{1,2-bis{di(<i>p</i> -ethylphenyl)phosphino}benzene]tungsten(0)]	90
	bis(pentacarbonylchromium(0))	
3.4.5	Attempted synthesis of μ -C,C'-[bis(<i>p</i> -diisocyanotetramethylbenzene)bis{1,2-bis{di(<i>p</i> -ethylphenyl)phosphino}benzene]molybdenum(0)]	91
	bis(η^5 -cyclopentadienyldicarbonylmanganese(0))	
3.4.6	Attempted synthesis of μ -C,C'-[bis(<i>p</i> -diisocyanotetramethylbenzene)bis{1,2-bis{di(<i>p</i> -ethylphenyl)phosphino}benzene]molybdenum(0)]	92
	bis([1,2-bis(di(<i>p</i> -ethylphenyl)phosphino)ethane]carbonylmolybdenum(0))	
5.1.1	The "cracking" of dicyclopentadiene	97
5.1.2	The deprotonation of cyclopentadiene by (A) strong base and (B) sodium metal	98
5.1.3	Experimental route to sodium cyclopentadienide, NaCp	100
5.1.4	Ligand displacement and introduction of Cp	100
6.1.2.1	Bragg's Law	123

List of Figures

Figure	Page
1.1.1 Metal “acting” as a Lewis acid	1
1.1.2 A “Dewar-Chatt-Duncanson” representation of the bonding of a carbonyl to a transition metal	5
1.1.3 Valence Bond Theory representation of the bonding of a carbonyl ligand	5
1.1.4 A “Dewar-Chatt-Duncanson” representation of the bonding of an isocyanide ligand to a transition metal	7
1.1.5 Valence Bond Theory model for an isocyanide ligand	8
1.1.6 A “Dewar-Chatt-Duncanson” model representation for the bonding of an alkene ligand to a transition metal	9
1.1.7 Valence Bond Theory representation of the bonding of a metal-olefin and metallocyclopropane	10
1.1.8 A “Dewar-Chatt-Duncanson” representation for the bonding of the bidentate dppe ligand to a transition metal	11
1.1.9 A “Dewar- Chatt-Duncanson” model representation for the bonding of a dinitrogen ligand to a transition metal	12
1.1.10 Valence Bond Theory representation of the bonding of a dinitrogen ligand to a transition metal	12
1.2.1 Structures of polyphosphazene, polysiloxane, and polysilane	15
1.2.2 Transition metal based polymers containing ferrocene with organosiloxane spacers	16

1.2.3	Example of a rigid-rod polyynes	17
1.2.4	Some examples of main-chain organometallic polymers	17
1.2.5	A first-generation organometallic dendrimer	18
1.3.1	An organometallic polymer containing aromatic isocyanides	20
1.3.2	Free isonitrile bridging molecular wire junctions	21
1.3.3	Metal phosphine center bridging aromatic isonitriles	22
1.3.4	Possible geometries of homoleptic metal complexes	22
1.3.5	Examples of some chelating phosphines	25
3.1.1	ORTEP representation of 1,2-bis({3,5-bis(trifluoromethyl)benzene} phosphino)benzene	67
3.2.2	ORTEP plot of bis(dinitrogen)bis[1,2-bis(di(<i>p</i> -ethylphenyl) phosphino)benzene]tungsten(0) showing the presence of liquid hexane channels	74
3.2.3	ORTEP plot of bis(dinitrogen)bis[1,2-bis(di(<i>p</i> -ethylphenyl) phosphino)benzene]tungsten(0)	75
3.3.1	ORTEP plot of bis(2,3,5,6-tetramethyl-1,4-diisocyanobenzene) bis(1,2-bis(diphenylphosphino)ethane)tungsten(0)	80
5.1.1	Examples of the different types of geometries present in cyclopentadienyl complexes	96
5.3.1	One possible solvation effect of butyl ether on NaCp	109
6.1.1.1	Figure depicting the defect sites that can result in crystal growth	115
6.2.1	ORTEP plot of 4-bromothiophene-2-carboxaldehyde	126
6.2.2	ORTEP plot of zinc di(pyridin-2-yl)methanone diiodide	129

6.2.3	ORTEP plot of zinc di(pyridin-2-yl)methanone dibromide	134
6.2.4	ORTEP plot of N-(9 H-fluoren-9-ylidene)-N-(4-methoxyphenyl)amine	138
6.2.5	ORTEP plot of 2,3-bis(5-bromothien-2-yl)quinoxaline	143
6.2.6	ORTEP plot of 5,10,15,20-tetrakis(5'-methylthien-2'-yl)porphyrin	149
6.2.7	ORTEP plot of 1,2-bis(4-bromothiopen-2-yl)ethane-1,2-dione	154
6.2.8	ORTEP plot of 5-nitro-2-thiophenecarboxaldehyde	157
6.2.9	ORTEP plot of N-(9 H-fluoren-9-ylidene)-3,4-dimethylbenzenamine	160
6.2.10	ORTEP plot of bis(2,3-di(5-bromothiophen-2-yl)quinoxaline)silver nitrate	165
6.2.11	ORTEP plot of bis(2,3-di(thiophen-2-yl)quinoxaline)silver nitrate	173
6.2.12	ORTEP plot of nitroanthracene	181
6.2.13	ORTEP plot of <i>o</i> -1-nitro-2-ethylbenzene and <i>p</i> -methylbenzenesulfonate	186
6.2.14	ORTEP plot of fluoren-9-ylidene-(4-nitrophenyl)amine	191
A1a	ORTEP plot of 1,2-bis({3,5-bis(trifluoromethyl)benzene}phosphino)benzene	197
A2a	ORTEP plot of <i>cis</i> -bis(2,3,5,6-tetramethyl-1,4-diisocyanobenzene)bis(1,2-bis(diphenylphosphino)ethane)tungsten(0)	207

List of Schemes

Scheme	Page
3.4.1 Possible mechanistic scheme for the reaction of benzyl propionate with a dinitrogen complex	87

List of Tables

Table	Page
1.1.1 Structure and bonding properties of some commonly encountered ligands	3
6.2.1a Crystal data for 4-bromothiophene-2-carboxaldehyde	125
6.2.1b Data collection parameters for 4-bromothiophene-2-carboxaldehyde	125
6.2.1c Refinement parameters for 4-bromothiophene-2-carboxaldehyde	126
6.2.1d Geometric parameters for 4-bromothiophene-2-carboxaldehyde	127
6.2.2a Crystal data for zinc di(pyridin-2-yl)methanone diiodide	128
6.2.2b Data collection parameters for zinc di(pyridin-2-yl)methanone diiodide	128
6.2.2c Refinement parameters for zinc di(pyridin-2-yl)methanone diiodide	129
6.2.2d Geometric parameters for zinc di(pyridin-2-yl)methanone diiodide	130
6.2.3a Crystal data for zinc di(pyridin-2-yl)methanone dibromide	132
6.2.3b Data collection parameters for zinc di(pyridin-2-yl)methanone dibromide	132
6.2.3c Refinement parameters for zinc di(pyridin-2-yl)methanone dibromide	134
6.2.3d Geometric parameters for zinc di(pyridin-2-yl)methanone dibromide	135
6.2.4a Crystal data for N-(9-H-fluoren-9-ylidene)-N-(4-methoxyphenyl)amine	137
6.2.4b Data collection parameters for N-(9-H-fluoren-9-ylidene)-N-(4-methoxyphenyl)amine	137
6.2.4c Refinement parameters for N-(9-H-fluoren-9-ylidene)-N-(4-methoxyphenyl)amine	138
6.2.4d Geometric parameters for N-(9-H-fluoren-9-ylidene)-N-(4-methoxyphenyl)amine	139

6.2.5a	Crystal data for 2,3-bis(5-bromothiien-2-yl)quinoxaline	142
6.2.5b	Data collection parameters for 2,3-bis(5-bromothiien-2-yl)quinoxaline	142
6.2.5c	Refinement parameters for 2,3-bis(5-bromothiien-2-yl)quinoxaline	143
6.2.5d	Geometric parameters for 2,3-bis(5-bromothiien-2-yl)quinoxaline	144
6.2.6a	Crystal data for 5,10,15,20-tetrakis(5'-methylthien-2'-yl)porphyrin	147
6.2.6b	Data collection parameters for 5,10,15,20-tetrakis(5'-methylthien-2'-yl)porphyrin	147
6.2.6c	Refinement parameters for 5,10,15,20-tetrakis(5'-methylthien-2'-yl)porphyrin	149
6.2.6d	Geometric parameters for 5,10,15,20-tetrakis(5'-methylthien-2'-yl)porphyrin	149
6.2.7a	Crystal data for 1,2-bis(4-bromothiopen-2-yl)ethane-1,2-dione	153
6.2.7b	Data collection parameters for 1,2-bis(4-bromothiopen-2-yl)ethane-1,2-dione	153
6.2.7c	Refinement parameters for 1,2-bis(4-bromothiopen-2-yl)ethane-1,2-dione	154
6.2.7d	Geometric parameters for 1,2-bis(4-bromothiopen-2-yl)ethane-1,2-dione	155
6.2.8a	Crystal data for 5-nitro-2-thiophenecarboxaldehyde	156
6.2.8b	Data collection parameters for 5-nitro-2-thiophenecarboxaldehyde	156
6.2.8c	Refinement parameters for 5-nitro-2-thiophenecarboxaldehyde	157
6.2.8d	Geometric parameters for 5-nitro-2-thiophenecarboxaldehyde	158
6.2.9a	Crystal data for N-(9 H-fluoren-9-ylidene)-3,4-dimethylbenzenamine	159
6.2.9b	Data collection parameters for N-(9 H-fluoren-9-ylidene)-3,4-dimethylbenzenamine	159

6.2.9c	Refinement parameters for N-(9 H-fluoren-9-ylidene)-3,4-dimethylbenzenamine	160
6.2.9d	Geometric parameters for N-(9 H-fluoren-9-ylidene)-3,4-dimethylbenzenamine	161
6.2.10a	Crystal data for bis[2,3-di(5-bromothiophen-2-yl)quinoxaline] silver nitrate	164
6.2.10b	Data collection parameters for bis[2,3-di(5-bromothiophen-2-yl)quinoxaline]silver nitrate	164
6.2.10c	Refinement parameters for bis[2,3-di(5-bromothiophen-2-yl)quinoxaline] silver nitrate	165
6.2.10d	Geometric parameters for bis[2,3-di(5-bromothiophen-2-yl)quinoxaline] silver nitrate	166
6.2.11a	Crystal data for bis[2,3-di(thiophen-2-yl)quinoxaline] silver nitrate	171
6.2.11b	Data collection parameters for bis[2,3-di(thiophen-2-yl)quinoxaline] silver nitrate	171
6.2.11c	Refinement parameters for bis[2,3-di(thiophen-2-yl)quinoxaline] silver nitrate	173
6.2.11d	Geometric parameters for bis[2,3-di(thiophen-2-yl)quinoxaline] silver nitrate	173
6.2.12a	Crystal data for nitroanthracene	180
6.2.12b	Data collection parameters for nitroanthracene	180
6.2.12c	Refinement parameters for nitroanthracene	181
6.2.12d	Geometric parameters for nitroanthracene	182

6.2.13a	Crystal data for <i>o</i> -1-nitro-2-ethylbenzene and <i>p</i> -methylbenzenesulfonate	184
6.2.13b	Data collection parameters for <i>o</i> -1-nitro-2-ethylbenzene and <i>p</i> -methylbenzenesulfonate	184
6.2.13c	Refinement parameters for <i>o</i> -1-nitro-2-ethylbenzene and <i>p</i> -methylbenzenesulfonate	186
6.2.13d	Geometric parameters for <i>o</i> -1-nitro-2-ethylbenzene and <i>p</i> -methylbenzenesulfonate	186
6.2.14a	Crystal data for fluoren-9-ylidene-(4-nitrophenyl)amine	190
6.2.14b	Data collection parameters for fluoren-9-ylidene-(4-nitrophenyl)amine	190
6.2.14c	Refinement parameters for fluoren-9-ylidene-(4-nitrophenyl)amine	191
6.2.14d	Geometric parameters for fluoren-9-ylidene-(4-nitrophenyl)amine	192
A1a	Crystal data for 1,2-bis[{3,5-bis(trifluoromethyl)benzene}phosphino] benzene	196
A1b	Data collection parameters for 1,2-bis[{3,5-bis(trifluoromethyl)benzene} phosphino]benzene	196
A1c	Refinement parameters for 1,2-bis[{3,5-bis(trifluoromethyl)benzene} phosphino]benzene	197
A1d	Geometric parameters for 1,2-bis[{3,5-bis(trifluoromethyl)benzene} phosphino]benzene	197
A2a	Crystal data for <i>cis</i> -bis(2,3,5,6-tetramethyl-1,4-diisocyanobenzene) bis[1,2-bis(diphenylphosphino)ethane]tungsten(0)	206
A2b	Data collection parameters for <i>cis</i> -bis(2,3,5,6-tetramethyl-1,4- diisocyanobenzene)bis[1,2-bis(diphenylphosphino)ethane]tungsten(0)	206

A2c	Refinement parameters for <i>cis</i> -bis(2,3,5,6-tetramethyl-1,4-diisocyanobenzene)bis[1,2-bis(diphenylphosphino)ethane]tungsten(0)	207
A2d	Geometric parameters for <i>cis</i> -bis(2,3,5,6-tetramethyl-1,4-diisocyanobenzene)bis[1,2-bis(diphenylphosphino)ethane]tungsten(0)	207

List of Abbreviations

a	Length of unit cell axis (as in X-ray diffraction)
α	Alpha angle (as in X-ray diffraction) between a and b axis
Å	Angstrom
Ar	Substituted aryl group
as	Asymmetric stretch (as in Infrared spectroscopy)
b	Length of unit cell axis (as in X-ray diffraction)
β	Beta angle (as in X-ray diffraction) between a and c axis
<i>t</i> -Bu	<i>tert</i> -Butyl
c	Length of unit cell axis (as in X-ray diffraction)
CDCl ₃	Deuteriochloroform
CH ₂ Cl ₂	Dichloromethane
cm ⁻¹	Reciprocal centimeters, wave numbers
CO	Carbonyl ligand
“CN”	Coordination number
CNR	Isocyanide ligand
Cp	Cyclopentadienyl (η^5 -C ₅ H ₅)
CV	Cyclic voltammogram
d	Doublet (as in NMR spectroscopy)
δ	Chemical shift (as in NMR spectroscopy)
Δ	Heat (thermal reaction)
dd	Doublet of doublet (as in NMR spectroscopy)
dppe	1,2-bis(diphenylphosphino)ethane
DMF	Dimethylformamide
Dx	Density (as in X-ray diffraction)
Eq	Equivalents
Et	Ethyl
EtOH	Ethanol
F	Structure factor (as in X-ray diffraction)
F_c	Calculated structure factor (as in X-ray diffraction)

F_o	Observed structure factor (as in X-ray diffraction)
FTIR	Fourier transform infrared
g	Grams
γ	Gamma angle (as in X-ray diffraction) between b and c axis
h	Hour, Miller indices (as in X-ray diffraction)
Hz	Hertz
HOMO	Highest occupied molecular orbital
IR	Infrared (as in spectroscopy)
J	Coupling constant (as in NMR spectroscopy) in Hz
k	Miller indices (as in X-ray diffraction)
l	Miller indices (as in X-ray diffraction)
L	Ligand; liter
LAH	Lithium aluminum hydride
LUMO	Lowest unoccupied molecular orbital
μ	Mu
m	multiplet (as in NMR)
Me	Methyl
MHz	Megahertz
mL	Milliliters
mm	Millimeters
Mo K_α	Molybdenum K alpha (as in X-ray diffraction)
mol	Mole
mmol	Millimole
MO	Molecular Orbital
Mr	Molecular weight (as in X-ray diffraction)
M_w	Molecular weight
η	Eta
N	Normality
NLO	Nonlinear optical
NMR	Nuclear Magnetic Resonance
o	<i>Ortho</i>

OMe	Methoxy
π	Bonding pi orbital
π^*	Anti-bonding pi orbital
<i>p</i>	<i>Para</i>
pd	pseudo-doublet (as in NMR spectroscopy)
Ph-	Phenyl
ppm	Parts per million (as in NMR)
PR ₃	Phosphine or Phosphite
R	Alkyl or aryl group
<i>R</i>	Discrepancy index (as in X-ray diffraction)
σ	Bonding sigma orbital
S	Goodness of fit (as in X-ray diffraction)
s	Singlet (as in NMR spectroscopy); strong (as in IR spectroscopy)
sy	Symmetric stretch (as in Infrared spectroscopy)
T	Temperature
<i>T_{min}</i>	Minimum transmission (as in X-ray diffraction)
<i>T_{max}</i>	Maximum transmission (as in X-ray diffraction)
ω	Omega (<i>e.g.</i> , measurement angle used in X-ray diffraction)
θ	Theta (<i>e.g.</i> , Angle between the incident and the diffracted beams, as in X-ray diffraction)
θ_{\max}	Theta (<i>e.g.</i> , maximum Bragg angle as in X-ray diffraction)
t	Triplet (as in NMR spectroscopy)
THF	Tetrahydrofuran
UV-Vis	Ultraviolet visible (as in spectroscopy)
V	Cell volume (as in X-ray diffraction)
ν	Stretching frequency (as in IR spectroscopy)
<i>in vacuo</i>	High vacuum manifold
<i>wR</i>	Weighted discrepancy index (as in X-ray diffraction)
w	weak (as in Infrared spectroscopy)
X	Cl, Br, or I ligand
Z	Number of molecules in unit cell (as in X-ray diffraction)

Chapter One - Introduction

Section One

1. Organometallic Structure and Bonding

Organometallic chemistry combines features of inorganic and organic chemistry. Roughly fifty years ago, research in this area went through a renaissance driven by breakthroughs in both synthetic methods and bonding theories thus beginning its current growth phase. Much of the interest in organometallic compounds has been due to their efficiency as catalysts for organic and polymer syntheses.¹ In turn, this efficacy stems from the seemingly infinite number of derivatives, which can be obtained by varying the ligands and metals of organometallic complexes. A transition metal organometallic compound is composed of one or more metal centers surrounded by a set of ligands. In the most basic terms, the ligands may be thought of as Lewis bases that donate pairs of electrons to the central metal atom(s), which acts as a Lewis acid(s).

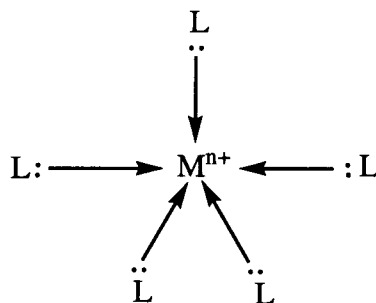


Figure 1.1.1

Metal "acting" as a Lewis acid

The relative stability of each complex is related to the valence electron count of the metal. The 18-electron rule predicts that a complex will be relatively stable if it has eighteen valence electrons associated with each metal center (*i.e.*, in the non-bonding orbitals of the metal and in the metal-ligand bonds). There are some exceptions to the rule, but metals in the middle of the transition series in low formal oxidation states generally obey the rule, (*e.g.*, the complexes that will be discussed in this thesis which contain chromium, molybdenum and tungsten).^{1,2}

Organometallic ligands may vary in the manner in which their valence electrons interact with the metal. For π -complexes in which unsaturated organic ligands are bonded "side on" to the metal (*e.g.*, olefins and aromatics), one or more π -bonds on the ligand may donate electrons to one or more metal atoms. The hapticity of the ligand (*i.e.*, its η^n number) is defined as the number of atoms that are within bonding distance of the metal atom. The total number and the nature of the ligands that are coordinated to a metal center determine its coordination number, CN. The number of coordination positions that a ligand occupies typically is equal to the number of electron pairs donated to the metal. While metal oxidation states and formal charges assigned to ligands do not accurately reflect the net electron charges in the complexes, they are useful bookkeeping tools and so are still widely used. Different ligands may vary in formal charge, the number of electrons that may be donated to the metal atom, and the number of coordination positions around the metal as shown in Table 1.1.²

Table 1.1.1 Structure and bonding properties of some commonly encountered ligands			
Ligand	Formal Charge(s)	Electrons Donated	Coordination Positions
Acyl	-1	2	1
η^2 -alkene	0	2	1
Alkyl	-1	2	1
Alkylidene	-2	4	1
Alkylidyne	-3	6	1
η^1 -allyl	-1	2	1
η^3 -allyl	-1	4	2
η^2 -alkyne	0	2 to 4	1
Amine	0	2	1
η^2 -arene	0	2	1
η^6 -arene	0	6	3
Carbene	0	2	1
Carbine	0	3	1
Carbonyl	0	2	1
η^1 -cyclopentadienyl	-1	2	1
η^3 -cyclopentadienyl	-1	4	2
η^5 -cyclopentadienyl	-1	6	3
Dinitrogen	0	2	1
Halide (<i>e.g.</i> , Cl ⁻)	-1	2	1
Hydride	-1	2	1
Isonitrile	0	2	1

Ligand	Formal Charge(s)	Electrons Donated	Coordination Positions
Nitrile	0	2	1
Nitrosyl (linear)	+1	2	1
Nitrosyl (bent)	-1	2	1
Phosphate	0	2	1
Phosphine	0	2	1
Pyridine	0	2	1

The carbonyl ligand is perhaps the most common ligand in transition metal organometallic chemistry. Its bonding in the linear terminal geometry is typical of other linear π -acidic ligands such as N_2 , NO^+ , and $CN-R$. In linear carbonyl complexes, the carbonyl is attached to the metal *via* the carbon atom, and the metal-carbon-oxygen bond angle is approximately 180° . According to the Dewar-Chat-Duncanson model,² σ -bonding occurs when a lone pair is donated from a filled σ -symmetry orbital on carbon (*i.e.*, the approximately sp hybrid orbital) to an empty σ -symmetry orbital on the metal (*i.e.*, the approximately d^2sp^3 hybrid orbital in an octahedral complex). There are also two π -back-bonding interactions, which are perpendicular to one another. In each of the two back bonds, there is a filled π -symmetry orbital on the metal (*e.g.*, the approximately d_{xy} , d_{xz} , or d_{yz} in an octahedral complex), which donates a pair of electrons into an empty π -symmetry orbital on carbon monoxide (*i.e.*, the approximately $CO \pi^*$ -antibonding orbital).

These σ -bonding and π -back-bonding components are synergic and the overall metal-

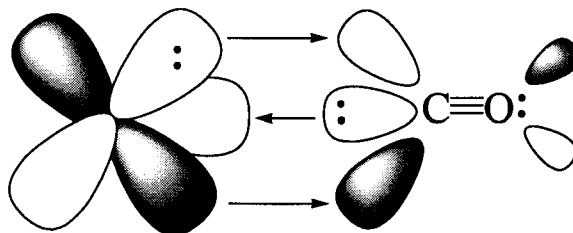


Figure 1.1.2 A “Dewar-Chatt-Duncanson” representation of the bonding of a carbonyl ligand to a transition metal.³

carbonyl bond is thus stronger than a linear sum of the two components. The electron transfer back to the ligand *via* π -back-bonding effectively neutralizes the electron transfer of the σ -bonding interaction to the metal. Thus, the overall metal-carbonyl bond is not polarized very much and there is only a small net electron transfer to the carbonyl ligand.

An alternate and complementary explanation for the bonding of metal carbonyls

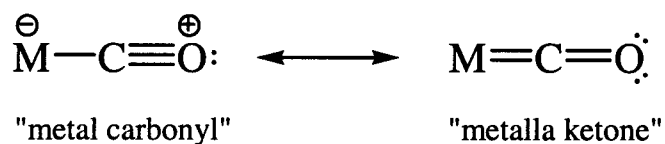


Figure 1.1.3 Valence Bond Theory representation of the bonding of a carbonyl ligand.

is provided by Valence Bond Theory.² Valence Bond Theory represents the bonding as contributions from two resonance forms. The first resonance form has metal-carbon single and carbon-oxygen triple bonds, with a formal charge of +1 on an sp hybridized oxygen. The second resonance form has both metal-carbon and carbon-oxygen interactions as double bonds, has no formal charges on carbon monoxide, and has oxygen sp² hybridized. In this interpretation, increased back-bonding to the carbonyl is reflected in an increased contribution from the second “metallo-ketone” resonance form.

Spectroscopy and X-ray diffraction may be used to provide experimental evidence of the nature and extent of the metal-carbonyl interaction. Infrared spectroscopy may be used to measure the amount of back-bonding of the metal to the ligand. The IR stretching frequencies of carbonyls decrease from 2120 cm⁻¹ to below 1850 cm⁻¹ as the metal becomes more electron rich and, consequently, as the amount of back-bonding increases. In turn, as the amount of back-bonding increases, the CO bond order decreases and the carbon-metal bond order increases. Various studies have shown carbonyl ligands are poor σ -donors and strong π -acceptors. Thus, carbonyls act as net electron withdrawing ligands. Nuclear magnetic resonance spectroscopy may also be used to examine the electron richness of the complex. As the amount of back-bonding increases, the chemical shift of the carbonyl carbon correlates with the electron richness of the complex (*i.e.*, shifting either downfield or up-field for a series of related complexes). X-ray diffraction may also be used to examine metal-ligand interactions. Thus, as the bond order of the carbon-metal bond increases the corresponding bond length decreases and as the carbon-oxygen bond order decreases its bond length increases.⁴

Isonitrile ligands are isoelectronic with carbonyl ligands and their bonding is therefore closely related. However, isocyanides are less electronegative than carbon monoxide and the lobes of the π^* -antibonding orbitals on the carbon atom are less polarized. Thus, isocyanides are generally better net electron donors than are carbonyls. In terms of the Dewar-Chatt-Duncanson model, there is σ -donation from the lone pair of electrons on the carbon (*i.e.*, the approximately sp hybrid orbital) to an empty σ -symmetry orbital of the metal (*i.e.*, approximately d^2sp^3 in octahedral complexes). There is also π -back donation from a pair of filled orbitals of π -symmetry on the metal (*i.e.*, the approximately d_{xy} , d_{xz} , or d_{yz} orbitals in octahedral metals) to a pair of empty π -symmetry orbitals on the isocyanide ligand (*i.e.*, the approximately π^* -orbitals localized on $C\equiv N$).^{3,4}

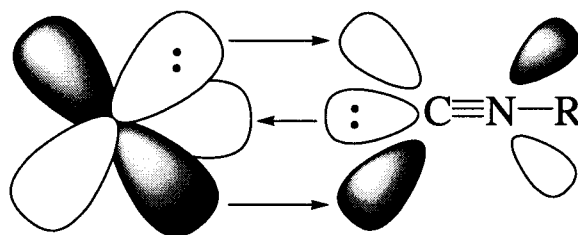


Figure 1.1.4 A Dewar-Chatt-Duncanson model representation of the bonding of an isocyanide ligand to a transition metal.

Valence Bond Theory provides an alternative and complementary explanation of the bonding that occurs during the coordination of an isocyanide to a transition metal. In Valence Bond terms, the coordination is explained *via* resonance. Thus, greater back-bonding results in an increased contribution from the second resonance form and hence a

decreased CN-R bond angle due to the sp^2 hybridization of the nitrogen atom on the

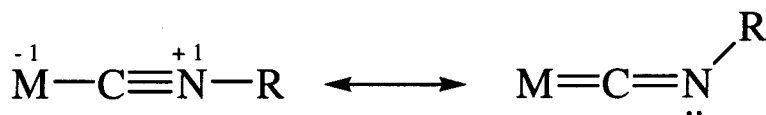


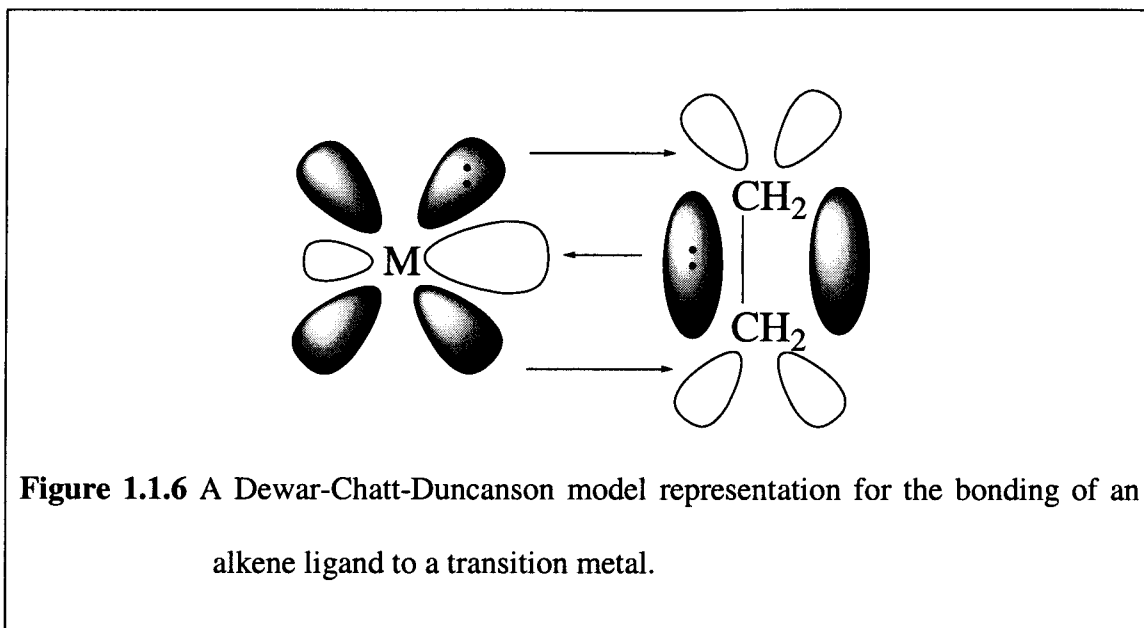
Figure 1.1.5 Valence Bond Theory model for the isocyanide ligand.

latter.⁵

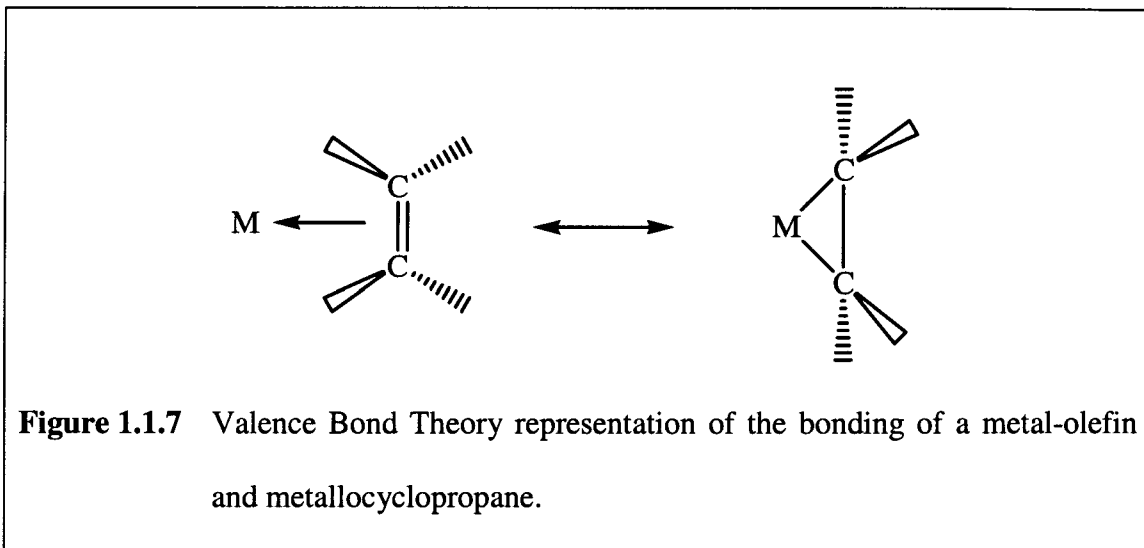
Both the Dewar-Chatt-Duncanson and Valence Bond Theory explanations can be used to rationalize the same experimental observations. The electron richness of the metal center affects the bond orders for the metal-carbon and carbon-nitrogen bonds as well as the CN-R bond angles. If the electron richness of the metal is increased, there is more back-bonding and the second resonance form is favored. The metal-carbon bond order therefore increases and the carbon-nitrogen bond order decreases while the CN-R angle decreases. As with carbonyls, the electron richness of isonitrile complexes may be measured through infrared spectroscopy. The $\text{C}\equiv\text{N}$ stretching frequency for isonitrile complexes is 250-350 wavenumbers lower than the stretching frequency for the free isonitrile reflecting both the weakening of the net $\text{C}\equiv\text{N}$ σ - and π -bonds upon coordination.^{3,4}

Olefins and related unsaturated organics are also common ligands. In the Dewar-Chatt-Duncanson model, the bonding of olefins involves a forward donation of π -electron density from the occupied π -bonding orbitals of the alkene (*i.e.*, σ -symmetry with respect to the metal) to empty σ -symmetry valence orbitals on the metal atom (*e.g.*,

approximately d^2sp^3 on an octahedral complex). Back donation occurs from filled π -symmetry orbitals on the metal (*e.g.*, approximately d_{xz} , d_{yz} , and d_{xy} on an octahedral metal center) into an empty π^* molecular orbital on the ligand, (*i.e.*, which have π -symmetry with respect to the metal).



In Valence Bond terms, the two resonance forms of olefins are referred to as the metal-olefin and metallo-cyclopropane forms, which differ in both their metal-carbon and carbon-carbon bond orders and in the hybridizations of the carbon atoms. Thus, increased back-bonding increases the contribution of the second resonance form, which increases the metal-carbon bond order, decreases the carbon-carbon bond order, and changes the carbon hybridization from sp^2 towards sp^3 .



As with carbon monoxide and CN-R, the electron richness of the metal containing olefin and related complexes may be measured through spectroscopy and X-ray diffraction. Increasing the electron richness on the metal produces increased back-bonding and, therefore, the net bond order of the carbon-carbon bond decreases. X-ray diffraction has shown that increased electron richness on the metal and the subsequent back-bonding, decreases the metal to ligand bond distance, increases the carbon-carbon bond length, and decreases the H-C-H bond angles from 120° towards 109° . The π -bonded hydrocarbons such as olefins and η^6 -arenes generally increase the net electron density on the metal in contrast to π -acidic ligands such as carbonyls and isocyanates, which typically decrease the net electron density on the metal.

The PR_3 ligand is widely used in metal coordination chemistry because it is a soft ligand and can be incorporated into metal complexes having central atoms in low oxidation states. The stability of complexes with PR_3 ligands results from the soft acceptor nature of the metal in low oxidation states and the stability of soft-donor/soft-acceptor combinations.⁶ It is generally accepted that the bonding of phosphines to metals

is almost entirely σ -donor in nature for alkyl phosphines. However, for aryl phosphines, phosphites, and fluorinated phosphines π -back-bonding into phosphorus orbitals that have phosphorus-carbon σ^* orbital character become increasingly important in the order given. The 1,2-bis(diphenylphosphino)ethane ligand, dppe, is typically a bidentate ligand in most complexes meaning that both phosphorus atoms coordinate to the metal. Each phosphorus atom has a lone pair of electrons from an sp^3 hybrid orbital that is donated to an empty σ -symmetry orbital on the metal (*e.g.*, approximately d^2sp^3 orbital on an octahedral metal center). For the phosphine ligands such as those used in this research, back-bonding plays little or no role because the aryl substituents are relatively electron rich.⁷

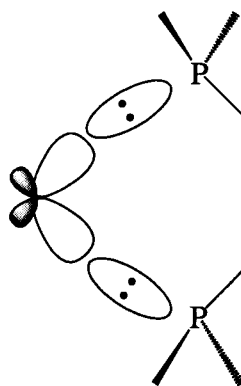


Figure 1.1.8 A Dewar-Chatt-Duncanson representation for the bonding of the bidentate dppe ligand to a transition metal.

The dinitrogen ligand is usually a linear monodentate ligand because only one pair of electrons from the dinitrogen molecule coordinates to the metal. As with carbon monoxide and $CN-R$,^{2,7} one can describe $M-N_2$ bonding in both Dewar-Chatt-Duncanson

(*i.e.*, σ -donation and π -back-donation) and Valence Bond (*i.e.*, two resonance contributions) terms. Free dinitrogen is IR inactive due to its lack of a dipole moment, but it is Raman active. The polarization that results from its synergic bonding to metal atoms leads to the observation of a N-N stretching vibration between 1920-2150 cm^{-1} and to chemical activation of the dinitrogen ligand.

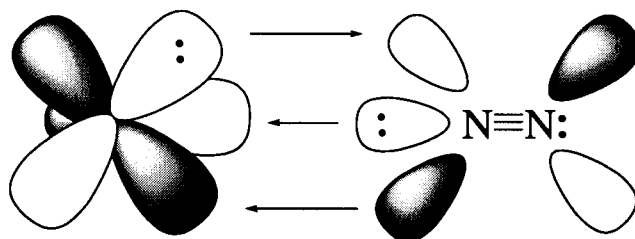


Figure 1.1.9 A Dewar-Chatt-Duncanson model representation for the bonding of a dinitrogen ligand to a transition metal.

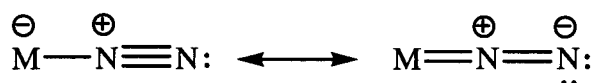
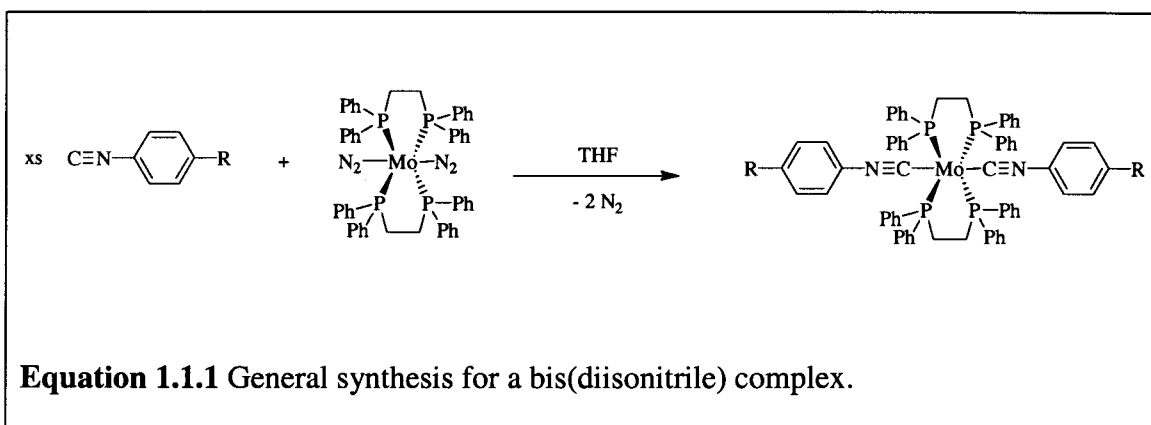


Figure 1.1.10 Valence Bond Theory representation of the bonding of a dinitrogen ligand to a transition metal.

However, for the terminal N_2 ligand net σ and π interactions are weaker than for other π -acidic ligands such as carbonyls and isocyanides. Therefore, dinitrogen ligands can be readily displaced by these π -acidic ligands, *e.g.*, as in equation 1.1.⁸



Section Two

Organometallic Polymers and Dendrimers

Metal-ligand complexes may be incorporated into polymers to produce new classes of organometallic polymers that are at least formally related to conventional organic and/or inorganic polymers. Most transition elements have a higher coordination number than carbon. This allows inorganic fragments incorporated into polymers to have more side groups. In addition, metal-ligand bonds are typically longer than conventional carbon bonds (*e.g.* carbon-carbon, carbon-nitrogen, and carbon-oxygen bonds). These differences in bonding and valences between carbon and transition metals produce different bond angles, internuclear distances, and backbone rigidities.⁷ Due to their variable bonding characteristics, organometallic polymers may also possess intriguing electrical, conductivity, magnetic, optical, liquid crystalline, and redox properties. Polymers with organometallic fragments in their repeating unit have many actual and/or potential advantages compared to conventional organic polymers. In particular, organometallic fragments are expected to induce properties in polymers that cannot easily be induced using conventional organic fragments.^{9,10} Organometallic polymers of most relevance to this research are polymers having transition elements that possess M-C σ or π bonds in the backbone. Polyphosphazenes, polysiloxanes, and polysilanes are some inorganic polymers that have been produced commercially because of their novel properties.⁷

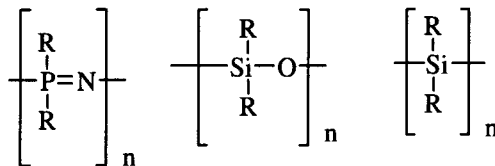
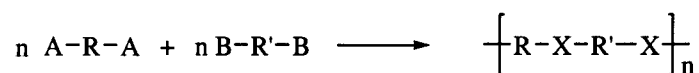
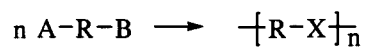


Figure 1.2.1 Structures of a polyphosphazene, polysiloxane, and polysilane.

To facilitate practical applications, a main goal of organometallic polymer researchers is to synthesize organometallic polymers with favorable materials processing characteristics (*e.g.*, melting point, solubility, and high or controllable molecular weights [$M_n > 10,000$]). Since the early 1950's, many organometallic polymers have been synthesized; however, these polymers typically had low molecular weights. They were also often insoluble or could not be melted without decomposing. In order to overcome these obstacles, researchers have attempted various synthetic approaches. Step growth polycondensation reactions involving the reaction of bifunctional monomers were used because addition polymerization reactions could not usually be employed for main-chain organometallic polymers.¹¹ There are two approaches for preparing polymers using step growth polymerization.¹²



Equations 1.2.1 and 1.2.2 Methods to prepare polymers by step growth polymerization.

The first method uses a molecule that has two functional groups and the second method uses two different difunctional monomers.

The first soluble, well-characterized transition metal based polymers of appreciable molecular weight were ferrocene-containing materials with organosiloxane spacers, which were reported in 1974 by Pittman and co-workers.¹³

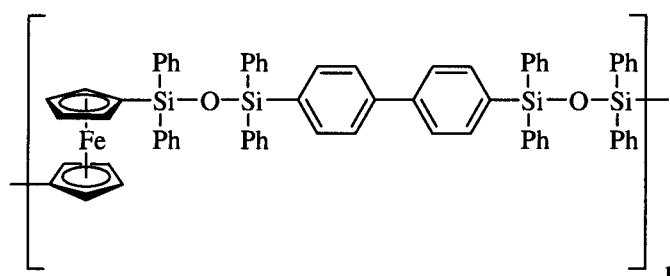


Figure 1.2.2 Transition metal based polymers containing ferrocene with organosiloxane spacers.

In 1977, the first high molecular weight rigid-rod metal polyynes were described by Hagihara *et al.*¹⁴

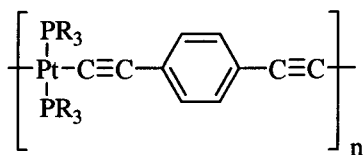


Figure 1.2.3 Example of a rigid-rod metal polyne.

These are prototypical examples of main chain organometallic polymers: Poly(metallocenes) and rigid-rod acetylide polymers.

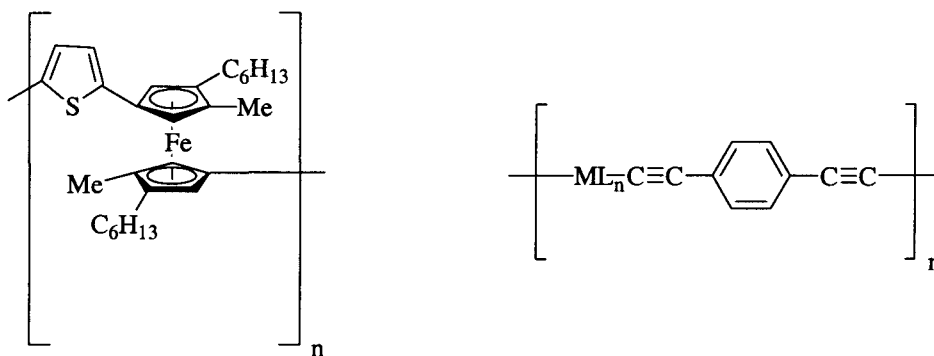
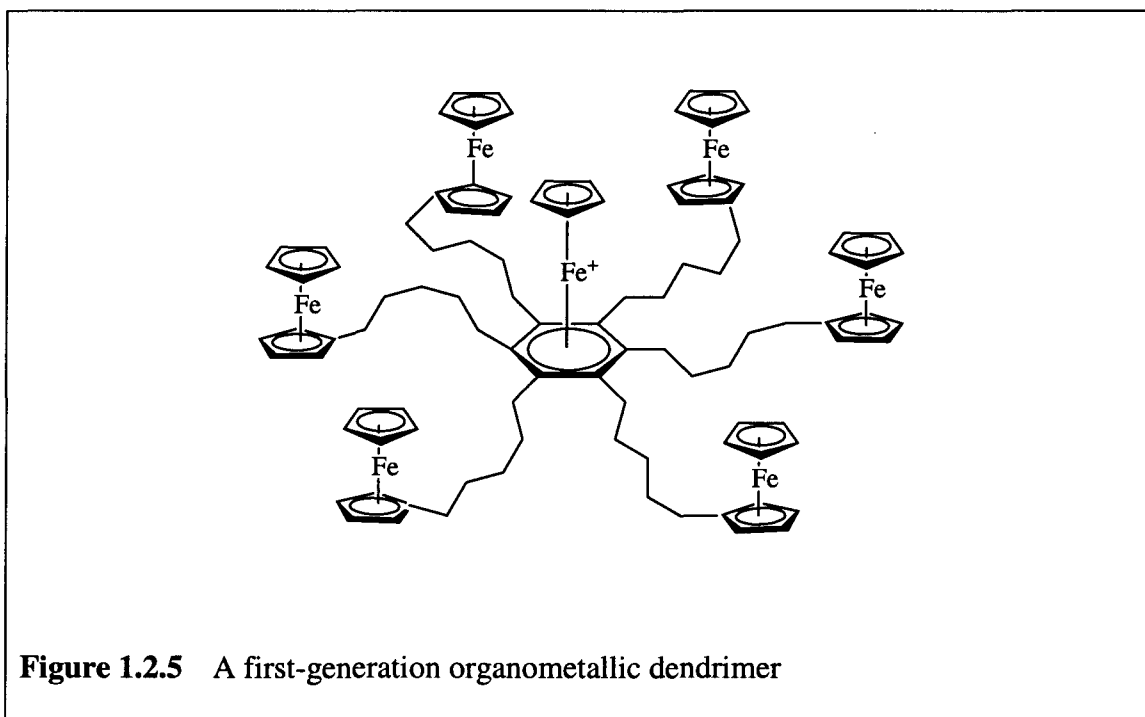


Figure 1.2.4 Some examples of main-chain organometallic polymers.

Many of the polymers shown in Figure 2.4 are soluble in common organic solvents such as benzene, toluene, tetrahydrofuran, and dichloromethane. They also have good electrical, optical, and nonlinear optical properties.⁹

Another type of organometallic compounds of interest are dendrimers (Greek: *dendron* = tree). Dendrimers are hyper-branched nanoscale materials that have potential applications as sequestration agents, micro-catalyst chambers, viscosity modifiers, analogues of proteins and enzymes, etc. Dendrimers are also being used in analytical and NLO applications. The generation number of a dendrimer is essentially the number of branching points along each arm.



As the size of a dendrimer increases, steric crowding increases in the outermost layers. Thus, a typical high generation number dendrimer is sterically crowded on its surface layers, but has significant free space near its central core. This crowding gradient sets the

maximum dendrimer generation number at about seven and is responsible for many of their useful properties.^{15, 16}

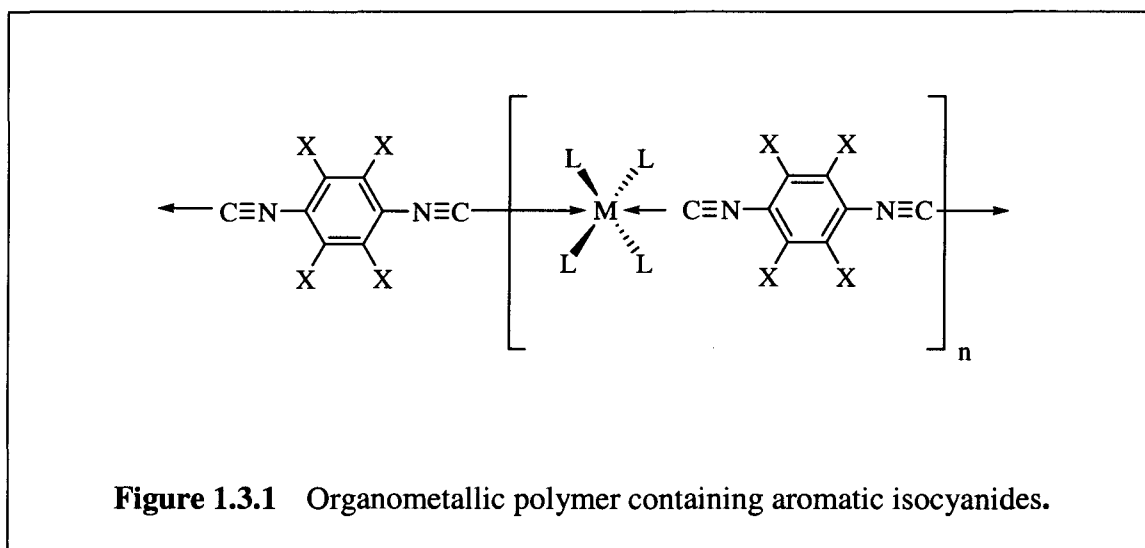
Many rigid-rod organometallic main chain oligomers and polymers are 0.5 to 1.0 nm in diameter and several hundreds of nanometers in length and are thus classified as nanomaterials. These materials may have potential uses for their electronic and nonlinear (NLO) properties.¹⁷ Non-linear optical properties arise from interactions of the electromagnetic fields of light with those of matter. Materials possessing nonlinear optical, NLO, properties are able to change the nature of light as it propagates through them and also to change their electronic and other properties as a function of the incident light. This allows different frequencies, amplitudes, polarization, or propagation characteristics to be produced and may also produce coupled changes in electrical and optical properties. Materials with NLO properties are of technological importance in areas that use optical devices such as optical data storage, optical communication, optical switching, image processing, and optical computing.^{12,18}

Section Three

Organometallic Nanomaterials

1. Introduction

Aromatic isocyanides are of interest in the synthesis of organometallic nanomaterials because they are relatively stable, non-toxic, non-volatile and because they form strong complexes (with transition metals) with rationally tunable bonding characteristics.



In addition, free aromatic diisocyanide ligands are also of interest because they are effective molecular-level conductors.¹⁹ These ligands are capable of bridging transition metal centers while mediating communication between the centers through a conjugated $d\pi$ - $p\pi$ - $d\pi$ network.²⁰ Thus, aromatic diisocyanide ligands could be deposited on a gold surface (**Figure 1.3.2**) to enhance the surface's electrochemical properties.

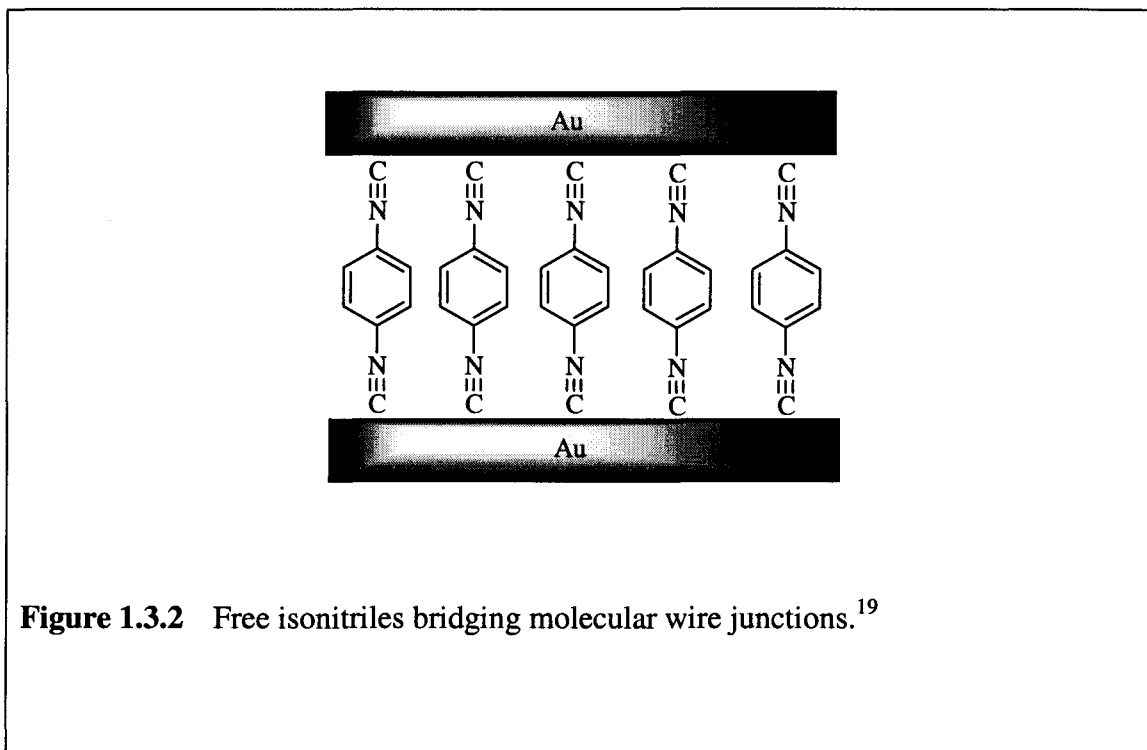


Figure 1.3.2 Free isocyanides bridging molecular wire junctions.¹⁹

If one uses metal phosphine centers, the steric and electronic properties of the resultant nanomaterials should also be tunable by varying the metal and PR_3 groups. There is a wide variety of structural data available from previous work on monometallic metal isocyanides and metal phosphines that should enable the prediction of the geometries of these complexes.

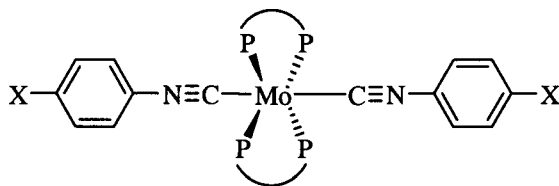


Figure 1.3.3 Metal phosphine center bridging aromatic isonitriles.

Some inorganic materials having from three to seven ligands bound to a central metal atom or ion are expected to have a star like shapes due to the geometry of the bonding orbitals. Examples of these types of systems are:

- Two coordinate: Au^+
- Three coordinate: Ag^+
- Some four coordinate systems: Ni^0 , Ag^+ , Cu^+ , Rh^+ , Ni^{+2} , Pd^{+2} , Co^{+2} .
- Some five coordinate systems: Fe^0 , Re^0 , Co^+ , Co^{+2} .
- Some six coordinate systems: Cr^0 , Mo^0 , W^0 , Cr^+ , Mn^+ , Cr^{+2} , Fe^{+2} .
- Some seven coordinate systems: Mo^{+2} , W^{+2} , W^{+3} .

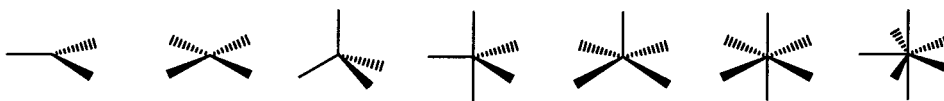


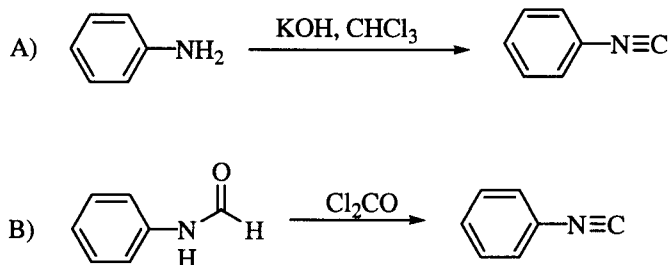
Figure 1.3.4 Possible geometries of homoleptic metal complexes.

Whether they are fluxional or rigid, many homoleptic complexes have such geometries about their metal centers. By using linear organometallic chains instead of simple ligands such as carbon monoxide with these centers, analogous organometallic nanostars having isocyanide-bridged arms should result.

2. Requisite Organic and Organometallic Reagents

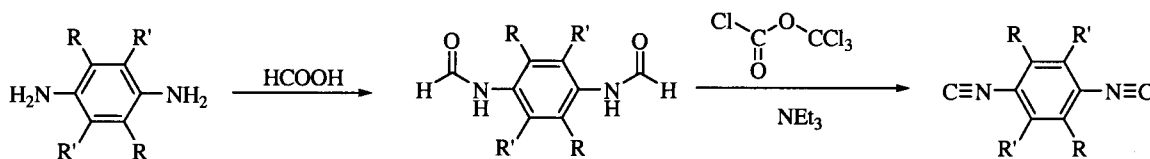
The organometallic nanomaterials described in this thesis contain bifunctional isonitrile ligands of the type $1,4\text{-C}_6\text{H}_4(\text{NC})_2$ and $1,4\text{-C}_6\text{Me}_4(\text{NC})_2$, and monofunctional isonitriles such as $\text{MeO-C}_6\text{H}_4\text{-NC}$. The chelating phosphines, $(1,4\text{-C}_6\text{H}_4\text{Y})_2\text{PCH}_2\text{CH}_2\text{P}(1,4\text{-C}_6\text{H}_4\text{Y})_2$ and $(1,4\text{-C}_6\text{H}_4\text{Y})_2\text{PC}_6\text{H}_4\text{P}(1,4\text{-C}_6\text{H}_4\text{Y})_2$ (where $\text{Y} = \text{OMe}, \text{Me}, \text{and Et}$) have been chosen because it is thought that these phosphines will improve the solubilities of the complexes compared to the parent phenyl species. In turn, the phosphines will be used to synthesize the dinitrogen starting materials $\text{Mo}(\text{R}_2\text{PC}_n\text{H}_m\text{PR}_2)_2(\text{N}_2)_2$. Based on molecular orbital arguments, it is expected that more electron rich metal centers (*e.g.*, $\text{Y} = \text{Me}$ or Et) and electron poor bridges (*e.g.*, $\text{C}\equiv\text{N-C}_6\text{F}_4\text{-N}\equiv\text{C}$) will give increased electronic communication down the oligomer backbones.

Aromatic isonitriles have been prepared by a variety of methods. The two most common are treatment of aromatic amines with hydroxide in chloroform (A) and the dehydration of formamides with phosgene (B) or its precursors.²¹



Equations 1.3.1 and 1.3.2 Synthetic methods for preparing isonitriles.

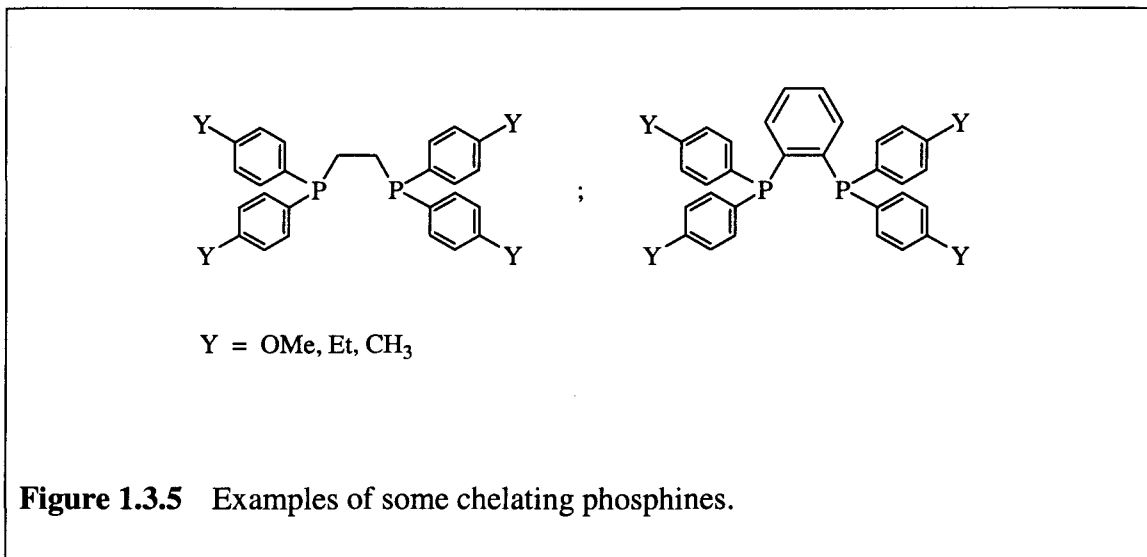
For the synthesis of diisocyanides, method A typically gives poor results so method B is preferred. As an alternative to hazardous phosgene gas, the safer “diphosgene” (trichloromethyl chloroformate) liquid or “triphosgene” (bis(trichloromethyl)carbonate) solid may be used as the dehydrating agent.²²



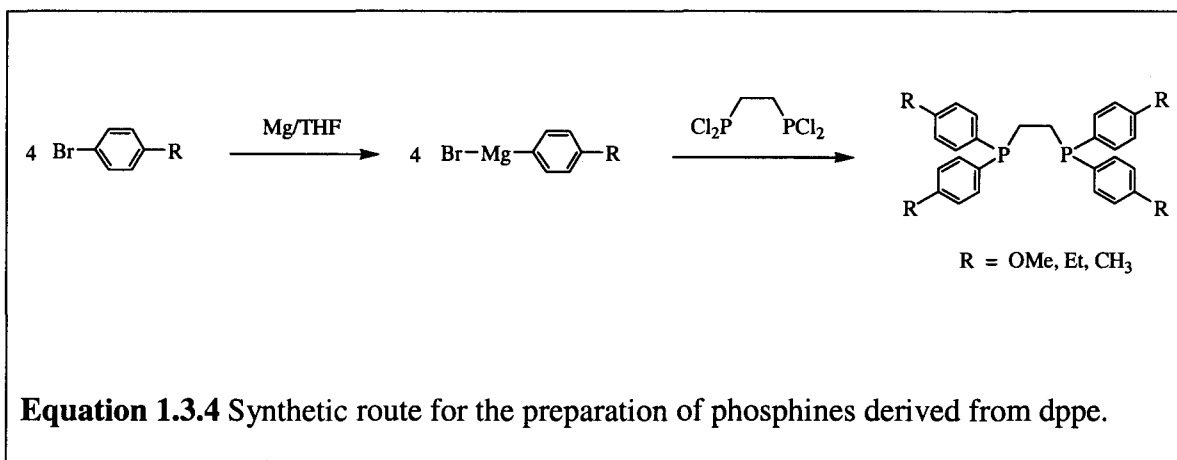
Equation 1.3.3 General synthesis for bis(isonitriles).

Phosphines will be used as ancillary ligands because they will allow us to tune the solubilities and electron richness of the products. To improve the solubilities of these species over the relatively insoluble dppe complexes, substituted dppe derivatives (*i.e.*,

$\text{dppe}' = (1,4\text{-C}_6\text{H}_4\text{Y})_2\text{PCH}_2\text{CH}_2\text{P}(1,4\text{-C}_6\text{H}_4\text{Y})_2$ and $(1,2\text{-C}_6\text{H}_4\text{Y})_2\text{PC}_6\text{H}_4\text{P}(1,4\text{-C}_6\text{H}_4\text{Y})_2$ where $\text{Y} = \text{OMe}, \text{Me}, \text{Et}, \text{etc.}$) will be used to systematically change the electron richness at Mo and the materials' steric bulk.



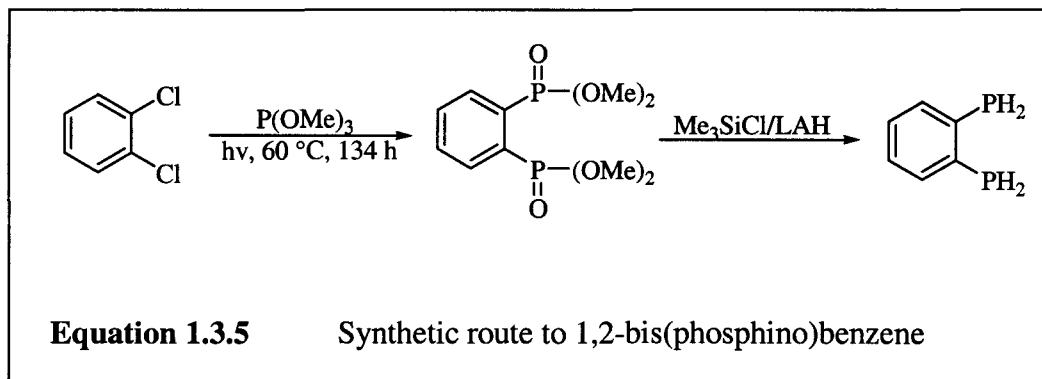
The typical synthetic route for preparing phosphines that are derivatives of dppe is shown below.²³



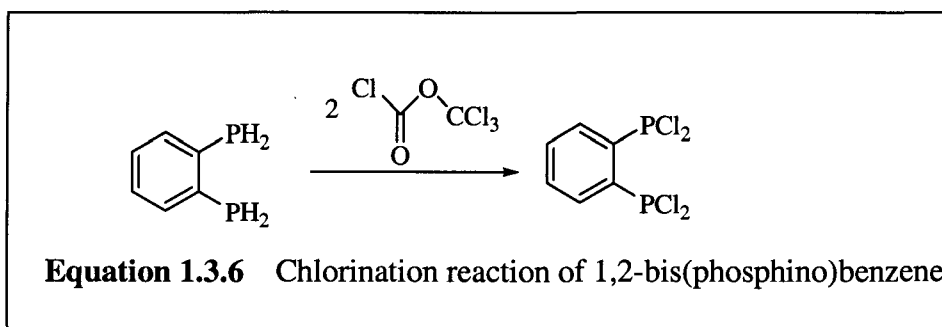
In this reaction, commercially available bis(dichlorophosphino)ethane is used as the starting material. Reaction of this compound with a Grignard or organolithium reagent in THF generally produces the desired dppe derivatives.

In addition to the phosphines derived from dppe, 1,2-bis(phosphino)benzene derivative will also be used. Instead of possessing an ethyl bridge between the phosphorus atoms, there is a benzene bridge (this type of phosphine is shown on the right in **Fig. 1.3.5**). The addition of the benzene backbone is expected to provide the polymer with a greater amount of stability since there is less rotational freedom present in a benzene ring than there is with an alkanediyl bridge.

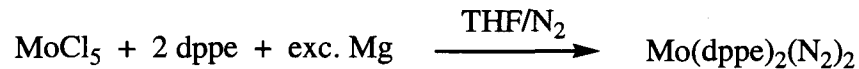
The synthetic route to preparing the “benzene backbone” phosphines and its derivatives is similar to the route shown in **Equation 1.3.4**. Thus, the aryl Grignard reagent is first prepared and is then combined with 1,2-bis(dichlorophosphino)benzene. Unlike 1,2-bis(dichlorophosphino)ethane, which is commercially available, the starting material for the dppe derivative phosphines, 1,2-bis(dichlorophosphino)benzene, must be synthesized. A useful synthetic route to 1,2-bis(phosphino)benzene has been reported by Kyba *et. al.*²⁴ and is detailed below.



The chlorination reaction is carried out by a method similar to the method reported by Dahlenburg *et. al.*²⁵

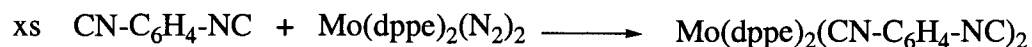


The precursors used for the synthesis of our organometallic materials are molybdenum and tungsten dinitrogen complexes of the type $M(N_2)_2(PR_3)_4$. They are generally well known compounds for the phenyl derivatives and have been extensively investigated as possible models and/or catalysts for chemical low-pressure nitrogen fixation.²⁶ In our new chemistry, the dinitrogen ligands will be exchanged with diisonitrile molecules to give the first generation metal-diisonitrile building blocks. Bisisonitrile complexes of the molybdenum phosphine complex (*e.g.*, $Mo(PR_3)_4(C\equiv N-C_6H_5)_2$) have previously been prepared by displacement of a weak ligand such as N_2 from the metal center. These starting materials (*e.g.*, $Mo(PR_3)_4(N_2)_2$ and $Mo(PR_3)_4(N_2)(CNMe)$) can be made by several routes, most commonly by the reduction of a molybdenum halide under an atmosphere of dinitrogen using a variety of reducing agents, or by analogous multistep procedures involving the isolation of intermediate products of this process.²⁷



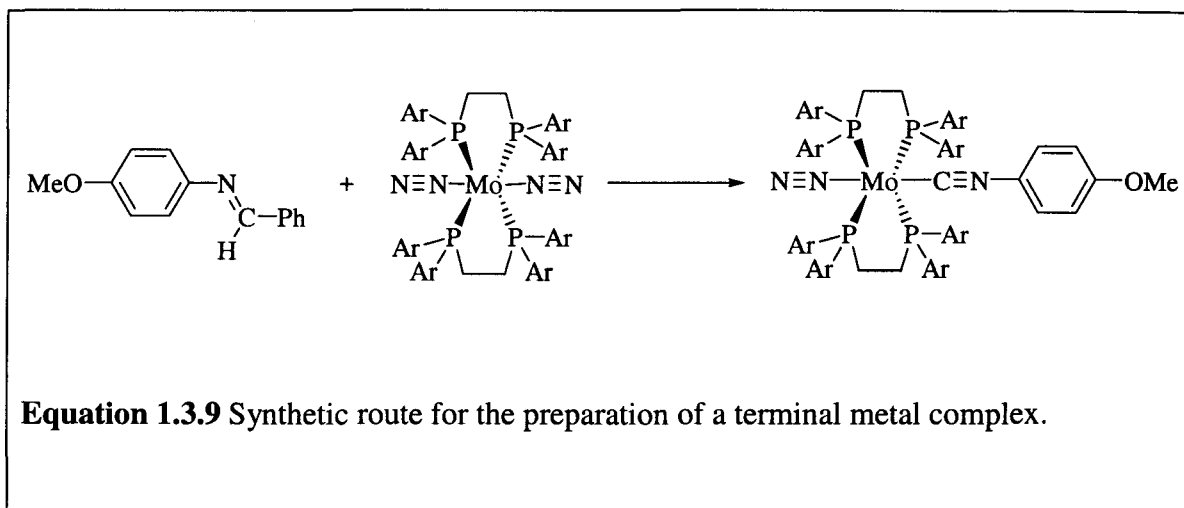
Equation 1.3.7 Synthetic route for the preparation of dinitrogen complexes.

In the next step, the first new nanorod building blocks will be synthesized. To avoid the uncontrollable formation of polymers, an excess of the isonitrile ligand will be used:

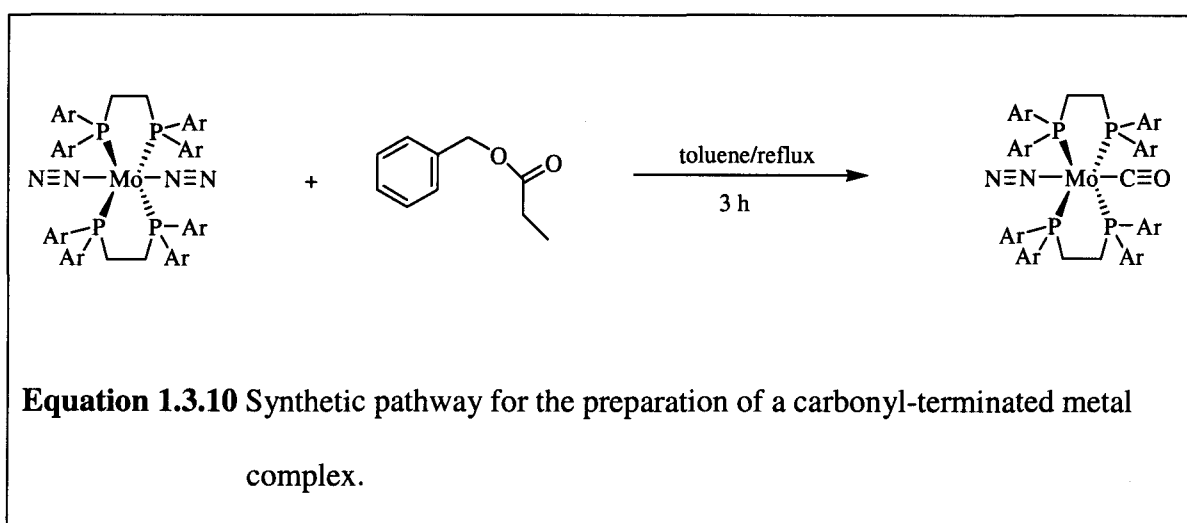


Equation 1.3.8 Synthetic route for the preparation of bis(diisonitrile) complexes.

Similar monoisonitrile complexes with only one isonitrile ligand per molybdenum center have been reported using a slightly different approach starting with imines instead of diisonitriles.²⁸

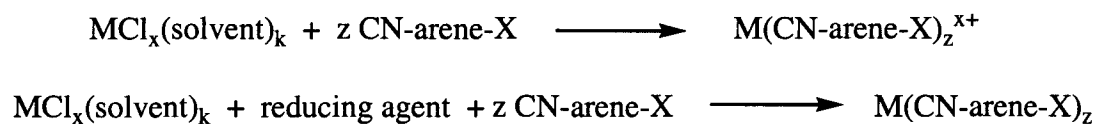


Longer oligomers will then be synthesized by combining the dinitrogen terminated first generation nanorods, the isocyanide terminated first generation nanorods, the bifunctional isocyanides, and/or the bis-dinitrogen complexes in appropriate proportions. When oligomers of the final desired chain length are made, they will be capped with terminal organometallic groups, including: $M(\text{CO})_5$ ($M = \text{Cr}, \text{Mo}, \text{W}$), $\text{CpFe}(\text{CO})_2^+$, $\text{CpMn}(\text{CO})_2$, $\text{Mo}(\text{dpppe}')_2\text{CO}$, or $\text{Mo}(\text{dpppe}')_2(\text{CN-R})$. The organometallic 'caps' will be prepared *via* published routes (equation 3.8).²⁹



However, the syntheses will require careful exploration of the reaction conditions to optimize conditions and prevent mixtures of non-capped, mono-capped, and di-capped species from forming. When electron poor caps such as $\text{Mo}(\text{CO})_5$ are used, it is expected that they will tend to polarize the organometallic isocyanide backbone and will also influence the degree of conjugation between the backbones and the caps. The most electron rich caps are expected to display the best conjugation. These 'capped' complexes will then be used to form organometallic nanostars.

Many metal-isocyanide complexes of the transition metals are known. They are typically prepared in excellent yields, either by reacting isocyanides with a metal salt or reducing the metal salt in the presence of isocyanides.²⁷



Equation 1.3.11 and 1.3.12 General pathways for the preparation of metal-isonitrile complexes.

Each nanostar will be prepared by using the specific reaction conditions used for the metal and conventional aryl isocyanides. It is expected that high yields will be obtained, but a major synthetic challenge will be the purification of the nanostars. Possible methods for purification are fractional crystallization and chromatography. Fractional crystallization works remarkably well if the synthesis is designed so that any

byproducts have different solubility than that of the desired material. Chromatography is very effective at removing byproducts that have different end-groups. However, column chromatography is quite tedious and often unsuccessful if there is a mixture of oligomers varying only in the number of repeating units.

The proposed organometallic nanostars are expected to have varying degrees of electronic conjugation down their arms and across their central vertices. They possibly may have fascinating electrical, conductive/semiconductive (i.e., when doped/partially oxidized, and NLO behavior when attached to surfaces. In molecular orbital terms, the maximum degree of electronic communication of the nanostars is expected when the metal fragment's highest occupied molecular orbitals, HOMOs (of predominately metal d-character), are of relatively high energy and the isonitrile's lowest unoccupied molecular orbitals, LUMOs (of π^* character), are of relatively low energy. It is also expected that increasing the electron richness at the molybdenum centers and decreasing it at the isonitriles should result in increased HOMO-LUMO overlap and hence conjugation.

3. Characterization of the Organometallic Building Blocks

It is expected that the new organometallic materials will be relatively air and thermally stable. Elemental analysis, IR, and ^1H , ^{13}C , and ^{31}P NMR spectroscopy will be used to characterize the physical and spectroscopic properties of the complexes and for information on purity and identity. X-ray diffraction will be used to determine the solid-state crystal structures of these building blocks. This will provide detailed structural information including: the degree of linearity down their oligomer backbones, the three

dimensional geometries at the central metal cores, and the extent of steric interactions. Intermetallic interactions can be quantitatively evaluated by cyclic voltammetric studies and qualitatively inferred from IR spectroscopy.

Section four

References

1. P. R. Jenkins. *Organometallic Reagents in Synthesis*; Oxford University Press: New York, **1992**.
2. (a) B. Douglas, D. McDaniel, J. Alexander. *Concepts and Models of Inorganic Chemistry*; John Wiley and Sons Inc.: New York, **1994**. (b) J. J. Eisch. *The Chemistry of Organometallic Compounds: The Main Group Elements*; The Macmillan Company; New York, **1967**. (c) J. E. Huheey. *Inorganic Chemistry: Principles of Structure and Reactivity*; Harper Collins Publishers Inc.: New York, **1983**.
3. R. F. Heck. *Organotransition Metal Chemistry: A Mechanistic Approach*; Academic Press: New York, **1974**.
4. C. M. Lukehart. *Fundamental Transition Metal Organometallic Chemistry*; Brooks/Cole Publishing Company: Monterey, California, **1985**.
5. (a) H. K. Hall Jr. *J. Amer. Chem. Soc.*, **1956**, 78, 2717 (1956). (b) E. L. Wittbecker, P. W. Morgan. *J. Polymer Sci.*, **1959**, 40, 289. (c) H. F. Mark, S. M. Atlas, N. Ogata. *J. Polymer Sci.* **1962**, 61, S49.
6. D. F. Shriver, P. W. Atkins. *Inorganic Chemistry*: 3rd ed; Oxford University Press: Oxford, **1999**; p 278.
7. J. E. Mark, H. E. Allcock, R. West. *Inorganic Polymers*; Prentice-Hall Inc.: Englewood Cliffs, New Jersey, **1992**.
8. T. A. George, C. D. Seibold, *Inorg. Chem.* **1973**, 12, 2544-2547.

9. P. Nguyen, P. Gomez-Elipe, I. Manners. *Chem. Rev.* **1999**, *99*, 1515-1548.
10. J. E. Keaton. *Organic Semiconducting Polymers* **1968**, p240, Marcel Dekker: New York.
11. I. Manners. *Angew. Chem., Int. Ed. Engl.* **1996**, *35*, 1602.
12. M. P. Stevens. *Polymer Chemistry: An Introduction*; 3rd ed; Oxford University Press: New York, 1999; p 12, 120.
13. C. U. Pittman Jr., O. E. Ayers, B. Suryanarayanan, S. P. McManus, J. E. Sheats. *Makromol. Chem.* **1974**, *175*, 1427.
14. (a) Y. Fujikura, K. Sonogashira, N. Hagihara. *Chem. Lett.* **1975**, 1067. (b) K. Sonogashira, S. Takahashi, N. Hagihara. *Macromolecules* **1977**, *10*, 879.
15. A. W. Bosman, H. M. Janssen, E. W. Meijer. *Chem. Rev.*, **1999**, *99*, 1665-1668.
16. C. E. Carraher Jr. *Polymer Chemistry*; 5th ed; Marcel Dekker, Inc.: New York, 2000; p 380.
17. A. M. McDonagh, N. T. Lucas, M. P. Cifuentes, M. G. Humphrey, S. Houbrechts, A. Persoons. *J. Organomet. Chem.* **2000**, *605*, 184-192.
18. I. R. Whittall, A. M. McDonagh, M. G. Humphrey. *Adv. Organomet. Chem.* **1998**, *42*, 291-362.
19. J. Chen, L. C. Clavet, M. A. Reed, D. W. Carr, D. S. Grubisha, D. W. Bennett. *Chem. Phys. Lett.* **1999**, *313*, 741-748.
20. N. L. Wagner, F. E. Laib, D. W. Bennett. *Inorg. Chem. Comm.* **2000**, *3*, 87-90.
21. I. Ugi, U. Fetzner, U. Ebholzer, H. Knuemper, K. Offermann. *Angew. Chem., Int. Ed. Engl.* **1965**, *4*, 472.

22. A. Efraty, I. Feinstein, L. Wackerle, A. Goldman. *J. Org. Chem.* **1980**, *45*, 4059-4061.
23. J. Chatt, W. Hussain, G. J. Leigh, H. M. Ali, C. J. Pickett, K. A. Rankin. *J. Chem. Soc. Dalton. Trans.* **1985**, 1131-1136.
24. Adapted from E. P. Kyba, S-T Jui, R. L. Harris. *Organometallics* **1983**, *2*, 1877-1879 and E. P. Kyba, M. C. Kerby, S. P. Rines. *Organometallics* **1986**, *5*, 1189-1194.
25. Adapted from L. Dahenburg, A. Kaunert. *Eur. J. Inorg. Chem.* **1998**, 885-887
26. M. Hidai, K. Tominari, Y. Uchida, A. Misono. *Chem. Commun.* **1969**, 1392.
27. J. Chatt, J. R. Dilworth, R. L. Richards. *Chem. Rev.* **1978**, *78*, 589.
28. G. Nakamura, Y. Harada, C. Arita, H. Seino, Y. Mizobe, M. Hidai. *Organometallics* **1998**, *17*, 1010-1012.
29. M. Sato, T. Tatsumi, T. Dodama, M. Hidai, T. Uchida, Y. Uchida. *J. Am. Chem. Soc.* **1978**, *100*, 4447-52.

Chapter II –Experimental

Unless otherwise stated, all reactions were carried out under a dry, inert atmosphere using standard Schlenk techniques for the handling of air-sensitive materials.

1. Reagents

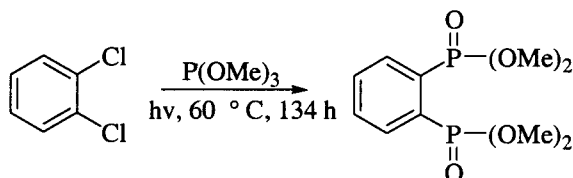
All reagents used were either purchased commercially or were synthesized prior to use. The reagents that were purchased were of reagent grade or comparable purity and were not further purified prior to use. Samples were deaerated by either bubbling ultra high purity nitrogen through the chemical or by the *freeze-pump-thaw* method (the reagent to be purified is frozen using liquid nitrogen, the air pumped off, then the reagent is allowed to thaw; the process is repeated at a minimum of three times). Solvents were dried and deaerated using standard methods¹ and stored under nitrogen. Thus, THF, diethyl ether and toluene were distilled from benzophenone ketyl radical over Na-K amalgam for THF and diethyl ether and Na for toluene. Hexane was distilled over Na-K amalgam. Dichloromethane was distilled over calcium hydride.

2. Instrumentation

Infrared spectra were measured using a JASCO FT/IR-410 infrared spectrophotometer. NMR spectra were measured on a Varian Gemini 2000 400 MHz spectrometer with reference to the deuterium signal of the solvent used. The ¹H, ¹³C, and

^{31}P NMR chemical shifts were measured in parts per million (ppm) downfield from external Me_4Si and 85% H_3PO_4 , as appropriate.

3. 1,2-Bis(dimethoxyphosphoryl)benzene²

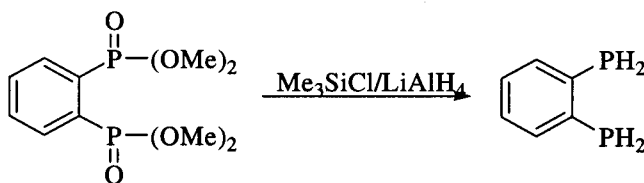


The photochemical reaction vessel used was purchased from Ace Glass, catalog number 7861-255 1000mL. The power supply has catalog number 7830-60, with a power rating of 450 watts. The lamp used was catalog number 7825-34 for a 450W UV immersion lamp with a 4.3" arc length. Trimethyl phosphite (Aldrich, 97%, 900 mL, 947 g, 8 mol) and 1,2-dichlorobenzene (Aldrich, 99%, 300 mL, 391.5 g, 2.66 mol) are photolyzed for 134 h at 60 °C under an atmosphere of nitrogen. The solution is then transferred to a 3 L flask and reduced in volume by half (i.e. to 600 mL). Acetone (approximately 200 mL) is added and the solution is placed in the freezer (-19 °C) to crystallize. Re-crystallization (when needed) can be done by dissolving the crystals in hot acetone and placing the mixture in the freezer (-19 °C) overnight giving 106.63 g (362.46 mmol, 13.6%) of 1,2-bis(dimethoxyphosphoryl)benzene as clear, colorless crystals. The supernatant can then be recycled for use in this reaction as it contains a mixture primarily composed of the starting material, the monosubstitution product, and the desired product.

Spectroscopic Data

NMR data: ^{31}P NMR (161.884 MHz, CDCl_3): $\delta = -4.634(\text{s})$; ^1H NMR (399.905 MHz, CDCl_3): $\delta = 7.895$ (m, 2 H, C_6H_4), 7.411 (m, 2 H, C_6H_4), 3.580 (pd, 12 H, CH_3)

4. 1,2-Bis(phosphino)benzene¹



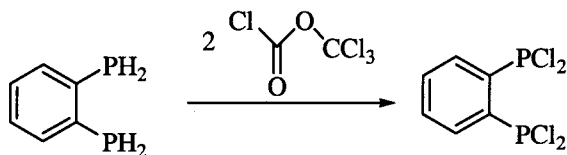
Lithium aluminum hydride (Aldrich, 95%, 15.6 g, 410 mmol) is added to a 1 L 3-neck flask fitted with a stopper, N_2 adaptor, and an over-sized bean-shaped stirring bar. The flask is evacuated and filled with nitrogen. THF (500 mL) is added and the flask is cooled to $-78\text{ }^\circ\text{C}$ using a dry ice-ethanol bath. Trimethylchlorosilane (Aldrich, 98%, 51.8 mL, 44.5g, 410 mmol) is then added drop-wise to the cold solution and the solution is stirred while warming to room temperature for 2 h. 1,2-Bis(dimethoxyphosphoryl)benzene (20.0 g, 68 mmol) is dissolved in THF (200 mL). This solution is then added drop-wise *via* syringe to the reducing mixture after it has cooled back down to $-78\text{ }^\circ\text{C}$. This addition must be done slowly as gas and heat evolve from this reduction. The solution is stirred for 36 h. **Note:** the next step should be done **slowly**, as the excess LAH reacts **violently** with water. The reaction is quenched with water (100 mL), followed by 1M KOH (250 mL; both degassed prior to use). The organic layer is removed and the aqueous layer is extracted with diethyl ether (4×200 mL portions). The ether portions are then combined, concentrated to 30 mL, and dried over magnesium

sulfate overnight. After the magnesium sulfate is removed by filtration, the extracts are fractionally distilled *in vacuo* to give 6.27 g (44.13 mmol, 64%) of the desired product as a clear, colorless to slightly yellow liquid with a boiling point (in oil pump vacuum) of 60 °C.

Spectroscopic Data

^1H NMR (399.905 MHz, CDCl_3) δ 7.25 (m, 2H, C_6H_4), 6.90 (m, 2H, C_6H_4), 3.90 (pd, 4H, PH_2). ^{31}P NMR (161.884 MHz, CDCl_3) δ -147.69

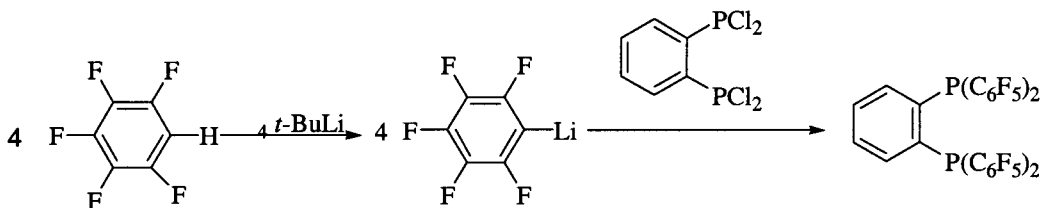
5. 1,2-Bis(dichlorophosphino)benzene³



A 500 mL 3-neck flask is fitted with a stopper, N_2 adaptor, and a 50 mL addition funnel. It is then evacuated and filled with nitrogen. 1,2-Bis(phosphino)benzene (10.13 g, 71.3 mmol) and THF (200 mL) are added to the flask. Trichloromethyl chloroformate (Lancaster, 98%, 17.4 mL, 144.3 mmol) in THF (30 mL) are added *via* the addition funnel drop-wise to the solution of 1,2-bis(phosphino)benzene over 1 h. After addition is complete, the reaction mixture is allowed to stir for an additional 2 h. The solution is then concentrated to 50 mL and fractionally vacuum distilled, resulting in 7.35 g (26.27 mmol, 36.8%) of a yellow tinted liquid with a boiling point (under vacuum) of 85-90 °C for 1,2-

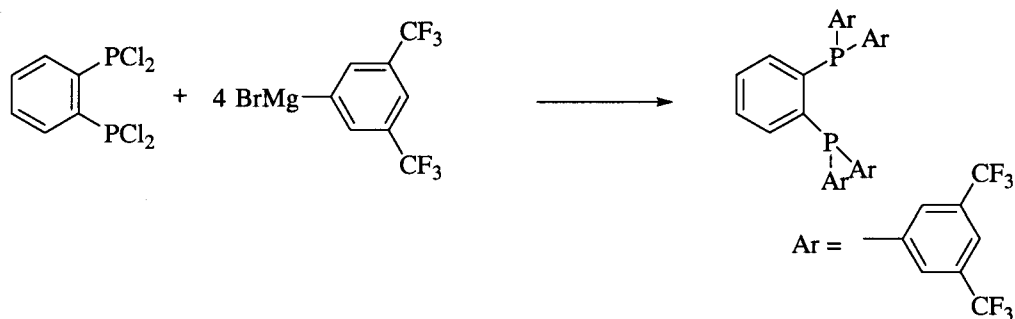
$C_6H_4(PCl_2)_2$. Due to its reactivity, this product was not further characterized except by its products.

6. Attempted synthesis of 1,2-bis(di(pentafluorobenzene)phosphino)benzene⁴



To a 250 mL 3-neck flask fitted with a nitrogen adapter, addition funnel, and a stopper, are added 30 mL diethyl ether and 3.3 mL (5 g, 29.8 mmol) 1,2,3,4,5-pentafluorobenzene (Aldrich, 99%) (The reaction vessel is evacuated and filled with nitrogen prior to the addition). The solution is then cooled to $-55\text{ }^{\circ}\text{C}$ using a dry ice/ethanol bath. The 17.5 mL (12.3 g, 29.8 mmol) of *t*-butyl lithium is added *via* syringe and the solution is stirred for 1 h. 1,2-Bis(dichlorophosphino)benzene (1.60 g, 5.72 mmol) and 20 mL diethyl ether are then combined in the addition funnel and added to the mixture drop-wise over the course of 1 h. The resulting orange solution is stirred for an additional 2 h. The mixture is then placed in the freezer ($-19\text{ }^{\circ}\text{C}$) to crystallize. No product was isolated.

7. 1,2-Bis({3,5-bis(trifluoromethyl)benzene}phosphino)benzene³



Grignard Reagent Preparation

To a 500 mL 3-neck flask fitted with a nitrogen adapter, stopper, and a 50 mL addition funnel, are added 0.73 g (30 mmol) magnesium turnings (Aldrich, 99+%) and 150 mL THF. The addition funnel is then charged with 4.4 g (15 mmol, 2.6 mL) 3,5-bis(trifluoromethyl)bromobenzene (Aldrich, 99%) and 30 mL THF. This mixture is added drop-wise to the Mg/THF slurry over the course of 45 min. The resulting orange-brown solution is stirred for an additional hour.

Phosphine Synthesis

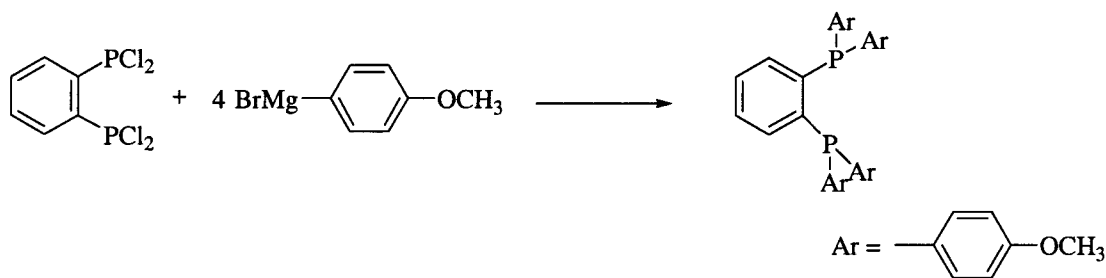
To a 500 mL Schlenk flask fitted with a 250 mL Schlenk filter, are added 1.08 g (3.58 mmol) of 1,2-bis(dichlorophosphino)benzene and 250 mL toluene (Fisher, ACS grade, 99.9%). This solution is then cooled to 0 °C. The Schlenk filter is charged with the Grignard reagent in A, which is slowly filtered so that it is added drop-wise to the solution of 1,2-bis(dichlorophosphino)benzene over the course of 45 min at 0 °C. The reaction mixture is stirred for an additional 2 h. The solution is then concentrated *in vacuo* to approximately 50 mL and hexane (100 mL) is added. The resulting dark orange-

brown solution is then placed in the freezer (-19 °C) to crystallize. The resulting brown crystals are re-dissolved in toluene (20 mL) and filtered through Celite. 100 mL Toluene and 250 mL hexane are added and the solution is placed in the freezer and left to crystallize over the course of 5 days. The solution is decanted off from the resulting quartz-like crystals and they are slurried in hexane and filtered through Whatman 41 filter paper. The crystals are then allowed to dry on the filter paper to give 0.71 g (0.71 mmol, 18.5%) of the desired phosphine.

Spectroscopic Data

$^1\text{H NMR}$ (399.886 MHz, CDCl_3) δ 7.88 (s), 7.57 (m, 2 H, Ph-H), 7.11 (m, 2 H, Ph-H)

8. 1,2-Bis(di(*p*-anisole)phosphino)benzene³



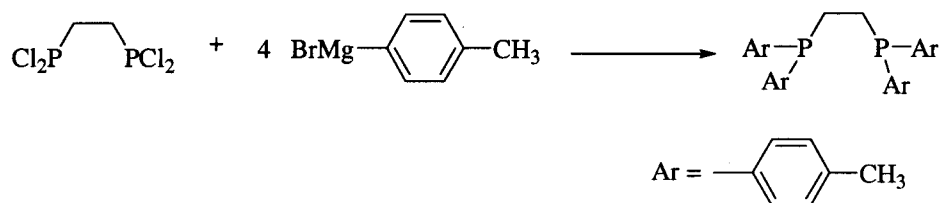
To a 500 mL 3 neck flask fitted with a nitrogen adapter, stopper, and 25 mL addition funnel, is added 2.06 g (84.76 mmol) magnesium turnings (Aldrich, 99+%) and 250 mL THF (Aldrich, HPLC grade, 99.9%). The addition funnel is charged with 6.5 mL (53.6 mmol) of 4-bromoanisole (Aldrich, 99%) and 15 mL of THF. The solution is then added drop-wise to the magnesium slurry over the course of 1 h. The solution is heated to reflux for an additional 10 min and is then stirred for an additional 2 h. To a 500 mL

Schlenk flask fitted with a 250 mL Schlenk filter, is added 100 mL THF and 3.0 g (10.72 mmol) 1,2-bis(dichlorophosphino)benzene. The filter frit is then charged with the anisole Grignard reagent described above. The Grignard reagent is added to the 1,2-bis(dichlorophosphino)benzene solution drop-wise *via* the filter frit over the course of 1h. This reaction mixture is then allowed to stir for an additional 2h. The excess Grignard reagent is hydrolyzed with a 10% solution of ammonium chloride (3 × 100 mL). The organic layer is removed and then stirred over anhydrous magnesium sulfate (Fisher, anhydrous) overnight. The yellow-green solution is filtered and the solvents are removed from the filtrate *in vacuo*. The resulting pale yellow residue is re-dissolved in diethyl ether (100 mL) and the solution is left to crystallize in the freezer (-19 °C) giving 0.71 g (1.25 mmol, 11.7%) of the white phosphine.

Spectroscopic Data

^1H NMR (399.886 MHz, CDCl_3): δ = 7.26 (m, 2 H, Ph-H), 7.09 (m, 2 H, Ph-H), 6.74 (d, J ($^1\text{H}^1\text{H}$) = 8 Hz, 4 H Ph-H), 3.78 (s, 12 H, CH₃)

9. Bis(di(*p*-tolyl)phosphino)ethane⁵

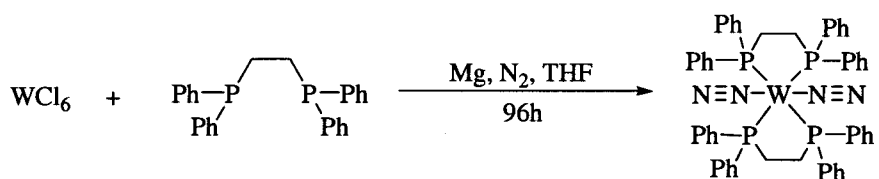


To a 500 mL 3 neck flask fitted with a nitrogen adapter, stopper, and 50 mL addition funnel, is added 11.47 g (472 mmol) of magnesium turnings (Aldrich, 99+ %) and 160 mL of THF (Aldrich, HPLC grade, 99.9 %). The addition funnel is charged with 37 mL (51 g, 298 mmol) of 4-bromotoluene (Aldrich, 99 %) and 10 mL of THF. This solution is then added drop-wise to the magnesium slurry over the course of 1 h and is stirred for an additional 1 h. To a 500 mL Schlenk flask fitted with a 250 mL Schlenk filter is added 100 mL of THF and 15.36 g (66.26 mmol, 10 mL) of 1,2-bis(dichlorophosphino)ethane. The sintered glass filter is then charged with the toluene Grignard reagent prepared previously. The Grignard reagent is then added to the 1,2-bis(dichlorophosphino)ethane solution drop-wise *via* the Schlenk filter over the course of 1 h. The reaction mixture is stirred for an additional 2 h. The excess Grignard reagent is then hydrolyzed with a 10% solution of ammonium chloride (3 × 100 mL). The organic layer is removed *via* a separatory funnel and stirred over anhydrous magnesium sulfate (Fisher, anhydrous) overnight. The yellow solution is filtered off and the solvents are removed from the filtrate *in vacuo*. The resulting pale yellow residue is re-dissolved in toluene (100 mL) and hexane (40 mL) is added. The solution is placed in the freezer (-19 °C), where it is left to crystallize. The solvent is removed using a syringe and the phosphine is re-crystallized from a 1:3 toluene/hexane mixture (the phosphine is first dissolved in toluene, and then layered with three times as much hexane (approximately 60 mL) giving 6.34 g (13.95 mmol, 21.1%) of the white crystalline phosphine.

Spectroscopic Data

^1H NMR (399.886 MHz, C_6D_6): δ = 7.36 (m), 6.89 (d, $J(^1\text{H } ^1\text{H})$ = 8 Hz), 2.32 (t, $J(^1\text{H } ^1\text{H})$ = 4 Hz, 4 H, $\underline{\text{CH}_2}$), 2.03 (s, 12 H, $\underline{\text{CH}_3}$). ^{13}C NMR (100.560 MHz, C_6D_6): δ = 139.00 (s, $\underline{\text{C}_6\text{H}_4}$), 136.63 (s, $\underline{\text{C}_6\text{H}_4}$), 133.82 (s, $\underline{\text{C}_6\text{H}_4}$), 130.20 (s, $\underline{\text{C}_6\text{H}_4}$), 25.91 (s, $\underline{\text{CH}_2}$), 22.10 (s, $\underline{\text{CH}_3}$).

10. Bis(dinitrogen)bis(diphenylphosphinoethane)tungsten (0)⁶



To a 1 L Schlenk flask equipped with a stir bar and stopper are added 24 g (1 mol) of Mg turnings (Aldrich, 99.9+ %; note: it is important that the Mg turnings are as clean as possible) and 25 g (62.75 mmol) of 1,2-bis(diphenylphosphino)ethane (Aldrich, 97 %). The reaction vessel is evacuated and then THF (300 mL) followed by 11.89 g (30 mmol) of tungsten hexachloride (Aldrich, 99+ %) are added. The reaction solution is vigorously stirred for 4 days (96 h) under an atmosphere of ultra high purity (UHP) N_2 . The reaction mixture is filtered through a Celite packed Schlenk filter to remove the Mg turnings. At this point, orange crystals can be seen on the Celite bed. These crystals are then dissolved off of the Celite and the initial reaction flask is rinsed with THF (1.5 – 2 L). Once the crystals have been dissolved, the solvent is reduced in volume by half (i.e. to 500 mL) and degassed methanol (300 mL; Acros, anhydrous, 99.8 %) is added. The flask is cooled to 0 °C for 1 h. The orange micro crystals are then filtered off and re-

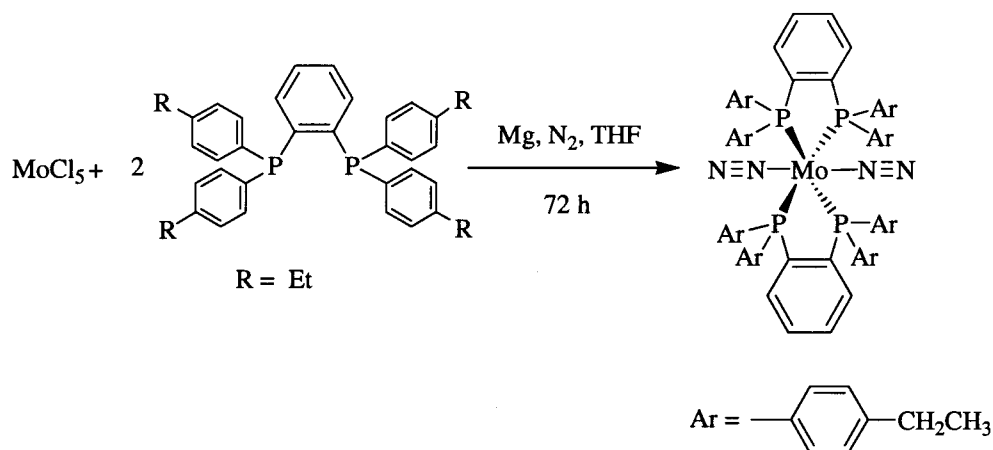
crystallized by dissolving them in THF (50 mL). Slight heating may be required to get the crystals fully into solution. After three times as much methanol (150 mL) is added, 13 g (12.54 mmol, 41.8%) of the orange dinitrogen complex is obtained by filtration as an orange crystalline solid.

Spectroscopic Data

^1H NMR (399.905 MHz, C_6D_6): $\delta = 2.26$ (t, $J(^1\text{H}^1\text{H}) = 8$ Hz, 8 H, CH_2), 7.01 (s, 20 H, C_6H_5), 7.02 (s, 20 H, C_6H_5), 7.19 (s, 32 H, C_6H_5). ^{31}P (161.884 MHz, C_6D_6): $\delta = 45.71$.

IR (CaF_2 plates, toluene solvent) $\nu(\text{N}\equiv\text{N})$ 1948.72 (s, sy), 2009.46 (w, as).

11. Bis(dinitrogen)bis[1,2-bis(di(*p*-ethylphenyl)phosphino)benzene]molybdenum(0)⁵



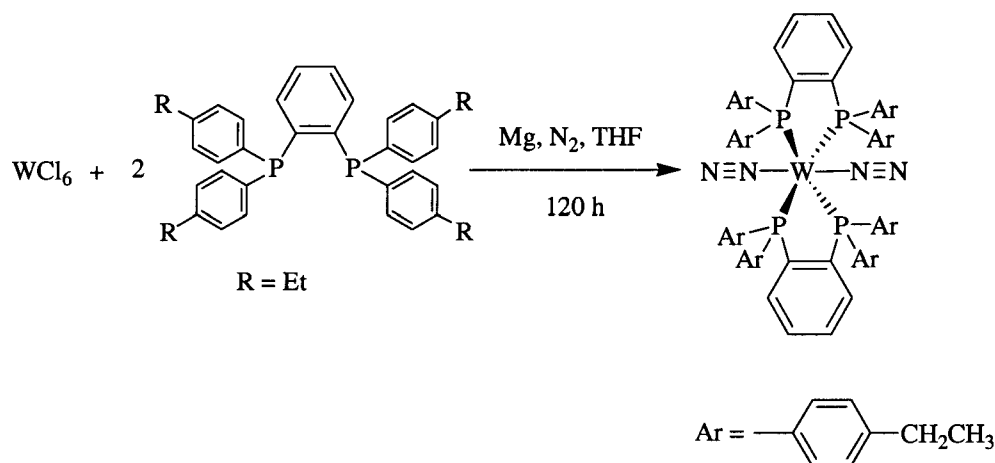
To a 1 L Schlenk flask equipped with a stir bar and stopper, is added 2.38 g (97.9 mmol) of Mg turnings (Aldrich, 99.9+ %; note: it is important that the Mg turnings be as clean as possible) and 6.71 g (12.01 mmol) of 1,2-bis(di(*p*-ethylbenzene)phosphino)benzene. The reaction vessel is evacuated and then THF (400

mL) followed by 1.64 g (6.0 mmol) of molybdenum pentachloride (Aldrich, 99+ %) are added. The reaction solution is stirred vigorously for 3 days (72 h) under an atmosphere of ultra high purity (UHP) N₂. The reaction mixture is then filtered through a Celite packed Schlenk filter to remove the Mg turnings. Degassed methanol (600 mL; Acros, anhydrous, 99.8%) is then added to precipitate the orange red product. The flask is cooled to 0 °C for 1 h. The suspension is again filtered through Celite. The resulting red-orange dinitrogen complex is dissolved off of the Celite into a different 1000 mL flask using THF (approximately 200 mL) and methanol (600 mL; Acros, anhydrous, 99.8%) is again added to precipitate 5.1 g (4.02 mmol, 66.8%) of the red dinitrogen complex. These crystals are collected on a filter frit and dried *in vacuo*. The purity of the product can be determined by ¹H NMR and additional purification by re-crystallization (THF/methanol mixture) can be done if necessary.

Spectroscopic Data

¹H NMR (399.905 MHz, C₆D₆): δ = 7.21 (d, *J* (¹H¹H) = 7.6 Hz, 20 H, C₆H₅), 6.94 (d, *J* (¹H¹H) = 8 Hz, 20 H, C₆H₅), 2.43 (q, *J* (¹H¹H) = 8 Hz, 16 H, CH₂), 1.07 (t, *J* (¹H¹H) = 7.6 Hz, 24 H, CH₃). ³¹P NMR (161.884 MHz, C₆D₆): δ = 70.10. IR (CaF₂ plates, toluene solvent) ν(N≡N) 1980.54 (s, sy), 2054.78 (w, as).

12. Bis(dinitrogen)bis[1,2 bis (di(*p*-ethylphenyl)phosphino)benzene]tungsten(0)⁵

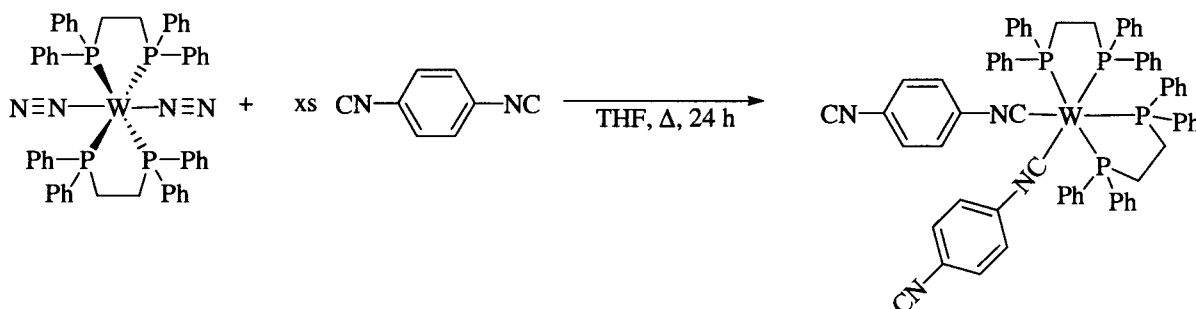


To a 500 mL Schlenk flask equipped with a stir bar and stopper, are added 1.02 g (42 mmol) of Mg turnings (Aldrich, 99.9+ %; note: it is important that the Mg turnings be as clean as possible) and 2.50 g (4.48 mmol) of 1,2 bis(di(*p*-ethylbenzene)phosphino)benzene. The reaction vessel is evacuated and then THF (300 mL) followed by 0.89 g (2.2 mmol) of tungsten hexachloride (Aldrich, 99+ %) are added. The reaction solution is stirred for 5 days (120 h) under an atmosphere of N₂. The reaction mixture is filtered through a Celite packed Schlenk filter to remove the Mg turnings and degassed methanol (800 mL; Acros, anhydrous, 99.8%) is added. The flask is then placed in the freezer (-19 °C) overnight. The solution mixture is again filtered through a Schlenk filter to remove any solid impurities and methanol (800 mL; Acros, anhydrous, 99.8%) is again added to precipitate the complex. These crystals are then collected on a filter frit. ¹H NMR confirms the product's identity.

Spectroscopic Data

$^1\text{H NMR}$ (399.905 MHz) δ 6.94 (d, $J = 8$ Hz, 40H, C_6H_5), 2.43 (q, $J = 8$ Hz 16H, CH_2), 1.07 (t, $J = 7.6$ Hz, 24H, CH_3). IR (CaF_2 plates, toluene solvent) $\nu(\text{N}\equiv\text{N})$ 1952.57(s, sym), 2023.93 (w, asym).

13. *cis*-Bis(1,4-diisocyanobenzene)bis[diphenylphosphinoethane]tungsten(0)

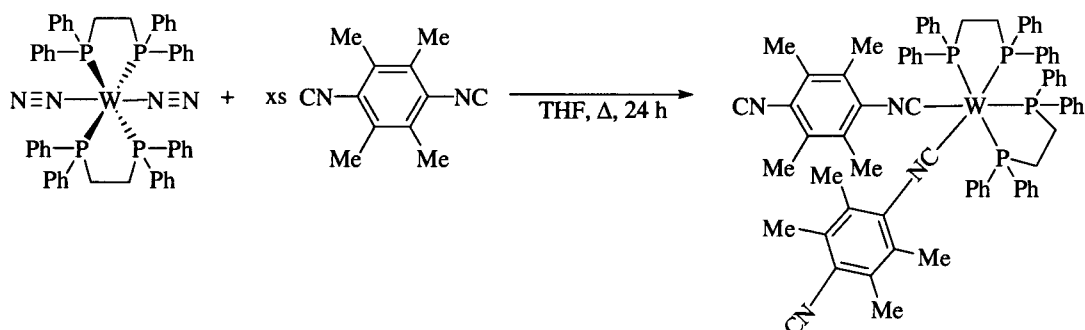


To a 500 mL 3-neck flask equipped with a stir bar, stopper, nitrogen adapter, and reflux condenser, are added 0.60 g. (0.58 mmol) of *trans*-bis(dinitrogen)bis(1,2-bis(diphenylphosphino)ethane)tungsten(0) and 0.74 g (5.8 mmol) of 1,4-diisocyanobenzene. The reaction vessel is evacuated and THF (200 mL) is added. The solution is heated to reflux for 24 h. The solvent is reduced *in vacuo* to 60 mL and 100 mL hexanes are added to precipitate the product as dark red crystals. The mixture is allowed to further crystallize in the refrigerator at 3 °C for 48 h. The mixture is filtered through a Schlenk filter and the resulting crystals are washed with hexane resulting in 0.229 g (0.19 mmol, 32%) of the bis(diisonitrile) complex.

Spectroscopic Data

No NMR data was recorded due to the poor solubility of the target complex

14. *cis*-Bis(2,3,5,6-tetramethyl-1,4-diisocyanobenzene)bis[diphenylphosphinoethane]tungsten(0)



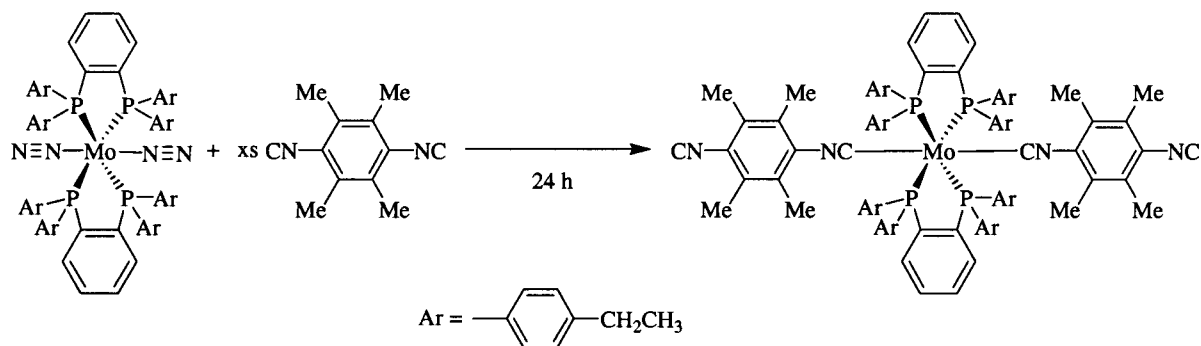
To a 500 mL 3-neck flask equipped with a stir bar, stopper, nitrogen adapter, and reflux condenser are added 0.60 g. (0.58 mmol) of *trans*-bis(dinitrogen)bis(1,2-bis(diphenylphosphino)ethane)tungsten(0) and 1.07 g (5.8 mmol) of 2,3,5,6-tetramethyl-1,4 diisocyanobenzene. The reaction vessel is evacuated and THF (200 mL) is added. The solution is heated to reflux for 24 h. The solvent is reduced *in vacuo* to 60 mL and 100 mL hexanes are added to precipitate the product as dark red crystals. The mixture is allowed to further crystallize in the refrigerator at 3 °C for 48 h. The mixture is collected on a Schlenk filter and the resulting purple crystals are washed with hexane (100 mL). In an attempt to further purify these crystals, THF (2.5 L) was used to dissolve the product (Note: product is only sparingly soluble in polar solvents) and the solution was placed in

the $-80\text{ }^{\circ}\text{C}$ freezer and later discarded. The hexane washing were placed in the refrigerator ($3\text{ }^{\circ}\text{C}$). After 5 days, black crystals could be seen in the flask. The target bis(diisonitrile complex was produced in a 34% (0.27 g, 0.20 mmol) yield.

Spectroscopic Data

No NMR data due to poor solubility of the complex. X-ray diffraction showed the product to be the *cis* isomer of the target isonitrile complex.

15. Bis(2,3,5,6-tetramethyl-1,4-diisocyanobenzene)bis[1,2-bis(di(*p*-ethylphenyl)phosphino)benzene]molybdenum(0)



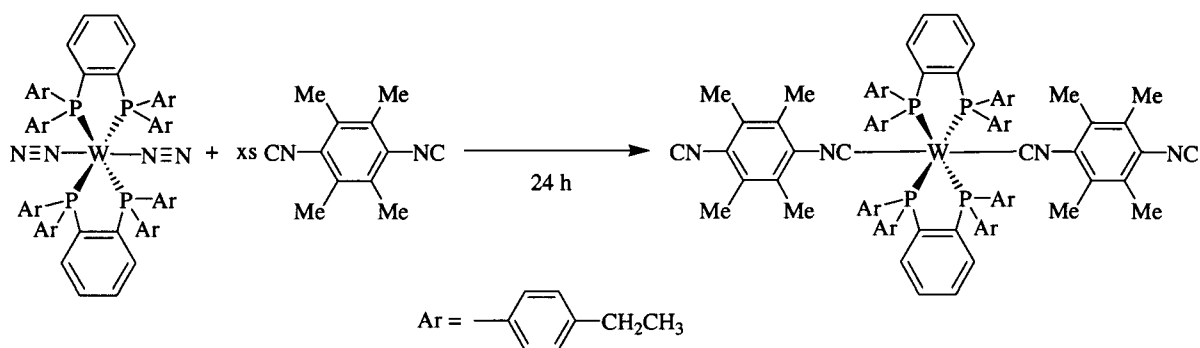
To a 500 mL 3-neck flask equipped with a stir bar, nitrogen adapter, addition funnel, and stopper are added 2.40 g (13.03 mmol) of 2,3,5,6-tetramethyl-1,4-diisocyanobenzene and toluene (120 mL). To the addition funnel are added 1.515 g (1.19 mmol) of bis(dinitrogen)bis[1,2-bis(di(*p*-ethylphenyl)phosphino)benzene]molybdenum(0) and toluene (60 mL). The flask is cooled to $0\text{ }^{\circ}\text{C}$ with an ice bath and the bis(dinitrogen) bis[1,2-bis(di(*p*-ethylbenzene)phosphino)benzene]

molybdenum(0)/toluene solution is added drop-wise over the course of 1 h. Toluene (20 mL) is used to rinse the addition funnel and the reaction progress is monitored by IR spectroscopy. The reaction mixture is stirred for a total of 24 h. The solvent is reduced in volume *in vacuo* to 100 mL at which point dark green to blue micro crystals were observed in the flask. The flask is then placed in the freezer (-19 °C) and allowed to crystallize overnight. Hexane (120 mL) is added and the solution is again placed in the freezer to crystallize over the course of two days. The green-blue crystals are collected on a filter frit giving 1.89 g (1.20 mmol, 89.4%) of the bis(diisonitrile) complex.

Spectroscopic Data

^1H NMR (399.905 MHz, C_6D_6): δ = 7.88 (s, 10 H, C_6H_5), 7.21 (d, J ($^1\text{H}^1\text{H}$) = 6.8 Hz, 10 H, C_6H_5), 7.14 (s, 10 H, C_6H_5), 6.81 (d, J ($^1\text{H}^1\text{H}$) = 8 Hz, 10 H, C_6H_5), 2.34 (q, J ($^1\text{H}^1\text{H}$) = 7.6 Hz, 16 H, CH_2), 2.00 (s, 12 H, Ar- CH_3), 1.00 (t, J ($^1\text{H}^1\text{H}$) = 7.6 Hz, 24 H, CH_3), 0.83 (s, 12 H, Ar- CH_3). ^{31}P NMR (161.884 MHz, C_6D_6): δ = 71.19 (s). IR (CaF_2 plates, toluene solvent) $\nu(\text{N}\equiv\text{C})$ 1865.79 (s).

16. Bis(2,3,5,6-tetramethyl-1,4-diisocyanobenzene)bis[1,2 bis (di(*p*-ethylphenyl)phosphino)benzene]tungsten(0)



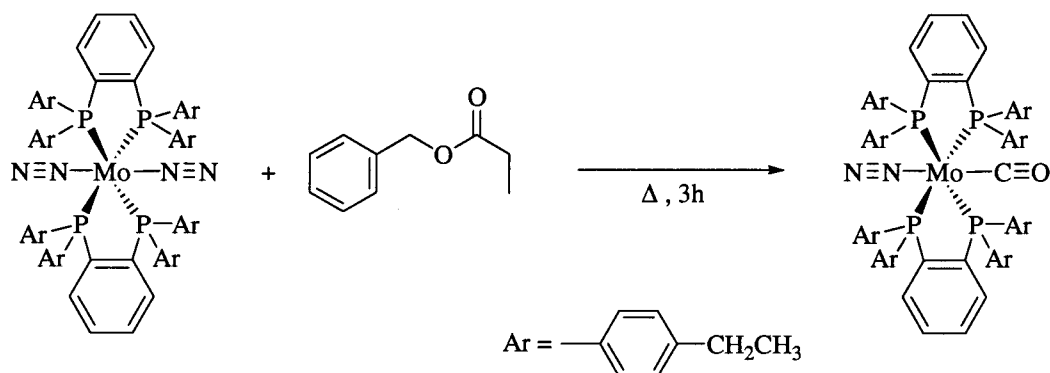
To a 500 mL 3-neck flask equipped with a stir bar, nitrogen adapter and stopper, are added 0.351 g (1.90 mmol) of 2,3,5,6-tetramethyl-1,4-dicyanobenzene and 0.515 g (0.380 mmol) of bis(dinitrogen)bis[1,2-bis(di(p-ethylphenyl)phosphino)benzene] tungsten(0). The flask is evacuated and toluene (300 mL) is added. The reaction mixture is stirred for a total of 168 h. The solvent is evaporated down to 20 mL and hexane (60 mL) is added. The flask is then placed in the freezer (-19 °C) and the product is allowed to crystallize over the course of five days. The resulting product is shown by ^1H NMR spectroscopy to be unreacted starting materials. The solvent is reduced to dryness *in vacuo*, toluene (150 mL) is added and the solution is heated to reflux for 18 h. The solution is then allowed to cool to room temperature and the solvent is reduced *in vacuo* to 20 mL. Hexane (100 mL) is added and the solution is again placed in the freezer to crystallize over the course of five days. The brown-to-black crystals are collected on a filter frit giving 0.25 g (0.150 mmol, 39.5%) of the bis(diisonitrile) complex.

Spectroscopic Data

^1H NMR (399.905 MHz, C_6D_6): δ = 7.88 (s, 16 H, C_6H_5), 7.21 (d, $J(^1\text{H}^1\text{H})$ = 6.8 Hz, 4 H, C_6H_5), 7.14 (s, 16 H, C_6H_5), 6.81 (d, $J(^1\text{H}^1\text{H})$ = 8 Hz, 4 H, C_6H_5), 2.34 (q, $J(^1\text{H}^1\text{H})$ =

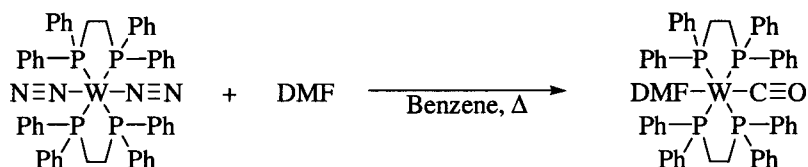
7.6 Hz, 16 H, CH_2), 2.00 (s, 12 H, Ar- CH_3), 1.00 (t, $J(^1\text{H}^1\text{H}) = 7.6$ Hz, 24 H, CH_3), 0.83 (s, 12 H, Ar- CH_3). ^{31}P NMR (161.884 MHz, C_6D_6): $\delta = 71.19$ (d, $J = 42.1$ Hz). IR (CaF_2 plates, toluene solvent) $\nu(\text{N}\equiv\text{C})$ 1858.08 (s).

17. Attempted synthesis of bis[1, 2-bis (di(*p*-ethylphenyl))phosphinobenzene] dinitrogencarbonylmolybdenum(0)



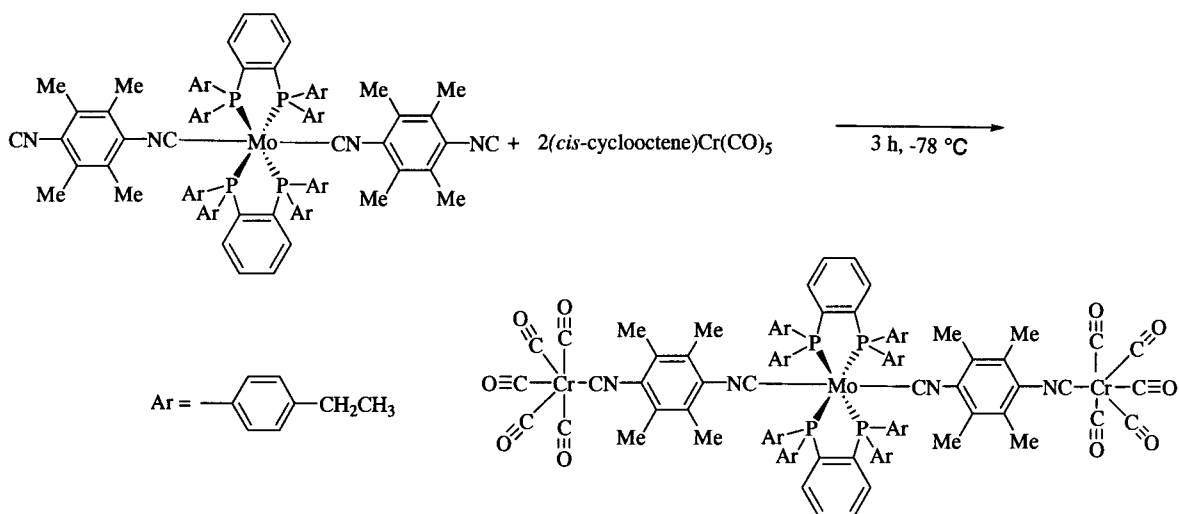
To a 250 mL 3-neck flask fitted with a nitrogen adaptor, stopper, reflux condenser, and stir bar is added 0.205 g (0.169 mmol) of bis(dinitrogen)bis[1,2-bis{di(*p*-ethylphenyl)}phosphinobenzene]molybdenum(0). The flask is evacuated and 10 mL of toluene and 0.30 mL (0.169 mmol) of benzyl propionate are added. The solution is heated to reflux for 3 h. The solution is allowed to cool to room temperature and 65 mL of hexane is added. The flask is placed in the refrigerator at 4 °C to crystallize. After two days, another 60 mL hexane is added in an attempt to crystallize the product. The mixture is placed in the freezer (-19 °C) to crystallize. No product was isolated.

18. Attempted synthesis of bis(diphenylphosphinoethane)carbonyl(DMF)tungsten(0)



To a 150 mL 3-neck flask fitted with a stir bar, reflux condenser, nitrogen adaptor and stopper are added 0.314 g (0.29 mmol) of bis(1,2-bis(diphenylphosphino)ethane)bis(dinitrogen)tungsten(0). The flask is evacuated and 0.2 mL (0.87 mmol) of DMF, along with 60 mL of benzene are added. The mixture is heated to reflux for 16 h. The solution is allowed to cool to room temperature and 100 mL hexane is added. The mixture is then filtered through a Schlenk filter to remove the impurities and the filtrate was placed in the freezer (-19 °C) to crystallize. A mixture of small red and white crystals is visible after a day in the freezer. The solution is then removed *via* syringe and the crystals are dried under a stream of nitrogen for 2 h. These crystals were found to be starting material by ¹H NMR.

19. μ -C,C'-[bis[bis(di(*p*-ethylphenyl)phosphino)benzene]bis(*p*-diisocyanotetramethylbenzene)molybdenum(0)]bis(pentacarbonylchromium(0))



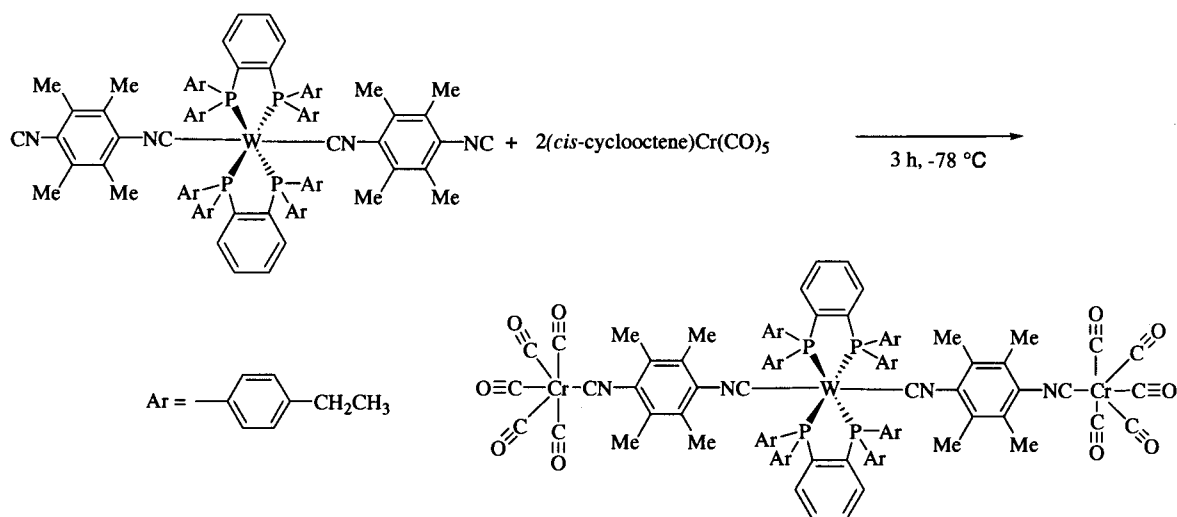
To a 100 mL Schlenk flask are added 0.301 g (0.190 mmol) of bis(2,3,5,6-tetramethyl-1,4-dicyanobenzene)bis[1,2-bis{di(*p*-ethylphenyl)}phosphinobenzene]molybdenum(0) and 0.131 g (0.433 mmol) of *cis*-cyclooctenechromiumpentacarbonyl (synthesized by Matthias Zeller). The flask is evacuated and 20 mL of toluene is added. The stirred reaction mixture is cooled with an ethanol/dry ice bath to $-30 \text{ }^\circ\text{C}$ for 3 h. The ethanol/dry ice bath is removed and the mixture is allowed to warm to room temperature over the course of 1 h. Hexane (60 mL) is added and the mixture is placed in the freezer ($-19 \text{ }^\circ\text{C}$) for three days to crystallize. The mother liquor is then removed *via* canula and the crystals washed with cold hexane ($2 \times 20 \text{ mL}$) and collected on filter paper to give 0.16 g (0.0814 mmol, 42.8%) of the desired product.

Spectroscopic Data

^1H NMR (399.905 MHz, C_6D_6): $\delta = 7.22$ (d, J ($^1\text{H}^1\text{H}$) = 7.6 Hz, 4 H, C_6H_5), 6.84 (d, J ($^1\text{H}^1\text{H}$) = 8 Hz, 4 H, C_6H_5), 2.36 (q, J ($^1\text{H}^1\text{H}$) = 6.4 Hz, 16 H, CH_2), 1.86 (s, 12 H, Ar-CH_3), 0.99 (t, J ($^1\text{H}^1\text{H}$) = 7.6 Hz, 24 H, CH_3), 0.86 (s, 12 H, Ar-CH_3). IR (CaF_2 plates, toluene solvent) $\nu(\text{C}\equiv\text{O})$ 2053.82 (w), $\nu(\text{C}\equiv\text{O})$ 1954.50 (s), $\nu(\text{N}\equiv\text{C})$ 1859.04 (s).

Anal. Calcd Cr, 5.06; C, 64.33; H, 5.10; N, 2.73. Found: Cr, 5.18; C, 63.73; H, 5.38; N, 2.82.

20. $\mu\text{-C,C'}$ -[bis[bis{di(*p*-ethylphenyl)phosphino}benzene]bis(*p*-diisocyanotetramethylbenzene)tungsten(0)]bis(pentacarbonylchromium(0))



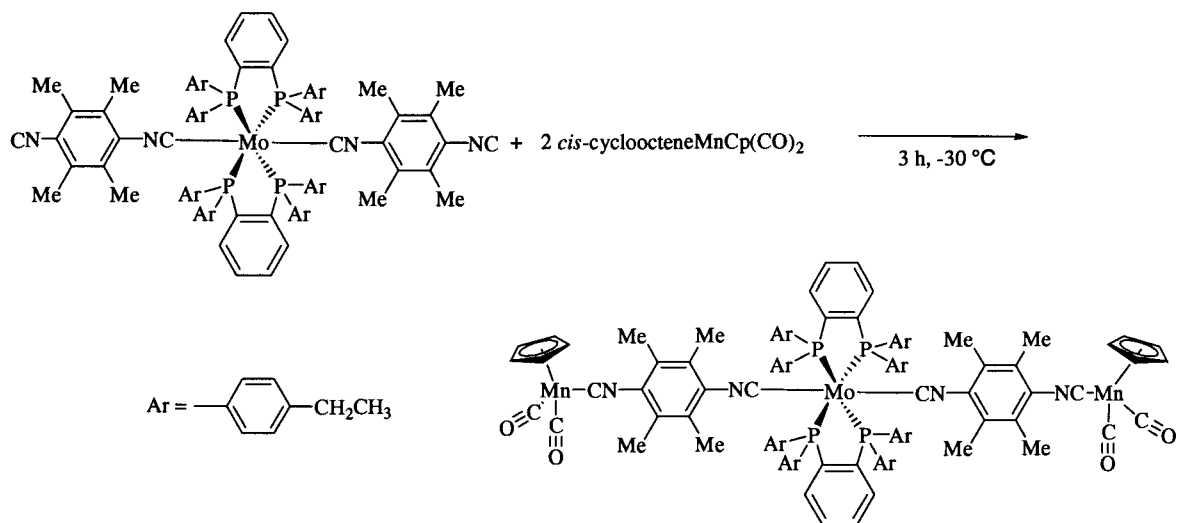
To a 100 mL Schlenk flask are added 0.100 g (0.058 mmol) of bis(2,3,5,6-tetramethyl-1,4-diisocyanobenzene)bis[1,2-bis{di(*p*-

ethylphenyl)}phosphinobenzene]tungsten(0) and 0.039 g (0.128 mmol) of *cis*-cyclooctenechromiumpentacarbonyl. The flask is evacuated and 25 mL of toluene is added. The stirred reaction mixture is cooled with an ethanol/dry ice bath (-78 °C) for 5 h. The ethanol/dry ice bath is removed and the mixture is allowed to warm to room temperature over the course of 1/2 h. The solvent is reduced in volume *in vacuo* to 15 mL, hexane (40 mL) is added, and the mixture is placed in the freezer (-19 °C) for three days to crystallize. The mother liquor is then removed *via* a canula and the crystals washed with cold hexane (2 × 20 mL) and collected on filter paper to give 0.06 g (0.0292 mmol, 48.8%) of the desired product.

Spectroscopic Data

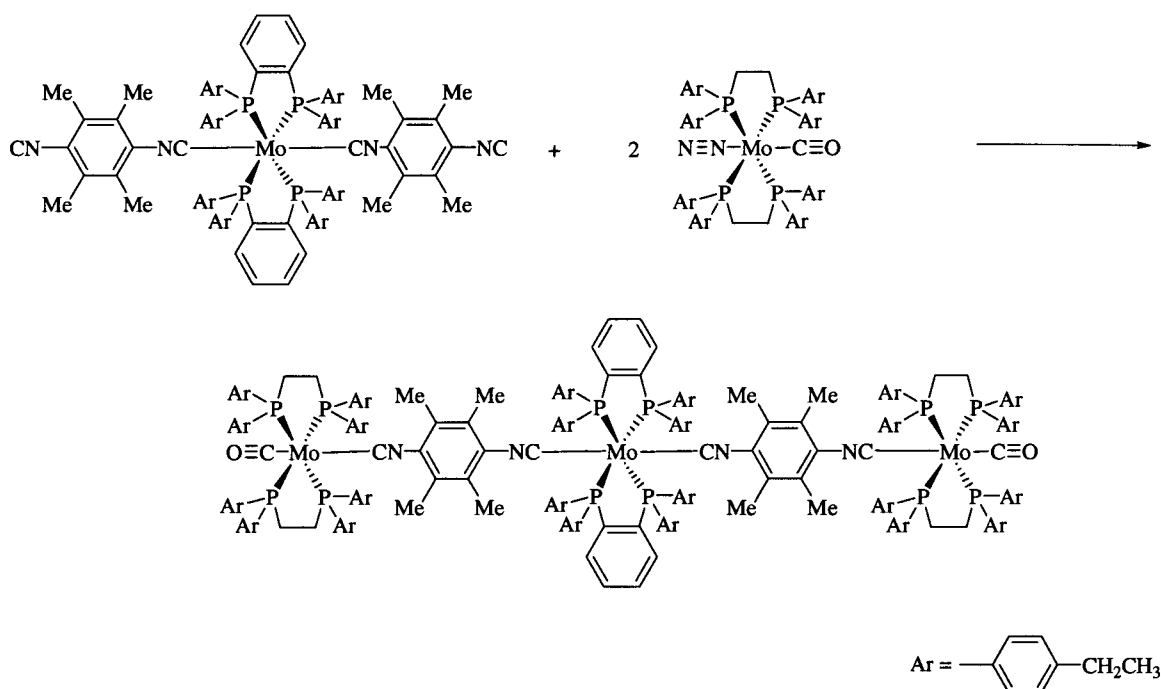
¹H NMR (399.905 MHz, C₆D₆): δ = 6.84 (d, *J* (¹H¹H) = 8 Hz, 4 H, C₆H₅), 2.36 (q, *J* (¹H¹H) = 6.4 and 7.6 Hz, 16 H, CH₂), 1.86 (s, 12 H, Ar-CH₃), 0.99 (t, *J* (¹H¹H) = 7.6 Hz, 24 H, CH₃), 0.84 (s, 12 H, Ar-CH₃). IR (CaF₂ plates, toluene solvent) ν(C=O) 2054.78 (w), ν(C≡O) 1953.54 (s), ν(N≡C) 1851.33 (s).

21. Attempted synthesis of μ-C,C'-[bis[bis{di(*p*-ethylphenyl)phosphino}benzene]bis(*p*-diisocyanotetramethylbenzene)molybdenum(0)] bis(η⁵-cyclopentadienyl dicarbonylmanganese(0))



To a 250 mL Schlenk flask are added 0.202 g (0.131 mmol) of bis(2,3,5,6-tetramethyl-1,4-dicyanobenzene)bis[1,2-bis{di(*p*-ethylphenyl)}phosphino benzene]molybdenum(0) and 0.078 g (0.270 mmol) of cis-cyclooctene- η^5 -cyclopentadienyldicarbonylmanganese(0) synthesized by Matthias Zeller). The flask is evacuated and 120 mL of toluene is added. The reaction mixture is stirred for 120 h. The solvent is reduced *in vacuo* to 20 mL and hexane (100 mL) is added and the mixture is placed in the freezer (-19 °C) to crystallize. After one week, the reaction vessel was placed in the -80 °C freezer. No product was isolated.

22. Attempted synthesis of μ -C,C'-[bis[bis(di(*p*-ethylphenyl))phosphino} benzene]bis(*p*-diisocyanotetramethylbenzene)molybdenum(0)]bis([bis(di(*p*-ethylbenzene)phosphino)ethane]carbonylmolybdenum(0))



To a 250 mL Schlenk flask that had been cooled in a dry ice/ethanol bath (-78 °C) are added 0.101 g (0.064 mmol) of bis(2,3,5,6-tetramethyl-1,4-dicyanobenzene)bis[1,2-bis{di(*p*-ethylphenyl)}phosphinobenzene]molybdenum(0) and 0.150 g (0.128 mmol) of bis(di(*p*-ethylphenyl)dinitrogencarbonylmolybdenum(0). The flask is evacuated and 120 mL of toluene is added. The reaction mixture is allowed to warm to room temperature over the course of 1 h and then stirred for an additional 5 h. The solution is filtered using a canula and filter paper and the solvent is reduced in volume to 20 mL. Hexane (100 mL) is added and the solution is placed in the freezer (-19 °C) to crystallize. After one week, a small amount of small black crystals can be seen in the flask. In an attempt to further crystallize the product, the reaction mixture is placed in the -80 °C freezer. No product was isolated.

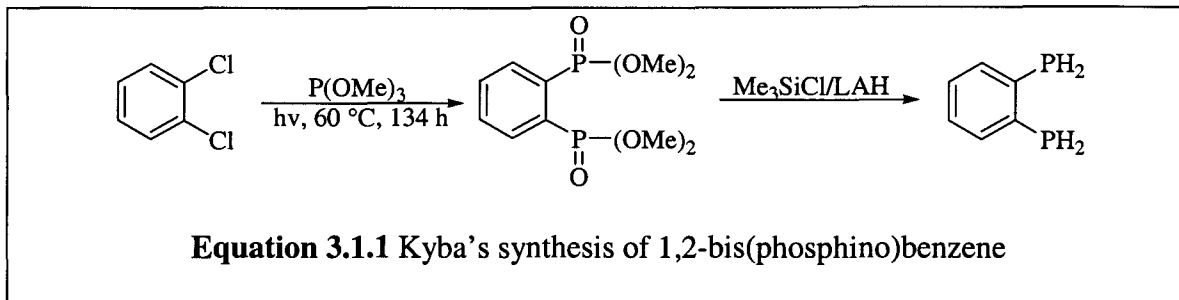
References

-
1. W. L. F. Armarego, D. D. Perrin. *Purification of Laboratory Chemicals*, 4th ed.; BH: Boston, 1996.
 2. E. P. Kyba, S-T. Jui, R. L. Harris. *Organometallics* **1983**, 2, 1877-1879
 3. Adapted from L. Dahenburg, A. Kaunert. *Eur. J. Inorg. Chem.* **1998**, 885-887
 4. E. P. Kyba, M. C. Kerby, S. P. Rines. *Organometallics* **1986**, 5, 1189-1194
 5. G. J. Kubas, C. J. Burns, J. Eckert, S. W. Johnson, A. C. Larson, P. J. Vergamini, C. J. Unkefer, G. R. K. Khalsa, S. A. Jackson, O. Eisenstein, *J. Am. Chem. Soc.* **1993**, 115, 569-581
 6. T. A. George, M. E. Noble, *Inorg. Chem.* **1978**, 17, 1678-1679

Chapter III –Results and Discussion

1. Phosphines

The derivatives of 1, 2-bis(phosphino)benzene were synthesized according to the previously published method by Kyba¹ shown below:



In the first step of this reaction, the two C-Cl bonds in 1,2-dichlorobenzene are photolytically cleaved in the presence of trimethylphosphite, resulting in the formation of 1,2-bis(dimethylphosphoryl)benzene. In the second step of **Equation 3.1.1**, 1,2-bis(dimethylphosphoryl)benzene is reduced to 1,2-bis(phosphino)benzene by a suspension of lithium aluminum hydride, LAH, and trimethylchlorosilane in diethyl ether.

The workup of 1,2-bis(phosphino)benzene uses both water (100 mL) and potassium hydroxide (1N, 250 mL). This must be done with extreme caution, as LAH reacts violently with water. After hydrolysis is complete, extraction can then be done with diethyl ether (approx. 1 L). This extraction is often mechanically difficult due to the amount of solid hydrolysis by-products. In order to deal with this, a piece of filter paper is folded into a cone and inserted into the 3-necked flask. The diethyl ether is then removed *via* syringe through the filter paper.

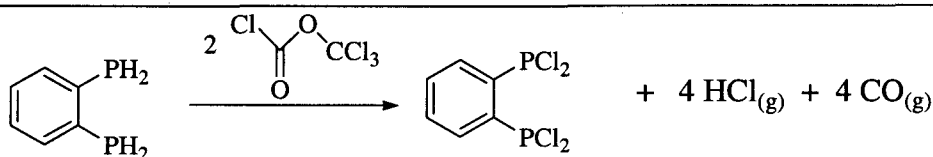
The first step of **Equation 3.1.1** produces about 20-50 g of the phosphoryl compound in a 14-38% yield after crystallization from acetone. The colorless crystals obtained are air stable. The ^{31}P NMR spectrum exhibits one peak at -4.63 ppm. The ^1H NMR spectrum shows multiplets with an AA'BB' coupling pattern at 7.90 and 7.41 ppm. A pseudo-doublet at 3.58 ppm is found due to the coupling of the methyl hydrogens with the phosphorus atoms.

In the second step of **Equation 3.1.1**, 1,2-bis(phosphino)benzene is produced in a 28-64% yield after distillation. The colorless to slightly yellow liquid has a boiling point (in oil pump vacuum) of 60 °C and is pyrophoric and extremely air sensitive. The ^{31}P NMR spectrum exhibits one peak at -147.69 ppm. The ^1H spectrum shows two AA'BB' multiplets at 7.25 and 6.90 ppm. Again, this can be attributed to the aromatic hydrogen atoms. A pseudo-doublet of doublets ($J(^1\text{H}^{31}\text{P}) = 25.2$ Hz) at 3.90 ppm is likely due to coupling between each of the phosphorous atoms and each hydrogen directly bonded to it.

The isolated yield for 1,2-bis(phosphino)benzene varied drastically from reaction to reaction and was low compared to the yield reported by Kyba (83%). The difference can be attributed to both the extraction process and the extreme sensitivity of the compound. In contrast to the findings here, Kyba reports using only 400 mL (2×200 mL) of diethyl ether. The phosphine is extremely air sensitive (as a neat compound, it is self-igniting in the presence of oxygen), thus great care must be taken to avoid oxygen during the synthesis. Failure to do so will result in loss of product due to oxidation. With the tedious and lengthy work-up procedure in mind, the diethyl ether must then be separated

from the solid by-products. This is done *via* syringe and may also contribute to the low isolated yield of this compound.

The chlorination reaction of 1,2-bis(phosphino)benzene is adapted from a method published by Dahlenburg *et al.*² as illustrated below:

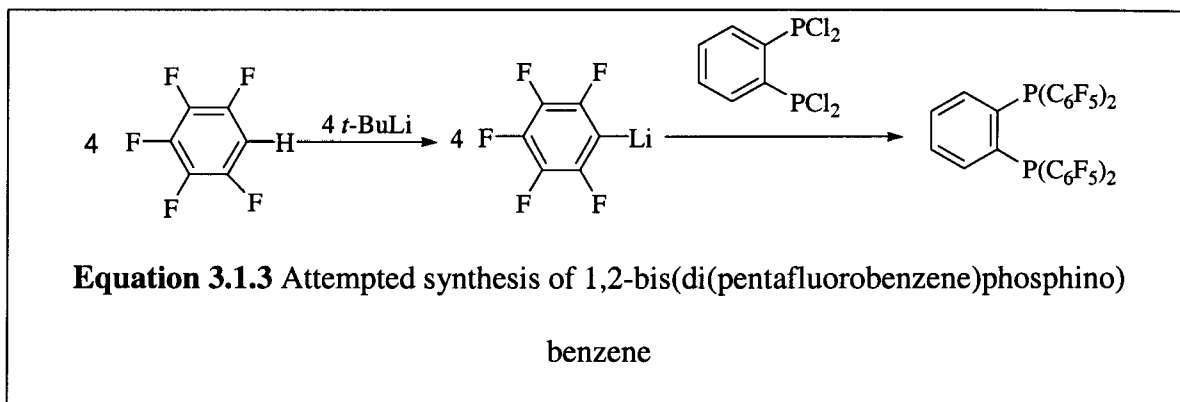


Equation 3.1.2 Synthesis of 1,2-bis(dichlorophosphino)benzene

Trichloromethyl chloroformate (diphosgene) is used as the chlorination agent and both carbon monoxide and hydrochloric acid gases are produced as by-products. The reaction proceeds smoothly over three hours. The chlorinated species is produced in a 36.8% yield and has a boiling point (in oil pump vacuum) of 85-90 °C. It is interesting to note that independent of the scale of the reaction, the yield is consistently about 37% each time. The side products are higher boiling than 1,2-bis(dichlorophosphino)benzene. Thus it can be surmised that condensation products (dimers, trimer) are formed by the reaction of the P-Cl groups with the unreacted P-H moieties.

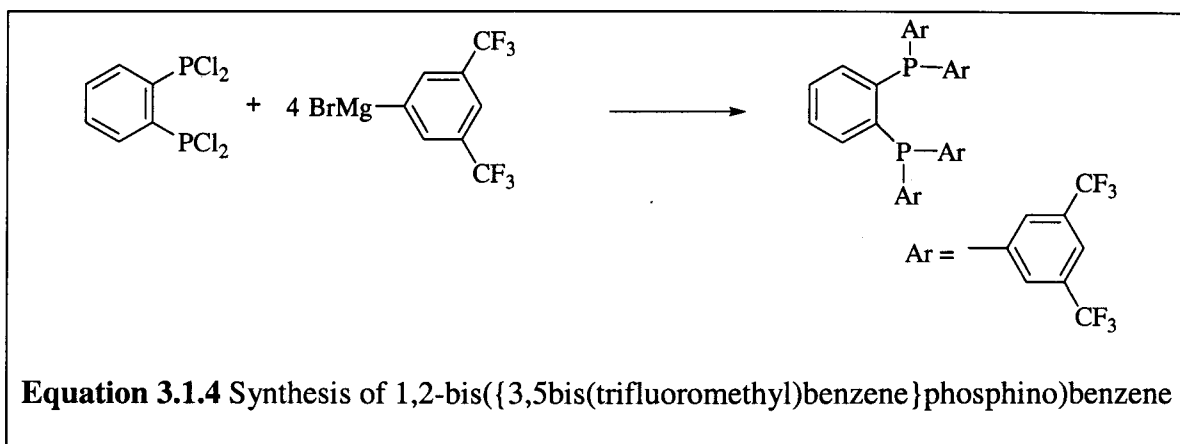
1,2-Bis(dichlorophosphino)benzene is the starting compound in the synthesis of a wide range of aryl phosphines. The excellent leaving ability of the chloride ion allows for a wide range of reactions to be performed: Grignard addition and nucleophilic attack are the most common. As mentioned in the introduction, aryl phosphines are preferred over alkyl phosphines because of the π -back-bonding contributions. Electron withdrawing substituents, such as fluorinated groups, will increase the degree of back-bonding present within the aryl phosphines.

The attempted synthesis of 1,2-bis(di(pentafluorobenzene)phosphino)benzene is shown below:



Pentafluorobenzene is deprotonated in THF using *t*-butyl lithium.³ The resulting nucleophile was then reacted with 1,2-bis(dichlorophosphino)benzene at -78 °C in an attempt to displace the chlorine atoms in a nucleophilic substitution reaction. After work-up, no product has yet been isolated from the reaction solution. A possible explanation for this is that since the fluorine atoms themselves are highly electronegative, thus they will evenly distribute the negative charge of the carbon atom where deprotonation occurred within the ring. This, in turn, will weaken the strength of the nucleophile to the point where it can no longer displace all of the chlorine atoms, resulting in a mixture of half reacted products or even no product at all.

In a second attempt to synthesis a fluorinated aromatic phosphine, 1,2-bis({3,5-bis(trifluoromethyl)benzene}phosphino)benzene was synthesized by the route shown below:



In the first step in this reaction, the Grignard reagent is synthesized. This is done by combining 3,5-bis(trifluoromethyl)bromobenzene and very clean magnesium turnings (99.9+% pure) in THF. It is important to use clean magnesium turnings as conventional magnesium will give poor yields for this step, which will then decrease the overall yield. The next step is a simple Grignard addition/substitution reaction. The resulting solution is hydrolyzed with a 10% solution of NH_4Cl to remove the excess Grignard reagent, and the phosphine is isolated by crystallization from a concentrated toluene solution.

The crystals of the target phosphine are clear and quartz-like in appearance. They are air stable and produced in an 18.5% yield. One molecule of toluene is present in the crystal lattice as shown in **Figure 3.1.1**. The ^1H NMR spectrum shows one singlet at 7.88 ppm. This is due to the *para*-hydrogen atoms between the $-\text{CF}_3$ groups as they will be the furthest downfield due to the electron withdrawing effect of the two $-\text{CF}_3$ groups. There is also a multiplet at 7.57 ppm. This is from the *ortho*-hydrogen atoms next to each one of the $-\text{CF}_3$ groups as they would be the next furthest downfield. The final multiplet at 7.11 ppm has to be due to the two AA'BB' type signals of the aromatic hydrogen atoms on the benzene backbone.

X-Ray structure analysis has determined that this phosphine crystallizes in the monoclinic space group $P2_1/n$. The unit cell dimensions are $a = 11.367(6)$ Å, $b = 16.374(8)$ Å, $c = 22.225(11)$ Å, α and $\gamma = 90^\circ$, and $\beta = 94.756(10)^\circ$. Some of the trifluoromethyl groups exhibit a pronounced rotational disorder, resulting in the residual electron density being modeled as if these CF_3 groups were actually CF_6 groups. A final R_1 value for all data of 0.0871 and a wR_2 for all data of 0.1818 was obtained. Due to the amount of disorder present and the amount of parameters that were used, the overall quality of the structure solution was poor, resulting in such high R values. The ORTEP plot is shown in **Figure 3.1.1**. The table of geometric parameters as well as refinement statistics can be found in Appendix I.

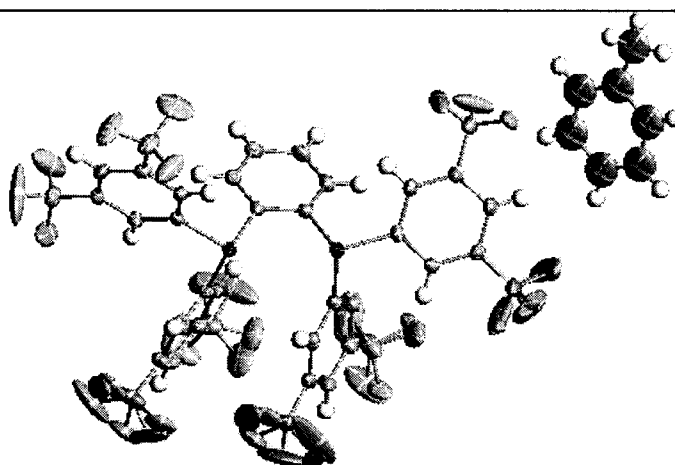
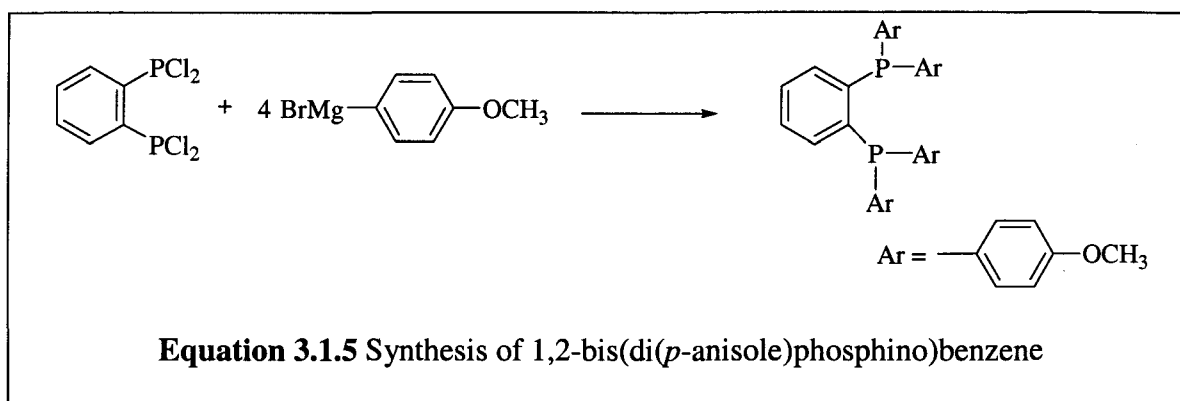


Figure 3.1.1 ORTEP representation of 1,2-bis(bis{3,5-bis(trifluoromethyl)benzene}phosphino)benzene. The thermal displacement ellipsoids are drawn at the 30% probability level and the disorder of the CF_3 groups as well as the one solvate of toluene are shown.

1,2-Bis(di(*p*-anisole)phosphino)benzene was synthesized by the method shown

below:



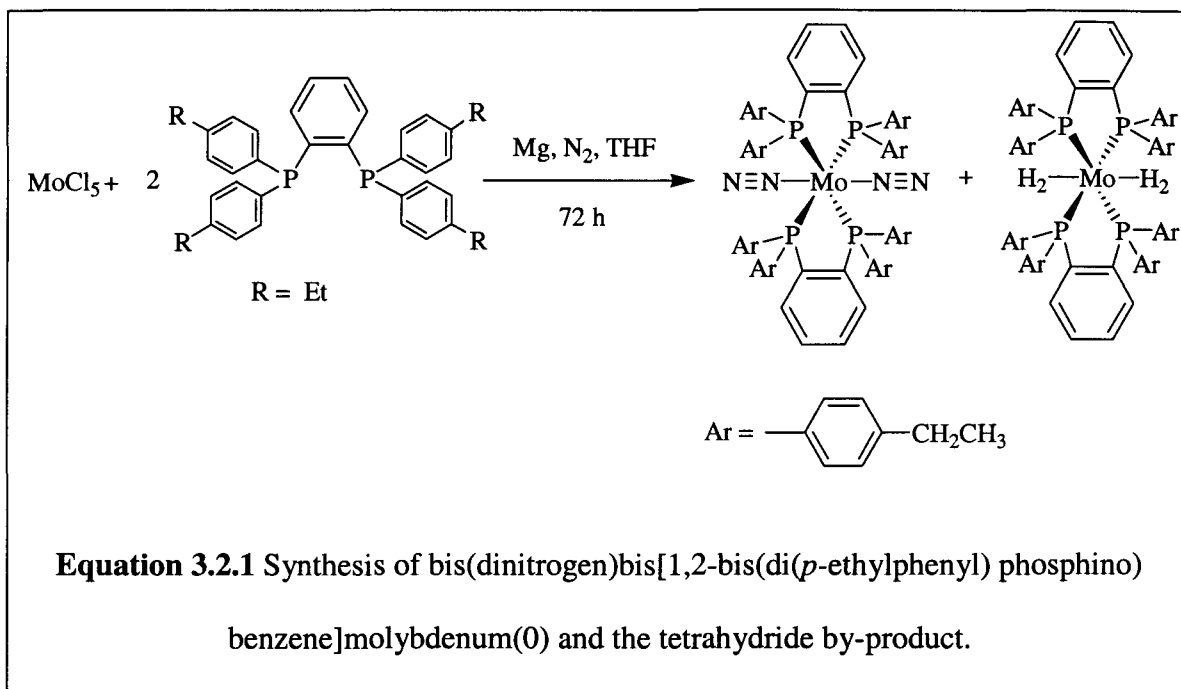
This phosphine is synthesized by a route similar to the one used in **Equation 3.1.4**. The white, air stable phosphine was isolated in a yield of 11.7%. The ^1H NMR spectrum exhibits two multiplets at 7.26 and 7.09 ppm. These are likely due to the AA'BB' interactions occurring between the hydrogen atoms of the benzene backbone. A doublet is found at 6.74 ppm ($J(^1\text{H}^1\text{H}) = 8$ Hz), due to the hydrogen atoms of the anisole rings. The singlet at 3.78 can be assigned to the methoxy hydrogen atoms.

Overall, the yields of the 1,2-bis(phosphino)benzene derivatives (i.e. those created *via* Grignard reagents) needs to be improved. A useful amount of phosphine would be approximately 20 g. At present, that would need twenty of these syntheses. Scaling these two reactions up may give higher yields. A method for synthesizing the pentafluorinated phosphine also has to be investigated.

2. Dinitrogen Complexes

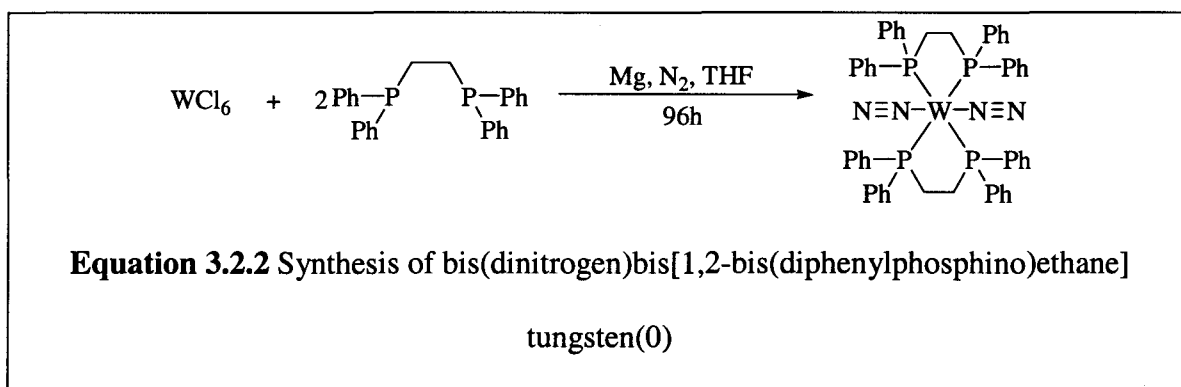
The molybdenum and tungsten dinitrogen complexes are synthesized by a route similar to that published by Hussain *et. al*⁴ in which the appropriate metal halide is reduced in the presence of N₂ and the desired phosphine by magnesium metal. In a similar method reported by George and Nobel⁵ sodium-mercury amalgam was used as the reducing agent. The magnesium route was chosen because of its one distinct advantage over the sodium-mercury amalgam route: mercury has a rather high toxicity level, while magnesium does not. The two routes show usually comparable yields, with the yield from the sodium-mercury amalgam method being slightly (~5%) higher. The magnesium method does, however, require the magnesium turnings to be absolutely clean (99.999+% pure) if one hopes to get reasonable yields. This is because the reduction reaction occurs on the surface of the magnesium metal; the cleaner the surface, the more efficient the reduction reaction will be.

George and Nobel also documented a competing reaction that is present in the method reported by Hussain *et. al*, namely, the formation of the tetrahydride complex (i.e. the two N₂ groups are replaced by four hydrogen atoms, M(R₂PC_xH_xPR₂)₂H₄). This is a competing reaction in which the source of hydrogen is thought⁵ to be from solvent decomposition and traces of humidity on the glass walls.



The formation of the tetrahydride complex was not witnessed in the synthesis of the three dinitrogen complexes described in this thesis. Slight modifications in procedure, such as removal of the solvent under high vacuum instead of *via* rotary evaporation and precipitation of the complex at 0 °C instead of at room temperature, may have helped to avoid the formation of the tetrahydride complex.

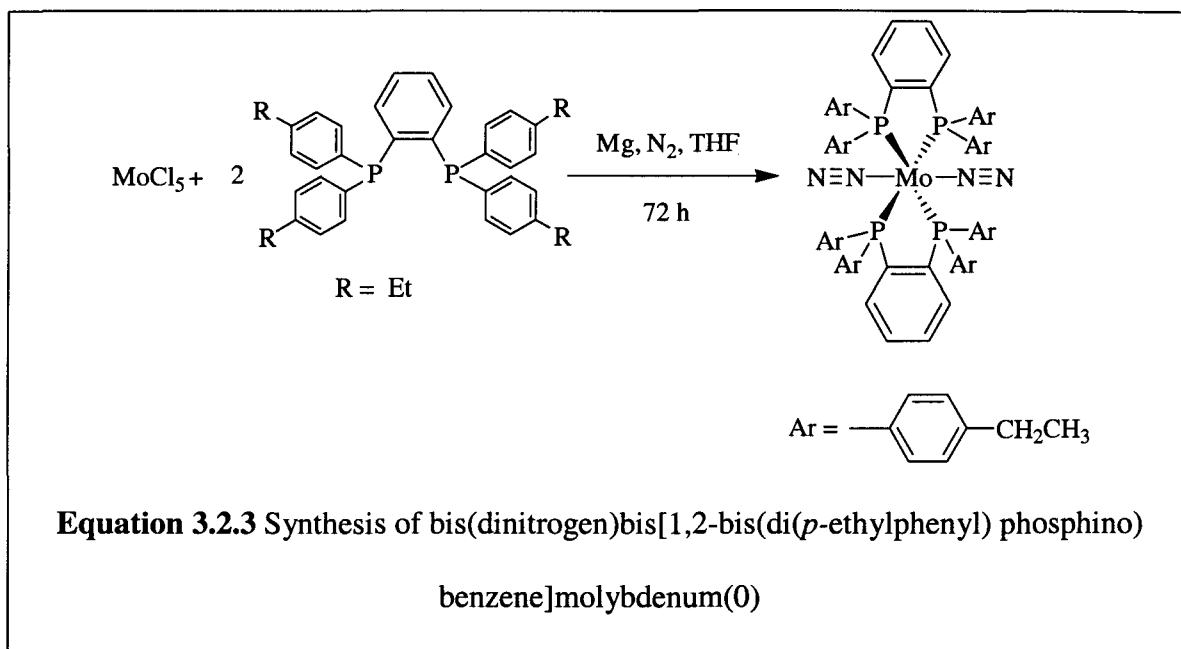
The first dinitrogen complex synthesized was bis(dinitrogen)bis((1,2-bisdiphenylphosphino)ethane)tungsten (0) by the route shown below:



The reaction proceeds as mentioned above. The workup is carried out by first filtering the reaction mixture to remove excess magnesium turnings then reducing the solvent *in vacuo* to half of its original volume, and, finally, precipitating the dinitrogen complex with methanol.

The orange dinitrogen complex is isolated in a 41.8% yield and is air stable as a solid for months, but is air sensitive in solution. The ^{31}P NMR spectrum shows a single peak at 45.71 ppm, indicating that all four phosphorus atoms are equivalent, thus the complex is the *trans* isomer. The ^1H NMR spectrum shows three singlets at 7.19, 7.02, and 7.01 ppm which integrate to a 1:2:3 ratio and can be attributed to the three types of aromatic hydrogen atoms present. The pseudo-triplet at 2.26 ppm ($J(^1\text{H}^{31}\text{P}) = 8$ Hz) are due to the methylene hydrogens forming the bridge between the phosphorus atoms. The two characteristic IR $\text{N}\equiv\text{N}$ stretching frequencies are at 1949 (strong) and 2009 (weak) cm^{-1} . In the *trans* isomer, the asymmetric stretching mode is expected to be the more intense of the two, as it has the greatest effect on the dipole moment.

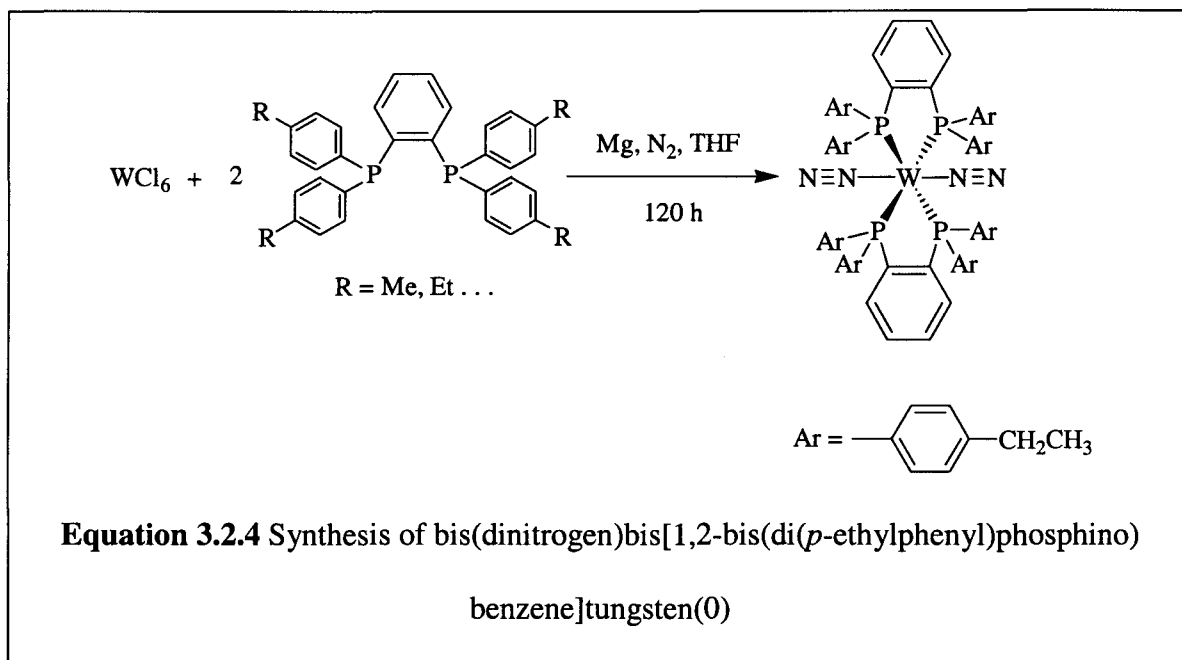
The second dinitrogen complex synthesized, bis(dinitrogen)bis[1,2-bis(di(*p*-ethylphenyl)phosphino)benzene]molybdenum(0), was synthesized according to the route shown:



The reaction and work-up is done in the same manner as the procedure outlined for bis(dinitrogen)bis(1,2-bis(diphenylphosphino)ethane)tungsten(0). The orange to red dinitrogen complex is isolated in a 66.8% yield. The ^{31}P NMR spectrum has a singlet at 70.1 ppm, indicating the presence of the *trans* isomer. The ^1H NMR spectrum shows two pseudo-doublets, which have integration ratios of 1:2, at 7.21 ppm ($J(^1\text{H}^1\text{H}) = 7.8$ Hz) and 6.94 ppm ($J(^1\text{H}^1\text{H}) = 7.8$ Hz) representing the aromatic hydrogen atoms of the benzene backbone and the *p*-ethylphenyl respectively. Two other aromatic proton signals are not observed, likely due to overlap with one of the above signals or overlap with the solvent signal. The quartet at 2.43 ppm ($J(^1\text{H}^1\text{H}) = 8$ Hz) can be attributed to the methylene protons of the ethyl groups. The triplet at 1.07 ppm ($J(^1\text{H}^1\text{H}) = 7.6$ Hz) is due to the methyl protons of the ethyl groups. The IR spectrum shows the two characteristic stretching frequencies of the dinitrogen ligand at 1981 and 2055 cm^{-1} . Again, the stronger vibrational mode at 1981 cm^{-1} can be attributed to the asymmetric stretching mode.

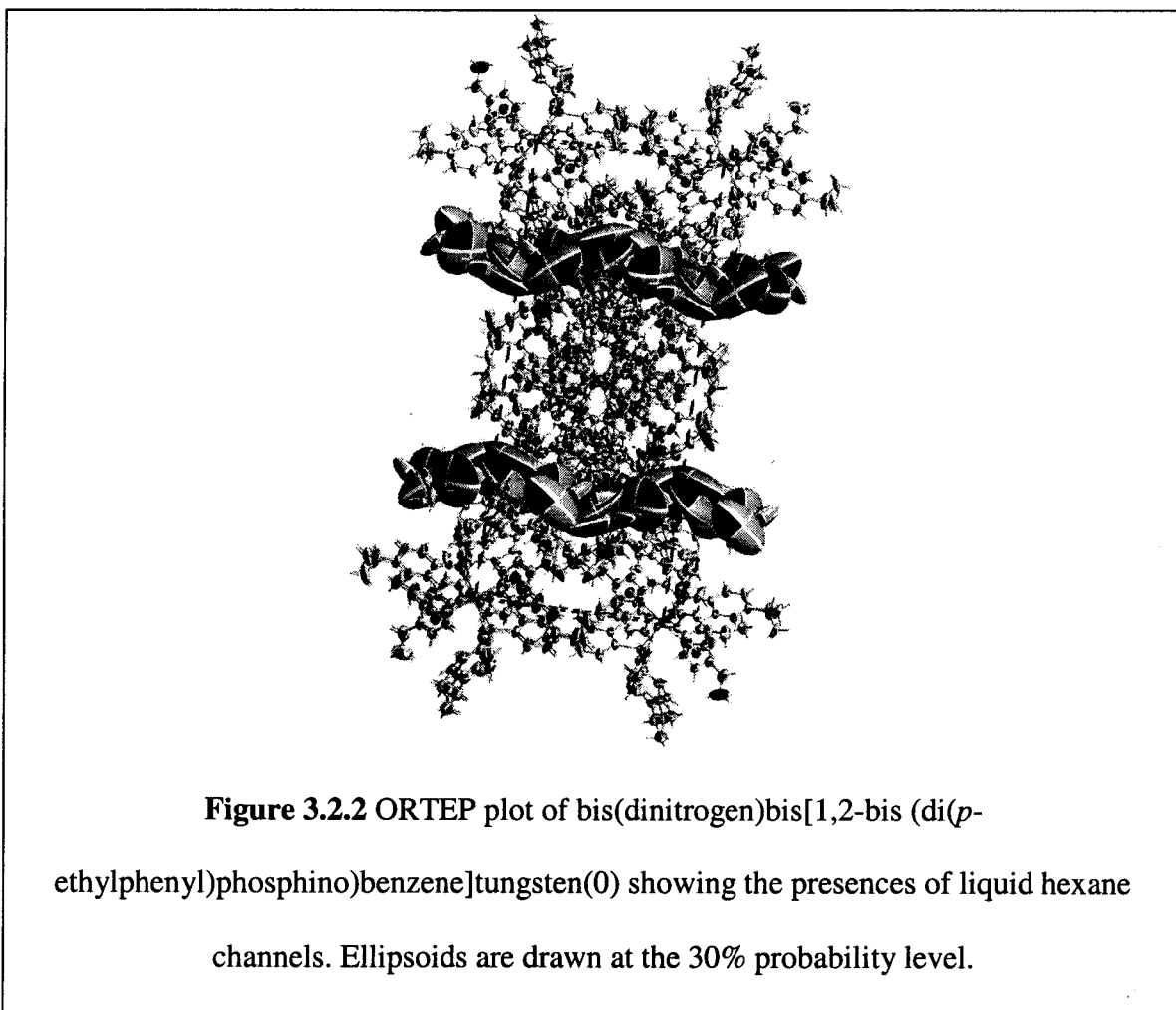
The final dinitrogen complex synthesized, bis(dinitrogen)bis[1,2-bis(di(*p*-ethylphenyl)phosphino)benzene]tungsten(0), is the tungsten derivative of the previously mentioned molybdenum complex. The reaction conditions and the work-up are the same.

The synthetic route is shown below:



The red fiber-like product is obtained in a 54% yield. It too is air stable as a solid but air-sensitive in solution. The ^1H NMR spectrum shows a doublet at 6.94 ppm ($J = 8$ Hz). This can be assigned to the aromatic hydrogen atoms. Three aromatic proton signals are missing. This again can be attributed to signal overlap. The quartet at 2.43 ppm ($J = 8$ Hz) is due to the methylene protons of the ethyl groups. The triplet at 1.07 ppm ($J = 7.6$ Hz) can be attributed to the methyl protons of the ethyl groups. The IR spectrum again exhibits the two characteristic dinitrogen stretching frequencies at 1953 and 2024 cm^{-1} . X-Ray diffraction shows that this complex is the *trans* isomer, thus the strong band at 1953 cm^{-1} is the asymmetric stretching mode.

X-Ray structure analysis was used to confirm the structure of the ethylphenyldinitrogen complex of tungsten. This complex crystallizes in the tetragonal space group $I4_1/a$. In **Figure 3.3.2**, it can be seen that there are channels present within the unit cell that contains highly disordered (i.e. pseudo liquid) hexane. The unit cell parameters are $a = 32.331(16) \text{ \AA}$, $b = 32.331 \text{ \AA}$, $c = 13.251(7) \text{ \AA}$, $\alpha = 90^\circ$, $\beta = 90^\circ$ and $\gamma = 90^\circ$. A final value of 0.0990 for R_1 and 0.2085 for wR_2 was obtained for all data. The unexpectedly high R values are the result of the disordered hexane present within the channels. The ORTEP plot showing the *trans* configuration of this complex is shown in **Figure 3.3.3**.



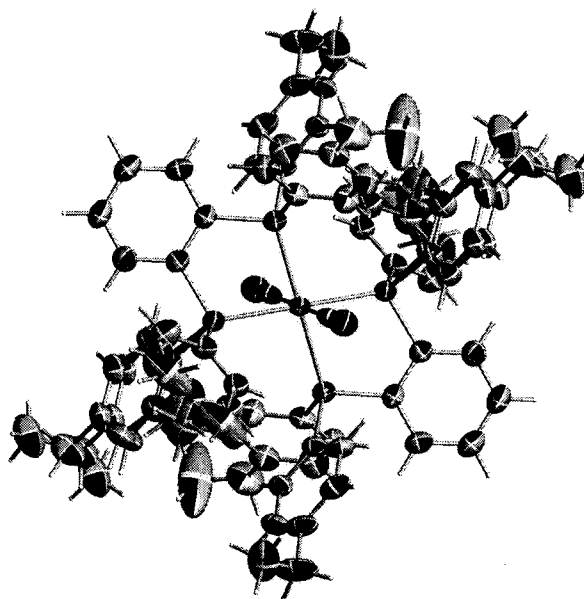


Figure 3.2.3 ORTEP plot of bis(dinitrogen)bis[1,2-bis (di(*p*-ethylphenyl)phosphino)benzene]tungsten(0). The hexane channels are omitted for clarity.

Ellipsoids are drawn at the 30% probability level.

Overall, the synthetic routes for the dinitrogen complexes all work according to the literature methods. The bis(dinitrogen)bis(dppe)tungsten(0) complex is only sparingly soluble in the solvents employed (THF, diethyl ether, toluene, and dichloromethane) because of the unsubstituted phenyl rings of the phosphine. This made full characterization of this complex difficult and boded poorly for the solubility of the eventual nanostar products. For this reason, the unsubstituted dppe ligand complex was abandoned as a starting material for future reactions. Bis(dinitrogen)bis[1,2-bis(di(*p*-ethylphenyl)phosphino)benzene]molybdenum(0) and its tungsten derivative did not exhibit the insolubility shown by bis(dinitrogen)bis(dppe)tungsten(0). Thus, the presence

of the alkyl substituents on the phenyl rings of the phosphine greatly enhances the solubility of these complexes. They are soluble in the solvents mentioned above and also standard NMR solvents.

A few important observations can be made concerning the nature of the dinitrogen complexes. In the ^{31}P NMR, the chemical shift of the tungsten complexes are consistently shifted to higher field than that of the molybdenum complexes which agrees with the expected trends,⁶ although the origin of this difference in shift is not fully understood. This difference may likely be due to the lanthanide contraction and, thus, the paramagnetic screening term associated with it.

The next important observation about the dinitrogen complexes is that regardless of what metal is used (Mo or W), the resulting complex has the *trans* configuration. This is important because, when assembling a nanorod, *trans* symmetry is desired so that conjugation between the metal centers will be maximized. A *cis* conformation in nanorods will likely result in reduced conjugation between the metal centers because of the nature of the two metal-isonitrile overlaps.

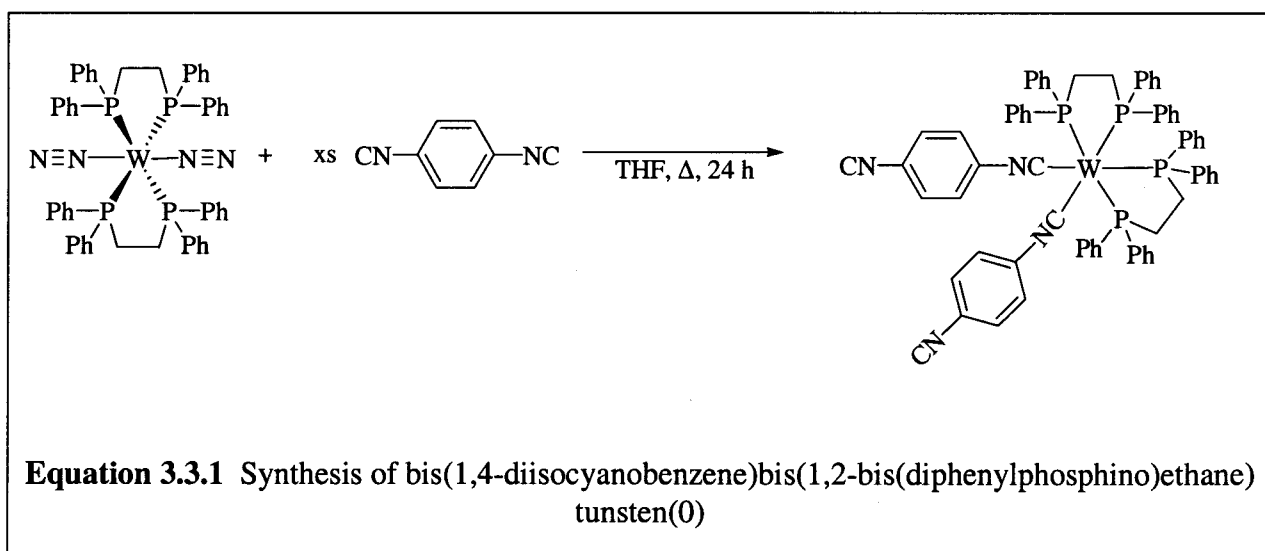
The final observation regarding the dinitrogen complexes is that the complexes are all orange to red. They are not very intensely colored in solution. This has to do with the type of electronic transitions that are present within the complex. The dinitrogen complexes are d^6 complexes with the metal in the zero oxidation state. A charge transfer transition would not occur since there is no strong acceptor molecule. Thus, the metal can act as either a donor or acceptor, the phosphine is a spectator ligand that does nothing more than shield the metal against oxidation, and the dinitrogen ligand is a rather labile ligand that has very little to no π - acceptor ability. A d-d transition is spin allowed since

promoting one of the paired electrons to the e orbital does not create a condition where two electrons have a parallel spin. However, this type of transition is Laporte forbidden since the dinitrogen complex has a center of inversion. Such d-d transitions tend not to be intensely colored, especially those that are not allowed. Even though this d-d transition is not allowed, molecular vibrations resulting in deviation from the perfect octahedral symmetry allows these transitions to be seen, albeit at low intensities. This accounts for the orange to red color of the dinitrogen complexes.

3. Bis(diisonitrile) complexes

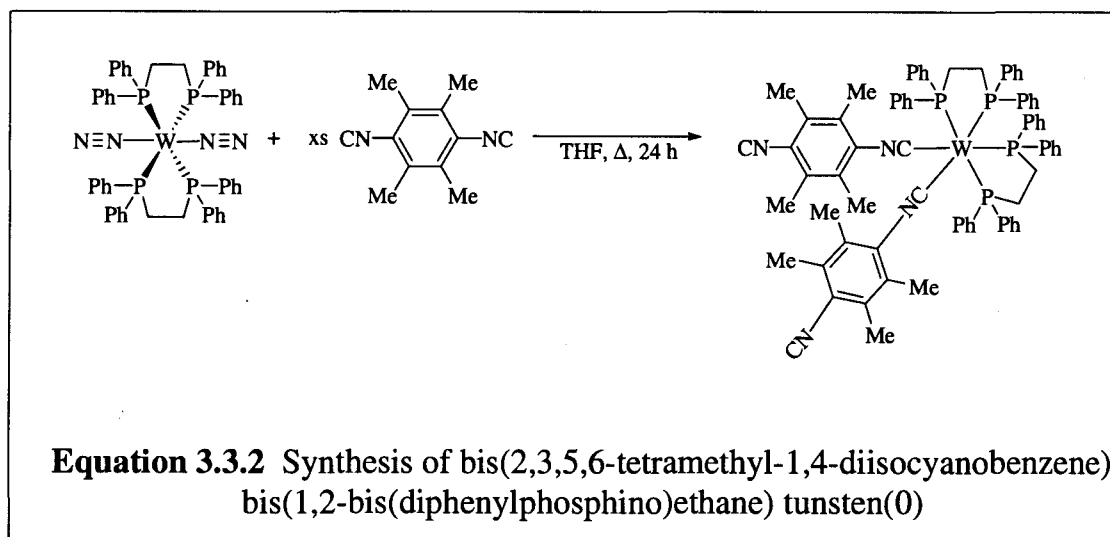
In general, the bis(diisonitrile) complexes were synthesized using a ten-fold molar excess of isonitrile compared to the dinitrogen complex.

The first bis(diisonitrile) complex synthesized was bis(1,4-diisocyanobenzene)bis(1,2-bis(diphenylphosphino)ethane)tungsten(0) by the route shown below:



1,4-Diisocyanobenzene⁷ is combined with bis(dinitrogen)bis(1,2-bis(diphenylphosphino)ethane)tungsten(0) in THF. This solution is then heated to reflux for 24 h. With molybedum, heating of the reaction mixture is usually not required. However, because of the lower reactivity of the tungsten complexes, heating is required to activate the complex. The solvent is reduced in volume and hexane is added to precipitate the bis(diisonitrile) complex as a dark red, almost black powder in a 32% yield. Due to the insolubility of this material (because of the un-substituted dppe ligand as well as the un-substituted 1,4-diisonitrile ligand), no further reactions were done with this material. Full characterization was also difficult, as this complex was not soluble in standard NMR solvents.

The next bis(isonitrile) complex synthesized was bis(2,3,5,6-tetramethyl-1,4-diisocyanobenzene)bis(1,2-bis(diphenylphosphino)ethane)tungsten(0) according to the procedure published by Bennett *et al.*⁸ as illustrated below:



2,3,5,6-Tetramethyl-1,4-diisocyanobenzene was chosen as the bridging isonitrile in an effort to increase the solubility of the eventual product. This reaction was carried

out using the same procedure as that described in **Equation 3.3.1**. The target tungsten bis(isonitrile) complex was produced as a black crystalline solid. Like the complex in **Equation 3.3.1**, this bis(isonitrile) complex also proved to be insoluble in standard NMR solvents and proved to be only sparingly soluble in THF. X-Ray structure analysis was used to confirm the presence of the *cis* isomer in the solid state. Bennett *et al.* report this complex to have *trans* symmetry, based on the spectroscopic data gathered.⁸ The ³¹P NMR spectrum we collected shows only one peak; IR spectroscopy revealed the C≡N stretching frequency to be *cis*. Bennett *et al.* showed that *trans* complexes have stretching frequencies in the range of 1940 to 1970 cm⁻¹, while the *cis* isomers exhibit these stretching frequencies in the range of 1740 to 1830 cm⁻¹. By comparing the data gathered on this complex and comparing it to data gathered on complexes with known geometries, it was deduced by Bennett *et al.* that this complex has *trans* symmetry. The origin of this difference is not clear and perhaps reflects preferential crystallization of the *cis* species. This complex crystallizes in the triclinic space group P-1. Two THF molecules and one hexane molecules (per unit cell) have been incorporated into the crystal lattice. The unit cell parameters are $a = 12.490(25) \text{ \AA}$, $b = 14.298(28) \text{ \AA}$, $c = 21.133(42) \text{ \AA}$, $\alpha = 71.067(34)^\circ$, $\beta = 81.897(36)^\circ$ and $\gamma = 82.440(36)^\circ$. The ORTEP plot is shown in **Figure 3.3.1**. The geometric parameters and cell data can be found in Appendix II.

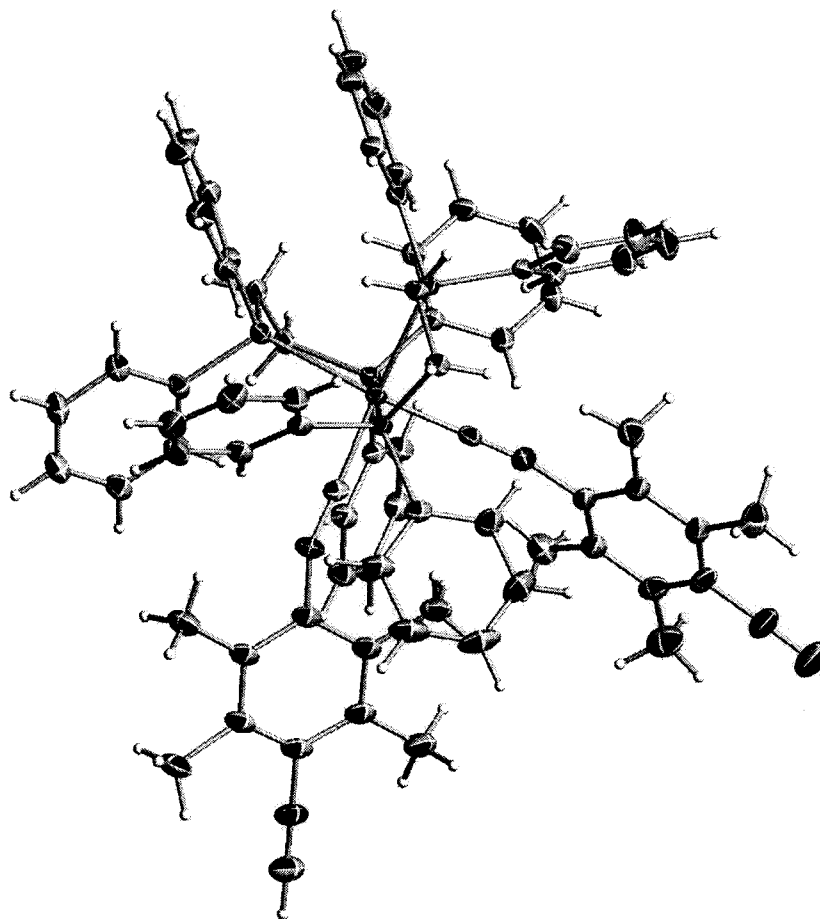
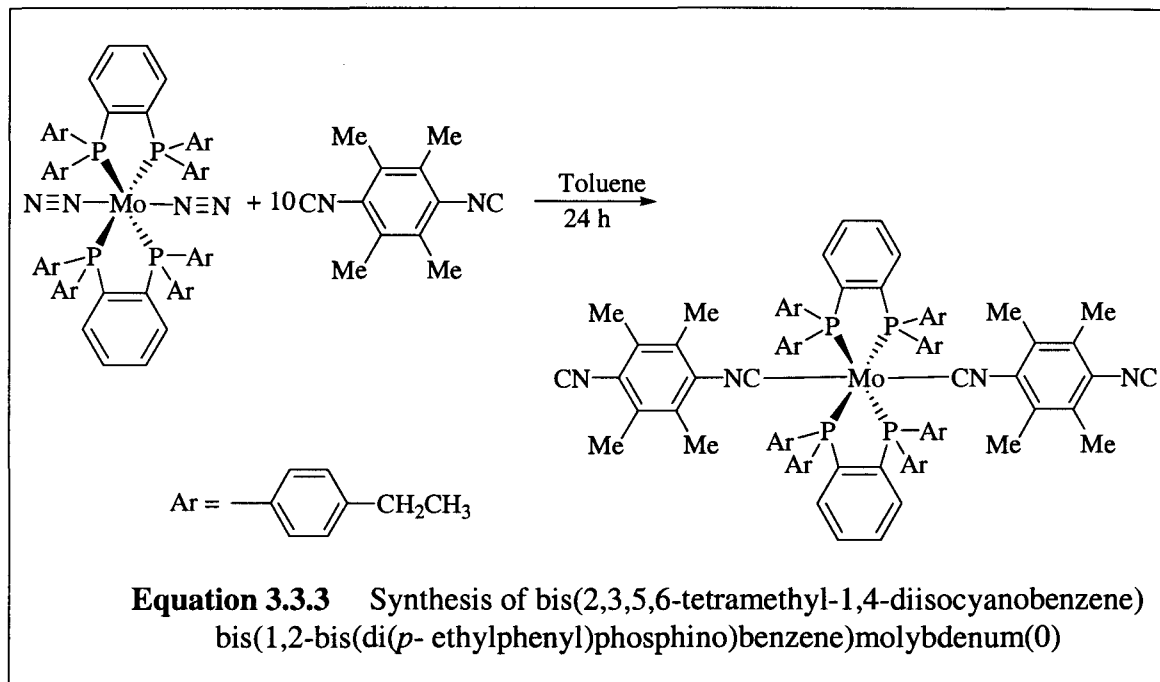


Figure 3.3.1 ORTEP plot of bis(2,3,5,6-tetramethyl-1,4-diisocyanobenzene))bis[1,2-bis(diphenylphosphino)ethane]tungsten(0). Thermal displacement ellipsoids are shown at the 30% probability level. Solvent molecules omitted for clarity.

Bis(2,3,5,6-tetramethyl-1,4-diisocyanobenzene))bis[1,2-bis(di(*p*-ethylphenyl)phosphino)benzene]molybdenum(0) was synthesized by the route shown below:

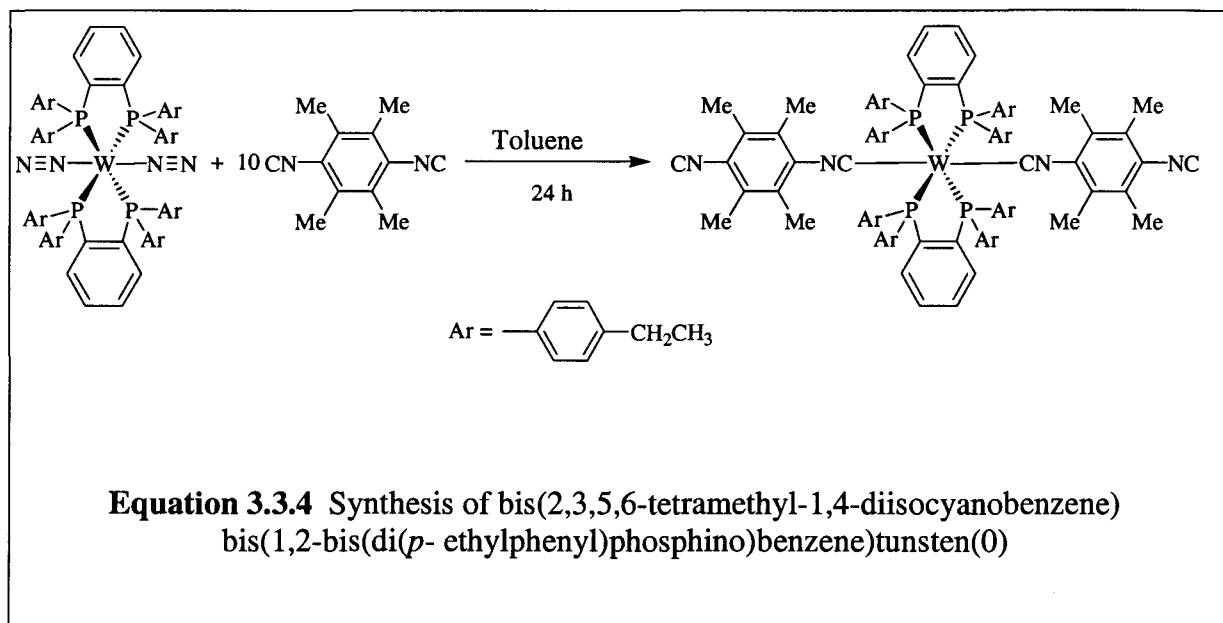


In this reaction, a solution of the molybdenum dinitrogen complex was added drop-wise to a solution of 2,3,5,6-tetramethyl-1,4-disocyanobenzene in toluene. In order to avoid side reactions, the reaction was carried out at 0 °C. The completeness of the reaction was monitored by IR spectroscopy. Thus, after 24 h, the N≡N stretching frequencies at 1981 and 2055 cm⁻¹ were replaced by the C≡N stretching frequencies at 1867 and 2114 cm⁻¹.

In the solid state, the bis(diisonitrile) complex is isolated as very dark green to blue microcrystals in a 89.4% yield. The ³¹P NMR spectrum has a single peak at 71.19 ppm, indicating that all four phosphorus atoms are in the same environment and, thus, the complex has a *trans* configuration. This is further confirmed by the ¹H NMR spectrum, in which there is only one set of each type of signals. The broad signals at 7.88 ppm as well as doublets which have integration ratio of 1:1 at 7.21 (*J*(¹H¹H) = 7.4 Hz) and 6.81 (*J*(¹H¹H) = 7.4 Hz) ppm can be assigned to the aromatic hydrogens. A quartet at 2.34

($J(^1\text{H}^1\text{H}) = 7.6 \text{ Hz}$) is due to the methylene protons of the ethyl groups. Singlets at 2.00 and 0.83 ppm are from the two types of methyl groups of the isocyanide: the 2,6 methyl groups and the 3,5 methyl groups, respectively. The triplet at 1.0 ($J(^1\text{H}^1\text{H}) = 7.6 \text{ Hz}$) ppm can be attributed to the methyl protons of the ethyl groups.

Bis(2,3,5,6-tetramethyl-1,4-diisocyanobenzene)bis[1,2-bis(di(*p*-ethylphenyl)phosphino)benzene]tungsten(0) was synthesized *via* the route below:



Although this is the tungsten congener of the product in **Equation 3.3.3** the reaction conditions are slightly different. In particular, the slow reaction kinetics associated with tungsten removes the need to do this reaction at 0 °C. In fact, in order to force this reaction to completion, it was necessary to reflux the reaction mixture. After 18 h of heating, the solution was then allowed to cool to room temperature and it was worked up using the same method as its molybdenum congener. The crude bis(diisocyanide) complex was isolated in a 39.5% yield.

The bis(diisonitrile) tungsten complex is a $5d^6$ complex, whereas the molybdenum derivative is a $4d^6$ complex. The $5d$ complexes have a higher activation barrier for substitution due to the Lanthanide contraction.

Both tungsten bis(diisonitrile) complexes synthesized with the dppe phosphine, bis(1,4-diisocyanobenzene)bis(1,2-bis(diphenylphosphino)ethane)tungsten(0) and bis(2,3,5,6-tetramethyl-1,4-diisocyanobenzene)bis(1,2-bis(diphenylphosphino)ethane)tungsten(0), are only sparingly soluble in common organic solvents (THF, diethyl ether, toluene) and were even less soluble in standard NMR solvents. Bis(1,4-diisocyanobenzene)bis(1,2-bis(diphenylphosphino)ethane)tungsten(0) has both unsubstituted phenyl rings on the phosphines and unsubstituted isonitrile arenes. The methyl substituents of the bis(diisonitrile) ligands have only a minor effect on the solubility of bis(2,3,5,6-tetramethyl-1,4-diisocyanobenzene)bis(1,2-bis(diphenylphosphino)ethane)tungsten(0), as the tetramethyl isonitrile complex shows only a slight increase in solubility over the perhydro isonitrile complex. Thus, five grams of the tetramethyl complex will dissolve in approximately 1.5 L THF as opposed to five grams of the perhydro complex dissolving in 2.5 L of THF. It can be concluded that the solubility of the bis(diisonitrile) complexes, like that of the corresponding dinitrogen complexes, is influenced more by the solubility properties of the phosphines and that the solubility of the bis(diisonitrile) serves only to augment the solubility dictated by the phosphine ligands. Bis(2,3,5,6-tetramethyl-1,4-diisocyanobenzene)bis[1,2-bis(di(*p*-ethylbenzene)phosphino)benzene]molybdenum(0) and bis(2,3,5,6-tetramethyl-1,4-diisocyanobenzene)bis[1,2-bis(di(*p*-ethylbenzene)phosphino)benzene]tungsten(0) do not exhibit these solubility problem because of the ethyl substituents that are present on the phenyl rings of

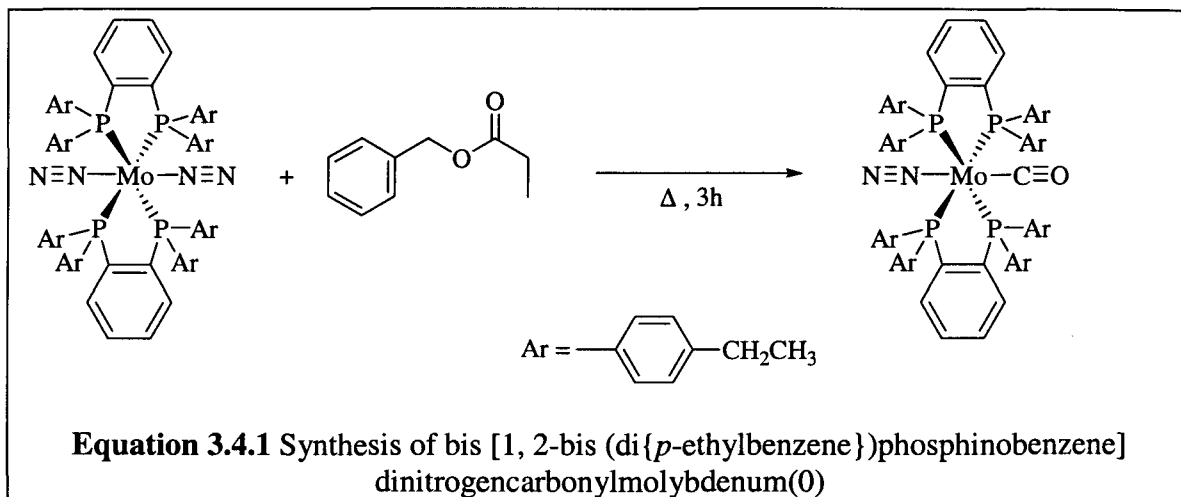
the phosphines. Indeed, it appears that the ethyl phosphines increase the solubility of the complex by a factor of 200.

The bis(diisonitrile) complexes all have one thing in common: in solution, they are all very intensely colored, usually dark purple to almost black. This is a major difference from the color found in the dinitrogen complexes and has to do with the types of electronic transitions that are present. As mentioned previously, for the dinitrogen complexes, the only transitions present are Laporte forbidden d-d transitions. The bis(diisonitrile) complexes also possess this transition, but more importantly, the bis(diisonitrile) complexes now have a metal to ligand (MLCT) charge transfer. In order to have these types of charge transfers, there must be a donor species (the metal “d” orbitals in this case) and an acceptor species [the bis(diisonitrile)]. Since the acceptor species has a delocalized π system of electrons, this will allow a donated electron to be dispersed throughout the bis(diisonitrile) itself and will enhance the charge transfer.

4. Capping Reactions

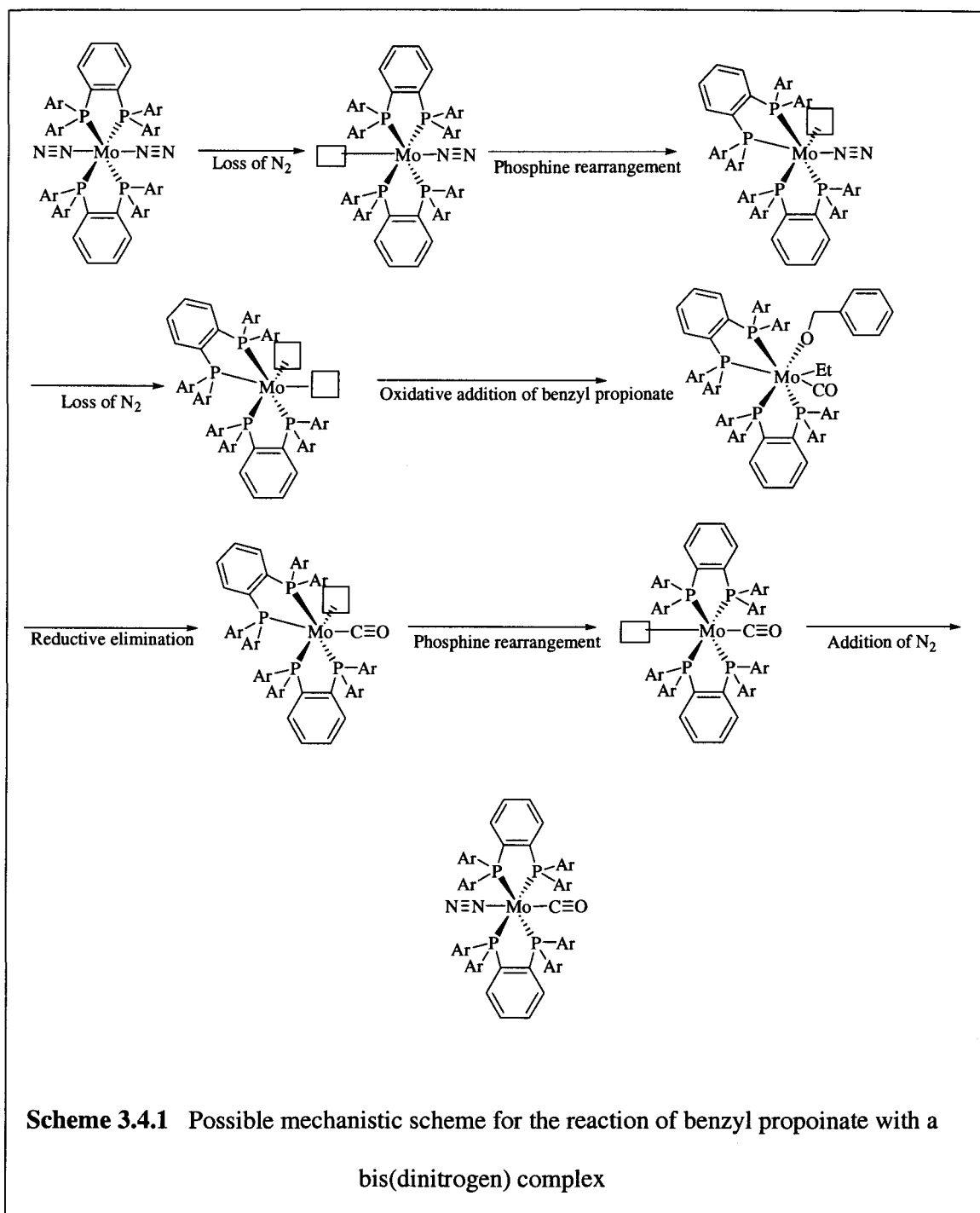
All wires, whether macroscopic or molecular, must have a distinct starting as well as ending point; the “caps” described in this section will provide these. In a capping reaction, a bis(diisonitrile) complex is combined with a monofunctional, usually organometallic, fragment. This fragment will very often contain one or more carbonyl groups.

The attempted synthesis of bis [1,2-bis(di{*p*-ethylphenyl})phosphinobenzene] dinitrogencarbonylmolybdenum(0) as a potential capping group is shown below:

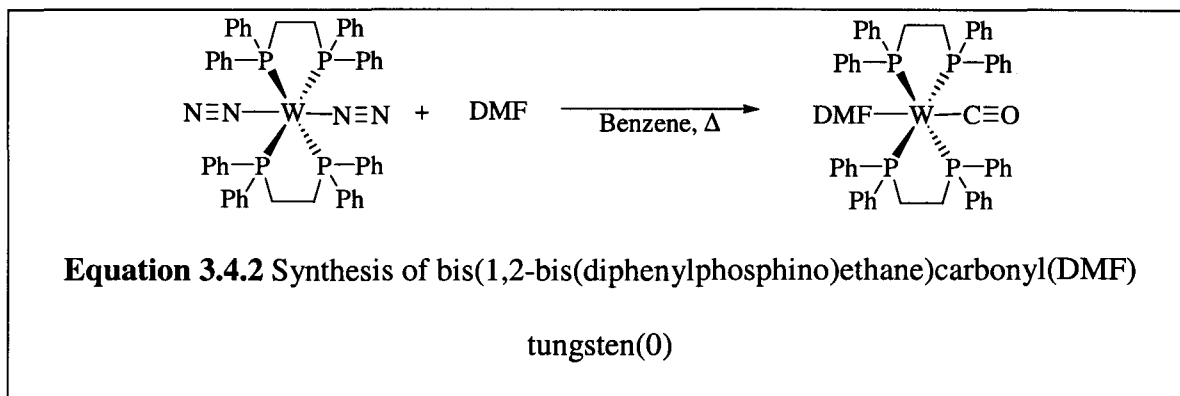


This is an oxidative addition/reductive elimination reaction in which the metal is inserted into either the carbon-carbon bond or the oxygen-carbon bond. The mechanism of this reaction has not been established. However, it is known that this reaction occurs only when there are two empty and adjacent coordination sites present at the metal center. These two adjacent empty coordination sites may be obtained through a few steps as illustrated in **Scheme 3.4.1**. First, a dinitrogen ligand is lost. One phosphorus atom of a phosphine ligand migrates (perhaps *via* an intermediate dissociative step) and fills the site vacated by the dinitrogen ligand. The overall effect of this is that the empty coordination site is shifted next to the remaining dinitrogen ligand. The remaining dinitrogen ligand dissociates and the metal is inserted into one of the bonds of the benzyl propionate molecule. This is followed by a second oxidative addition- bond cleavage. The benzoate and alkyl groups are then reductively eliminated, leaving only the carbonyl attached to the metal. Migration of one of the phosphines and reattachment of a dinitrogen ligand *para* to the new carbonyl completes the reaction sequence. Multiple attempts of this reaction resulted in no product being isolated despite its success with dppe for both molybdenum and tungsten. A possible reason for this is that due to the

rigidity provided by the 1,2-phenylene backbone of the phosphine. Thus this phenylene phosphine cannot readily dissociate and/or migrate, and two adjacent empty coordination sites cannot be created. This observation is consistent with the great stability reported for many 1,2- $R_2PC_6H_4PR_2$ complexes.

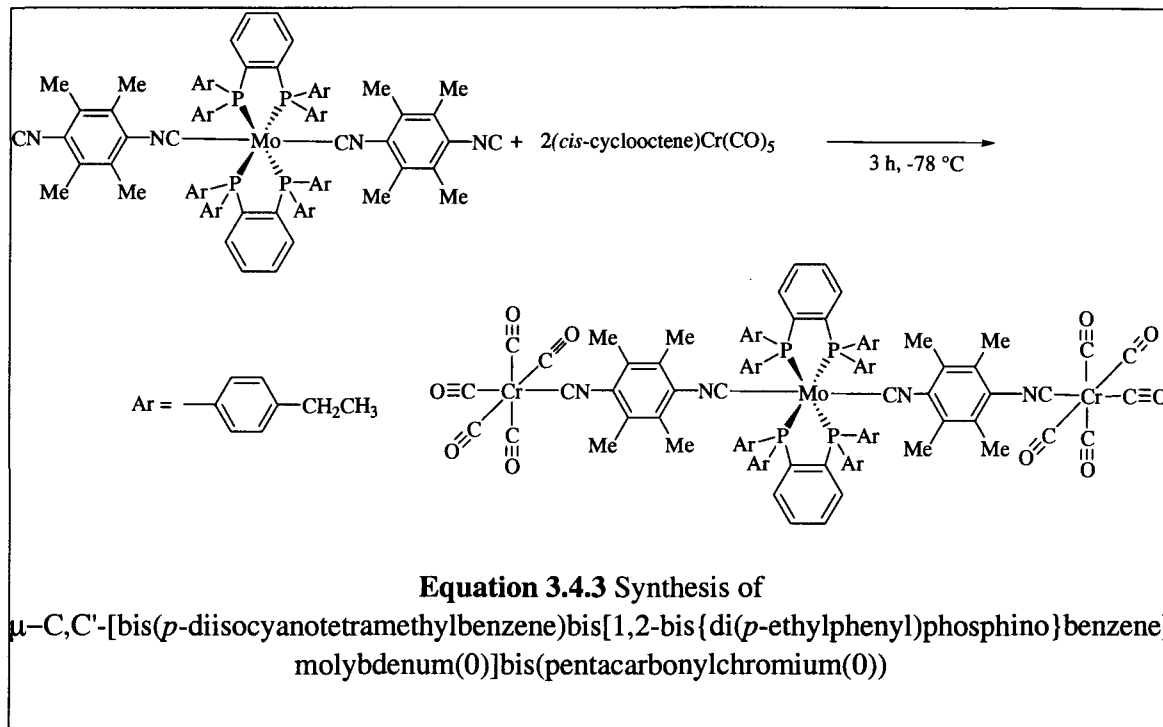


The synthesis of bis(1,2-bis(diphenylphosphino)ethane)carbonyl(DMF) tungsten (0) was attempted by the route shown:



This reaction is very similar to that in **Equation 3.4.1**, with the exception that dinitrogen does not re-attach to the metal because of the more strongly coordinated DMF molecule. A similar reaction in which a large excess of DMF was reacted with bis(dinitrogen)bis(1,2-bis(diphenylphosphino)ethane)molybdenum(0) to yield the molybdenum congener of the product shown in **Equation 3.4.2** was published by Tatsumi *et.al.*⁹ The product recovered after 2 h of reflux proved to be starting material in our case. Even under reflux, the solubility and/or the reactivity of the tungsten dinitrogen complex resulted in no formation of the desired product.

The trimetallic $\mu\text{-C,C'}$ -[bis(*p*-diisocyanotetramethylbenzene)bis[1,2-bis{di(*p*-ethylphenyl)phosphino}benzene]molybdenum(0)]bis(pentacarbonylchromium(0)) was synthesized as shown below:

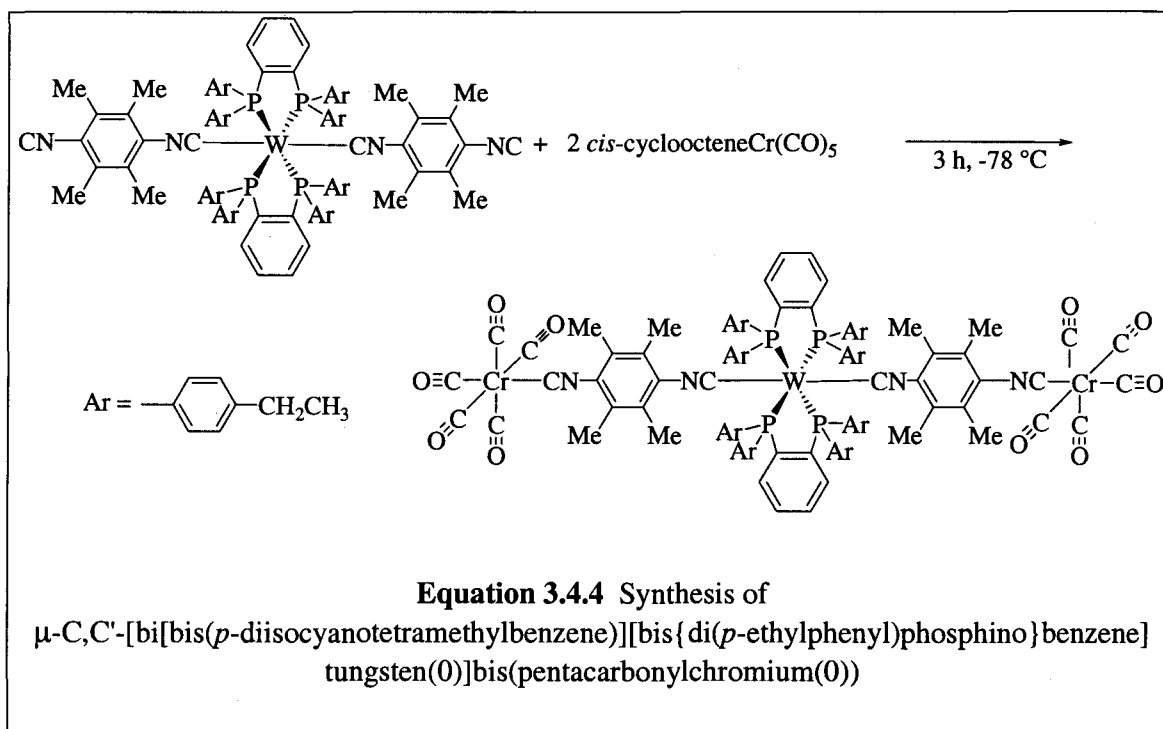


The reaction is carried out at $-78\text{ }^{\circ}\text{C}$ in order to minimize any side reactions that may occur. Two molar equivalents of the chromiumpentacarbonyl complex are added to one equivalent of the bis(diisocyanitrile) complex. The reaction is stirred for 3 h at $-78\text{ }^{\circ}\text{C}$ and is then allowed to warm to room temperature over an additional hour. Hexanes are then added and the solution is left to crystallize in the freezer.

The trimetallic complex is isolated as black iridescent very thin plates in a yield of 42.8%. The IR spectrum shows one $\text{N}\equiv\text{C}$ stretching frequency at 1859 cm^{-1} and two $\text{C}\equiv\text{O}$ stretching vibrations at 2054 and 1955 cm^{-1} . The ^1H NMR spectrum reveals the product in **Equation 3.4.3** to be exclusively the *trans* isomer as there is only one set of signals. The doublets at 7.22 ($J(^1\text{H}^1\text{H}) = 7.6\text{ Hz}$) and 6.84 ($J(^1\text{H}^1\text{H}) = 8\text{ Hz}$) ppm are due to the aromatic hydrogen atoms of the phosphine. Two aromatic proton signals are not observed, apparently due to signal overlap. The quartet at 2.36 ($J(^1\text{H}^1\text{H}) = 6.4\text{ Hz}$) ppm

is from the methylene protons of the ethyl groups. The singlets at 1.86 and 0.86 ppm are from the methyl groups of the bis(diisonitrile) ligands. The triplet at 0.990 ($J(^1\text{H}^1\text{H}) = 7.6$ Hz) is due to the methyl protons of the ethyl groups.

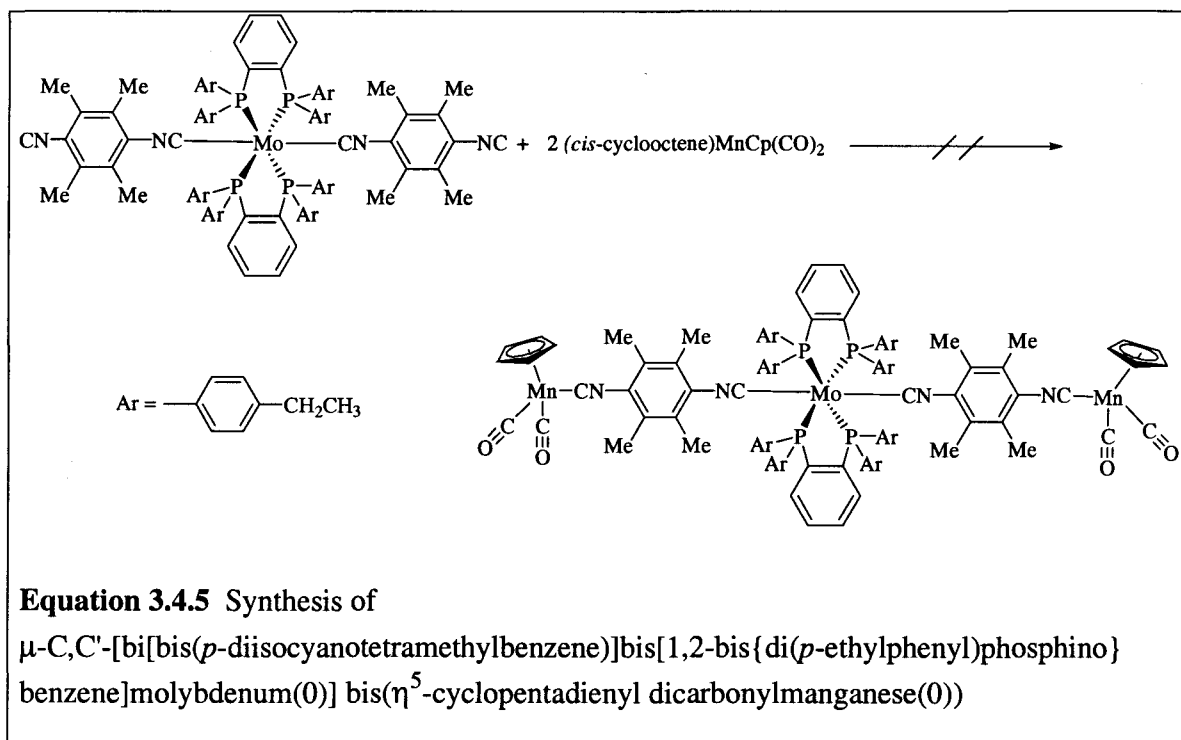
The trimetallic $\mu\text{-C,C'}$ -[bis(*p*-diisocyanotetramethylbenzene)bis[1,2-bis{di(*p*-ethylphenyl)phosphino}benzene]tungsten(0)]bis(pentacarbonylchromium(0)) was synthesized by a route similar to the one used for its molybdenum congener:



The trimetallic complex was isolated in a 48.8% yield as black iridescent, very thin plates. The IR spectrum shows one $\text{N}\equiv\text{C}$ stretching frequency at 1851 cm^{-1} and two $\text{C}\equiv\text{O}$ stretching frequencies at 2055 and 1954 cm^{-1} . The ^1H NMR spectrum shows this trimetallic to be again exclusively the *trans* isomer. The doublet at 6.84 ($J(^1\text{H}^1\text{H}) = 8$ Hz) is one of the aromatic proton signals from the phosphine. The other three aromatic proton signals are not observed due to signal overlap. The quartet at 2.36 ($J(^1\text{H}^1\text{H}) = 7.6$ Hz) is

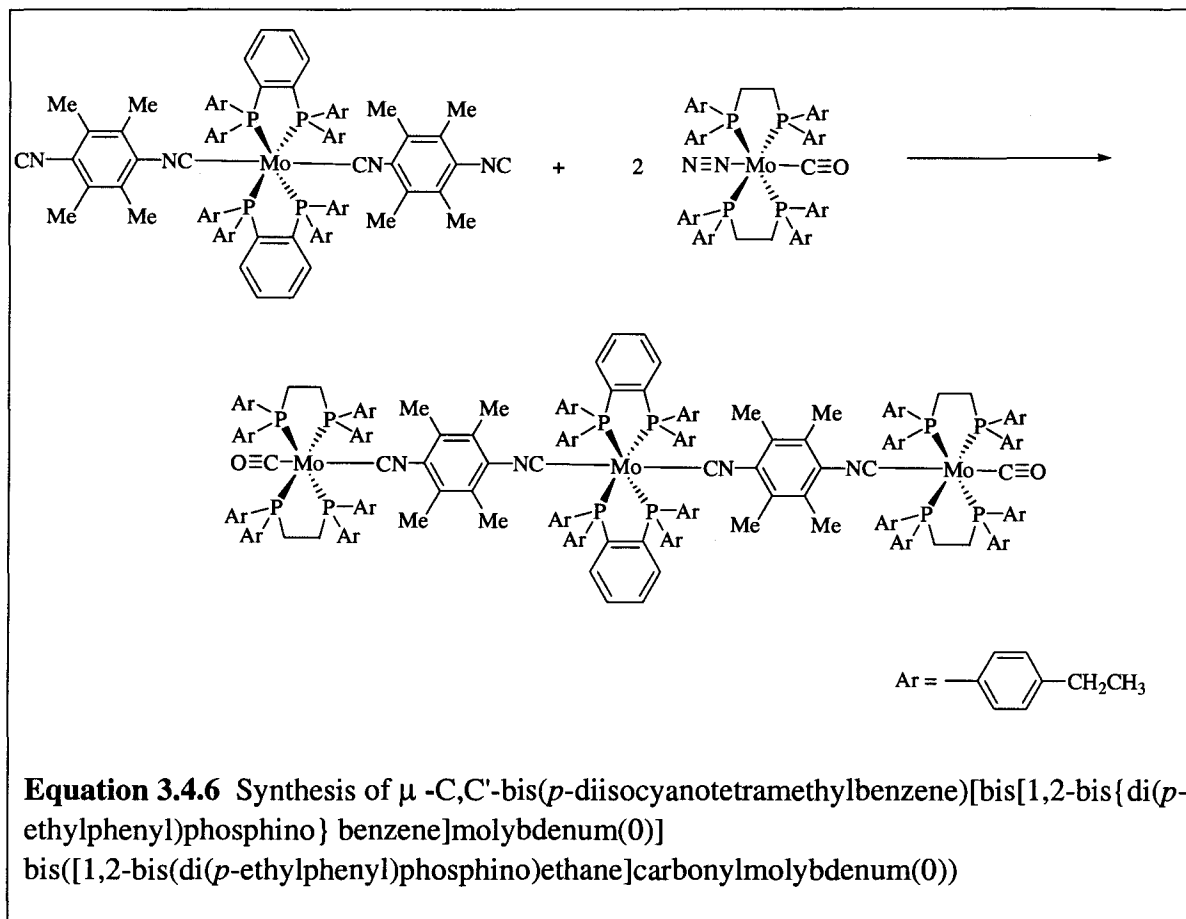
due to the methylene protons of the ethyl groups. The singlets at 1.86 and 0.84 ppm can be assigned to the methyl groups on the bis(diisonitrile). The triplet at 0.99 ($J(^1\text{H}^1\text{H}) = 7.6$ Hz) can be assigned to the methyl protons of the ethyl groups.

The attempted synthesis of $\mu\text{-C,C}'\text{-[bis}(p\text{-diisocyanotetramethylbenzene})\text{bis[1,2-bis}\{di(p\text{-ethylphenyl})\text{phosphino}\}\text{benzene]molybdenum(0)}\text{]bis}(\eta^5\text{-cyclopentadienyl dicarbonylmanganese(0))}$ is shown below:



Two molar equivalents of *cis*-cyclooctene- η^5 -cyclopentadienyl-dicarbonylmanganese were combined with one molar equivalent of the bis(isocyanide) complex. Since the manganese reagent does not easily lose its cyclooctene ligand, the reaction was stirred for five days and the reaction was monitored using IR spectroscopy. After five days, hexanes were added in an attempt to crystallize the desired product from the reaction solution. No product crystallized from the pale red-to-pink solution.

The attempted synthesis of $\mu\text{-C,C}'\text{-[bis}(p\text{-diisocyanotetramethylbenzene})\text{bis[1,2-bis}\{di(p\text{-ethylphenyl})\text{phosphino}\}\text{benzene]molybdenum(0)}\text{]bis}([1,2\text{-bis}(di(p\text{-ethylphenyl})\text{phosphino})\text{ethane})\text{carbonylmolybdenum(0)})$ is shown below:



In this reaction, solid bis(tetramethyl-*p*-diisocyanobenzene)bis[1,2-bis{di(*p*-ethylbenzene)}phosphinobenzene]molybdenum(0) and solid bis(di(*p*-ethylbenzene)phosphinoethane)dinitrogencarbonylmolybdenum(0) are combined in a cooled (-78 °C) flask. Toluene is added and the solution is stirred for 6 h (one of which is needed for the solution to warm to room temperature). Hexane is then added in an attempt to crystallize the product. No product was isolated from the dark blue solution.

Like the bis(diisonitrile) complexes, the three trimetallic complexes (those in **Equations 3.4.3, 4, and 6**) are very promising. In solution, all three complexes are very dark blue, almost black in color. As solids, all three have a metallic shine to them as well. The color is indicative of either a LMCT or MLCT taking place as in the bis(diisonitrile) complexes. Again, this implies that these complexes are highly conjugated and thus these higher oligomers should be capable of conducting electrons. The iridescent sheen of the solid chromiumpentacarbonyl complexes resembles that found in most metals. With most metals having at least semi-conducting properties, it can be inferred that the chromiumpentacarbonyl complexes might also have semi-conducting properties as well. The goal of synthesizing conducting nanowires becomes even closer with these trimetallic complexes.

References

-
1. a) E. P. Kyba, S-T. Jui, R. L. Harris. *Organometallics* **1983**, *2*, 1877-1879, b) E. P. Kyba, M. C. Kerby, S. P. Rines. *Organometallics* **1986**, *5*, 1189-1194.
 2. Adapted from L. Dahlenburg, A. Kaunert. *Eur. J. Inorg. Chem.* **1998**, 885-887.
 3. R. L. Cook and J. G. Morse. *Inorg. Chem.* **1982**, *21*, 4103-4105.
 4. W. Hussain, G. J. Leigh, H. M. Ali, J. Pickett, D. Rankin. *A. J. Chem. Soc. Dalton Transactions* **1984**, 1703-1708.
 5. T. A. George, M. E. Noble. *Inorg. Chem.* **1978**, *17*, 1678-1679.
 6. Mtunzi-S. Donovan, M. Hughes, G. J. Leigh, H. Mohd. Ali, R. L. Richards, J. Mason. *J. Organomet. Chem.* **1983**, *246*, C1.
 - 7 C. L. Perrine. "0th and 1st Generation Organometallic Nanostars from Ferrocenylamine and Ferrocenylaniline." M.S. Thesis. August, **2004**
 - 8 . N. L. Wagner, F. E. Laib, D. W. Bennett. *J. Am. Chem. Soc.* **2000**, *122*, 10856-10867.
 - 9 . T. Tatsumi, H. Tominaga, M. Hidai, Y. Uchida. *J. Organomet. Chem.* **1981**, *215*, 67-76.

Chapter IV- Conclusions

The first step towards the goal of synthesizing electronically conducting nanorods is the synthesis of molybdenum and tungsten dinitrogen complexes. The majority of the dinitrogen complexes containing these metals adopt the *trans* configurations (some are *cis*) as do the bis(diisonitrile) complexes reported here. The bis(diisonitrile) complexes can be made by the direct reaction of the dinitrogen complex with an excess of the appropriate bis(diisonitrile), the labile dinitrogen ligand being easily replaced by the stronger coordinating diisonitrile ligands. Trimetallic complexes can then be synthesized from the bis(diisonitrile) complexes. In going from the dinitrogen complexes to the bis(diisonitrile) complexes and then to the trimetallic complexes, charge transfer transitions (indicated by color intensity) become increasingly more important. This points towards an increase in conjugation along the backbone of the metal complexes.

Further studies to be undertaken include electrochemical (CV) analysis, DFT calculations, finding a better synthetic route for the fluorinated phosphines, as well as investigating the exact nature of the transitions that are occurring in both the bis(isonitrile) complexes as well as the trimetallic complexes. A measurement of the UV-Vis spectrum may provide useful information about the type of charge transfer transition and, thus the color changes, occurring in these complexes. The bis(diisonitrile) complexes and the trimetallic complexes both show promise. Thus, with the successful synthesis of the trimetallic complexes, the goal of synthesizing conducting nanowires comes closer.

Chapter V- Solid Sodium Cyclopentadienide, NaCp

Section one- Introduction

The cyclopentadienyl anion, Cp^{\ominus} , remains one of the most common and widely used ligands in organometallic chemistry. This cyclic polyene ligand can co-ordinate through up to five of its carbon atoms, donating up to six electrons to the metal it is coordinated to.¹ The Cp containing complexes can have one, two, or three cyclopentadienyl rings and the dicyclopentadienyl complexes can have either straight or angular (bent) “sandwich” structures (“metallocenes”, as in 1 and 2 of Fig. 5.1.1). They can also be derivatives of the sandwich form with other ligands present (Fig. 5.1.1 number 3) or be half sandwich (“piano stool”) (Fig. 5.1.1 number 4) complexes.^{2,3}

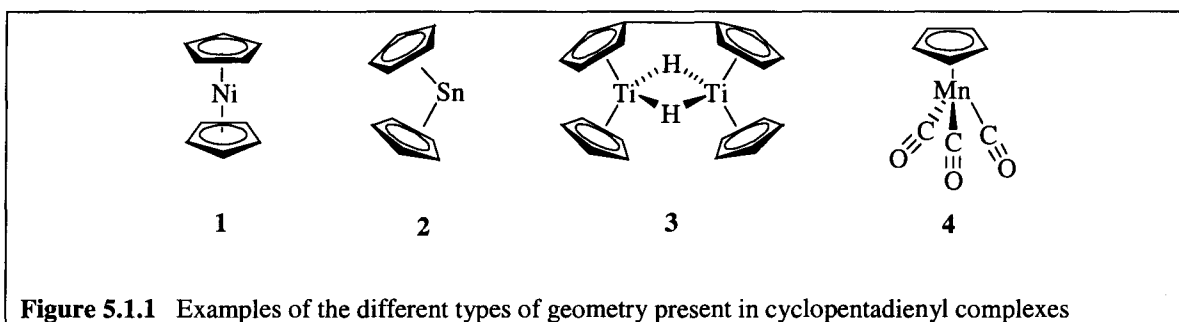
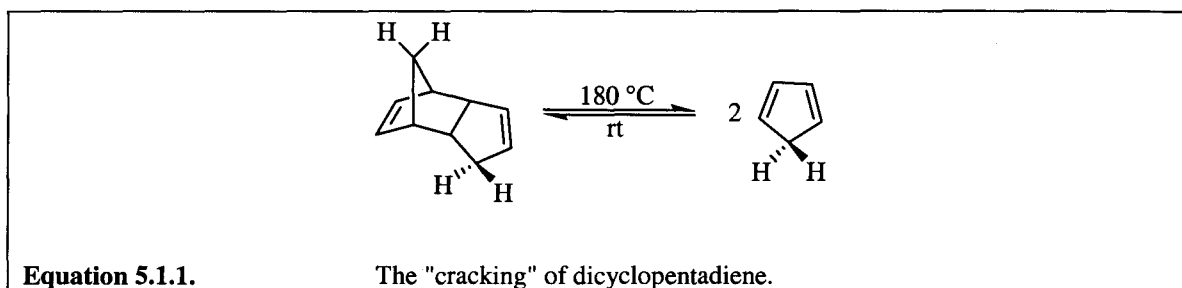


Figure 5.1.1 Examples of the different types of geometry present in cyclopentadienyl complexes

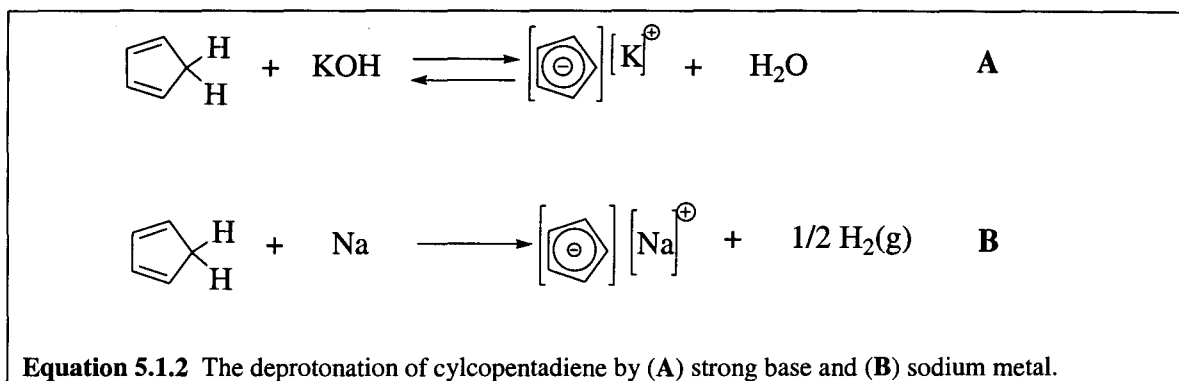
Cyclopentadiene itself does not usually exist as the free molecule C_5H_6 , CpH , since the five-membered diene ring has limited thermal stability and readily undergoes dimerization. Instead, the dimeric dicyclopentadiene, $\text{C}_{10}\text{H}_{12}$, $(\text{CpH})_2$, must be “cracked”, meaning it undergoes a retro-Diels-Alder addition reaction to produce the monomeric form of CpH as shown in **Equation 5.1.1**.² It is important to use this freshly cracked

CpH as soon as possible as the neat liquid will readily re-dimerize even at room temperature and its solutions are only stable towards dimerization for a few hours at ambient temperature or days in the freezer.



Methylcyclopentadiene, $C_5H_5CH_3$, Cp^*H , like the parent compound cyclopentadiene, will also dimerize at or near room temperature (the dimerization of Cp^*H is measurable above $0\text{ }^\circ\text{C}$ and is complete within two hours at $60\text{ }^\circ\text{C}$).⁴ The Cp^*H dimer, $(Cp^*H)_2$, (CpH , Cp^*H , etc., may also form trimers and higher weight oligomers) has the same *endo*-dicyclopentadiene structure as dicyclopentadiene itself. The two dimers also exhibit similar cracking temperatures, namely: $172\text{ }^\circ\text{C}$ for the methylcyclopentadiene dimer and $180\text{ }^\circ\text{C}$ for dicyclopentadiene.⁴ 1,2,3,4,5-Pentamethylcyclopentadiene, C_5Me_5H , Cp^*H , however, does not show a tendency towards dimerization at room temperature, presumably because it is hindered by the steric bulk of the pentamethylated Cp ring.

Once the monomeric CpH has been produced, it has to be introduced into the coordination sphere of the metal. Cyclopentadiene is a weak acid ($pK_a = 10^{-15}$), but is still one of the more acidic hydrocarbons. As such, it can easily be deprotonated by a strong base or alkali metals² to form the aromatic cyclopentadienyl anion.



Cp-alkali metal complexes are the most common reagent for the introduction of the Cp ligand into a metal's coordination sphere.⁵ The most common such reagent is sodium cyclopentadienide, NaCp. NaCp is the first known Cp-containing complex. It was first synthesized *in situ* by Thiele for use in subsequent reactions⁵ in 1900.⁶ He later isolated the first pure Cp-alkali metal compound, KCp, which was synthesized from the reaction of cyclopentadiene and potassium metal in benzene.⁷

The metal-Cp bonding in Cp-alkali metal complexes is mainly ionic in character - the value of 80-90% being well established.⁸⁻¹⁰ This is to be expected since the bond between an electropositive alkali metal and a less electropositive carbon atom is expected to possess substantial ionic character.⁶ The resulting Cp-alkali metal complexes are therefore more accurately described as being ionic clusters in which anion-cation interactions make up the majority of the bonding. The polarity of this bond is not only dependent upon the alkali metal that is present but also on the nature of the organic anion.⁶ It has been shown^{8, 9} that Cp-alkali metal bonds are more ionic than alkyl-alkali metal bonds. For this reason, Cp-alkali metal complexes are better described as contact ion pairs with no delocalization of the Cp's electron cloud towards the alkali metal.

It has already been mentioned that Cp can have hapticity of up to five. Through a computational haptotropic search in which the lithium cation was moved from side to

side above the Cp anion, it was found¹¹ that the preference in LiCp is η^5 coordination. The same type of bonding can be assumed to be present in NaCp since it has been shown *via* the use of high-resolution powder X-ray diffraction¹² that LiCp and NaCp are isomorphous in the solid state, that they show very similar unit cell parameters, and also that they crystallize in the same crystal system and space group.

NaCp, with its highly ionic character and thus its high reactivity, remains the most common reagent through which Cp is introduced into a metal complex. The experimental procedure^{2,13} for making NaCp involves three main steps:

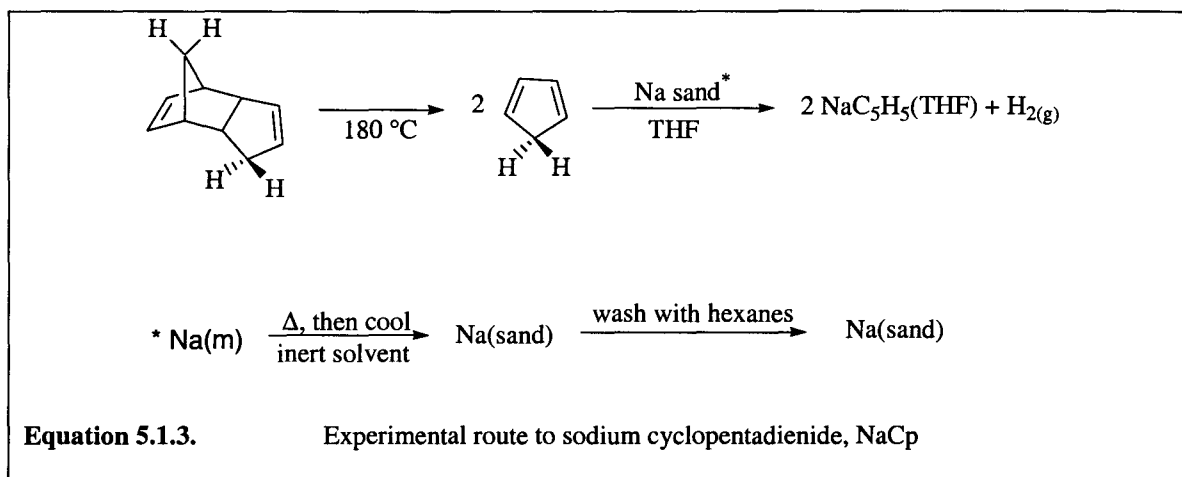
- (1) Dicyclopentadiene is “cracked” as mentioned before to give monomeric CpH.

- (2) A sample of metallic sodium is placed in a high boiling inert solvent (under inert atmosphere) which is heated above the melting point of sodium while being vigorously stirred. This gives a suspension of very finely divided sodium. The suspension is then cooled to room temperature while stirring is constant to give sodium sand (care should be taken when using the sodium sand as it is very reactive towards moisture, and is thus air sensitive). The inert solvent is removed by canulation, filtration, etc., to give a finely divided solid. Alternatively, commercial sodium sand in a medium such as paraffin can be heated (below the melting point of sodium) in an inert solvent such as hexanes and then the solvent is removed, the sand washed to give a similar finely divided sodium.

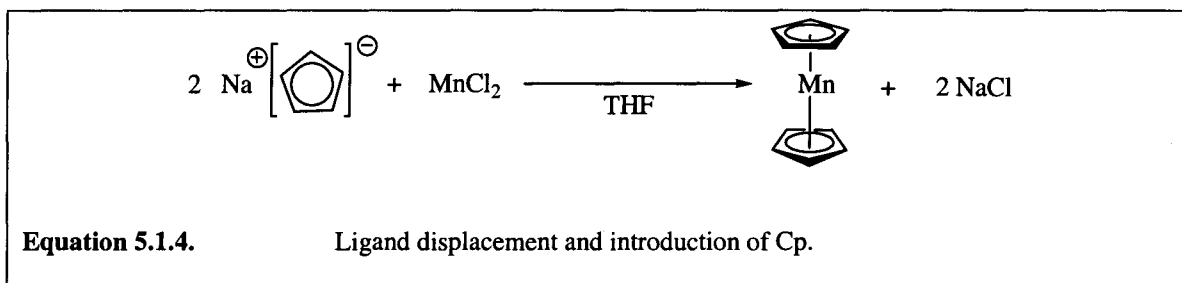
- (3) A solvent that is suitable for dissolving NaCp, typically THF as Cp-alkali metal compounds are insoluble in apolar solvents⁵ is then added to the sodium sand and the CpH monomer is added drop-wise. After the reaction to give a colorless (pure) to purple (partially oxidized) solution is complete one has a THF solution of reactive

NaCp(THF). The THF can then be removed *in vacuo* and an alternative solvent added but this solid NaCp is a very air sensitive, pyrophoric material that is very hard to handle.

The overall reaction scheme for this is illustrated in **Equation 5.1.3**.



Cyclopentadiene anion can then be introduced into a metal's coordination sphere by reacting a metal precursor (often a metal chloride or carbonyl) with the cyclopentadienyl reagent previously generated (NaCp).² This occurs through simple ligand displacement as shown in **Equation 5.1.4**.¹



Although the traditional method to make NaCp is reliable (roughly 70% yield), it is rather time consuming. Given the evolution of flammable hydrogen gas, the need to handle pyrophoric sodium sand, multiple reaction steps, and a product that is often rather air sensitive, the need for an easier method is apparent. This chapter deals with such a

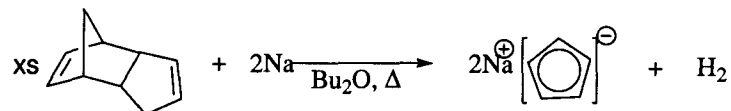
method: a one-step, one-pot synthesis of solid NaCp. One can imagine that if a solvent can be chosen that is both inert and has a high enough boiling point, the dicyclopentadiene can be cracked *in situ* while the sodium is being melted and finely divided. The freshly cracked Cp can then immediately react with the sodium droplets. The solvent should also be non-polar so that the NaCp will precipitate from the solution. Collection of the product can then be done *via* filtration under an inert atmosphere or canulation of the supernatant away from the desired product. This new method would both eliminate the multiple steps and might be expected to be safer since the possibility of air getting into the reaction apparatus, the sodium sand catching fire, and/or that the dropping funnel will leak are drastically reduced and/or avoided all together. This new method is basically a “one-pot” reaction: sodium metal, an excess of dicyclopentadiene, and the appropriate solvent are combined in a single flask, heated, and stirred until the sodium metal has been consumed. Butyl ether was chosen as the solvent because it has a pleasant smell, is nonpolar, is relatively inert, and has an appropriately high boiling point of 142-143 °C.

Once it has been determined whether or not the method works, certain fundamental questions will then be investigated and answered. The first of which is how this new method compares to the traditional method, i.e. are the yields similar, how time consuming is it, and how do the products compare (purity, sensitivity, etc.)? The next question is how general is this reaction? To answer this, other ligands in the Cp family will be used (indene and 1,2,3,4,5-pentamethylcyclopentadiene, Cp*). The final question is what kind of transfer properties does the NaCp generated by this new method have (i.e. will a reaction as illustrated in **Equation 5.1.4** work using this new NaCp).

Section two – Experimental

Unless otherwise stated, all manipulations were carried out under an inert atmosphere of N_2 using standard Schlenk techniques. Dicyclopentadiene, indene, 1,2,3,4,5-pentamethylcyclopentadiene, and butyl ether (anhydrous) were purchased commercially through Aldrich chemical company and were degassed by bubbling N_2 through them. Solvents were distilled over the appropriate drying agent under a nitrogen atmosphere prior to use (except for butyl ether, which was used without further purification). All of the reactions documented below should be done in a properly working fume hood as dicyclopentadiene has a very pungent odor.

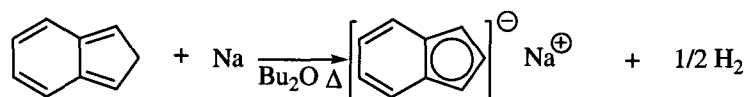
A. Sodium cyclopentadienide (NaC_5H_5)¹³



To a 1000 mL 3-necked flask fitted with a septum, reflux condenser with a combination nitrogen inlet/bubbler on top, and nitrogen inlet adapter on the side, are added 400 mL of butyl ether (99.3%, anhydrous, Aldrich) and 30 mL (29.58 g, 223.7 mmol) of dicyclopentadiene (Aldrich). The solution is then degassed by bubbling N_2 through it *via* a syringe needle through the septum for 30 minutes. Clean sodium metal, 6.24 g (271.3 mmol) is cut fresh from sodium sticks and added to the flask. The supply of N_2 to the side arm is stopped and the suspension is heated to reflux (oil bath temperature

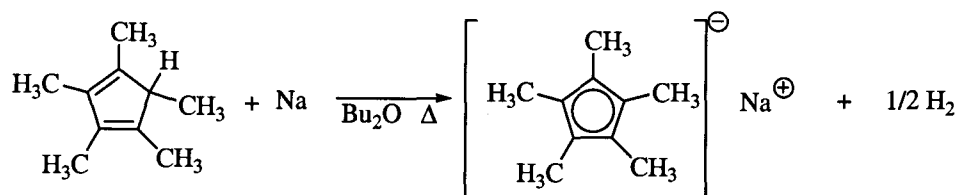
of 120 °C) with vigorous stirring until all of the sodium metal has been consumed (approximately 48 h). No water flow is used in the condenser due to the potential explosion hazard if the apparatus were to break and then water were to come in contact with alkali metals. If the sodium metal is not all consumed after 70 h, additional dicyclopentadiene (in a degassed butyl ether solution) may be added (the reaction mixture is allowed to cool down to room temperature before the addition of additional reagents) and the mixture is heated to reflux for an additional 48 h. [Note: hydrogen gas is generated in this reaction. The pressure that arises from this evolution of gas is alleviated through the use of a mercury bubbler.] After the reaction is finished, the resulting pale yellow suspension is allowed to cool to room temperature and is filtered through a Schlenk filter. The white to beige solid sodium cyclopentadiene is allowed to dry *in vacuo* for 2 h, washed with hexanes (~ 50 mL) and 33.37g (383.2 mmol, 141%) of the air-sensitive NaCp is isolated. Alternatively, the supernatant may be removed by cannulation, the solid washed with hexane (3 × 40 mL), and the solid dried *in vacuo*. It is believed that solvent is incorporated in the crystal lattice, resulting in a percent yield above 100.

B. Sodium Indenide (NaC₉H₇)¹³



To a 1000 mL 3-necked flask fitted with a septum, reflux condenser with a combination nitrogen inlet/bubbler on top, and nitrogen inlet adapter on the side, are added 300 mL of butyl ether (99.3%, anhydrous, Aldrich) and 25 mL (24.9 g, 214.4 mmol) of indene. The solution is then degassed by bubbling N₂ through it *via* a syringe through the septum for 30 minutes. Sodium metal, 3.79 g (164.8 mmol) is cut fresh from sodium sticks and added to the flask. The supply of N₂ to the side arm is stopped and the suspension is heated to reflux (with an oil bath temperature of 120 °C) with vigorous stirring until all of the sodium metal is consumed (48 h). After 45min, the solution takes on a brown-yellow color. [Note: hydrogen gas is generated in this reaction. The pressure that arises from this evolution of gas is alleviated through the use of a mercury bubbler.] After the reaction has gone to completion, the solution is allowed to cool down to room temperature. The now greenish solution is filtered t cold hrough a Schlenk filter and placed in the freezer (-19 °C) to crystallize. No product was isolated.

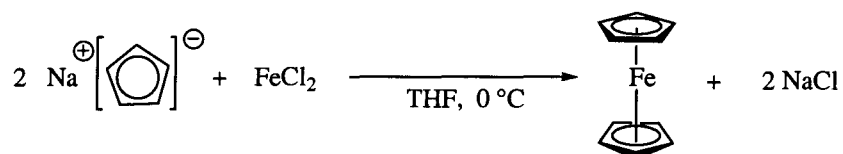
C. 1,2,3,4,5-Pentamethylcyclopentadienylsodium (NaC₁₀H₁₅)¹³



To a 150 mL 3-neck flask fitted with a septum, reflux condenser with a combination nitrogen inlet/bubbler on top, and nitrogen inlet adapter on the side, are added 55 mL of butyl ether (99.3%, anhydrous, Aldrich) and 17 mL (14.79 g, 108.6

mmol) of 1,2,3,4,5-pentamethylcyclopentadiene (Aldrich). The solution is then degassed by bubbling N_2 through it *via* a syringe through the septum for 2 h. Sodium metal, 1.7 g (73.95 mmol) is cut fresh from sodium sticks and added to the flask. The supply of N_2 to the side arm is stopped and the suspension is heated to reflux (with an oil bath temperature of 120 °C) with vigorous stirring until all of the sodium is consumed (72 h). [Note: hydrogen gas is generated in this reaction. The pressure that arises from this evolution of gas is alleviated through the use of a mercury bubbler.] After the reaction is finished, the resulting suspension is allowed to cool to room temperature and filtered through a Schlenk filter and the slightly gray pentamethylcyclopentadienyl sodium is allowed to dry *in vacuo* for 2 h. 4.30 g (27.2 mmol, 36.8%) of the very air-sensitive product are isolated.

D. Ferrocene ($FeC_{10}H_{10}$)¹³



To a 100 mL Schlenk flask is added 0.68 g (5.36 mmol, anhydrous) of $FeCl_2$ and the flask is evacuated and filled with nitrogen. To a second 100 mL Schlenk flask are added 1.18 g (13.55 mmol) of sodium cyclopentadienide and 25 mL of THF. This solution is then added to the $FeCl_2$ along with an additional 25 mL of THF. The solution is stirred at 0 °C for 18 h. The THF is evaporated off, leaving crude yellow-orange ferrocene. The product is purified by dissolving the crystals in diethyl ether (Aldrich) and

then by sublimation *in vacuo* at 80 °C for 2 h. 0.35 g (2.08 mmol, 35%) of the air-stable, yellow-orange ferrocene are obtained.

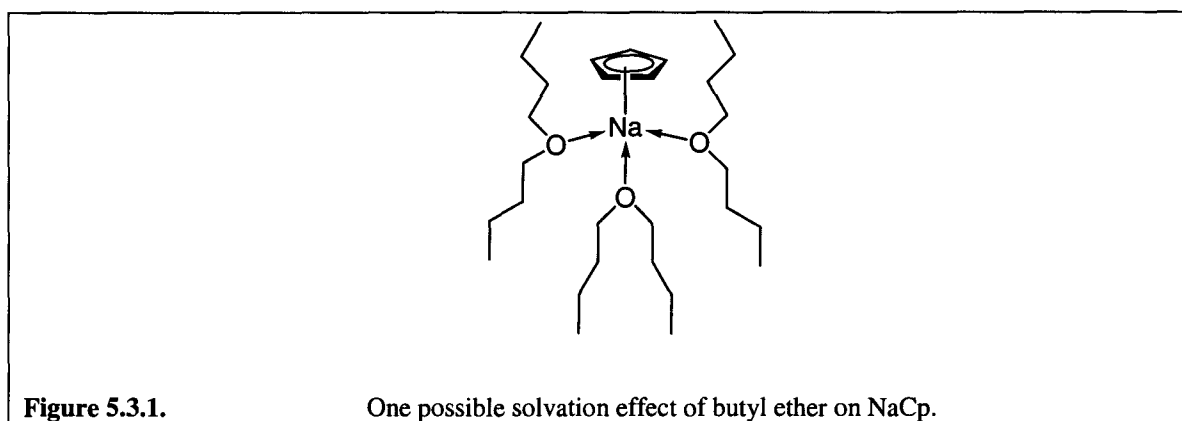
Section three - Results and Discussion

1. Synthesis and physical properties of sodium cyclopentadienide, NaCp

As was previously mentioned¹³, the traditional route to sodium cyclopentadienide is very tedious and involves multiple steps. In these multiple steps, the possibility that the reaction apparatus is not air tight, thus allowing humid air to enter and, consequently, oxidize or hydrolyze the desired product, is a major concern. This new one-step, one-pot method seems to have eliminated this concern. On the average, once the starting materials have been combined in the reaction vessel, the reaction needs to be run for ninety-six hours (four days). Although this is a longer reaction time than the traditional method, the advantages are obvious: the possibility that air can enter the reaction vessel has been drastically reduced and the investigator is not doing multiple steps that take up his/her time and equipment. The investigator needs only to ensure that the joints of the glassware are tight upon initial set-up only. The traditional method also requires the removal of the solvent from the sodium sand after it is created and then the addition of another nonpolar solvent so that the NaCp product may precipitate from solution. This removal/addition process not only leaves the newly-formed and highly activated sodium sand exposed to possible oxidation, but it also creates a potential explosion hazard if any moisture or halogenated solvents are present. Again, the new method alleviates this problem since there is no removal of the solvent after the sodium sand is created. The sodium sand is created in an inert solvent that is relatively nonpolar so that the NaCp may precipitate from it and the sodium sand is all consumed in the reaction flask.

The sodium cyclopentadienide created by the traditional method is typically pyrophoric. The NaCp created by the new method did not exhibit this pyrophoric nature. In fact, the off-white to beige product showed remarkable stability: it remained exposed to air for a period of one hour before any decomposition effects were demonstrated. The decomposition of the NaCp created *via* the new method was not violent in nature; the product simply “melted” to give a clear, brown liquid that had an odor similar to that of dicyclopentadiene. This enhanced stability may be explained by first examining the percent yield for this reaction. Upon doing the calculation to determine the percent yield, it is noticed that a percent yield of well over a hundred is obtained. This is usually an indication that the product is still “wet”, meaning that the solvent has not been completely removed by drying the product using an oil pump vacuum. One possible explanation could be that the solvent has been incorporated into the crystal lattice. In the traditional method, it is not uncommon for at least one solvent molecule to be incorporated into the crystal lattice of NaCp.⁴ This solvent molecule is usually a polar one, coordinating to the sodium cation. These polar solvent molecules interact with the alkali metal electrostatically; a large electrostatic component (cation-dipole interaction) and a smaller polarization component (cation-induced dipole interaction) are present with negligible ligand-to-metal charge transfer effects.^{4,14,15} This “solvent effect” serves only to shield the relatively inert cation, leaving the reactive anion readily accessible to oxidation or hydrolysis. The accessibility of the electron-rich anion results in the pyrophoric decomposition event often exhibited by Cp-alkali metal complexes synthesized by the traditional method. The new method, however, does not leave the reactive anion as unprotected. It uses butyl ether, a large and relatively nonpolar solvent,

which may, if incorporated into the crystal lattice, create a protective barrier for the sensitive cyclopentadienyl anion. This can be accomplished in two ways. There could be no interaction between the solvent and the NaCp - the solvent simply fills holes present in the crystal lattice, thus providing added "bulk" around the anion. Alternatively, the butyl ether could be co-coordinated to the sodium through the oxygen atom, in a manner similar to THF. The bulky butyl groups could then create a shield around either side of the Cp anion. A diagram of this proposed shielding effect is shown below in **Fig. 5.3.1**.



This shielding effect partially stabilizes the cyclopentadienyl anion, resulting in a decomposition event that is a much milder overall.

The cyclopentadienyl ring transfer capability is now called into question. The way that the ring transfer capability was tested was by synthesizing ferrocene from ferrous chloride and two equivalents of NaCp. The textbook yield for this reaction can be as high as 90%, with the average yield being 67-73%.¹⁶ For the new method to even be considered viable, an atom transfer rate at least equal to that of the old method must be obtained. When this synthesis was done, a yield of 35% was obtained. This is half of the standard literature value for this reaction. While this low yield is discouraging, it can be attributed to the inexperience of the investigator since yields of 90+% have been reported by other individuals using solid NaCp in more demanding reactions.

2. Synthesis and physical properties of pentamethylcyclopentadienyl sodium, NaCp*

Pentamethylcyclopentadienyl sodium was produced as an off white-to-gray powder in a 38.6% yield. The use of a non-polar solvent seemed to have had no effect on the stability of the product, as the powder remained pyrophoric and air sensitive: the NaCp* would “crackle” and spark simply upon transferring the material from one flask to the other. The product is also moisture sensitive. During the writing of this thesis, a flask with ca. two grams of NaCp* that was stored in the freezer leaked. This resulted in not only air getting into the flask, but moisture as well. The violent reaction that followed not only blew the freezer door open, it also melted the plastic clamp that held the glass stopper on, and shot the stopper across the room. An explanation for the higher reactivity of NaCp* compared to NaCp are the methyl ring substituents. A methyl group is electron donating in character. It will then donate electron density to the cyclopentadienyl ring. The cyclopentadienyl ring now has more electron density localized in the aromatic ring, making it more reactive towards oxidation and/or hydrolyses. Thus, when decomposition occurs, the event is rapid, resulting in a more violent event overall. In contrast to NaCp, no stabilizing effect of the butyl ether was observed for NaCp*. An explanation for this is that steric repulsion between the ring substituents and the butyl ether prohibits the butyl ether from forming the “protective wall” close enough to the cyclopentadienyl anion. No attempts to investigate the ring transfer capabilities were undertaken due to the pyrophoric nature of the product as well as the inconclusive results achieved from the NaCp study.

Section four- Conclusions

This study has shown that, while the new method presents fewer hazards to the investigator and does indeed produce NaCp that is remarkably air-stable, the cyclopentadiene ring transfer capabilities of only 50% of literature values for the synthesis of ferrocene can be attributed to the inexperience of the investigator. NaCp is used as a transfer reagent because of its reactivity and relatively inexpensive cost. The new method yields NaCp that is more stable. This method did not, however, yield NaCp* that showed enhanced stability. Other Cp-like ligands, such as indene, resisted isolation. This could have been due to isolation issues, with the sodium indenide being soluble in the butyl ether (another solvent, such as decane, may be better suited to this reaction due to its lower polarity). Further investigations are needed to determine exactly what effects the solvent does have on both the stability and the reactivity of the NaCp that is produced in this one-step-one-pot method.

During the writing of this thesis, another research group did, in fact, investigate this one-pot synthesis for both NaCp and KCp. Instead of using a non-polar solvent, their reaction was carried out in neat dicyclopentadiene, resulting in the formation of analytically pure NaCp in excellent yield (99%).¹⁷

Section five- References

1. D.F Shiver, P.W Atkins. *Inorganic Chemistry*, 3rd ed.; Oxford University Press: New York, 1999; Chapter 16.
2. C. Elschenbroich, A Salzer. *Organometallics A Concise Introduction*, 2nd rev. ed.; VCH: New York, 1992; Chapter 15.
3. T. Aoyagi, H.M.M. Shearer, K. Wade, G. Whitehead. *J. Organomet. Chem.* **1979**, *175*, 21.
4. S.M. Csicsery. *J. Org. Chem.* **1960**, *25*, 518-521.
5. J. Thiele. *Dtsch. Chem. Ges.* **1900**, *33*, 666.
6. S. Harder. *Coordination Chemistry Reviews* **1998**, *176*, 17-66.
7. J. Thiele. *Dtsch. Chem. Ges.* **1901**, *34*, 68.
8. C. Lambert, P. von R. Schleyer. *Angew. Chem.* **1994**, *106*, 1187.
9. C. Lambert, P. von R. Schleyer. *Angew. Chem., Int. Ed. Engl.* **1994**, *33*, 1129.
10. S. Harder. Ph.D. Thesis, University of Ultrescht, The Netherlands, 1990, p.2.
11. S. Alexandratos, A. Streitwieser, H. F. Schaefer III. *J. Am. Chem. Soc.* **1976**, *98*, 7959.
12. R. E. Dinnebier, U. Behrens, F. Olbrich. *Organometallics* **1997**, *16*, 3855.
13. A. D. Hunter. "Evaluation of Air Stable Cyclopentadienyl Ligands". Grant proposal 2002
14. G. Corongui, E. P. Clementi, W. Simone. *J. Chem. Phys.* **1980**, *72*, 3096.
15. E. Kaufmann, B. Tidor, P. von R. Schleyer. *J. Comput. Chem.* **1986**, *7*, 334.

16. G. Wilkinson. Ferrocene. In *Organic Syntheses Collective Volume*, 2nd Ed.; Rabjohn, N.; Wiley: New York, 1963, 4, 473-477.
17. T. K. Panda, M. T. Gamer, P. W. Roesky. *Organometallics*. **2003**, 22, 877-878.

Chapter VI- Crystallography

Section one- Introduction

SubSection One-Crystals

6.1.1a. Crystal growth

There are a variety of methods that can be used to grow crystals suitable for X-ray diffraction studies. These different methods all share the same basic steps for crystal growth: nucleation, growth, and termination.

Nucleation is the process of forming the initial aggregate that growth will occur from.¹ This aggregate is formed by the chance association of molecules in solution that happen to have the same orientation or, more commonly, on the surface of the vessel or an adventitious solid. The number of nucleation sites that form play an important role in the crystallization process. Too many sites will result in micro crystals that are not suitable (too small) for X-ray diffraction. Only a few nucleation sites should be present to obtain X-ray quality crystals.

Once the initial nucleus has been formed, crystal growth can now take place by deposition of material onto that nucleus. The strength of the interaction between molecules or ions determines whether or not growth will occur.¹ These interactions tend to be stronger at defect sites. These “defect sites” are sites at which there is a “hole” or “ledge” present from the asymmetrical growth of the crystal as shown in **Figure 6.1.1**. The new material can then “fill the gap”. Crystals of suitable quality are formed when the

rate at which material is deposited onto the nucleation site and the rate at which the curing of these defect in the crystal's growth is approximately equal. Rapid deposition may cause growth in too many directions (i.e. formation of dendrites), while a rapid rate of curing of the defect sites may result in early termination of the crystal's growth (i.e. there is still material left in solution, but it will not deposit onto the crystal because of weak interactions).¹

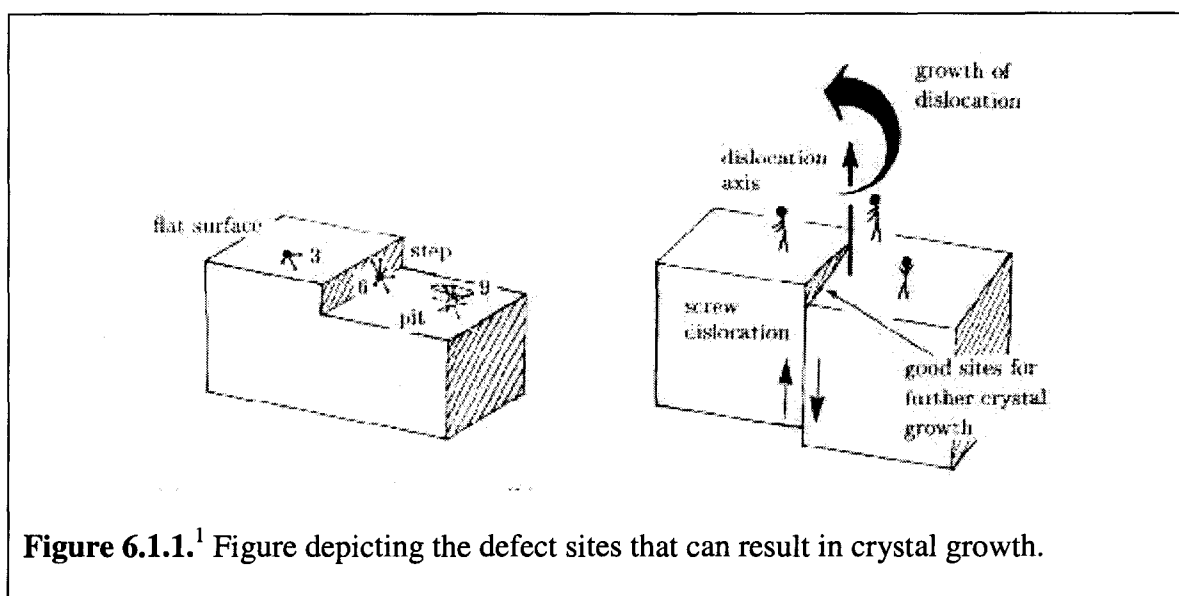


Figure 6.1.1.¹ Figure depicting the defect sites that can result in crystal growth.

Termination of the crystal's growth can occur by two methods. As mentioned above, termination can occur when the rate at which the healing of the defect sites is high. More commonly, termination occurs when there is simply no more material left to deposit onto the crystal because the solution is no longer supersaturated.

The most common method for growing crystals of small molecules (also the method used exclusively throughout the course of this work) is crystallization by slow solvent evaporation. A saturated solution of the compound to be crystallized is first made

from an appropriate solvent. A second solvent that the compound of interest is not soluble in is then layered on top of the first solvent and that second solvent is allowed to slowly diffuse into the mixture. The mixture is then allowed to stand undisturbed (usually in the refrigerator or freezer to decrease the solubility of the compound of interest) and, as the name implies, the rate of crystal growth is dependent upon the rate at which the solvent evaporates. Ideally, slow evaporation is desired in order to produce well defined, X-ray diffraction quality crystals. Fast solvent evaporation often produces crystals that have grown together and are of too low quality for diffraction studies.

Crystallization by hanging/sitting drop methods is the preferred method for growing crystals of proteins.¹ In this method, 5-15 μL of a concentrated protein solution containing insoluble precipitates is suspended from a silicone-treated glass slide and placed over a spot plate reservoir that contains an additional 500 μL of the concentrated precipitate solution. Protein crystals form as equilibrium between the hanging drop and the solution is reached.¹

6.1.1b. Crystal Selection

Crystal selection is often the hardest aspect of an X-ray diffraction study. Many different factors need to be considered when choosing a crystal: size, morphology, etc. Internal properties (i.e. ordering of the unit cell, solvent molecules incorporated into the crystal lattice, rotational freedoms of functional groups present) of the crystal will also play a role in whether or not it is suitable for diffraction studies. For this reason, just

because a crystal appears to be well defined and of the right size does not mean that that crystal will be suitable for X-ray diffraction studies.

In general, a suitable crystal should be no larger than $0.5 \text{ mm} \times 0.5 \text{ mm} \times 0.5 \text{ mm}$ and no smaller than 0.1 mm in all dimensions (these numbers only provide a guideline; smaller or larger crystals can be evaluated on a case-by-case basis). If the crystal is too small in one or more dimensions, the X-ray beam is not diffracted off of the crystal sufficiently strongly. This then, results in the loss of data, as the number of reflections that should be present from that particular orientation of the crystal are dramatically lowered, possibly to the point of none being present at all. If the crystal is too big in one of the dimensions, it projects outside of the homogeneous region of the X-ray or eventually out of the beam which will also badly systematically bias the data.

As noted, the internal properties of the crystal also play a role in whether or not a crystal is suitable for diffraction studies. A crystal may appear to be suitable, but when the diffraction study is done, the crystal is found to be unsuitable for a number of reasons. A crystal that appears to be crystalline can be made up of many micro crystals. This will result in the crystal giving a diffraction pattern which resembles that given by a powder with a greater or lesser degree of preferential alignment of the crystallites. Rotational disorder and/or flip disorder may be present within the crystal (i.e. CF_3 groups exhibit rotation disorder, while flip disorder can be seen in thiophene rings). Rotational disorder, like the name suggests, arises from the motion of atoms within the solid crystal. Flip disorder is seen primarily in compounds that contain substituents in the form of rings (i.e. thiophenes, phenyl, etc.). Flip disorder is much like rotational disorder, except that instead of the ring rotating, the ring is flipping back and forth rapidly. Although both

types of dynamic disorder (motion within a crystal) can usually be accommodated for, depending on the overall amount of disorder present, it may still have an effect on how well the structure of that given compound can be determined (i.e. the thermal displacement parameters of the atoms effected by the disorder may be abnormally large).

Subsection Two-Diffraction

6.1.2a Components of a Diffractometer

A. X-ray generators

The most common (and least inexpensive) type of X-ray generators is the sealed X-ray tube. Within these vacuum sealed tubes, a high DC voltage is used to accelerate electrons towards a metal anode target.^{1, 2} Upon striking the metal target, a 1s electron is ejected and sharp X-ray bands (K_{α} waves) are produced as electrons fall from the $n = 2$ quantum shell to the $n = 1$ shell.² The K_{α} wavelengths produced are dependant upon the metal being used as the target. Two suitable metals are Cu and Mo, which produce K_{α} waves at 1.54179 Å and 0.71073 Å, respectively (i.e. these are the composite values of the $K_{\alpha 1}$ and $K_{\alpha 2}$ of each).

The maximum power level of the X-ray tubes is limited primarily by how quickly heat can be removed from the tube.^{1, 2} As the electrons collide with the metal target and with themselves, heat is produced. This heat, if not properly dissipated, can melt the metal target. In order to remove this heat, the X-ray tubes are cooled by circulated water running through the back of the tube past the metal target. The tubes are not typically run at a power rating of 100%, but rather at 80% to extend the life of the tubes. This translates into a voltage of 40 kV and a current of 40 mA (1600 W of total power, 2000 W maximum power) for Cu tubes and 40 kV and 50 mA (2000 W of total power, 2500 W maximum power) for Mo tubes in our lab.

Another type of X-ray generator is the rotating anode generator. The workings of this tube are very similar to that of the sealed tubes except that the metal target now rotates. The advantages of this type of generator are that the heat is removed over a much larger area due to the tube rotation. Because of the increased power now useable, the signal-to-noise (S/N) ratio may increase up to six times that obtained by a sealed tube generator, resulting in a better data set. The disadvantages, however, outweigh the advantages for many applications. These types of generators are more costly, much bigger, and require much more user maintenance to keep them functioning properly (i.e. monthly). Since the metal target rotates while under high voltage and vacuum and with water flowing through it, it is much less reliable.

B. Detectors

The simplest type of detector used is the scintillation or point detector. This detector relies on directly measuring the X-ray beam flux rather than measuring the effects of the beam (i.e. the effects of the X-ray beam on photographic film).¹ The X-ray beam enters the detector and strikes a compound that emits photons of visible light, such as NaI.¹ The intensity of the emitted light is proportional to the intensity of the X-ray beam and is measured by a photomultiplier tube (PMT).¹ Although these types of detectors have very high counting efficiencies and are very reliable, they can only collect data on one single point at a time. Therefore, collection time tends to be rather long when a point detector is employed.

Multi-wire detectors are in the category of area detectors. Area detectors can collect a wide range of reflections at one time, meaning that the collection time when an area detector is used is much shorter than when a point detector is used. Because these types of detectors are flat, the data must be corrected to account for the differences in path length of the refracted X-ray beam. In a multi-wire detector, a wire anode array is sandwiched between two wire cathode arrays. The chamber is filled with a mixture of Xe/CO₂. The Xe is ionized upon X-rays entering the detector; the Xe⁺ ions migrate to the cathode while the electrons produced from the ionization migrate towards the anode (the CO₂ serves to absorb UV light which can erroneously activate the signal cascade). The electronic potential generated is then recorded by the detector.¹

A charge-coupled device, CCD, detector also belongs to the area detector family. Upon entering the detectors, X-rays strike a phosphor (usually doped ZnS) that emits visible light. This light is then transferred to a photocathode either directly (our APEX CCD) or *via* a fiber optic taper (other CCDs). One potential problem inherent to a CCD is that signal loss can occur through the fiber optic taper. Recent advances have corrected this problem and have also allowed for 1:1 imaging.

C. Monochromator and Collimator

A graphite crystal monochromator is often used to filter out the undesired radiation bands (Bremstrahlung, K_β, etc.) from the desired K_α band. The undesired bands are absorbed, while the K_α bands are allowed to pass through the monochromator.² This process also produces some collimation.

The collimator is a hollow tube with an internal diameter of 0.1 to 1.0 mm (0.5 mm diameter set by “pinholes” was used in the work herein).^{1, 2} The collimator reduces the angular spread of the X-ray beam and makes it nearly collinear.² The diameter of the collimator’s pin holes also determines the maximum size of the crystal. Thus, the size of the crystal cannot exceed the width of the X-ray beam as mentioned previously in this introduction.

D. Goniometer and Goniometer heads

Once a crystal has been selected, it needs to be held in place and oriented in the X-ray beam. This is done by the goniometer and the goniometer head. The crystal (if air stable) is first glued on the end of a very thin glass capillary (if the crystal is air sensitive, it can be sealed inside of a capillary tube). The capillary is fixed into a brass pin with epoxy which is then inserted into the goniometer head. This head is adjustable and allows for precise centering of the crystal so that it will constantly remain in the center of the X-ray beam. The goniometer head is then attached to the χ circle. There are four axes through which the crystal can be oriented by the goniometer: ϕ (spindle axis of the goniometer head), ω (the angle between the diffraction vector and the plane of the χ circle), χ (the angle between the ϕ axis and the base of the diffractometer), and 2θ (angle between the incident and diffracted beams). The goniometer, through direction from the host computer, can then orient the crystal at any or almost any, depending on the goniometer design, arbitrary angle along these axes.^{1, 2}

6.1.2b. Basic Principles of Diffraction

X-rays can be diffracted by electrons just as light can be diffracted by very small objects.¹ When X-rays are diffracted, a path difference is created between X-rays diffracting off of different parts of the lattice that is dependent upon the angle at which these beams are diffracted. Either constructive or deconstructive interference is then a result of the path differences.

One can think of a crystal lattice as having an infinite number of parallel planes running through it where these planes are spaced by a distance, d , from each other. The angle of the incidence of radiation is given by $90^\circ - \theta$ and is set equal to the angle of reflection.¹ For the n th reflection then, the difference in path length is given by

$$n\lambda = 2d\sin \theta$$

Equation 6.2.1. Bragg's Law

This equation is known as Bragg's Law. In order for coherent diffraction (diffraction in which the wavelength of the diffracted beam does not change, only the phase changes) to occur, the Bragg Equation must be met.¹ Since only a small number of reflections are diffracted at angles that satisfy Bragg's Law, the crystal is rotated through a number of different angular positions as described above in **subsection 1D**.

Using the analogy of diffraction of visible light by a series of slits, just as the diffraction pattern of the visible light is a result of the periodicity of the slits, the diffraction pattern of X-rays is a result of the periodicity of the crystal lattice.¹ The diffraction pattern for X-rays is determined by the atoms and the spacing of the atoms that are diffracting the X-ray beams. The diffraction pattern of X-rays by a crystal can then be further simplified into the sampling of the lattice points of an individual unit cell (smallest repeating unit in a crystal) within the crystal lattice.¹ The directions in space and the intensity of the diffracted beams can then be measured and attributed to the geometry and the arrangement of the atoms within the unit cell, respectively.

Section two- Experimental

1. 4-bromothiophene-2-carboxaldehyde

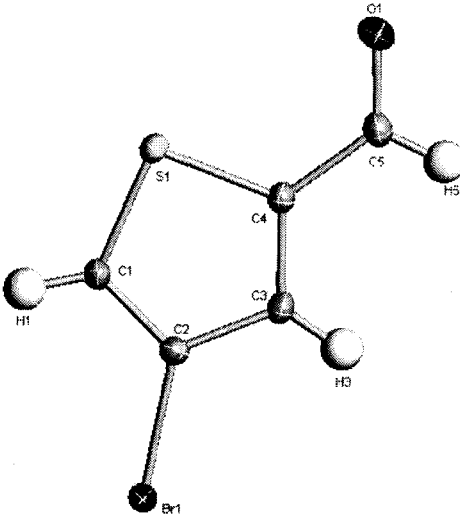
Comment

G. Crundwell from Central Connecticut State University provided the crystal investigated. It was grown from ethanol at 273 K.

All H atoms were placed in calculated positions, with C–H distances of 0.93 Å, and were included in the refinement in riding-motion approximation, with $U_{\text{iso}}(\text{H}) = 1.2U_{\text{eq}}$ of the adjacent carbon atom. This constraint was necessary due to the presences of the heavy atom bromine as the heavy atom would mask the presences of the hydrogen atoms next to it.

Table 6.2.1a. Crystal data for 03JU06am	Table 6.2.1b. Data collection
C ₅ H ₃ BrOS	Bruker SMART CCD area-detector
Mr = 191.04	diffractometer
Monoclinic, P2 ₁ /c	ω scans
$a = 4.1169 (4) \text{ \AA}$	Absorption correction: multi-scan
$b = 8.4929 (8) \text{ \AA}$	$T_{\text{min}} = 0.141, T_{\text{max}} = 0.159$
$c = 17.1626 (16) \text{ \AA}$	5955 measured reflections
$\beta = 90.788 (2)^\circ$	1499 independent reflections
$V = 600.02 (10) \text{ \AA}^3$	1408 reflections with $I > 2\sigma(I)$
Z = 4	$R_{\text{int}} = 0.034$
$D_x = 2.115 \text{ Mg m}^{-3}$	$\theta_{\text{max}} = 28.3^\circ$

Mo K_{α} radiation	$h = -5 \rightarrow 5$
Cell parameters from 5955 reflections	$k = -11 \rightarrow 11$
$\theta = 2.4 \pm 28.3^{\circ}$	$l = -22 \rightarrow 22$
$\mu = 7.08 \text{ mm}^{-1}$	
$T = 100 (2) \text{ K}$	
Cube, colorless	
$0.26 \times 0.26 \times 0.26 \text{ mm}$	

Table 6.2.1c. Refinement	Figure 6.2.1. ORTEP plot of title compound. Ellipsoids are at the 50% probability level.
<p>Refinement on F^2</p> <p>$R[F^2 > 2\sigma(F^2)] = 0.019$</p> <p>$wR(F^2) = 0.047$</p> <p>$S = 1.05$</p> <p>1499 reflections</p> <p>73 parameters</p> <p>H-atom parameters constrained</p> <p>$w = 1/[\sigma^2(F_o^2) + (0.0039P)^2 + 0.449P]$</p> <p>where $P = (F_o^2 + 2F_c^2)/3$</p> <p>$(\Delta/\sigma)_{\text{max}} = 0.004$</p> <p>$\Delta\rho_{\text{max}} = 0.50 \text{ e}\times\text{\AA}^{-3}$</p>	

$\Delta\rho_{\min} = -0.32 \text{ e}\times\text{\AA}^{-3}$	
------------------------------------------------------------	--

Table 6.2.1d

Selected geometric parameters (Å, °).

Br1–C4 1.8804 (18)	C4–C5–S1 111.27 (14)
C5–C4 1.371 (2)	C5–C4–C3 113.67 (16)
C5–S1 1.7118 (19)	C5–C4–Br1 123.40 (14)
C4–C3 1.414 (2)	C3–C4–Br1 122.92 (13)
C3–C2 1.374 (2)	C2–C3–C4 111.23 (16)
C2–C1 1.457 (2)	C3–C2–C1 125.71 (16)
C2–S1 1.7218 (17)	C3–C2–S1 112.23 (13)
O1–C1 1.213 (2)	C1–C2–S1 122.03 (14)
	C5–S1–C2 91.61 (9)
	O1–C1–C2 124.39 (18)

2. Zinc di(pyridin-2-yl)methanone diiodide

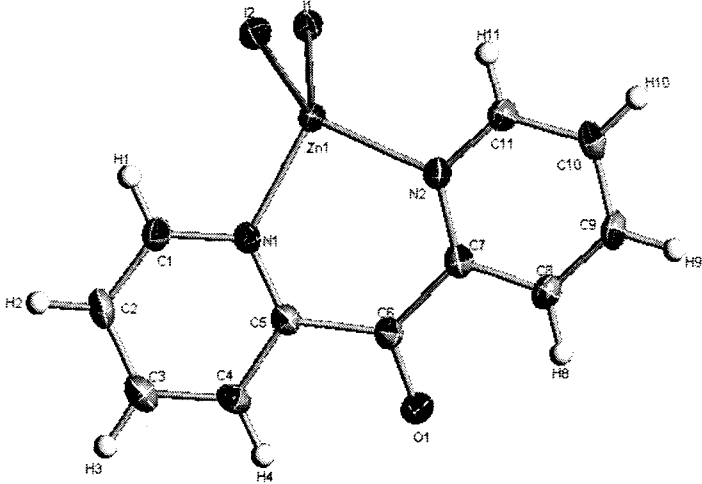
Comment

G. Crundwell from Central Connecticut State University provided the crystal investigated. It was grown from 1-butanol.

All H atoms were placed in calculated positions, with C–H distances of 0.95 Å, and were included in the refinement in riding-motion approximation, with $U_{\text{iso}}(\text{H}) = 1.2U_{\text{eq}}$ of the adjacent carbon atom. This constraint was necessary due to the presences of the heavy atom iodine as the heavy atom would mask the presences of the hydrogen atoms next to it.

Table 6.2.2a. Crystal data for 03JU07am	Table 6.2.2b. Data collection
$\text{C}_{11}\text{H}_8\text{I}_2\text{N}_2\text{OZn}$	Bruker SMART CCD area-detector
Mr = 503.36	diffractometer
Monoclinic, $P2_1/c$	ω scans
$a = 12.6266$ (5) Å	Absorption correction: multi-scan
$b = 8.3959$ (3) Å	$T_{\text{min}} = 0.42557$, $T_{\text{max}} = 0.73$
$c = 13.1079$ (5) Å	13480 measured reflections
$\beta = 103.6490$ (10)°	3344 independent reflections
$V = 1350.35$ (9) Å ³	3114 reflections with $I > 2\sigma(I)$
$Z = 4$	$R_{\text{int}} = 0.0344$
$D_x = 2.476$ Mg m ⁻³	$\theta_{\text{max}} = 28.28^\circ$
Mo K_α radiation	$h = -16 \rightarrow 16$

Cell parameters from 9564 reflections	$k = -11 \rightarrow 11$
$\theta = 2.906 \pm 28.271^\circ$	$l = -17 \rightarrow 17$
$\mu = 6.376 \text{ mm}^{-1}$	
$T = 100 (2) \text{ K}$	
Plate, yellow	
$0.29 \times 0.14 \times 0.05 \text{ mm}$	

Table 6.2.2c. Refinement	Figure 6.2.2. ORTEP plot of title compound. Ellipsoids are at the 50% probability level.
<p>Refinement on F^2</p> <p>$R[F^2 > 2\sigma(F^2)] = 0.0281$</p> <p>$wR(F^2) = 0.0742$</p> <p>$S = 1.070$</p> <p>3344 reflections</p> <p>186 parameters</p> <p>H-atom parameters constrained</p> <p>$w = 1/[\sigma^2(F_o^2) + (0.0408P)^2 + 2.3356P]$</p> <p>where $P = (F_o^2 + 2F_c^2)/3$</p> <p>$(\Delta/\sigma)_{\max} = 0.001$</p> <p>$\Delta\rho_{\max} = 1.768 \text{ e}\times\text{\AA}^{-3}$</p>	 <p>The ORTEP plot shows a complex organic molecule coordinated to a zinc atom (Zn1). The molecule consists of a fused ring system including a benzene ring (C1-C6), a five-membered ring with nitrogen (N1), and another five-membered ring with nitrogen (N2). A side chain is attached to N2, containing atoms C7, C8, C9, C10, C11 and H7, H8, H9, H10, H11. An oxygen atom (O1) is also present. Hydrogen atoms are shown as small spheres of arbitrary radii. The zinc atom (Zn1) is coordinated to the nitrogen atoms and other ligands not fully shown in this view.</p>

$\Delta\rho_{\min} = -0.618 \text{ e}\times\text{\AA}^{-3}$	
-------------------------------------------------------------	--

Table 6.2.2d.

Selected geometric parameters (Å, °).

I1—Zn1 2.5321 (5)	N2—C1—H1 118 (2)
I2—Zn1 2.5520 (5)	C2—C1—H1 120 (2)
Zn1—N1 2.036 (3)	C11—N1—C7 118.4 (3)
Zn1—N2 2.042 (3)	C11—N1—Zn1 114.9 (2)
C1—N2 1.337 (5)	C7—N1—Zn1 126.6 (2)
C1—C2 1.389 (5)	O1—C6—C5 117.0 (3)
C1—H1 0.94 (4)	O1—C6—C7 117.4 (3)
N1—C11 1.342 (5)	C5—C6—C7 125.5 (3)
N1—C7 1.346 (5)	C11—C10—C9 118.6 (3)
C6—O1 1.212 (5)	C11—C10—H10 115 (3)
C6—C5 1.516 (5)	C9—C10—H10 127 (3)
C6—C7 1.522 (5)	N2—C5—C4 121.4 (3)
C10—C11 1.375 (5)	N2—C5—C6 123.1 (3)
C10—C9 1.387 (6)	C4—C5—C6 115.6 (3)
C10—H10 0.97 (6)	C1—N2—C5 118.9 (3)
C5—N2 1.353 (5)	C1—N2—Zn1 115.0 (2)
C5—C4 1.386 (5)	C5—N2—Zn1 125.9 (2)
C9—C8 1.375 (5)	C8—C9—C10 118.9 (4)

C9—H9 0.84 (5)	C8—C9—H9 117 (3)
C3—C2 1.381 (6)	C10—C9—H9 124 (3)
C3—C4 1.392 (5)	C2—C3—C4 119.3 (3)
C3—H3 0.93 (5)	C2—C3—H3 121 (3)
C11—H11 0.85 (5)	C4—C3—H3 119 (3)
C4—H4 0.92 (4)	N1—C11—C10 123.1 (4)
C8—C7 1.393 (5)	N1—C11—H11 111 (4)
C8—H8 0.91 (4)	C10—C11—H11 126 (4)
C2—H2 1.05 (5)	C5—C4—C3 119.2 (4)
N1—Zn1—N2 93.89 (12)	C5—C4—H4 119 (3)
N1—Zn1—I1 113.98 (8)	C3—C4—H4 122 (3)
N2—Zn1—I1 111.35 (8)	C9—C8—C7 119.6 (4)
N1—Zn1—I2 108.79 (9)	C9—C8—H8 119 (3)
N2—Zn1—I2 112.14 (8)	C7—C8—H8 121 (3)
I1—Zn1—I2 114.860 (17)	C3—C2—C1 118.3 (3)
N2—C1—C2 122.9 (3)	C3—C2—H2 121 (3)
	C1—C2—H2 120 (3)
	N1—C7—C8 121.3 (3)
	N1—C7—C6 122.7 (3)
	C8—C7—C6 115.9 (3)

3. Zinc di(pyridin-2-yl)methanone dibromide

Comment

G. Crundwell from Central Connecticut State University provided the crystal investigated. It was grown from an acetonitrile/dichloromethane mixture.

All H atoms were placed in calculated positions, with C–H distances of 0.95 Å, and were included in the refinement in riding-motion approximation, with $U_{\text{iso}}(\text{H}) = 1.2U_{\text{eq}}$ of the adjacent carbon atom.

The bromine analogue, like the iodine version, crystallizes in $P2_1/c$. The cell parameters are on average 0.3 Å shorter than that of its iodine brethren, as are the Zn–Br bond distances compared to the Zn–I bond distances. This is to be expected, as iodine is bigger than bromine. The iodine analogue appears to have refined better (judging by the R values) than its bromine counterpart.

Table 6.2.3a. Crystal data for 03JU13am	Table 6.2.3b. Data collection
$\text{C}_{11}\text{H}_8\text{N}_2\text{Br}_2\text{OZn}$	Bruker SMART CCD area-detector
Mr = 409.38	diffractometer
Monoclinic, $P2_1/c$	ω scans
$a = 12.300$ (2) Å	Absorption correction: multi-scan
$b = 8.0699$ (16) Å	$T_{\text{min}} = 0.15$, $T_{\text{max}} = 0.27$
$c = 12.751$ (3) Å	11266 measured reflections

$\beta = 103.229 (3)^\circ$	3052 independent reflections
$V = 1232.1 (4) \text{ \AA}^3$	2600 reflections with $I > 2\sigma(I)$
$Z = 4$	$R_{\text{int}} = 0.0579$
$D_x = 2.207 \text{ Mg m}^{-3}$	$\theta_{\text{max}} = 28.36^\circ$
Mo K_α radiation	$h = -16 \rightarrow 16$
Cell parameters from 7592 reflections	$k = -10 \rightarrow 10$
$\theta = 2.62 \pm 28.381^\circ$	$l = -16 \rightarrow 17$
$\mu = 8.461 \text{ mm}^{-1}$	
$T = 100 (2) \text{ K}$	
Block, colorless	
$0.264 \times 0.195 \times 0.152 \text{ mm}$	

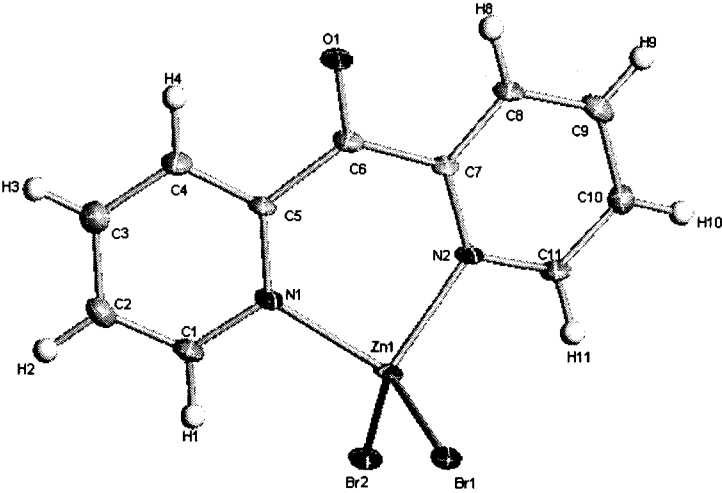
Table 6.2.3c. Refinement	Figure 6.2.3. ORTEP plot of title compound. Ellipsoids are at the 50% probability level.
Refinement on F^2 $R[F^2 > 2\sigma(F^2)] = 0.0408$ $wR(F^2) = 0.1005$ $S = 1.003$ 3052 reflections 154 parameters H-atom parameters constrained $w = 1/[\sigma^2(F_o^2) + (0.0605P)^2 + 0.0000P]$ where $P = (F_o^2 + 2F_c^2)/3$ $(\Delta/\sigma)_{\max} = 0.001$ $\Delta\rho_{\max} = 1.973 \text{ e}\times\text{\AA}^{-3}$ $\Delta\rho_{\min} = -1.356 \text{ e}\times\text{\AA}^{-3}$	 <p>The ORTEP plot shows a complex organic molecule with a central zinc atom (Zn1) coordinated to two bromine atoms (Br1, Br2) and two nitrogen atoms (N1, N2). The organic part consists of two fused six-membered rings containing nitrogen atoms (N1, N2) and a side chain with an oxygen atom (O1). Carbon atoms are labeled C1 through C11, and hydrogen atoms are labeled H1 through H11. The structure is shown with ellipsoids at the 50% probability level.</p>

Table 6.2.3d.

Selected geometric parameters (Å, °).

Br1—Zn1 2.3435 (7)	C1—N1—C5 118.1 (3)
Br2—Zn1 2.3658 (7)	C1—N1—Zn1 115.2 (3)
Zn1—N1 2.029 (3)	C5—N1—Zn1 126.7 (3)
Zn1—N2 2.040 (3)	O1—C6—C7 116.9 (3)
N2—C11 1.346 (5)	O1—C6—C5 116.8 (3)
N2—C7 1.357 (5)	C7—C6—C5 126.0 (3)
N1—C1 1.347 (5)	N2—C7—C8 120.8 (3)
N1—C5 1.359 (5)	N2—C7—C6 122.7 (3)
C6—O1 1.213 (5)	C8—C7—C6 116.6 (3)
C6—C7 1.518 (5)	N1—C1—C2 123.1 (4)
C6—C5 1.521 (5)	N1—C1—H1 118.4
C7—C8 1.395 (5)	C2—C1—H1 118.4
C1—C2 1.382 (6)	C1—C2—C3 118.7 (4)
C1—H1 0.9500	C1—C2—H2 120.6
C2—C3 1.383 (6)	C3—C2—H2 120.6
C2—H2 0.9500	N1—C5—C4 121.6 (3)
C5—C4 1.386 (5)	N1—C5—C6 122.0 (3)
C3—C4 1.388 (6)	C4—C5—C6 116.4 (3)
C3—H3 0.9500	C2—C3—C4 119.0 (4)
C11—C10 1.386 (5)	C2—C3—H3 120.5
C11—H11 0.9500	C4—C3—H3 120.5

C9—C10 1.380 (6)	N2—C11—C10 122.5 (4)
C9—C8 1.384 (5)	N2—C11—H11 118.7
C9—H9 0.9500	C10—C11—H11 118.7
C8—H8 0.9500	C10—C9—C8 119.1 (4)
C10—H10 0.9500	C10—C9—H9 120.5
C4—H4 0.9500	C8—C9—H9 120.5
N1—Zn1—N2 94.16 (13)	C9—C8—C7 119.8 (4)
N1—Zn1—Br1 113.32 (9)	C9—C8—H8 120.1
N2—Zn1—Br1 110.52 (9)	C7—C8—H8 120.1
N1—Zn1—Br2 108.42 (9)	C9—C10—C11 118.9 (4)
N2—Zn1—Br2 111.46 (9)	C9—C10—H10 120.6
Br1—Zn1—Br2 116.72 (2)	C11—C10—H10 120.6
C11—N2—C7 118.9 (3)	C5—C4—C3 119.5 (4)
C11—N2—Zn1 115.1 (2)	C5—C4—H4 120.2
C7—N2—Zn1 125.9 (3)	C3—C4—H4 120.2

4. N-(9 H-fluoren-9-ylidene)-N-(4-methoxyphenyl)amine

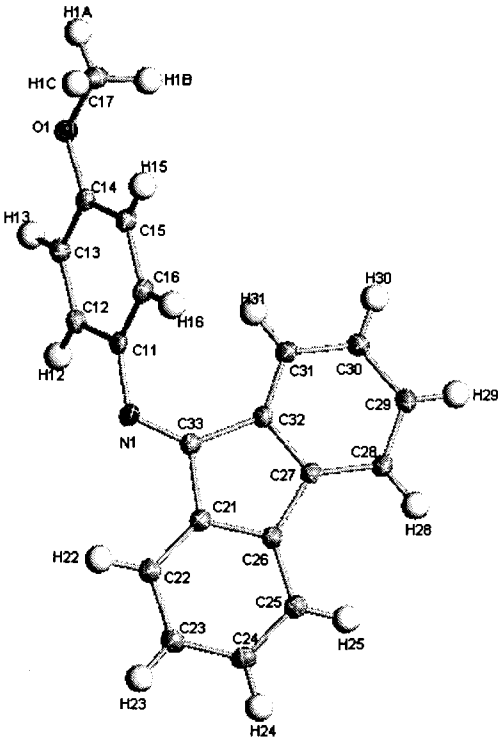
Comment

G. Crundwell from Central Connecticut State University provided the crystal investigated. It was made by heating 9-fluorenone, 4-methoxyaniline, *p*-toluenesulfonic acid and toluene under reflux for 24 h.

All H atoms were placed in calculated positions, with aromatic and methyl C–H distances of 0.95 and 0.98 Å, respectively, and were included in the refinement in riding-motion approximation, with $U_{\text{iso}}(\text{H}) = 1.2U_{\text{eq}}$ of the adjacent carbon atom.

Table 6.2.4a. Crystal data for 03JU10am	Table 6.2.4b. Data collection
$\text{C}_{20}\text{H}_{15}\text{NO}$	Bruker SMART CCD area-detector
$M_r = 285.33$	diffractometer
Monoclinic, $C2/c$	ω scans
$a = 19.0275 (10) \text{ \AA}$	Absorption correction: multi-scan
$b = 9.8262 (5) \text{ \AA}$	$T_{\text{min}} = 0.922, T_{\text{max}} = 0.968$
$c = 17.4862 (10) \text{ \AA}$	14415 measured reflections
$\beta = 118.4860 (10)^\circ$	3565 independent reflections
$V = 2873.5 (3) \text{ \AA}^3$	3287 reflections with $I > 2\sigma(I)$
$Z = 8$	$R_{\text{int}} = 0.042$
$D_x = 1.319 \text{ Mg m}^{-3}$	$\theta_{\text{max}} = 28.3^\circ$
Mo K_α radiation	$h = -25 \rightarrow 25$
Cell parameters from 14878 reflections	$k = -13 \rightarrow 13$

$\theta = 2.4 \pm 28.3^\circ$ $\mu = 0.08 \text{ mm}^{-1}$ $T = 100 (2) \text{ K}$ Parallelepiped, orange $0.60 \times 0.56 \times 0.35 \text{ mm}$	$l = -23 \rightarrow 23$
-----------------------------------------------------------------------------------------------------------------------------------------------------------------	--------------------------

Table 6.2.4c. Refinement	Figure 6.2.4. ORTEP plot of title compound. Ellipsoids are at the 50% probability level.
Refinement on F^2 $R[F^2 > 2\sigma(F^2)] = 0.042$ $wR(F^2) = 0.115$ $S = 1.08$ 3287 reflections 199 parameters H-atom parameters constrained $w = 1/[\sigma^2(F_o^2) + (0.0646P)^2 + 1.5364P]$ where $P = (F_o^2 + 2F_c^2)/3$ $(\Delta/\sigma)_{\text{max}} = 0.003$ $\Delta\rho_{\text{max}} = 0.37 \text{ e}\times\text{\AA}^{-3}$	

$$\Delta\rho_{\min} = -0.28 \text{ e}\times\text{\AA}^{-3}$$

Table 6.2.4d.

Selected geometric parameters (Å, °).

O1—C14 1.3758 (11)	C31—C32—C33 132.28 (9)
O1—C17 1.4235 (12)	C27—C32—C33 107.71 (8)
N1—C33 1.2816 (12)	C16—C11—C12 118.84 (9)
N1—C11 1.4186 (12)	C16—C11—N1 121.79 (9)
C16—C11 1.3914 (13)	C12—C11—N1 118.93 (9)
C16—C15 1.3953 (13)	C13—C12—C11 120.59 (9)
C16—H16 0.973 (14)	C13—C12—H12 119.8 (8)
C33—C21 1.4874 (13)	C11—C12—H12 119.6 (8)
C33—C32 1.4983 (12)	C12—C13—C14 119.99 (9)
C15—C14 1.3915 (13)	C12—C13—H13 121.0 (8)
C15—H15 0.955 (14)	C14—C13—H13 119.0 (8)
C32—C31 1.3904 (13)	C24—C23—C22 120.45 (9)
C32—C27 1.4125 (13)	C24—C23—H23 117.9 (8)
C11—C12 1.4008 (13)	C22—C23—H23 121.6 (8)
C12—C13 1.3853 (14)	C25—C26—C21 120.57 (9)
C12—H12 0.961 (14)	C25—C26—C27 131.06 (9)
C13—C14 1.3966 (13)	C21—C26—C27 108.27 (8)
C13—H13 0.982 (14)	C22—C21—C26 121.30 (9)

C23—C24 1.3950 (14)	C22—C21—C33 129.55 (9)
C23—C22 1.3955 (14)	C26—C21—C33 109.12 (8)
C23—H23 0.966 (14)	C26—C25—C24 118.06 (9)
C26—C25 1.3881 (13)	C26—C25—H25 120.6 (8)
C26—C21 1.4025 (13)	C24—C25—H25 121.3 (8)
C26—C27 1.4717 (13)	O1—C14—C15 124.18 (8)
C21—C22 1.3846 (13)	O1—C14—C13 115.74 (8)
C25—C24 1.3962 (14)	C15—C14—C13 120.08 (9)
C25—H25 0.991 (14)	C27—C28—C29 118.36 (9)
C28—C27 1.3855 (13)	C27—C28—H28 120.5 (8)
C28—C29 1.3934 (14)	C29—C28—H28 121.1 (8)
C28—H28 0.979 (14)	C32—C31—C30 118.54 (9)
C31—C30 1.3994 (13)	C32—C31—H31 121.5 (8)
C31—H31 0.995 (14)	C30—C31—H31 120.0 (8)
C29—C30 1.3920 (14)	C28—C27—C32 121.45 (9)
C29—H29 0.995 (16)	C28—C27—C26 129.11 (9)
C30—H30 1.001 (14)	C32—C27—C26 109.30 (8)
C22—H22 0.998 (15)	C30—C29—C28 120.63 (9)
C24—H24 0.982 (14)	C30—C29—H29 119.1 (9)
C17—H1C 0.977 (16)	C28—C29—H29 120.2 (9)
C17—H1B 1.015 (16)	C29—C30—C31 121.19 (9)
C17—H1A 0.980 (16)	C29—C30—H30 120.6 (8)
C14—O1—C17 116.75 (7)	C31—C30—H30 118.2 (8)

C33—N1—C11 122.13 (8)	C21—C22—C23 118.28 (9)
C11—C16—C15 121.02 (9)	C21—C22—H22 121.5 (9)
C11—C16—H16 120.4 (8)	C23—C22—H22 120.2 (9)
C15—C16—H16 118.6 (8)	C23—C24—C25 121.32 (9)
N1—C33—C21 121.05 (8)	C23—C24—H24 119.1 (8)
N1—C33—C32 133.31 (9)	C25—C24—H24 119.6 (8)
C21—C33—C32 105.59 (7)	O1—C17—H1C 109.5 (9)
C14—C15—C16 119.44 (9)	O1—C17—H1B 110.2 (9)
C14—C15—H15 121.0 (8)	H1C—C17—H1B 110.2 (13)
C16—C15—H15 119.5 (8)	O1—C17—H1A 106.6 (9)
C31—C32—C27 119.80 (9)	H1C—C17—H1A 108.5 (13)
	H1B—C17—H1A 111.7 (12)

5. 2,3-bis(5-bromothien-2-yl)quinoxaline

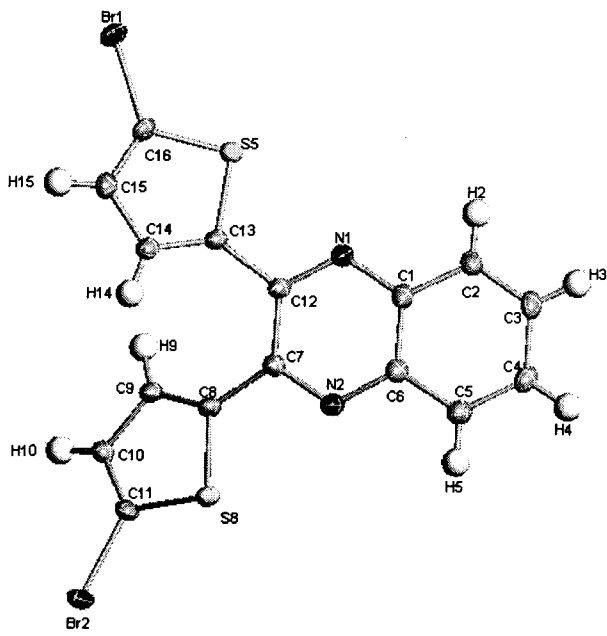
Comment

G. Crundwell from Central Connecticut State University provided the crystal investigated. It was made by reacting 1,2-phenylenediamine and 1,2-bis(5-bromothien-2-yl)-1,2-ethanedione in boiling ethanol.

All H atoms were placed in calculated positions, with C–H distance of 0.95 Å, and were included in the refinement in riding-motion approximation, with $U_{\text{iso}}(\text{H}) = 1.2U_{\text{eq}}$ of the adjacent carbon atom.

Table 6.2.5a. Crystal data for 03JU11am	Table 6.2.5b. Data collection
$\text{C}_{16}\text{H}_8\text{Br}_2\text{N}_2\text{S}_2$	Bruker SMART CCD area-detector
Mr = 452.18	diffractometer
Triclinic, $P\bar{1}$	ω scans
$a = 8.8701$ (9) Å	Absorption correction: multi-scan
$b = 9.0664$ (9) Å	$T_{\text{min}} = 0.018$, $T_{\text{max}} = 0.466$
$c = 11.1751$ (11) Å	7531 measured reflections
$\beta = 79.998$ (2)°	3818 independent reflections
$V = 781.51$ (13) Å ³	3126 reflections with $I > 2\sigma(I)$
$Z = 2$	$R_{\text{int}} = 0.044$
$D_x = 1.922$ Mg m ⁻³	$\theta_{\text{max}} = 28.4^\circ$

Mo K_{α} radiation	$h = -11 \rightarrow 11$
Cell parameters from 7531 reflections	$k = -12 \rightarrow 12$
$\theta = 1.9 \pm 28.4^{\circ}$	$l = -14 \rightarrow 14$
$\mu = 5.45 \text{ mm}^{-1}$	
$T = 100 (2) \text{ K}$	
Thick plate, yellow	
$0.88 \times 0.35 \times 0.14 \text{ mm}$	

Table 6.2.5c.	Figure 6.2.5. ORTEP plot of title compound. Ellipsoids are at the 50% probability level.
Refinement	
Refinement on F^2	
$R[F^2 > 2\sigma(F^2)] = 0.044$	
$wR(F^2) = 0.119$	
$S = 0.85$	
3818 reflections	
199 parameters	
H-atom parameters constrained	
$w = 1/[\sigma^2(F_o^2) + (0.0927P)^2]$	
where $P = (F_o^2 + 2F_c^2)/3$	
	

$(\Delta/\sigma)_{\max} = 0.001$ $\Delta\rho_{\max} = 1.39 \text{ e}\times\text{\AA}^{-3}$ $\Delta\rho_{\min} = -1.08 \text{ e}\times\text{\AA}^{-3}$	
-------------------------------------------------------------------------------------------------------------------------------------------------------------	--

Table 6.2.5d.Selected geometric parameters (\AA , $^\circ$).

Br2—C18 1.875 (3)	N1—C10—C15 114.6 (3)
Br1—C14 1.877 (3)	C1—C10—C15 124.2 (3)
S2—C18 1.721 (3)	C1—N2—C3 118.6 (3)
S2—C15 1.730 (3)	N1—C8—C3 120.8 (3)
S1—C14 1.722 (3)	N1—C8—C7 120.1 (3)
S1—C11 1.736 (3)	C3—C8—C7 119.1 (3)
C13—C14 1.350 (5)	C10—N1—C8 118.2 (3)
C13—C12 1.424 (4)	C11—C12—C13 113.4 (3)
C13—H13 0.9500	C11—C12—H12 123.3
C10—N1 1.318 (4)	C13—C12—H12 123.3
C10—C1 1.451 (4)	C17—C18—S2 113.1 (2)
C10—C15 1.477 (4)	C17—C18—Br2 127.0 (3)
N2—C1 1.326 (4)	S2—C18—Br2 119.70 (18)
N2—C3 1.362 (4)	C15—C16—C17 113.3 (3)
C8—N1 1.361 (4)	C15—C16—H16 123.4
C8—C3 1.418 (5)	C17—C16—H16 123.4

C8—C7 1.423 (4)	C16—C15—C10 131.1 (3)
C12—C11 1.371 (4)	C16—C15—S2 111.4 (2)
C12—H12 0.9500	C10—C15—S2 117.1 (2)
C18—C17 1.360 (5)	C12—C11—C1 131.6 (3)
C16—C15 1.370 (4)	C12—C11—S1 110.9 (2)
C16—C17 1.415 (5)	C1—C11—S1 117.0 (2)
C16—H16 0.9500	C7—C6—C5 121.3 (3)
C11—C1 1.465 (4)	C7—C6—H6 119.4
C6—C7 1.368 (5)	C5—C6—H6 119.4
C6—C5 1.413 (5)	N2—C3—C4 119.5 (3)
C6—H6 0.9500	N2—C3—C8 120.1 (3)
C3—C4 1.412 (5)	C4—C3—C8 120.1 (3)
C4—C5 1.376 (5)	C5—C4—C3 119.5 (3)
C4—H4 0.9500	C5—C4—H4 120.2
C5—H5 0.9500	C3—C4—H4 120.2
C17—H17 0.9500	N2—C1—C10 120.1 (3)
C7—H7 0.9500	N2—C1—C11 114.5 (3)
C18—S2—C15 90.67 (15)	C10—C1—C11 125.4 (3)
C14—S1—C11 90.77 (15)	C4—C5—C6 120.4 (3)
C14—C13—C12 111.4 (3)	C4—C5—H5 119.8
C14—C13—H13 124.3	C6—C5—H5 119.8
C12—C13—H13 124.3	C18—C17—C16 111.5 (3)
C13—C14—S1 113.4 (2)	C18—C17—H17 124.2

C13—C14—Br1 126.4 (2)	C16—C17—H17 124.2
S1—C14—Br1 120.16 (19)	C6—C7—C8 119.5 (3)
N1—C10—C1 121.1 (3)	C6—C7—H7 120.3
	C8—C7—H7 120.3

6. 5,10,15,20-tetrakis(5'-methylthien-2'-yl)porphyrin

Comment

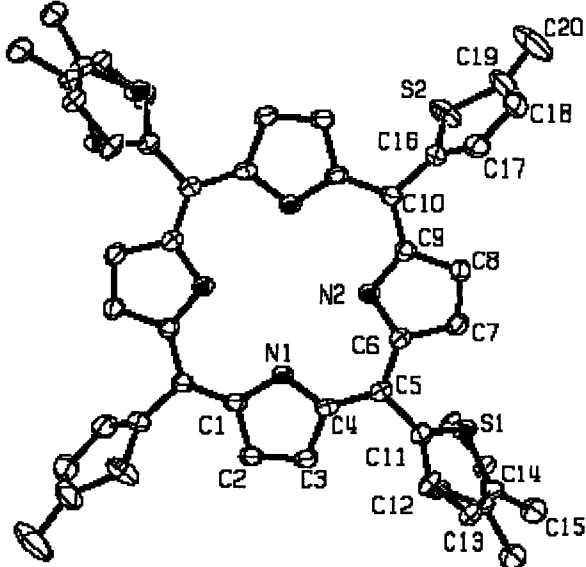
G. Crundwell from Central Connecticut State University provided the crystal investigated. It was prepared by the condensation of pyrrole and 5-methyl-2-thiophenecarboxaldehyde.

All H atoms were placed in calculated positions, with aromatic and methyl C–H distances of 0.95–0.98 Å, respectively, and were included in the refinement in riding-motion approximation, with $U_{\text{iso}}(\text{H}) = 1.2\text{--}1.5U_{\text{eq}}$ of the adjacent carbon atom. The placement of the imino hydrogen on N1 was arbitrary, or from a difference map (i.e. Q peaks): placement on N1 over N2 had no significant effect on the refinement.

The major and minor components of ring 1 were modeled to be structurally equivalent. Thus, restraints were applied so that the overall geometry of the two component rings were identical. Due to the closeness of some of the disordered atoms, it also became necessary to define the thermal displacement parameters (and consequently their thermal ellipsoids) to be the same (e.g. C11 and C11B were given the same displacement parameters, as were C12 and C12B, C13 and C13B, seven sets of atoms in total).

Table 6.2.6a. Crystal data for 03JU12am	Table 6.2.6b. Data collection
$\text{C}_{40}\text{H}_{30}\text{N}_4\text{S}_4$	Bruker SMART CCD area-detector
Mr = 452.18	diffractometer

Triclinic, $P\bar{1}$	ω scans
$a = 6.5126 (7) \text{ \AA}$	Absorption correction: multi-scan
$b = 10.499 (1) \text{ \AA}$	$T_{\min} = 0.659241, T_{\max} = 1$
$c = 12.635 (1) \text{ \AA}$	8653 measured reflections
$\beta = 79.141 (2)^\circ$	4124 independent reflections
$V = 846.7 (16) \text{ \AA}^3$	3692 reflections with $I > 2\sigma(I)$
$Z = 1$	$R_{\text{int}} = 0.0314$
$D_x = 1.363 \text{ Mg m}^{-3}$	$\theta_{\max} = 28.29^\circ$
Mo K_α radiation	$h = -8 \rightarrow 8$
Cell parameters from 7344 reflections	$k = -13 \rightarrow 13$
$\theta = 2.5095 \pm 28.2875^\circ$	$l = -16 \rightarrow 16$
$\mu = 0.317 \text{ mm}^{-1}$	
$T = 100 (2) \text{ K}$	
Thin plate, purple	
$0.7 \times 0.6 \times 0.033 \text{ mm}$	

<p>Table 6.2.6c. Refinement</p>	<p>Figure 6.2.6. ORTEP plot of title compound. Ellipsoids are at the 50% probability level.</p>
<p>Refinement on F^2</p> <p>$R[F^2 > 2\sigma(F^2)] = 0.0579$</p> <p>$wR(F^2) = 0.149$</p> <p>$S = 1.087$</p> <p>4124 reflections</p> <p>255 parameters</p> <p>H-atom parameters constrained</p> <p>$w = 1/[\sigma^2(F_o^2) + (0.0604P)^2 + 0.7520P]$</p> <p>where $P = (F_o^2 + 2F_c^2)/3$</p> <p>$(\Delta/\sigma)_{\max} = 0.000$</p> <p>$\Delta\rho_{\max} = 0.536 \text{ e}\times\text{\AA}^{-3}$</p> <p>$\Delta\rho_{\min} = -0.516 \text{ e}\times\text{\AA}^{-3}$</p>	

<p>Table 6.2.6d. Selected geometric parameters (\AA, $^\circ$).</p>	
<p>S1—C16 1.685 (3)</p> <p>S1—C19 1.743 (3)</p> <p>C16—C5 1.467 (3)</p> <p>C16—C17 1.473 (4)</p> <p>C17—C18 1.289 (5)</p>	<p>C5—C16A—C17A 120.56 (14)</p> <p>C18A—C17A—C16A 115.1</p> <p>C18A—C17A—H17A 122.4</p> <p>C16A—C17A—H17A 122.4</p> <p>C17A—C18A—C19A 113.6</p>

C17—H17 0.9500	C17A—C18A—H18A 123.2
C18—C19 1.340 (4)	C19A—C18A—H18A 123.2
C18—H18 0.9500	C20A—C19A—C18A 124.6
C19—C20 1.506 (3)	C20A—C19A—S1A 125.15 (11)
C20—H20A 0.9800	C18A—C19A—S1A 105.4
C20—H20B 0.9800	C19A—C20A—H20D 109.5
C20—H20C 0.9800	C19A—C20A—H20E 109.5
S1A—C16A 1.4121	H20D—C20A—H20E 109.5
S1A—C19A 1.7787	C19A—C20A—H20F 109.5
C16A—C5 1.516 (3)	H20D—C20A—H20F 109.5
C16A—C17A 1.7087	H20E—C20A—H20F 109.5
C17A—C18A 1.0785	C11—S2—C14 92.56 (15)
C17A—H17A 0.9500	C6—N2—C9 106.16 (18)
C18A—C19A 1.5079	C6—N2—H1B 120 (7)
C18A—H18A 0.9500	C9—N2—H1B 133 (7)
C19A—C20A 1.4940 (16)	C1—N1—C4 109.62 (17)
C20A—H20D 0.9800	C1—N1—H1A 126 (3)
C20A—H20E 0.9800	C4—N1—H1A 125 (3)
C20A—H20F 0.9800	N2—C6—C5 126.39 (19)
S2—C11 1.729 (3)	N2—C6—C7 110.29 (18)
S2—C14 1.729 (3)	C5—C6—C7 123.32 (19)
N2—C6 1.365 (3)	C4—C5—C6 125.38 (19)
N2—C9 1.369 (3)	C4—C5—C16 116.6 (2)

N2—H1B 0.66 (8)	C6—C5—C16 118.0 (2)
N1—C1 1.366 (3)	C4—C5—C16A 116.5 (3)
N1—C4 1.372 (3)	C6—C5—C16A 118.1 (3)
N1—H1A 0.79 (4)	C16—C5—C16A 1.3 (2)
C6—C5 1.409 (3)	N2—C9—C10 125.80 (19)
C6—C7 1.448 (3)	N2—C9—C8 110.00 (18)
C5—C4 1.401 (3)	C10—C9—C8 124.21 (19)
C9—C10 1.407 (3)	C2—C3—C4 107.63 (19)
C9—C8 1.448 (3)	C2—C3—H3 128.6 (16)
C3—C2 1.358 (3)	C4—C3—H3 123.7 (16)
C3—C4 1.439 (3)	N1—C4—C5 126.18 (18)
C3—H3 0.95 (3)	N1—C4—C3 107.31 (18)
C10—C1i 1.399 (3)	C5—C4—C3 126.43 (19)
C10—C11 1.480 (3)	C1i—C10—C9 125.65 (19)
C1—C10i 1.399 (3)	C1i—C10—C11 116.85 (18)
C1—C2 1.436 (3)	C9—C10—C11 117.50 (19)
C7—C8 1.350 (3)	N1—C1—C10i 126.69 (18)
C7—H7 0.94 (3)	N1—C1—C2 107.44 (18)
C2—H2 0.93 (3)	C10i—C1—C2 125.68 (19)
C8—H8 0.93 (3)	C8—C7—C6 106.64 (19)
C11—C12 1.362 (3)	C8—C7—H7 128.2 (16)
C14—C13 1.336 (5)	C6—C7—H7 125.0 (16)
C14—C15 1.506 (5)	C3—C2—C1 107.99 (19)

C12—C13 1.425 (4)	C3—C2—H2 130.9 (17)
C12—H12 0.92 (3)	C1—C2—H2 121.0 (17)
C13—H13 0.94 (4)	C7—C8—C9 106.91 (19)
C15—H15A 0.9800	C7—C8—H8 128.0 (16)
C15—H15B 0.9800	C9—C8—H8 125.1 (16)
C15—H15C 0.9800	C12—C11—C10 130.2 (2)
C16—S1—C19 93.57 (14)	C12—C11—S2 110.00 (19)
C5—C16—C17 130.4 (3)	C10—C11—S2 119.71 (17)
C5—C16—S1 124.6 (2)	C13—C14—C15 130.1 (3)
C17—C16—S1 105.0 (2)	C13—C14—S2 110.5 (2)
C18—C17—C16 117.3 (3)	C15—C14—S2 119.5 (3)
C18—C17—H17 121.3	C11—C12—C13 112.9 (3)
C16—C17—H17 121.3	C11—C12—H12 125.9 (18)
C17—C18—C19 113.4 (3)	C13—C12—H12 121.2 (18)
C17—C18—H18 123.3	C14—C13—C12 114.0 (3)
C19—C18—H18 123.3	C14—C13—H13 126 (2)
C18—C19—C20 129.3 (3)	C12—C13—H13 120 (2)
C18—C19—S1 110.74 (19)	C14—C15—H15A 109.5
C20—C19—S1 119.9 (2)	C14—C15—H15B 109.5
C16A—S1A—C19A 97.7	H15A—C15—H15B 109.5
S1A—C16A—C5 132.19 (14)	C14—C15—H15C 109.5
S1A—C16A—C17A 107.2	H15A—C15—H15C 109.5
	H15B—C15—H15C 109.5

7. 1,2-bis(4-bromothiopen-2-yl)ethane-1,2-dione

Comment

G. Crundwell from Central Connecticut State University provided the crystal investigated. It was grown from ethanol.

All H atoms were placed in calculated positions, with C–H distances of 0.95 Å, and were included in the refinement in riding-motion approximation, with $U_{\text{iso}}(\text{H}) = 1.2U_{\text{eq}}$ of the adjacent carbon atom.

Table 6.2.7a. Crystal data for 03JU15am	Table 6.2.7b. Data collection
$\text{C}_{10}\text{H}_4\text{S}_2\text{Br}_2\text{O}_2$	Bruker SMART CCD area-detector
Mr = 380.07	diffractometer
Orthorhombic, $P2_12_12$	ω scans
$a = 8.522(2) \text{ \AA}$	Absorption correction: multi-scan
$b = 16.890(4) \text{ \AA}$	$T_{\text{min}} = 0.0936, T_{\text{max}} = 0.28$
$c = 3.89331(9) \text{ \AA}$	5622 measured reflections
$V = 560.4(2) \text{ \AA}^3$	1402 independent reflections
$Z = 2$	1368 reflections with $I > 2\sigma(I)$
$D_x = 2.253 \text{ Mg m}^{-3}$	$R_{\text{int}} = 0.0750$
Mo K_{α} radiation	$\theta_{\text{max}} = 28.31^\circ$
Cell parameters from 5567 reflections	$h = -11 \rightarrow 11$
$\theta = 2.390 \pm 28.3075^\circ$	$k = -22 \rightarrow 22$

$\mu = 7.583 \text{ mm}^{-1}$	$l = -5 \rightarrow 5$
$T = 100 (2) \text{ K}$	
Block, colorless	
$0.49 \times 0.27 \times 0.17 \text{ mm}$	

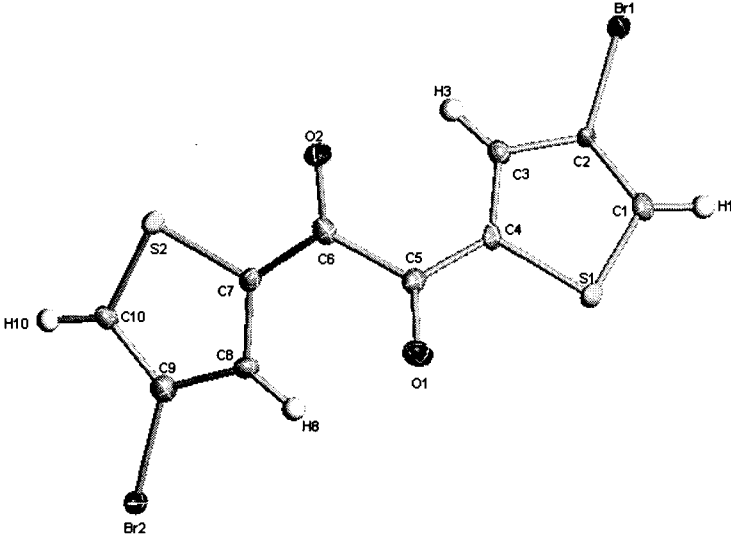
Table 6.2.7c. Refinement	Figure 6.2.7. ORTEP plot of title compound. Ellipsoids are at the 50% probability level.
<p>Refinement on F^2</p> <p>$R[F^2 > 2\sigma(F^2)] = 0.0303$</p> <p>$wR(F^2) = 0.0758$</p> <p>$S = 1.064$</p> <p>1402 reflections</p> <p>73 parameters</p> <p>H-atom parameters constrained</p> <p>$w = 1/[\sigma^2(F_o^2) + (0.0405P)^2 + 0.0000P]$</p> <p>where $P = (F_o^2 + 2F_c^2)/3$</p> <p>$(\Delta/\sigma)_{\max} = 0.001$</p> <p>$\Delta\rho_{\max} = 0.946 \text{ e}\times\text{\AA}^{-3}$</p> <p>$\Delta\rho_{\min} = -0.801 \text{ e}\times\text{\AA}^{-3}$</p>	

Table 6.2.7d.

Selected geometric parameters (Å, °).

Br1—C3 1.886 (3)	C4—C3—Br1 124.1 (2)
S1—C4 1.712 (3)	C2—C3—Br1 121.9 (2)
S1—C1 1.730 (3)	C2—C1—C5 129.0 (3)
C3—C4 1.363 (4)	C2—C1—S1 112.0 (2)
C3—C2 1.414 (4)	C5—C1—S1 119.0 (2)
C1—C2 1.377 (4)	C3—C4—S1 111.5 (2)
C1—C5 1.462 (4)	C3—C4—H4 124.3
C4—H4 0.9500	S1—C4—H4 124.3
C2—H2 0.9500	C1—C2—C3 111.0 (3)
O1—C5 1.226 (4)	C1—C2—H2 124.5
C5—C5i 1.531 (6)	C3—C2—H2 124.5
C4—S1—C1 91.42 (15)	O1—C5—C1 123.4 (3)
C4—C3—C2 114.1 (3)	O1—C5—C5i 120.0 (3)
	C1—C5—C5i 116.6 (3)

8. 5-nitro-2-thiophenecarboxaldehyde

Comment

G. Crundwell from Central Connecticut State University provided the crystal investigated. It was grown by re-crystallizing commercially available material from benzene (material purchased from Aldrich).

All H atoms were placed in calculated positions, with C–H distances of 0.95 Å, and were included in the refinement in riding-motion approximation, with $U_{\text{iso}}(\text{H}) = 1.2U_{\text{eq}}$ of the adjacent carbon atom.

Table 6.2.8a. Crystal data for 04JU06a	Table 6.2.8b. Data collection
$\text{C}_5\text{H}_3\text{SNO}_3$	Bruker SMART CCD area-detector
Mr = 157.14	diffractometer
Orthorhombic, $Pn_{a2(1)}$	ω scans
$a = 11.409 (5) \text{ \AA}$	Absorption correction: multi-scan
$b = 13.936 (6) \text{ \AA}$	$T_{\text{min}} = 0.77, T_{\text{max}} = 0.9$
$c = 3.8479 (17) \text{ \AA}$	5484 measured reflections
$V = 611.8 (5) \text{ \AA}^3$	1513 independent reflections
Z = 4	1482 reflections with $I > 2\sigma(I)$
$D_x = 1.706 \text{ Mg m}^{-3}$	$R_{\text{int}} = 0.0555$
Mo K_{α} radiation	$\theta_{\text{max}} = 28.35^\circ$
Cell parameters from 5589 reflections	$h = -14 \rightarrow 14$

$\theta = 2.307 \pm 28.348^\circ$	$k = -18 \rightarrow 18$
$\mu = 0.463 \text{ mm}^{-1}$	$l = -5 \rightarrow 5$
$T = 100 (2) \text{ K}$	
Block, brown	
$0.55 \times 0.24 \times 0.24 \text{ mm}$	

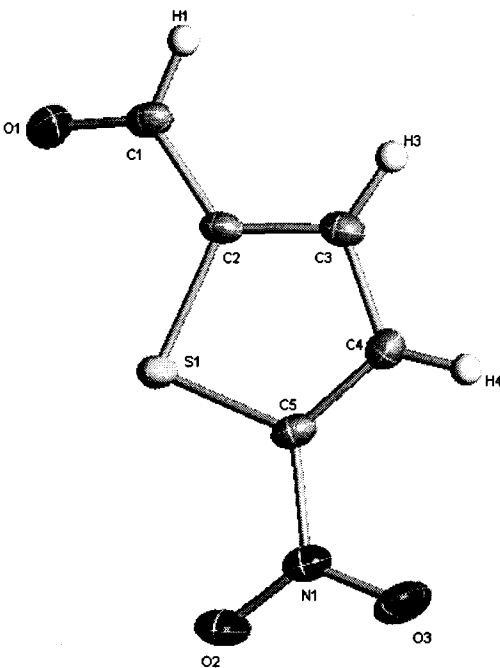
Table 6.2.8c.	Figure 6.2.8. ORTEP plot of title compound. Ellipsoids are at the 50% probability level.
Refinement	
Refinement on F^2	
$R[F^2 > 2\sigma(F^2)] = 0.0377$	
$wR(F^2) = 0.0951$	
$S = 1.067$	
1513 reflections	
103 parameters	
H-atom parameters constrained	
$w = 1/[\sigma^2(F_o^2) + (0.0664P)^2 + 0.0662P]$	
where $P = (F_o^2 + 2F_c^2)/3$	
$(\Delta/\sigma)_{\max} = 0.001$	
$\Delta\rho_{\max} = 0.482 \text{ e}\times\text{\AA}^{-3}$	
$\Delta\rho_{\min} = -0.337 \text{ e}\times\text{\AA}^{-3}$	

Table 6.2.8d.

Selected geometric parameters (Å, °).

S1—C5 1.7103 (19)	C2—C1—H1 114.5 (19)
S1—C2 1.7247 (19)	C5—C4—C3 110.45 (18)
O1—C1 1.213 (3)	C5—C4—H4 122.7 (16)
O2—N1 1.222 (2)	C3—C4—H4 126.9 (16)
C1—C2 1.463 (3)	C2—C3—C4 111.98 (17)
C1—H1 0.91 (3)	C2—C3—H3 124.4 (16)
C4—C5 1.357 (3)	C4—C3—H3 123.7 (16)
C4—C3 1.414 (2)	C3—C2—C1 126.74 (17)
C4—H4 0.95 (2)	C3—C2—S1 113.20 (14)
O3—N1 1.220 (2)	C1—C2—S1 120.03 (15)
C3—C2 1.378 (3)	O3—N1—O2 124.77 (17)
C3—H3 0.93 (3)	O3—N1—C5 117.56 (17)
N1—C5 1.444 (2)	O2—N1—C5 117.67 (16)
C5—S1—C2 88.84 (10)	C4—C5—N1 124.95 (17)
O1—C1—C2 122.77 (19)	C4—C5—S1 115.53 (15)
O1—C1—H1 122.7 (19)	N1—C5—S1 119.50 (14)

9. *N*-(9 *H*-fluoren-9-ylidene)-3,4-dimethylbenzenamine

Comment

G. Crundwell from Central Connecticut State University provided the crystal investigated. It was grown from hexane.

All H atoms were placed in calculated positions, with C–H distances of 0.95 Å, and were included in the refinement in riding-motion approximation, with $U_{\text{iso}}(\text{H}) = 1.2U_{\text{eq}}$ of the adjacent carbon atom.

Table 6.2.9a. Crystal data for 04JU07a	Table 6.2.9b. Data collection
$\text{C}_{21}\text{H}_{17}\text{N}$	Bruker SMART CCD area-detector
Mr = 283.355	diffractometer
Triclinic, $P\bar{1}$	ω scans
$a = 8.476(3) \text{ \AA}$	Absorption correction: multi-scan
$b = 8.870(3) \text{ \AA}$	$T_{\text{min}} = 0.972, T_{\text{max}} = 0.993$
$c = 10.376(4) \text{ \AA}$	7401 measured reflections
$V = 752.095(8) \text{ \AA}^3$	3722 independent reflections
$Z = 2$	3472 reflections with $I > 2\sigma(I)$
$D_x = 1.251 \text{ Mg m}^{-3}$	$R_{\text{int}} = 0.0351$
Mo K_{α} radiation	$\theta_{\text{max}} = 28.47^{\circ}$
Cell parameters from 6350 reflections	$h = -11 \rightarrow 11$
$\theta = 2.342 \pm 28.366^{\circ}$	$k = -11 \rightarrow 11$

$\mu = 0.07 \text{ mm}^{-1}$	$l = -13 \rightarrow 13$
$T = 100 (2) \text{ K}$	
Block, orange	
$0.40 \times 0.34 \times 0.10 \text{ mm}$	

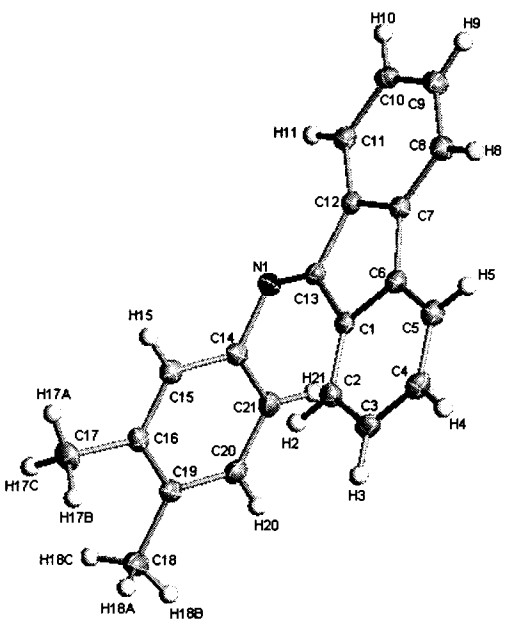
Table 6.2.9c. Refinement	Figure 6.2.9. ORTEP plot of title compound. Ellipsoids are at the 50% probability level.
Refinement on F^2	
$R[F^2 > 2\sigma(F^2)] = 0.0543$	
$wR(F^2) = 0.1463$	
$S = 1.032$	
3722 reflections	
201 parameters	
H-atom parameters constrained	
$w = 1/[\sigma^2(F_o^2) + (0.0808P)^2 + 0.24P]$	
where $P = (F_o^2 + 2F_c^2)/3$	
$(\Delta/\sigma)_{\text{max}} = 0.000$	
$\Delta\rho_{\text{max}} = 0.49 \text{ e}\times\text{\AA}^{-3}$	
$\Delta\rho_{\text{min}} = -0.28 \text{ e}\times\text{\AA}^{-3}$	

Table 6.2.9d.

Selected geometric parameters (Å, °).

N(1)-C(8)	1.2745(15)	N(1)-C(8)-C(9)	132.58(10)
N(1)-C(7)	1.4234(15)	C(20)-C(8)-C(9)	105.45(9)
C(5)-C(4)	1.3922(16)	C(13)-C(14)-C(9)	120.82(10)
C(5)-C(7)	1.3939(16)	C(13)-C(14)-C(15)	129.77(10)
C(5)-H(5)	0.983(16)	C(9)-C(14)-C(15)	109.41(9)
C(4)-C(2)	1.4046(17)	C(6)-C(3)-C(2)	121.77(11)
C(4)-C(21)	1.5057(17)	C(6)-C(3)-H(3)	118.8(10)
C(2)-C(3)	1.3912(17)	C(2)-C(3)-H(3)	119.4(10)
C(2)-C(1)	1.5054(16)	C(6)-C(7)-C(5)	119.42(10)
C(15)-C(16)	1.3866(16)	C(6)-C(7)-N(1)	120.25(10)
C(15)-C(20)	1.4035(15)	C(5)-C(7)-N(1)	120.21(10)
C(15)-C(14)	1.4712(16)	C(2)-C(1)-H(1B)	110.7(10)
C(8)-C(20)	1.4885(15)	C(2)-C(1)-H(1C)	111.0(12)
C(8)-C(9)	1.4982(15)	H(1B)-C(1)-H(1C)	107.7(15)
C(14)-C(13)	1.3885(15)	C(2)-C(1)-H(1A)	111.1(12)
C(14)-C(9)	1.4088(15)	H(1B)-C(1)-H(1A)	107.2(15)
C(3)-C(6)	1.3896(16)	H(1C)-C(1)-H(1A)	109.0(17)
C(3)-H(3)	0.981(16)	C(10)-C(9)-C(14)	120.47(10)
C(7)-C(6)	1.3891(17)	C(10)-C(9)-C(8)	131.69(10)
C(1)-H(1B)	0.995(18)	C(14)-C(9)-C(8)	107.84(9)

C(1)-H(1C)	1.02(2)	C(19)-C(20)-C(15)	121.06(10)
C(1)-H(1A)	1.00(2)	C(19)-C(20)-C(8)	129.78(10)
C(9)-C(10)	1.3901(16)	C(15)-C(20)-C(8)	109.15(10)
C(20)-C(19)	1.3842(16)	C(17)-C(18)-C(19)	120.47(11)
C(18)-C(17)	1.3937(16)	C(17)-C(18)-H(18)	119.2(9)
C(18)-C(19)	1.3953(16)	C(19)-C(18)-H(18)	120.4(9)
C(18)-H(18)	0.960(16)	C(15)-C(16)-C(17)	118.47(11)
C(16)-C(17)	1.3970(17)	C(15)-C(16)-H(16)	121.3(9)
C(16)-H(16)	0.991(16)	C(17)-C(16)-H(16)	120.2(9)
C(6)-H(6)	0.979(17)	C(7)-C(6)-C(3)	119.43(11)
C(13)-C(12)	1.3931(17)	C(7)-C(6)-H(6)	118.6(9)
C(13)-H(13)	0.992(17)	C(3)-C(6)-H(6)	122.0(9)
C(11)-C(12)	1.3894(18)	C(14)-C(13)-C(12)	118.40(11)
C(11)-C(10)	1.3983(16)	C(14)-C(13)-H(13)	121.0(9)
C(11)-H(11)	0.999(17)	C(12)-C(13)-H(13)	120.6(9)
C(19)-H(19)	0.990(17)	C(12)-C(11)-C(10)	120.91(11)
C(10)-H(10)	0.984(17)	C(12)-C(11)-H(11)	120.2(10)
C(17)-H(17)	1.004(16)	C(10)-C(11)-H(11)	118.9(10)
C(12)-H(12)	0.996(18)	C(20)-C(19)-C(18)	118.56(10)
C(21)-H(21A)	1.019(19)	C(20)-C(19)-H(19)	120.0(10)
C(21)-H(21C)	1.014(19)	C(18)-C(19)-H(19)	121.5(10)
C(21)-H(21B)	1.00(2)	C(9)-C(10)-C(11)	118.39(11)
C(8)-N(1)-C(7)	119.72(10)	C(9)-C(10)-H(10)	121.9(10)

C(4)-C(5)-C(7)	121.23(11)	C(11)-C(10)-H(10)	119.8(10)
C(4)-C(5)-H(5)	119.4(9)	C(18)-C(17)-C(16)	120.98(11)
C(7)-C(5)-H(5)	119.4(9)	C(18)-C(17)-H(17)	118.4(10)
C(5)-C(4)-C(2)	119.40(10)	C(16)-C(17)-H(17)	120.6(10)
C(5)-C(4)-C(21)	119.76(11)	C(11)-C(12)-C(13)	121.01(11)
C(2)-C(4)-C(21)	120.82(11)	C(11)-C(12)-H(12)	119.1(10)
C(3)-C(2)-C(4)	118.72(10)	C(13)-C(12)-H(12)	119.9(10)
C(3)-C(2)-C(1)	120.56(11)	C(4)-C(21)-H(21A)	110.9(11)
C(4)-C(2)-C(1)	120.70(11)	C(4)-C(21)-H(21C)	111.2(11)
C(16)-C(15)-C(20)	120.45(10)	H(21A)-C(21)-H(21C)	108.9(15)
C(16)-C(15)-C(14)	131.40(10)	C(4)-C(21)-H(21B)	112.7(11)
C(20)-C(15)-C(14)	108.15(10)	H(21A)-C(21)-H(21B)	104.5(15)
N(1)-C(8)-C(20)	121.96(10)	H(21C)-C(21)-H(21B)	108.4(15)

10. Bis(2,3-di(5-bromothiophen-2-yl)quinoxaline)silver nitrate

Comment

G. Crundwell from Central Connecticut State University provided the crystal investigated. It was grown from methanol.

All H atoms were placed in calculated positions, with C–H distances of 0.95 Å, and were included in the refinement in riding-motion approximation, with $U_{\text{iso}}(\text{H}) = 1.2U_{\text{eq}}$ of the adjacent carbon atom.

Table 6.2.10a. Crystal data for 04JU10am	Table 6.2.10b. Data collection
$\text{C}_{32}\text{H}_{16}\text{N}_5\text{AgBr}_4\text{O}_3\text{S}_4$	Bruker SMART CCD area-detector
Mr = 1074.25	diffractometer
Triclinic, $P\bar{1}$	ω scans
$a = 8.765$ (11) Å	Absorption correction: multi-scan
$b = 13.871$ (17) Å	$T_{\text{min}} = 0.203$, $T_{\text{max}} = 0.642$
$c = 15.192$ (19) Å	17117 measured reflections
$V = 1710.774$ (4) Å ³	8404 independent reflections
$Z = 2$	7507 reflections with $I > 2\sigma(I)$
$D_x = 2.085$ Mg m ⁻³	$R_{\text{int}} = 0.0418$
Mo K_{α} radiation	$\theta_{\text{max}} = 28.31^{\circ}$
Cell parameters from 12478 reflections	$h = -11 \rightarrow 11$

$\theta = 2.316 \pm 28.31^\circ$	$k = -18 \rightarrow 18$
$\mu = 5.548 \text{ mm}^{-1}$	$l = -20 \rightarrow 20$
$T = 100 (2) \text{ K}$	
Plate, yellow	
$0.45 \times 0.25 \times 0.08 \text{ mm}$	

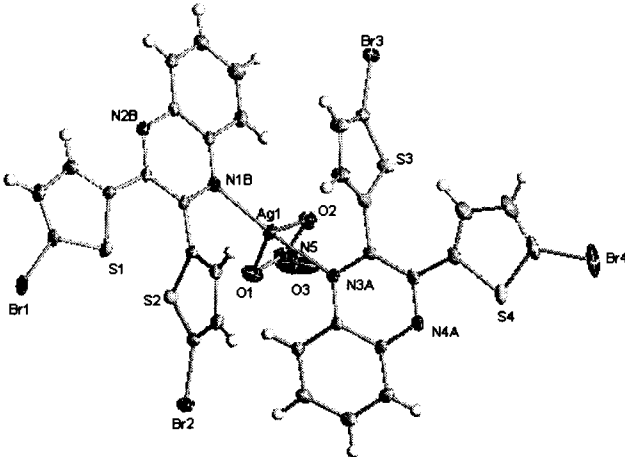
Table 6.2.10c.	Figure 6.2.10. ORTEP plot of title compound. Ellipsoids are at the 50% probability level.
Refinement	
Refinement on F^2	
$R[F^2 > 2\sigma(F^2)] = 0.0437$	
$wR(F^2) = 0.1017$	
$S = 1.024$	
8404 reflections	
442 parameters	
H-atom parameters	
constrained	
$w = 1/[\sigma^2(F_o^2) + (0.0355P)^2 + 1.1808P]$	
where $P = (F_o^2 + 2F_c^2)/3$	
$(\Delta/\sigma)_{\max} = 0.001$	
$\Delta\rho_{\max} = 1.510 \text{ e}\times\text{\AA}^{-3}$	
$\Delta\rho_{\min} = -1.324 \text{ e}\times\text{\AA}^{-3}$	

Table 6.2.10d.

Geometric parameters (Å, °).

Ag(1)-N(1B)	2.209(2)	C(6)-N(1B)-C(11)	119.0(2)
Ag(1)-N(3A)	2.248(2)	C(6)-N(1B)-Ag(1)	117.45(19)
Ag(1)-O(2)	2.481(2)	C(11)-N(1B)-Ag(1)	123.53(19)
Ag(1)-O(1)	2.535(3)	C(9)-C(10)-S(2)	112.7(2)
Br(3)-C(21)	1.870(3)	C(9)-C(10)-Br(2)	126.5(2)
Br(2)-C(10)	1.873(3)	S(2)-C(10)-Br(2)	120.73(17)
Br(1)-C(1)	1.874(3)	C(5)-N(2B)-C(16)	118.9(3)
Br(4)-C(30)	1.869(3)	C(26)-N(4A)-C(31)	118.5(3)
S(2)-C(10)	1.716(3)	N(4A)-C(31)-C(36)	120.8(3)
S(2)-C(7)	1.731(3)	N(4A)-C(31)-C(32)	119.7(3)
S(4)-C(30)	1.713(4)	C(36)-C(31)-C(32)	119.4(3)
S(4)-C(27)	1.742(3)	N(5)-O(2)-Ag(1)	96.07(18)
S(1)-C(1)	1.714(3)	C(25)-N(3A)-C(36)	118.5(2)
S(1)-C(4)	1.735(3)	C(25)-N(3A)-Ag(1)	117.03(18)
S(3)-C(21)	1.723(3)	C(36)-N(3A)-Ag(1)	123.90(18)
S(3)-C(24)	1.732(3)	C(23)-C(24)-C(25)	129.0(3)
C(35)-C(34)	1.378(4)	C(23)-C(24)-S(3)	111.4(2)
C(35)-C(36)	1.415(4)	C(25)-C(24)-S(3)	119.3(2)
C(35)-H(35)	0.9500	N(3A)-C(25)-C(26)	120.9(3)
C(28)-C(27)	1.363(4)	N(3A)-C(25)-C(24)	114.8(3)

C(28)-C(29)	1.418(5)	C(26)-C(25)-C(24)	124.2(3)
C(28)-H(28)	0.9500	C(2)-C(1)-S(1)	113.4(2)
C(8)-C(7)	1.371(4)	C(2)-C(1)-Br(1)	126.4(2)
C(8)-C(9)	1.424(4)	S(1)-C(1)-Br(1)	120.19(17)
C(8)-H(8)	0.9500	C(24)-C(23)-C(22)	113.0(3)
C(26)-N(4A)	1.327(4)	C(24)-C(23)-H(23)	123.5
C(26)-C(25)	1.436(4)	C(22)-C(23)-H(23)	123.5
C(26)-C(27)	1.458(4)	C(28)-C(27)-C(26)	133.8(3)
N(1B)-C(6)	1.325(4)	C(28)-C(27)-S(4)	110.5(2)
N(1B)-C(11)	1.368(4)	C(26)-C(27)-S(4)	115.7(2)
C(10)-C(9)	1.359(4)	N(2B)-C(16)-C(15)	120.0(3)
N(2B)-C(5)	1.327(4)	N(2B)-C(16)-C(11)	121.0(3)
N(2B)-C(16)	1.361(4)	C(15)-C(16)-C(11)	118.9(3)
N(4A)-C(31)	1.359(4)	C(32)-C(33)-C(34)	120.7(3)
C(31)-C(36)	1.411(4)	C(32)-C(33)-H(33)	119.7
C(31)-C(32)	1.412(4)	C(34)-C(33)-H(33)	119.7
O(2)-N(5)	1.255(4)	N(3A)-C(36)-C(31)	120.1(3)
N(3A)-C(25)	1.324(4)	N(3A)-C(36)-C(35)	119.8(3)
N(3A)-C(36)	1.372(3)	C(31)-C(36)-C(35)	120.1(3)
C(24)-C(23)	1.356(4)	N(5)-O(1)-Ag(1)	93.34(18)
C(24)-C(25)	1.483(4)	C(29)-C(30)-S(4)	112.8(3)
C(1)-C(2)	1.356(4)	C(29)-C(30)-Br(4)	127.9(3)
C(23)-C(22)	1.425(4)	S(4)-C(30)-Br(4)	119.2(2)

C(23)-H(23)	0.9500	C(8)-C(7)-C(6)	128.7(3)
C(16)-C(15)	1.414(4)	C(8)-C(7)-S(2)	111.3(2)
C(16)-C(11)	1.418(4)	C(6)-C(7)-S(2)	120.0(2)
C(33)-C(32)	1.370(4)	C(13)-C(12)-C(11)	119.0(3)
C(33)-C(34)	1.412(5)	C(13)-C(12)-H(12)	120.5
C(33)-H(33)	0.9500	C(11)-C(12)-H(12)	120.5
O(1)-N(5)	1.260(4)	C(14)-C(15)-C(16)	119.8(3)
C(30)-C(29)	1.347(6)	C(14)-C(15)-H(15)	120.1
C(7)-C(6)	1.477(4)	C(16)-C(15)-H(15)	120.1
C(12)-C(13)	1.371(4)	C(1)-C(2)-C(3)	110.9(3)
C(12)-C(11)	1.410(4)	C(1)-C(2)-H(2)	124.6
C(12)-H(12)	0.9500	C(3)-C(2)-H(2)	124.6
C(15)-C(14)	1.364(4)	C(22)-C(21)-S(3)	112.1(2)
C(15)-H(15)	0.9500	C(22)-C(21)-Br(3)	126.8(2)
C(2)-C(3)	1.421(4)	S(3)-C(21)-Br(3)	121.13(17)
C(2)-H(2)	0.9500	C(33)-C(32)-C(31)	119.8(3)
C(21)-C(22)	1.359(4)	C(33)-C(32)-H(32)	120.1
C(32)-H(32)	0.9500	C(31)-C(32)-H(32)	120.1
C(3)-C(4)	1.362(4)	C(4)-C(3)-C(2)	114.2(3)
C(3)-H(3)	0.9500	C(4)-C(3)-H(3)	122.9
C(9)-H(9)	0.9500	C(2)-C(3)-H(3)	122.9
C(34)-H(34)	0.9500	C(10)-C(9)-C(8)	112.0(3)
C(14)-C(13)	1.416(5)	C(10)-C(9)-H(9)	124.0

C(14)-H(14)	0.9500	C(8)-C(9)-H(9)	124.0
C(4)-C(5)	1.473(4)	C(35)-C(34)-C(33)	120.7(3)
C(13)-H(13)	0.9500	C(35)-C(34)-H(34)	119.6
C(6)-C(5)	1.438(4)	C(33)-C(34)-H(34)	119.6
C(22)-H(22)	0.9500	C(15)-C(14)-C(13)	121.1(3)
O(3)-N(5)	1.239(4)	C(15)-C(14)-H(14)	119.5
C(29)-H(29)	0.9500	C(13)-C(14)-H(14)	119.5
N(1B)-Ag(1)-N(3A)	141.77(8)	C(3)-C(4)-C(5)	124.3(3)
N(1B)-Ag(1)-O(2)	122.55(8)	C(3)-C(4)-S(1)	110.5(2)
N(3A)-Ag(1)-O(2)	90.47(8)	C(5)-C(4)-S(1)	125.2(2)
N(1B)-Ag(1)-O(1)	116.18(9)	C(12)-C(13)-C(14)	120.6(3)
N(3A)-Ag(1)-O(1)	99.12(8)	C(12)-C(13)-H(13)	119.7
O(2)-Ag(1)-O(1)	51.07(8)	C(14)-C(13)-H(13)	119.7
C(10)-S(2)-C(7)	91.22(14)	N(1B)-C(6)-C(5)	121.2(3)
C(30)-S(4)-C(27)	91.12(17)	N(1B)-C(6)-C(7)	115.3(2)
C(1)-S(1)-C(4)	91.06(14)	C(5)-C(6)-C(7)	123.6(2)
C(21)-S(3)-C(24)	91.25(14)	C(21)-C(22)-C(23)	112.2(3)
C(34)-C(35)-C(36)	119.1(3)	C(21)-C(22)-H(22)	123.9
C(34)-C(35)-H(35)	120.5	C(23)-C(22)-H(22)	123.9
C(36)-C(35)-H(35)	120.5	N(1B)-C(11)-C(12)	119.9(3)
C(27)-C(28)-C(29)	113.4(3)	N(1B)-C(11)-C(16)	119.5(3)
C(27)-C(28)-H(28)	123.3	C(12)-C(11)-C(16)	120.6(3)
C(29)-C(28)-H(28)	123.3	N(2B)-C(5)-C(6)	120.3(3)

C(7)-C(8)-C(9)	112.7(3)	N(2B)-C(5)-C(4)	115.4(2)
C(7)-C(8)-H(8)	123.6	C(6)-C(5)-C(4)	124.3(2)
C(9)-C(8)-H(8)	123.6	O(3)-N(5)-O(2)	120.0(3)
N(4A)-C(26)-C(25)	120.7(3)	O(3)-N(5)-O(1)	121.4(3)
N(4A)-C(26)-C(27)	114.6(3)	O(2)-N(5)-O(1)	118.6(3)
		C(30)-C(29)-C(28)	112.1(3)

11. Bis(2,3-di(thiophen-2-yl)quinoxaline)silver nitrate

Comment

G. Crundwell from Central Connecticut State University provided the crystal investigated. It was grown from methanol.

Three of the four thiophene rings exhibit flip disorder (the rings are rapidly flipping from “right-handed” to left handed”). The major and minor components were refined to be the same: restraints were applied so that the geometry of the two component rings was identical. Due to the flip disorder, it also became necessary for the thermal displacement parameter of the disordered atoms (thus their thermal ellipsoids) to be set the same.

All H atoms were placed in calculated positions, with C–H distances of 0.95 Å, and were included in the refinement in riding-motion approximation, with $U_{\text{iso}}(\text{H}) = 1.2U_{\text{eq}}$ of the adjacent carbon atom.

Table 6.2.11a. Crystal data for 04JU11am	Table 6.2.11b. Data collection
$\text{C}_{32}\text{H}_{16}\text{N}_5\text{AgO}_3\text{S}_4$ Mr = 758.64 Triclinic, $P\bar{1}$ $a = 10.4991 (7) \text{ \AA}$ $b = 11.9510 (8) \text{ \AA}$ $c = 12.5195 (8) \text{ \AA}$	Bruker SMART CCD area-detector diffractometer ω scans Absorption correction: multi-scan $T_{\text{min}} = 0.683, T_{\text{max}} = 0.885$ 15097 measured reflections

$V = 1467.81 (17) \text{ \AA}^3$	7234 independent reflections
$Z = 2$	6833 reflections with $I > 2\sigma(I)$
$D_x = 1.717 \text{ Mg m}^{-3}$	$R_{\text{int}} = 0.0164$
Mo K_α radiation	$\theta_{\text{max}} = 28.32^\circ$
Cell parameters from 12561 reflections	$h = -13 \rightarrow 13$
$\theta = 2.43 \pm 28.306^\circ$	$k = -15 \rightarrow 15$
$\mu = 1.017 \text{ mm}^{-1}$	$l = -16 \rightarrow 16$
$T = 100 (2) \text{ K}$	
Block, yellow	
$0.40 \times 0.32 \times 0.12 \text{ mm}$	

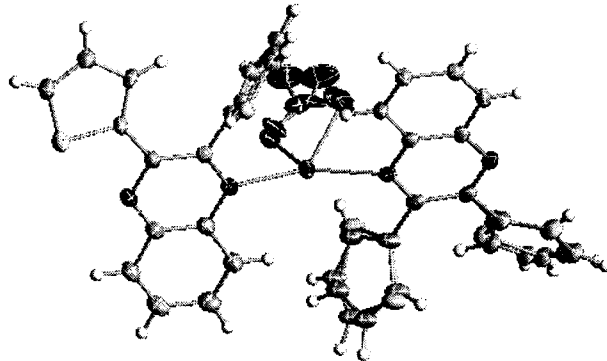
Table 6.2.11c. Refinement	Figure 6.2.11. ORTEP plot of title compound. Ellipsoids are at the 50% probability level. The flip disorder is also modeled.
Refinement on F^2 $R[F^2 > 2\sigma(F^2)] = 0.0372$ $wR(F^2) = 0.0954$ $S = 1.048$ 7234 reflections 416 parameters H-atom parameters constrained $w = 1/[\sigma^2(F_o^2) + (0.0475P)^2 + 2.32P]$ where $P = (F_o^2 + 2F_c^2)/3$ $(\Delta/\sigma)_{\max} = 0.000$ $\Delta\rho_{\max} = 1.769 \text{ e}\times\text{\AA}^{-3}$ $\Delta\rho_{\min} = -0.818 \text{ e}\times\text{\AA}^{-3}$	

Table 6.2.11d. Geometric parameters (Å, °).			
Ag(1)-N(4)	2.226(2)	N(1)-C(8)-C(9)	113.6(3)
Ag(1)-N(2)	2.226(2)	C(13)-C(8)-C(9)	124.8(3)

Ag(1)-O(2)	2.489(12)	N(1)-C(8)-C(9B)	121.5(5)
Ag(1)-O(1B)	2.56(3)	C(13)-C(8)-C(9B)	116.6(5)
C(1)-N(2)	1.370(3)	C(9)-C(8)-C(9B)	10.8(5)
C(1)-C(2)	1.411(3)	C(10)-C(9)-C(8)	137.5(4)
C(1)-C(6)	1.416(3)	C(10)-C(9)-S(3)	100.1(3)
C(2)-C(3)	1.372(3)	C(8)-C(9)-S(3)	120.1(3)
C(2)-H(2)	0.9500	C(11)-C(10)-C(9)	130.4(6)
C(3)-C(4)	1.414(3)	C(11)-C(10)-H(10)	114.8
C(3)-H(3)	0.9500	C(9)-C(10)-H(10)	114.8
C(4)-C(5)	1.366(4)	C(10)-C(11)-C(12)	103.9(4)
C(4)-H(4)	0.9500	C(10)-C(11)-H(11)	128.1
C(5)-C(6)	1.418(3)	C(12)-C(11)-H(11)	128.1
C(5)-H(5)	0.9500	C(11)-C(12)-S(3)	114.1(3)
C(6)-N(1)	1.362(3)	C(11)-C(12)-H(12)	123.0
N(1)-C(8)	1.322(3)	S(3)-C(12)-H(12)	123.0
C(8)-C(13)	1.440(3)	C(9)-S(3)-C(12)	89.3(2)
C(8)-C(9)	1.467(5)	C(10B)-C(9B)-C(8)	146.6(10)
C(8)-C(9B)	1.513(11)	C(10B)-C(9B)-S(3B)	105.0(9)
C(9)-C(10)	1.365(7)	C(8)-C(9B)-S(3B)	108.3(6)
C(9)-S(3)	1.737(4)	C(11B)-C(10B)-C(9B)	125.7(14)
C(10)-C(11)	1.214(6)	C(11B)-C(10B)-H(10B)	117.1
C(10)-H(10)	0.9500	C(9B)-C(10B)-H(10B)	117.1
C(11)-C(12)	1.333(6)	C(10B)-C(11B)-C(12B)	105.7(11)

C(11)-H(11)	0.9500	C(10B)-C(11B)-H(11B)	127.1
C(12)-S(3)	1.761(4)	C(12B)-C(11B)-H(11B)	127.1
C(12)-H(12)	0.9500	C(11B)-C(12B)-S(3B)	115.3(7)
C(9B)-C(10B)	1.423(15)	C(11B)-C(12B)-H(12B)	122.4
C(9B)-S(3B)	1.709(11)	S(3B)-C(12B)-H(12B)	122.4
C(10B)-C(11B)	1.213(14)	C(9B)-S(3B)-C(12B)	86.4(5)
C(10B)-H(10B)	0.9500	N(2)-C(13)-C(8)	120.7(2)
C(11B)-C(12B)	1.332(12)	N(2)-C(13)-C(14)	116.3(2)
C(11B)-H(11B)	0.9500	C(8)-C(13)-C(14)	123.0(2)
C(12B)-S(3B)	1.829(9)	C(15)-C(14)-C(13)	130.0(3)
C(12B)-H(12B)	0.9500	C(15)-C(14)-S(4)	106.0(3)
C(13)-N(2)	1.325(3)	C(13)-C(14)-S(4)	123.3(2)
C(13)-C(14)	1.474(4)	C(16)-C(15)-C(14)	119.3(5)
C(14)-C(15)	1.413(7)	C(16)-C(15)-H(15A)	120.4
C(14)-S(4)	1.706(3)	C(14)-C(15)-H(15A)	120.4
C(15)-C(16)	1.346(7)	C(15)-C(16)-C(17)	108.1(5)
C(15)-H(15A)	0.9500	C(15)-C(16)-H(16)	126.0
C(16)-C(17)	1.352(6)	C(17)-C(16)-H(16)	126.0
C(16)-H(16)	0.9500	C(16)-C(17)-S(4)	114.0(4)
C(17)-S(4)	1.729(5)	C(16)-C(17)-H(17)	123.0
C(17)-H(17)	0.9500	S(4)-C(17)-H(17)	123.0
C(15B)-C(16B)	1.426(13)	C(14)-S(4)-C(17)	91.8(2)
C(15B)-H(15B)	0.9500	C(16B)-C(15B)-H(15B)	125.0

C(16B)-C(17B)	1.356(11)	C(17B)-C(16B)-C(15B)	108.7(9)
C(16B)-H(16B)	0.9500	C(17B)-C(16B)-H(16B)	125.7
C(17B)-S(4B)	1.775(9)	C(15B)-C(16B)-H(16B)	125.7
C(17B)-H(17B)	0.9500	C(16B)-C(17B)-S(4B)	115.4(8)
C(18)-N(4)	1.369(3)	C(16B)-C(17B)-H(17B)	122.3
C(18)-C(19)	1.410(4)	S(4B)-C(17B)-H(17B)	122.3
C(18)-C(23)	1.411(3)	N(4)-C(18)-C(19)	119.7(2)
C(19)-C(20)	1.371(4)	N(4)-C(18)-C(23)	119.7(2)
C(19)-H(19)	0.9500	C(19)-C(18)-C(23)	120.6(2)
C(20)-C(21)	1.409(4)	C(20)-C(19)-C(18)	119.6(3)
C(20)-H(20)	0.9500	C(20)-C(19)-H(19)	120.2
C(21)-C(22)	1.368(4)	C(18)-C(19)-H(19)	120.2
C(21)-H(21)	0.9500	C(19)-C(20)-C(21)	120.0(3)
C(22)-C(23)	1.425(3)	C(19)-C(20)-H(20)	120.0
C(22)-H(22)	0.9500	C(21)-C(20)-H(20)	120.0
C(23)-N(3)	1.355(3)	C(22)-C(21)-C(20)	121.6(2)
N(3)-C(25)	1.327(3)	C(22)-C(21)-H(21)	119.2
C(25)-C(30)	1.441(3)	C(20)-C(21)-H(21)	119.2
C(25)-C(26)	1.466(3)	C(21)-C(22)-C(23)	119.4(2)
C(26)-C(27)	1.419(3)	C(21)-C(22)-H(22)	120.3
C(26)-S(2)	1.726(2)	C(23)-C(22)-H(22)	120.3
C(27)-C(28)	1.437(3)	N(3)-C(23)-C(18)	121.4(2)
C(27)-H(27)	0.9500	N(3)-C(23)-C(22)	119.9(2)

C(28)-C(29)	1.358(4)	C(18)-C(23)-C(22)	118.6(2)
C(28)-H(28)	0.9500	C(25)-N(3)-C(23)	118.4(2)
C(29)-S(2)	1.697(3)	N(3)-C(25)-C(30)	120.7(2)
C(29)-H(29)	0.9500	N(3)-C(25)-C(26)	115.5(2)
C(30)-N(4)	1.322(3)	C(30)-C(25)-C(26)	123.8(2)
C(30)-C(31)	1.481(3)	C(27)-C(26)-C(25)	132.1(2)
C(31)-C(32)	1.409(6)	C(27)-C(26)-S(2)	111.36(18)
C(31)-S(5)	1.687(3)	C(25)-C(26)-S(2)	116.48(17)
C(32)-C(33)	1.393(7)	C(26)-C(27)-C(28)	109.8(2)
C(32)-H(32)	0.9500	C(26)-C(27)-H(27)	125.1
C(33)-C(34)	1.359(6)	C(28)-C(27)-H(27)	125.1
C(33)-H(33)	0.9500	C(29)-C(28)-C(27)	113.9(2)
C(34)-S(5)	1.730(5)	C(29)-C(28)-H(28)	123.0
C(34)-H(34)	0.9500	C(27)-C(28)-H(28)	123.0
C(32B)-C(33B)	1.362(10)	C(28)-C(29)-S(2)	112.5(2)
C(32B)-H(32B)	0.9500	C(28)-C(29)-H(29)	123.7
C(33B)-C(34B)	1.351(8)	S(2)-C(29)-H(29)	123.7
C(33B)-H(33B)	0.9500	N(4)-C(30)-C(25)	120.7(2)
C(34B)-S(5B)	1.732(7)	N(4)-C(30)-C(31)	115.6(2)
C(34B)-H(34B)	0.9500	C(25)-C(30)-C(31)	123.7(2)
N(5)-O(3)	1.245(10)	C(32)-C(31)-C(30)	127.1(3)
N(5)-O(1)	1.248(10)	C(32)-C(31)-S(5)	109.9(3)
N(5)-O(2)	1.249(10)	C(30)-C(31)-S(5)	123.08(18)

N(5B)-O(2B)	1.236(14)	C(33)-C(32)-C(31)	115.5(5)
N(5B)-O(3B)	1.239(14)	C(33)-C(32)-H(32)	122.3
N(5B)-O(1B)	1.247(14)	C(31)-C(32)-H(32)	122.3
N(4)-Ag(1)-N(2)	151.74(7)	C(34)-C(33)-C(32)	109.0(5)
N(4)-Ag(1)-O(2)	83.7(3)	C(34)-C(33)-H(33)	125.5
N(2)-Ag(1)-O(2)	123.9(3)	C(32)-C(33)-H(33)	125.5
N(4)-Ag(1)-O(1B)	131.2(6)	C(33)-C(34)-S(5)	114.3(4)
N(2)-Ag(1)-O(1B)	76.0(5)	C(33)-C(34)-H(34)	122.8
O(2)-Ag(1)-O(1B)	54.8(5)	S(5)-C(34)-H(34)	122.8
N(2)-C(1)-C(2)	119.8(2)	C(31)-S(5)-C(34)	91.2(2)
N(2)-C(1)-C(6)	119.8(2)	C(33B)-C(32B)-H(32B)	122.6
C(2)-C(1)-C(6)	120.4(2)	C(34B)-C(33B)-C(32B)	108.7(8)
C(3)-C(2)-C(1)	119.5(2)	C(34B)-C(33B)-H(33B)	125.7
C(3)-C(2)-H(2)	120.3	C(32B)-C(33B)-H(33B)	125.7
C(1)-C(2)-H(2)	120.3	C(33B)-C(34B)-S(5B)	116.0(6)
C(2)-C(3)-C(4)	120.3(2)	C(33B)-C(34B)-H(34B)	122.0
C(2)-C(3)-H(3)	119.9	S(5B)-C(34B)-H(34B)	122.0
C(4)-C(3)-H(3)	119.9	C(13)-N(2)-C(1)	118.6(2)
C(5)-C(4)-C(3)	121.3(2)	C(13)-N(2)-Ag(1)	120.38(17)
C(5)-C(4)-H(4)	119.4	C(1)-N(2)-Ag(1)	118.97(15)
C(3)-C(4)-H(4)	119.4	C(30)-N(4)-C(18)	119.0(2)
C(4)-C(5)-C(6)	119.7(2)	C(30)-N(4)-Ag(1)	119.23(15)
C(4)-C(5)-H(5)	120.2	C(18)-N(4)-Ag(1)	120.86(16)

C(6)-C(5)-H(5)	120.2	O(3)-N(5)-O(1)	119.9(13)
N(1)-C(6)-C(1)	121.5(2)	O(3)-N(5)-O(2)	120.5(11)
N(1)-C(6)-C(5)	119.6(2)	O(1)-N(5)-O(2)	119.3(11)
C(1)-C(6)-C(5)	118.9(2)	N(5)-O(2)-Ag(1)	103.6(7)
C(8)-N(1)-C(6)	117.7(2)	O(2B)-N(5B)-O(3B)	122.8(18)
N(1)-C(8)-C(13)	121.6(2)	O(2B)-N(5B)-O(1B)	119.4(16)
		O(3B)-N(5B)-O(1B)	117.3(17)

12. Nitroanthracene

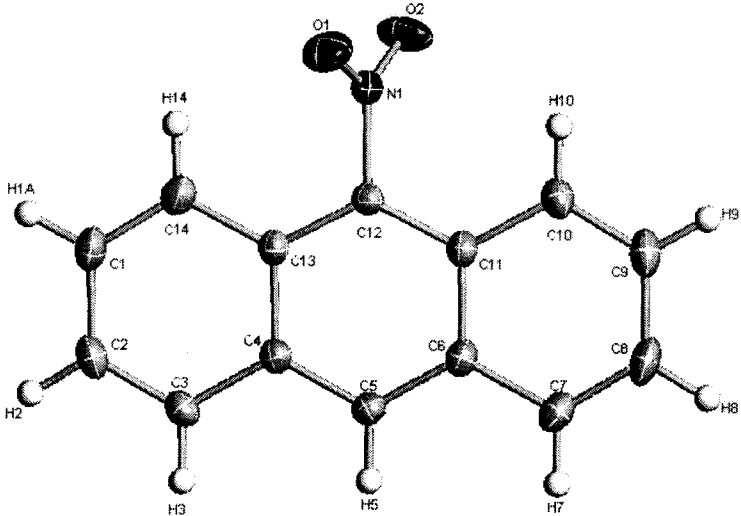
Comment

G. Crundwell from Central Connecticut State University provided the crystal investigated. It was grown from hexane.

All H atoms were placed in calculated positions, with C–H distances of 0.95 Å, and were included in the refinement in riding-motion approximation, with $U_{\text{iso}}(\text{H}) = 1.2U_{\text{eq}}$ of the adjacent carbon atom.

Table 6.2.12a. Crystal data for 04JU12a	Table 6.2.12b. Data collection
$\text{C}_{14}\text{H}_9\text{NO}_2$	Bruker SMART CCD area-detector
Mr = 268.22	diffractometer
Monoclinic, $P2_1/c$	ω scans
$a = 10.5117 (7) \text{ \AA}$	Absorption correction: multi-scan
$b = 13.5401 (9) \text{ \AA}$	$T_{\text{min}} = 0.981, T_{\text{max}} = 0.984$
$c = 7.4285 (5) \text{ \AA}$	10391 measured reflections
$\beta = 103.1970 (10)^\circ$	2545 independent reflections
$V = 1029.37 (12) \text{ \AA}^3$	2182 reflections with $I > 2\sigma(I)$
$Z = 3$	$R_{\text{int}} = 0.0247$
$D_x = 1.298 \text{ Mg m}^{-3}$	$\theta_{\text{max}} = 28.29^\circ$
Mo K_α radiation	$h = -14 \rightarrow 14$
Cell parameters from 5299 reflections	$k = -18 \rightarrow 18$

$\theta = 2.495 \pm 28.283^\circ$	$l = -9 \rightarrow 9$
$\mu = 0.098 \text{ mm}^{-1}$	
$T = 100 (2) \text{ K}$	
Needle, yellow	
$0.40 \times 0.16 \times 0.16 \text{ mm}$	

Table 6.2.12c. Refinement	Figure 6.2.12. ORTEP plot of title compound. Ellipsoids are at the 50% probability level.
Refinement on F^2 $R[F^2 > 2\sigma(F^2)] = 0.0438$ $wR(F^2) = 0.1255$ $S = 1.066$ 2545 reflections 154 parameters H-atom parameters constrained $w = 1/[\sigma^2(F_o^2) + (0.0791P)^2 + 0.20P]$ where $P = (F_o^2 + 2F_c^2)/3$ $(\Delta/\sigma)_{\text{max}} = 0.000$	

$\Delta\rho_{\max} = 0.471 \text{ e}\times\text{\AA}^{-3}$	
$\Delta\rho_{\min} = -0.202 \text{ e}\times\text{\AA}^{-3}$	

Table 6.2.12d.			
Geometric parameters (\AA , $^\circ$).			
C(11)-C(12)	1.3989(14)	C(11)-C(12)-N(1)	117.82(9)
C(11)-C(10)	1.4284(14)	C(12)-C(13)-C(14)	124.39(10)
C(11)-C(6)	1.4343(15)	C(12)-C(13)-C(4)	116.81(9)
C(4)-C(5)	1.3972(14)	C(14)-C(13)-C(4)	118.78(9)
C(4)-C(3)	1.4274(14)	C(6)-C(5)-C(4)	122.07(10)
C(4)-C(13)	1.4325(14)	C(6)-C(5)-H(5)	119.0
C(12)-C(13)	1.3976(14)	C(4)-C(5)-H(5)	119.0
C(12)-N(1)	1.4728(13)	C(5)-C(6)-C(7)	121.84(10)
C(13)-C(14)	1.4297(14)	C(5)-C(6)-C(11)	119.56(9)
C(5)-C(6)	1.3950(15)	C(7)-C(6)-C(11)	118.60(10)
C(5)-H(5)	0.9500	C(2)-C(3)-C(4)	121.10(10)
C(6)-C(7)	1.4286(14)	C(2)-C(3)-H(3)	119.4
C(3)-C(2)	1.3592(16)	C(4)-C(3)-H(3)	119.4
C(3)-H(3)	0.9500	C(9)-C(10)-C(11)	120.32(11)
C(10)-C(9)	1.3608(15)	C(9)-C(10)-H(10)	119.8
C(10)-H(10)	0.9500	C(11)-C(10)-H(10)	119.8
N(1)-O(2)	1.2170(13)	O(2)-N(1)-O(1)	123.25(10)

N(1)-O(1)	1.2201(12)	O(2)-N(1)-C(12)	118.55(9)
C(7)-C(8)	1.3591(16)	O(1)-N(1)-C(12)	118.20(9)
C(7)-H(7)	0.9500	C(8)-C(7)-C(6)	120.86(11)
C(14)-C(1)	1.3619(15)	C(8)-C(7)-H(7)	119.6
C(14)-H(14)	0.9500	C(6)-C(7)-H(7)	119.6
C(8)-C(9)	1.4213(18)	C(1)-C(14)-C(13)	120.35(10)
C(8)-H(8)	0.9500	C(1)-C(14)-H(14)	119.8
C(9)-H(9)	0.9500	C(13)-C(14)-H(14)	119.8
C(2)-C(1)	1.4194(17)	C(7)-C(8)-C(9)	120.33(10)
C(2)-H(2)	0.9500	C(7)-C(8)-H(8)	119.8
C(1)-H(1A)	0.9500	C(9)-C(8)-H(8)	119.8
C(12)-C(11)-C(10)	124.13(10)	C(10)-C(9)-C(8)	120.99(10)
C(12)-C(11)-C(6)	116.96(9)	C(10)-C(9)-H(9)	119.5
C(10)-C(11)-C(6)	118.90(10)	C(8)-C(9)-H(9)	119.5
C(5)-C(4)-C(3)	121.64(10)	C(3)-C(2)-C(1)	120.11(10)
C(5)-C(4)-C(13)	119.77(9)	C(3)-C(2)-H(2)	119.9
C(3)-C(4)-C(13)	118.59(9)	C(1)-C(2)-H(2)	119.9
C(13)-C(12)-C(11)	124.81(10)	C(14)-C(1)-C(2)	121.06(10)
C(13)-C(12)-N(1)	117.37(9)		

13. *o*-1-nitro-2-ethylbenzene and *p*-methylbenzenesulfonate

Comment

G. Crundwell from Central Connecticut State University provided the crystal investigated. It was grown from hexane and was the starting material of the intended compound.

All H atoms were placed in calculated positions, with C–H distances of 0.95 Å, and were included in the refinement in riding-motion approximation, with $U_{\text{iso}}(\text{H}) = 1.2U_{\text{eq}}$ of the adjacent carbon atom.

Table 6.2.13a. Crystal data for 04JU25am	Table 6.2.13b. Data collection
$\text{C}_{15}\text{H}_{19}\text{NO}_3\text{S}$ $M_r = 293.37$ Monoclinic, $P2_1/c$ $a = 5.9374 (7) \text{ \AA}$ $b = 21.805 (2) \text{ \AA}$ $c = 11.5549 (13) \text{ \AA}$ $\beta = 95.057 (2)^\circ$ $V = 1490.1 (3) \text{ \AA}^3$ $Z = 4$ $D_x = 1.308 \text{ Mg m}^{-3}$	Bruker SMART CCD area-detector diffractometer ω scans Absorption correction: multi-scan $T_{\text{min}} = 0.905, T_{\text{max}} = 0.984$ 12891 measured reflections 3618 independent reflections 3527 reflections with $I > 2\sigma(I)$ $R_{\text{int}} = 0.0381$ $\theta_{\text{max}} = 28.30^\circ$

Mo K_{α} radiation	$h = -7 \rightarrow 7$
Cell parameters from 13010 reflections	$k = -29 \rightarrow 29$
$\theta = 2.573 \pm 28.289^{\circ}$	$l = -15 \rightarrow 15$
$\mu = 0.224 \text{ mm}^{-1}$	
$T = 100 (2) \text{ K}$	
Plate, colorless	
$0.60 \times 0.37 \times 0.07 \text{ mm}$	

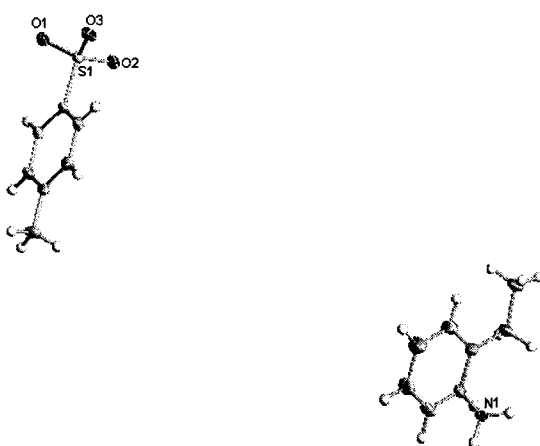
Table 6.2.13c. Refinement	Figure 6.2.13. ORTEP plot of title compound. Ellipsoids are at the 50% probability level.
<p>Refinement on F^2</p> <p>$R[F^2 > 2\sigma(F^2)] = 0.0614$</p> <p>$wR(F^2) = 0.1356$</p> <p>$S = 1.292$</p> <p>3618 reflections</p> <p>184 parameters</p> <p>H-atom parameters constrained</p> <p>$w = 1/[\sigma^2(F_o^2) + (0.0206P)^2 + 2.1666P]$</p> <p>where $P = (F_o^2 + 2F_c^2)/3$</p> <p>$(\Delta/\sigma)_{\max} = 0.000$</p> <p>$\Delta\rho_{\max} = 0.43 \text{ e} \times \text{\AA}^{-3}$</p> <p>$\Delta\rho_{\min} = -0.44 \text{ e} \times \text{\AA}^{-3}$</p>	

Table 6.2.13d.			
Geometric parameters (\AA , $^\circ$).			
C(15)-H(15B)	0.9800	H(4A)-N(1)-H(4C)	109.5
C(15)-H(15C)	0.9800	H(4B)-N(1)-H(4C)	109.5
S(1)-O(1)	1.4574(18)	C(5)-C(4)-C(3)	122.8(2)

S(1)-O(3)	1.4587(17)	C(5)-C(4)-N(1)	118.3(2)
S(1)-O(2)	1.4635(17)	C(3)-C(4)-N(1)	119.0(2)
S(1)-C(9)	1.774(2)	C(8)-C(3)-C(4)	116.8(2)
N(1)-C(4)	1.467(3)	C(8)-C(3)-C(2)	123.6(2)
N(1)-H(4A)	0.9100	C(4)-C(3)-C(2)	119.6(2)
N(1)-H(4B)	0.9100	C(6)-C(7)-C(8)	120.2(2)
N(1)-H(4C)	0.9100	C(6)-C(7)-H(7)	119.9
C(4)-C(5)	1.386(3)	C(8)-C(7)-H(7)	119.9
C(4)-C(3)	1.398(3)	C(4)-C(5)-C(6)	119.1(2)
C(3)-C(8)	1.392(3)	C(4)-C(5)-H(5)	120.4
C(3)-C(2)	1.516(3)	C(6)-C(5)-H(5)	120.4
C(7)-C(6)	1.387(4)	C(3)-C(2)-C(1)	116.2(2)
C(7)-C(8)	1.394(4)	C(3)-C(2)-H(2A)	108.2
C(7)-H(7)	0.9500	C(1)-C(2)-H(2A)	108.2
C(5)-C(6)	1.387(4)	C(15)-C(12)	1.508(3)
C(5)-H(5)	0.9500	C(15)-H(15A)	0.9800
C(2)-C(1)	1.522(3)	C(3)-C(2)-H(2B)	108.2
C(2)-H(2A)	0.9900	C(1)-C(2)-H(2B)	108.2
C(2)-H(2B)	0.9900	H(2A)-C(2)-H(2B)	107.4
C(1)-H(1A)	0.9800	C(2)-C(1)-H(1A)	109.5
C(1)-H(1B)	0.9800	C(2)-C(1)-H(1B)	109.5
C(1)-H(1C)	0.9800	H(1A)-C(1)-H(1B)	109.5
C(8)-H(8)	0.9500	C(2)-C(1)-H(1C)	109.5

C(6)-H(6)	0.9500	H(1A)-C(1)-H(1C)	109.5
C(12)-C(11)	1.392(3)	H(1B)-C(1)-H(1C)	109.5
C(12)-C(13)	1.401(3)	C(3)-C(8)-C(7)	121.4(2)
C(14)-C(9)	1.389(3)	C(3)-C(8)-H(8)	119.3
C(14)-C(13)	1.392(3)	C(7)-C(8)-H(8)	119.3
C(14)-H(14)	0.9500	C(5)-C(6)-C(7)	119.7(2)
C(11)-C(10)	1.394(3)	C(5)-C(6)-H(6)	120.1
C(11)-H(11)	0.9500	C(7)-C(6)-H(6)	120.1
C(13)-H(13)	0.9500	C(11)-C(12)-C(13)	118.6(2)
C(10)-C(9)	1.393(3)	C(11)-C(12)-C(15)	120.9(2)
C(10)-H(10)	0.9500	C(13)-C(12)-C(15)	120.6(2)
C(12)-C(15)-H(15A)	109.5	C(9)-C(14)-C(13)	119.5(2)
C(12)-C(15)-H(15B)	109.5	C(9)-C(14)-H(14)	120.2
H(15A)-C(15)-H(15B)	109.5	C(13)-C(14)-H(14)	120.2
C(12)-C(15)-H(15C)	109.5	C(12)-C(11)-C(10)	121.5(2)
H(15A)-C(15)-H(15C)	109.5	C(12)-C(11)-H(11)	119.3
H(15B)-C(15)-H(15C)	109.5	C(10)-C(11)-H(11)	119.3
O(1)-S(1)-O(3)	113.02(11)	C(14)-C(13)-C(12)	120.7(2)
O(1)-S(1)-O(2)	110.53(10)	C(14)-C(13)-H(13)	119.6
O(3)-S(1)-O(2)	112.31(10)	C(12)-C(13)-H(13)	119.6
O(1)-S(1)-C(9)	107.22(10)	C(9)-C(10)-C(11)	118.8(2)
O(3)-S(1)-C(9)	106.30(10)	C(9)-C(10)-H(10)	120.6
O(2)-S(1)-C(9)	107.06(10)	C(11)-C(10)-H(10)	120.6

C(4)-N(1)-H(4A)	109.5	C(14)-C(9)-C(10)	120.9(2)
C(4)-N(1)-H(4B)	109.5	C(14)-C(9)-S(1)	119.76(17)
H(4A)-N(1)-H(4B)	109.5	C(10)-C(9)-S(1)	119.28(17)
C(4)-N(1)-H(4C)	109.5		

14. Fluoren-9-ylidene-(4-nitrophenyl)-amine

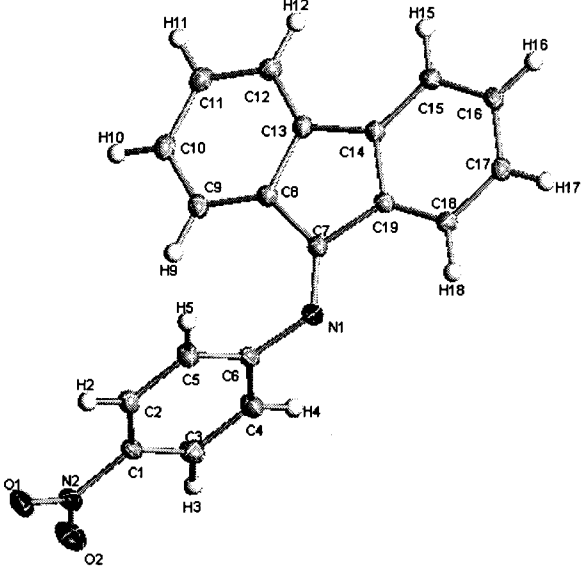
Comment

G. Crundwell from Central Connecticut State University provided the crystal investigated. It was grown from hexane.

All H atoms were placed in calculated positions, with C–H distances of 0.95 Å, and were included in the refinement in riding-motion approximation, with $U_{\text{iso}}(\text{H}) = 1.2U_{\text{eq}}$ of the adjacent carbon atom.

Table 6.2.14a. Crystal data for 04JU26am	Table 6.2.14b. Data collection
$\text{C}_{19}\text{H}_{12}\text{N}_2\text{O}_2$	Bruker SMART CCD area-detector
$M_r = 293.37$	diffractometer
Triclinic, $P\bar{1}$	ω scans
$a = 8.0894 (12) \text{ \AA}$	Absorption correction: multi-scan
$b = 9.0445 (14) \text{ \AA}$	$T_{\text{min}} = 0.950, T_{\text{max}} = 0.955$
$c = 9.8573 (15) \text{ \AA}$	7381 measured reflections
$\beta = 85.417 (3)^\circ$	3496 independent reflections
$V = 707.70 (19) \text{ \AA}^3$	3277 reflections with $I > 2\sigma(I)$
$Z = 2$	$R_{\text{int}} = 0.0292$
$D_x = 1.409 \text{ Mg m}^{-3}$	$\theta_{\text{max}} = 28.35^\circ$
Mo K_α radiation	$h = -10 \rightarrow 10$

Cell parameters from 6491 reflections	$k = -12 \rightarrow 12$
$\theta = 2.285 \pm 28.35^\circ$	$l = -13 \rightarrow 12$
$\mu = 0.093 \text{ mm}^{-1}$	
$T = 100 (2) \text{ K}$	
Block, yellow	
$0.55 \times 0.55 \times 0.50 \text{ mm}$	

Table 6.2.14c.	Figure 6.2.14. ORTEP plot of title compound. Ellipsoids are at the 50% probability level.
Refinement	
Refinement on F^2	
$R[F^2 > 2\sigma(F^2)] = 0.0443$	
$wR(F^2) = 0.1189$	
$S = 1.036$	
3496 reflections	
256 parameters	
H-atom parameters constrained	
$w = 1/[\sigma^2(F_o^2) + (0.0723P)^2 + 0.2346P]$	
where $P = (F_o^2 + 2F_c^2)/3$	
$(\Delta/\sigma)_{\text{max}} = 0.000$	
$\Delta\rho_{\text{max}} = 0.40 \text{ e} \times \text{\AA}^{-3}$	
	

$$\Delta\rho_{\min} = -0.30 \text{ e} \times \text{\AA}^{-3}$$

Table 6.2.14d.

Geometric parameters (Å, °).

N(1)-C(7)	1.2766(14)	C(6)-C(4)-H(4)	120.2(10)
N(1)-C(6)	1.4102(13)	C(17)-C(16)-C(15)	120.78(9)
O(1)-N(2)	1.2296(13)	C(17)-C(16)-H(16)	119.9(9)
N(2)-O(2)	1.2266(13)	C(15)-C(16)-H(16)	119.3(9)
N(2)-C(1)	1.4636(13)	C(15)-C(14)-C(19)	120.54(9)
C(1)-C(2)	1.3861(15)	C(15)-C(14)-C(13)	130.94(9)
C(1)-C(3)	1.3864(15)	C(19)-C(14)-C(13)	108.51(9)
C(6)-C(4)	1.3968(15)	C(12)-C(13)-C(8)	121.15(9)
C(6)-C(5)	1.3976(15)	C(12)-C(13)-C(14)	129.80(9)
C(4)-C(3)	1.3856(15)	C(8)-C(13)-C(14)	109.04(9)
C(4)-H(4)	0.957(17)	C(14)-C(15)-C(16)	118.47(9)
C(16)-C(17)	1.3927(15)	C(14)-C(15)-H(15)	120.9(9)
C(16)-C(15)	1.3966(14)	C(16)-C(15)-H(15)	120.6(9)
C(16)-H(16)	0.992(16)	N(1)-C(7)-C(19)	121.95(9)
C(14)-C(15)	1.3867(14)	N(1)-C(7)-C(8)	132.47(9)
C(14)-C(19)	1.4030(14)	C(19)-C(7)-C(8)	105.56(8)
C(14)-C(13)	1.4744(13)	C(4)-C(3)-C(1)	118.61(10)
C(13)-C(12)	1.3849(14)	C(4)-C(3)-H(3)	119.8(9)

C(13)-C(8)	1.4096(14)	C(1)-C(3)-H(3)	121.5(9)
C(15)-H(15)	0.983(15)	C(1)-C(2)-C(5)	118.55(10)
C(7)-C(19)	1.4899(13)	C(1)-C(2)-H(2)	120.8(10)
C(7)-C(8)	1.4985(14)	C(5)-C(2)-H(2)	120.7(10)
C(3)-H(3)	0.989(16)	C(2)-C(5)-C(6)	120.34(10)
C(2)-C(5)	1.3878(14)	C(2)-C(5)-H(5)	119.8(9)
C(2)-H(2)	0.965(16)	C(6)-C(5)-H(5)	119.8(9)
C(5)-H(5)	0.971(16)	C(9)-C(8)-C(13)	120.26(9)
C(8)-C(9)	1.3914(14)	C(9)-C(8)-C(7)	131.70(10)
C(17)-C(18)	1.3992(14)	C(13)-C(8)-C(7)	107.99(9)
C(17)-H(17)	0.950(16)	C(16)-C(17)-C(18)	120.95(9)
C(10)-C(11)	1.3922(16)	C(16)-C(17)-H(17)	119.6(9)
C(10)-C(9)	1.3981(15)	C(18)-C(17)-H(17)	119.4(9)
C(10)-H(10)	0.988(16)	C(11)-C(10)-C(9)	120.90(10)
C(18)-C(19)	1.3856(14)	C(11)-C(10)-H(10)	119.4(9)
C(18)-H(18)	0.988(16)	C(9)-C(10)-H(10)	119.7(9)
C(9)-H(9)	0.962(15)	C(19)-C(18)-C(17)	117.97(9)
C(11)-C(12)	1.3979(15)	C(19)-C(18)-H(18)	121.2(9)
C(11)-H(11)	0.978(16)	C(17)-C(18)-H(18)	120.9(9)
C(12)-H(12)	0.972(16)	C(8)-C(9)-C(10)	118.51(10)
C(7)-N(1)-C(6)	122.24(9)	C(8)-C(9)-H(9)	121.9(9)
O(2)-N(2)-O(1)	123.27(9)	C(10)-C(9)-H(9)	119.6(9)
O(2)-N(2)-C(1)	118.31(9)	C(18)-C(19)-C(14)	121.27(9)

O(1)-N(2)-C(1)	118.41(9)	C(18)-C(19)-C(7)	129.86(9)
C(2)-C(1)-C(3)	122.34(10)	C(14)-C(19)-C(7)	108.87(9)
C(2)-C(1)-N(2)	118.85(10)	C(10)-C(11)-C(12)	120.85(10)
C(3)-C(1)-N(2)	118.79(9)	C(10)-C(11)-H(11)	120.9(9)
C(4)-C(6)-C(5)	119.74(10)	C(12)-C(11)-H(11)	118.2(9)
C(4)-C(6)-N(1)	119.73(10)	C(13)-C(12)-C(11)	118.32(10)
C(5)-C(6)-N(1)	120.23(9)	C(13)-C(12)-H(12)	122.0(9)
C(3)-C(4)-C(6)	120.40(10)	C(11)-C(12)-H(12)	119.6(9)
C(3)-C(4)-H(4)	119.4(10)		

Section three- References

-
- 1 J.P. Glusker, M. Lewis, M. Rossi. *Crystal Structure Analysis for Chemists and Biologists*; Wiley-VCH: New York, 1994.
 - 2 A.D. Hunter. *X-ray Structure Analysis Lab Manual: A Beginner's Introduction*, 1998

Appendix I

X-Ray crystal data for 1,2-bis[3,5-bis(trifluoromethyl)benzene]phosphino]benzene

Table A1a. Crystal data for 03JU01a	Table A1b. Data collection
$C_{38}H_{16}F_{24}P_2$	Bruker SMART CCD area-detector
Mr = 990.45	diffractometer
Monoclinic, $P2_1/n$	ω scans
$a = 11.3667 (6) \text{ \AA}$	Absorption correction: multi-scan
$b = 16.3738 (8) \text{ \AA}$	$T_{\min} = 0.942, T_{\max} = 0.964$
$c = 22.2252 (11) \text{ \AA}$	42957 measured reflections
$\beta = 94.756 (1)^\circ$	10226 independent reflections
$V = 4122.22 (10) \text{ \AA}^3$	32068 reflections with $I > 2\sigma(I)$
$Z = 4$	$R_{\text{int}} = 0.0394$
$D_x = 1.596 \text{ Mg m}^{-3}$	$\theta_{\max} = 28.3^\circ$
Mo K_α radiation	$h = -15 \rightarrow 15$
Cell parameters from 17838 reflections	$k = -21 \rightarrow 21$
$\theta = 2.22 \pm 28.3^\circ$	$l = -29 \rightarrow 29$
$\mu = 0.24 \text{ mm}^{-1}$	
$T = 100 (2) \text{ K}$	
Rectangular, colorless	
$0.15 \times 0.20 \times 0.27 \text{ mm}$	

C(5)-H(5)	0.94(4)	C(28)-C(27)-C(26)	121.4(3)
C(6)-H(6)	0.95(3)	C(28)-C(27)-C(38)	118.9(3)
C(7)-C(12)	1.394(4)	C(26)-C(27)-C(38)	119.7(3)
C(7)-C(8)	1.401(4)	C(29)-C(28)-C(27)	118.2(3)
C(8)-C(9)	1.384(4)	C(29)-C(28)-H(28)	122(2)
C(8)-H(8)	0.97(3)	C(27)-C(28)-H(28)	120(2)
C(9)-C(10)	1.387(4)	C(28)-C(29)-C(30)	121.4(3)
C(9)-C(31)	1.498(4)	C(28)-C(29)-C(37)	119.8(3)
C(10)-C(11)	1.386(4)	C(30)-C(29)-C(37)	118.7(3)
C(10)-H(10)	0.92(4)	C(29)-C(30)-C(25)	120.5(3)
C(11)-C(12)	1.390(4)	C(29)-C(30)-H(30)	120(2)
C(11)-C(32)	1.503(4)	C(25)-C(30)-H(30)	119(2)
C(12)-H(12)	0.90(4)	F(31C)-C(31)-F(31B)	106.1(3)
C(13)-C(14)	1.394(4)	F(31C)-C(31)-F(31A)	106.8(3)
C(13)-C(18)	1.401(4)	F(31B)-C(31)-F(31A)	106.2(3)
C(14)-C(15)	1.387(4)	F(31C)-C(31)-C(9)	112.9(3)
C(14)-H(14)	0.90(4)	F(31B)-C(31)-C(9)	113.1(3)
C(15)-C(16)	1.387(5)	F(31A)-C(31)-C(9)	111.3(3)
C(15)-C(34)	1.498(4)	F(32A)-C(32)-F(32E)	92.7(12)
C(16)-C(17)	1.383(4)	F(32A)-C(32)-F(32B)	108.8(13)
C(16)-H(16)	0.93(4)	F(32E)-C(32)-F(32B)	19.5(16)
C(17)-C(18)	1.391(4)	F(32A)-C(32)-F(32D)	17.6(17)
C(17)-C(33)	1.508(5)	F(32E)-C(32)-F(32D)	105.1(12)

C(19)-C(20)	1.388(4)	F(32B)-C(32)-F(32D)	118.0(9)
C(19)-C(24)	1.394(4)	F(32A)-C(32)-F(32F)	119.9(14)
C(20)-C(21)	1.386(4)	F(32E)-C(32)-F(32F)	109.0(12)
C(20)-H(20)	0.93(4)	F(32B)-C(32)-F(32F)	91.1(9)
C(21)-C(22)	1.392(4)	F(32D)-C(32)-F(32F)	103.4(7)
C(21)-C(36)	1.500(4)	F(32A)-C(32)-F(32C)	110.3(13)
C(22)-C(23)	1.382(4)	F(32E)-C(32)-F(32C)	119.4(12)
C(22)-H(22)	0.99(3)	F(32B)-C(32)-F(32C)	102.4(8)
C(23)-C(24)	1.385(4)	F(32D)-C(32)-F(32C)	93.2(8)
C(23)-C(35)	1.502(4)	F(32F)-C(32)-F(32C)	12.5(8)
C(24)-H(24)	0.93(3)	F(32A)-C(32)-C(11)	109.8(9)
C(25)-C(30)	1.390(4)	F(32E)-C(32)-C(11)	111.5(7)
C(25)-C(26)	1.401(4)	F(32B)-C(32)-C(11)	113.8(7)
C(26)-C(27)	1.387(4)	F(32D)-C(32)-C(11)	114.9(6)
C(26)-H(26)	0.96(4)	F(32F)-C(32)-C(11)	112.2(6)
C(27)-C(28)	1.381(4)	F(32C)-C(32)-C(11)	111.4(7)
C(27)-C(38)	1.501(5)	F(33D)-C(33)-F(33C)	111(2)
C(28)-C(29)	1.380(4)	F(33D)-C(33)-F(33A)	87.7(18)
C(28)-H(28)	0.94(4)	F(33C)-C(33)-F(33A)	113.9(16)
C(29)-C(30)	1.385(4)	F(33D)-C(33)-F(33E)	118(2)
C(29)-C(37)	1.503(4)	F(33C)-C(33)-F(33E)	11(3)
C(30)-H(30)	0.91(3)	F(33A)-C(33)-F(33E)	104.1(16)
C(31)-F(31C)	1.315(4)	F(33D)-C(33)-F(33F)	106.6(13)

C(31)-F(31B)	1.324(4)	F(33C)-C(33)-F(33F)	107(2)
C(31)-F(31A)	1.327(4)	F(33A)-C(33)-F(33F)	18.9(15)
C(32)-F(32A)	1.300(11)	F(33E)-C(33)-F(33F)	96(2)
C(32)-F(32E)	1.301(10)	F(33D)-C(33)-F(33B)	21(2)
C(32)-F(32B)	1.308(9)	F(33C)-C(33)-F(33B)	96.0(14)
C(32)-F(32D)	1.312(9)	F(33A)-C(33)-F(33B)	107.0(9)
C(32)-F(32F)	1.316(8)	F(33E)-C(33)-F(33B)	104.8(13)
C(32)-F(32C)	1.323(9)	F(33F)-C(33)-F(33B)	126.0(14)
C(33)-F(33D)	1.306(11)	F(33D)-C(33)-C(17)	114.9(9)
C(33)-F(33C)	1.313(11)	F(33C)-C(33)-C(17)	110.8(9)
C(33)-F(33A)	1.323(10)	F(33A)-C(33)-C(17)	116.5(10)
C(33)-F(33E)	1.331(10)	F(33E)-C(33)-C(17)	112.9(7)
C(33)-F(33F)	1.339(13)	F(33F)-C(33)-C(17)	105.7(11)
C(33)-F(33B)	1.354(7)	F(33B)-C(33)-C(17)	110.5(6)
C(34)-F(34F)	1.283(15)	F(34F)-C(34)-F(34D)	107(2)
C(34)-F(34D)	1.287(14)	F(34F)-C(34)-F(34A)	35(3)
C(34)-F(34A)	1.305(5)	F(34D)-C(34)-F(34A)	127.5(13)
C(34)-F(34B)	1.315(5)	F(34F)-C(34)-F(34B)	128.4(18)
C(34)-F(34E)	1.326(14)	F(34D)-C(34)-F(34B)	61(2)
C(34)-F(34C)	1.343(5)	F(34A)-C(34)-F(34B)	108.5(4)
C(35)-F(35A)	1.318(4)	F(34F)-C(34)-F(34E)	103(3)
C(35)-F(35B)	1.321(4)	F(34D)-C(34)-F(34E)	102(3)
C(35)-F(35C)	1.330(5)	F(34A)-C(34)-F(34E)	71(4)

C(36)-F(36C)	1.287(4)	F(34B)-C(34)-F(34E)	44(4)
C(36)-F(36A)	1.301(4)	F(34F)-C(34)-F(34C)	73(3)
C(36)-F(36B)	1.302(4)	F(34D)-C(34)-F(34C)	44(2)
C(37)-F(37D)	1.276(11)	F(34A)-C(34)-F(34C)	106.3(4)
C(37)-F(37C)	1.291(7)	F(34B)-C(34)-F(34C)	104.7(4)
C(37)-F(37E)	1.310(8)	F(34E)-C(34)-F(34C)	137.7(18)
C(37)-F(37B)	1.310(7)	F(34F)-C(34)-C(15)	116.9(15)
C(37)-F(37A)	1.356(6)	F(34D)-C(34)-C(15)	117.4(12)
C(37)-F(37F)	1.369(10)	F(34A)-C(34)-C(15)	114.0(3)
C(38)-F(38A)	1.198(8)	F(34B)-C(34)-C(15)	111.8(3)
C(38)-F(38F)	1.241(10)	F(34E)-C(34)-C(15)	107.8(12)
C(38)-F(38D)	1.283(7)	F(34C)-C(34)-C(15)	111.1(3)
C(38)-F(38C)	1.297(8)	F(35A)-C(35)-F(35B)	108.1(3)
C(38)-F(38B)	1.434(8)	F(35A)-C(35)-F(35C)	105.8(3)
C(38)-F(38E)	1.456(8)	F(35B)-C(35)-F(35C)	106.0(3)
C(41)-C(40)-C(45)	120.0	F(35A)-C(35)-C(23)	112.5(3)
C(41)-C(40)-H(40)	120.0	F(35B)-C(35)-C(23)	112.7(3)
C(45)-C(40)-H(40)	120.0	F(35C)-C(35)-C(23)	111.3(3)
C(42)-C(41)-C(40)	120.0	F(36C)-C(36)-F(36A)	106.6(4)
C(42)-C(41)-H(41)	120.0	F(36C)-C(36)-F(36B)	104.9(3)
C(40)-C(41)-H(41)	120.0	F(36A)-C(36)-F(36B)	104.9(3)
C(41)-C(42)-C(43)	120.0	F(36C)-C(36)-C(21)	113.2(3)
C(41)-C(42)-H(42)	120.0	F(36A)-C(36)-C(21)	113.0(3)

C(43)-C(42)-H(42)	120.0	F(36B)-C(36)-C(21)	113.5(3)
C(44)-C(43)-C(42)	120.0	F(37D)-C(37)-F(37C)	125.2(8)
C(44)-C(43)-H(43)	120.0	F(37D)-C(37)-F(37E)	117.0(12)
C(42)-C(43)-H(43)	120.0	F(37C)-C(37)-F(37E)	68.4(11)
C(43)-C(44)-C(45)	120.0	F(37D)-C(37)-F(37B)	21.5(10)
C(43)-C(44)-H(44)	120.0	F(37C)-C(37)-F(37B)	108.8(6)
C(45)-C(44)-H(44)	120.0	F(37E)-C(37)-F(37B)	127.9(8)
C(44)-C(45)-C(40)	120.0	F(37D)-C(37)-F(37A)	83.8(9)
C(44)-C(45)-C(46)	129.0(8)	F(37C)-C(37)-F(37A)	107.2(5)
C(40)-C(45)-C(46)	111.0(8)	F(37E)-C(37)-F(37A)	41.1(12)
C(13)-P(1)-C(7)	101.08(12)	F(37B)-C(37)-F(37A)	102.6(6)
C(13)-P(1)-C(1)	99.05(12)	F(37D)-C(37)-F(37F)	102.1(8)
C(7)-P(1)-C(1)	103.34(12)	F(37C)-C(37)-F(37F)	34.4(4)
C(6)-C(1)-C(2)	118.9(2)	F(37E)-C(37)-F(37F)	101.5(9)
C(6)-C(1)-P(1)	123.7(2)	F(37B)-C(37)-F(37F)	81.5(7)
C(2)-C(1)-P(1)	117.35(19)	F(37A)-C(37)-F(37F)	135.2(7)
C(25)-P(2)-C(2)	101.60(12)	F(37D)-C(37)-C(29)	112.6(8)
C(25)-P(2)-C(19)	101.43(12)	F(37C)-C(37)-C(29)	113.0(4)
C(2)-P(2)-C(19)	103.09(12)	F(37E)-C(37)-C(29)	113.6(4)
C(3)-C(2)-C(1)	119.2(2)	F(37B)-C(37)-C(29)	114.5(5)
C(3)-C(2)-P(2)	122.4(2)	F(37A)-C(37)-C(29)	110.0(3)
C(1)-C(2)-P(2)	118.23(19)	C(14)-C(13)-C(18)	118.8(3)
C(4)-C(3)-C(2)	121.2(3)	C(14)-C(13)-P(1)	118.9(2)

C(4)-C(3)-H(3)	118(2)	C(18)-C(13)-P(1)	122.3(2)
C(2)-C(3)-H(3)	120(2)	C(15)-C(14)-C(13)	120.2(3)
C(5)-C(4)-C(3)	119.4(3)	C(15)-C(14)-H(14)	122(2)
C(5)-C(4)-H(4)	122(2)	C(13)-C(14)-H(14)	118(2)
C(3)-C(4)-H(4)	119(2)	C(16)-C(15)-C(14)	121.1(3)
C(4)-C(5)-C(6)	120.4(3)	C(16)-C(15)-C(34)	118.3(3)
C(4)-C(5)-H(5)	120(2)	C(14)-C(15)-C(34)	120.5(3)
C(6)-C(5)-H(5)	120(2)	F(37F)-C(37)-C(29)	108.3(6)
C(5)-C(6)-C(1)	120.8(3)	F(38A)-C(38)-F(38F)	121.1(9)
C(5)-C(6)-H(6)	119(2)	F(38A)-C(38)-F(38D)	52.7(10)
C(1)-C(6)-H(6)	121(2)	F(38F)-C(38)-F(38D)	116.4(8)
C(12)-C(7)-C(8)	118.1(2)	F(38A)-C(38)-F(38C)	113.3(10)
C(12)-C(7)-P(1)	122.0(2)	F(38F)-C(38)-F(38C)	22.6(10)
C(8)-C(7)-P(1)	119.4(2)	F(38D)-C(38)-F(38C)	131.3(6)
C(9)-C(8)-C(7)	120.7(3)	F(38A)-C(38)-F(38B)	108.1(9)
C(9)-C(8)-H(8)	121.5(19)	F(38F)-C(38)-F(38B)	72.9(9)
C(7)-C(8)-H(8)	117.8(19)	F(38D)-C(38)-F(38B)	58.7(5)
C(8)-C(9)-C(10)	121.0(3)	F(38C)-C(38)-F(38B)	95.4(6)
C(8)-C(9)-C(31)	120.0(3)	F(38A)-C(38)-F(38E)	43.8(11)
C(10)-C(9)-C(31)	119.0(3)	F(38F)-C(38)-F(38E)	100.1(9)
C(11)-C(10)-C(9)	118.6(3)	F(38D)-C(38)-F(38E)	96.2(5)
C(11)-C(10)-H(10)	120(2)	F(38C)-C(38)-F(38E)	81.3(6)
C(9)-C(10)-H(10)	122(2)	F(38B)-C(38)-F(38E)	143.2(5)

C(10)-C(11)-C(12)	120.9(3)	F(38A)-C(38)-C(27)	117.2(5)
C(10)-C(11)-C(32)	120.0(3)	F(38F)-C(38)-C(27)	117.9(7)
C(12)-C(11)-C(32)	119.0(3)	F(38D)-C(38)-C(27)	114.5(4)
C(11)-C(12)-C(7)	120.6(3)	F(38C)-C(38)-C(27)	112.5(5)
C(11)-C(12)-H(12)	121(2)	F(38B)-C(38)-C(27)	107.7(4)
C(7)-C(12)-H(12)	119(2)	F(38E)-C(38)-C(27)	107.3(4)
C(17)-C(16)-C(15)	118.8(3)	C5-S1-C2	91.61 (9)
C(17)-C(16)-H(16)	123(2)	O1-C1-C2	124.39 (18)

Appendix II

X-Ray crystal data for *cis*-bis(2,3,5,6-tetramethyl-1,4-diisocyanobenzene) bis[1,2-bis(diphenylphosphino)ethane]tungsten(0)

Table A2a. Crystal data for 03Mz48am	Table A2b. Data collection
$C_{85}H_{89}N_4P_4W$ $M_r = 1498.33$ Triclinic, P-1 $a = 12.486 (3) \text{ \AA}$ $b = 14.298 (3) \text{ \AA}$ $c = 21.133 (4) \text{ \AA}$ $\alpha = 71.067 (3)^\circ$ $\beta = 81.897 (4)^\circ$ $\gamma = 82.440 (4)^\circ$ $V = 3518.1 (12) \text{ \AA}^3$ $Z = 2$ $D_x = 1.414 \text{ Mg m}^{-3}$ Mo K_α radiation Cell parameters from 19900 reflections $\theta = 2.342 \pm 28.313^\circ$ $\mu = 1.785 \text{ mm}^{-1}$ $T = 100 (2) \text{ K}$ Rectangular, colorless $0.10 \times 0.14 \times 0.30 \text{ mm}$	Bruker SMART CCD area-detector diffractometer ω scans Absorption correction: multi-scan $T_{\min} = 0.741, T_{\max} = 0.837$ 36248 measured reflections 17391 independent reflections 14642 reflections with $I > 2\sigma(I)$ $R_{\text{int}} = 0.0388$ $\theta_{\max} = 28.313^\circ$ $h = -16 \rightarrow 16$ $k = -19 \rightarrow 19$ $l = -28 \rightarrow 28$

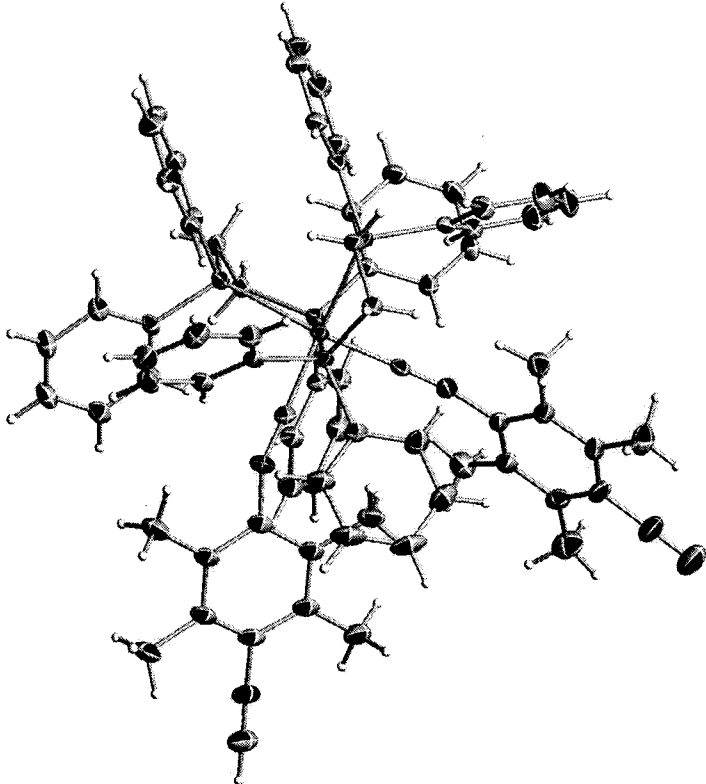
Table A2c. Refinement	Figure A2a. ORTEP plot of title compound. Ellipsoids are at the 50% probability level. Solvent molecules of THF and hexane are also shown.
Refinement on F^2 $R[F^2 > 2\sigma(F^2)] = 0.0530$ $wR(F^2) = 0.1033$ $S = 1.026$ 17391 reflections 862 parameters H-atom parameters constrained $w = 1/[\sigma^2(F_o^2) + (0.0652P)^2 + 0.0000P]$ where $P = (F_o^2 + 2F_c^2)/3$ $(\Delta\sigma)_{\max} = 0.002$ $\Delta\rho_{\max} = 3.679 \text{ e}\times\text{\AA}^{-3}$ $\Delta\rho_{\min} = -0.924 \text{ e}\times\text{\AA}^{-3}$	

Table A2d			
Selected geometric parameters (\AA , $^\circ$).			
W(1)-C(1)	1.973(4)	C(29)-C(22)-C(28)	121.4(3)
W(1)-C(8)	2.000(4)	C(30)-C(23)-C(29)	118.5(3)
W(1)-P(2)	2.4347(9)	C(30)-C(23)-C(69)	122.0(4)
W(1)-P(4)	2.4669(9)	C(29)-C(23)-C(69)	119.5(4)
W(1)-P(3)	2.5252(10)	C(26)-C(24)-C(9)	121.2(4)
W(1)-P(1)	2.5358(9)	C(26)-C(24)-H(24)	119.4

P(2)-C(25)	1.832(3)	C(9)-C(24)-H(24)	119.4
P(2)-C(5)	1.838(4)	C(17)-C(25)-P(2)	106.6(2)
P(2)-C(7)	1.843(4)	C(17)-C(25)-H(25A)	110.4
P(4)-C(11)	1.837(4)	P(2)-C(25)-H(25A)	110.4
P(4)-C(27)	1.843(4)	C(17)-C(25)-H(25B)	110.4
P(4)-C(6)	1.857(4)	P(2)-C(25)-H(25B)	110.4
P(1)-C(3)	1.838(4)	H(25A)-C(25)-H(25B)	108.6
P(1)-C(17)	1.843(3)	C(24)-C(26)-C(57)	120.1(4)
P(1)-C(4)	1.844(4)	C(24)-C(26)-H(26)	120.0
P(3)-C(10)	1.848(4)	C(57)-C(26)-H(26)	120.0
P(3)-C(9)	1.851(3)	C(15)-C(27)-P(4)	111.0(2)
P(3)-C(15)	1.861(4)	C(15)-C(27)-H(27A)	109.4
C(3)-C(42)	1.395(5)	P(4)-C(27)-H(27A)	109.4
C(3)-C(12)	1.399(5)	C(15)-C(27)-H(27B)	109.4
C(1)-N(2)	1.221(4)	P(4)-C(27)-H(27B)	109.4
C(4)-C(31)	1.386(5)	H(27A)-C(27)-H(27B)	108.0
C(4)-C(20)	1.396(5)	C(48)-C(28)-C(22)	118.9(3)
C(5)-C(16)	1.387(5)	C(48)-C(28)-C(60)	120.0(3)
C(5)-C(34)	1.392(5)	C(22)-C(28)-C(60)	121.0(3)
C(6)-C(43)	1.385(5)	C(23)-C(29)-C(22)	119.0(3)
C(6)-C(13)	1.392(5)	C(23)-C(29)-C(37)	119.5(3)
C(7)-C(56)	1.388(6)	P(3)-C(15)-H(15B)	109.6
C(7)-C(18)	1.390(5)	H(15A)-C(15)-H(15B)	108.1

N(1)-C(8)	1.187(5)	C(62)-C(16)-C(5)	121.3(4)
N(1)-C(22)	1.393(5)	C(62)-C(16)-H(16)	119.3
C(9)-C(14)	1.382(5)	C(5)-C(16)-H(16)	119.3
C(9)-C(24)	1.400(5)	C(25)-C(17)-P(1)	107.8(2)
C(10)-C(19)	1.387(5)	C(25)-C(17)-H(17A)	110.1
C(10)-C(36)	1.403(5)	P(1)-C(17)-H(17A)	110.1
C(11)-C(21)	1.393(5)	C(25)-C(17)-H(17B)	110.1
C(11)-C(32)	1.397(5)	P(1)-C(17)-H(17B)	110.1
C(12)-C(67)	1.372(5)	H(17A)-C(17)-H(17B)	108.5
C(12)-H(12)	0.9500	N(1)-C(8)-W(1)	171.1(3)
C(13)-C(39)	1.382(5)	C(71)-C(18)-C(7)	120.2(4)
C(13)-H(13)	0.9500	C(71)-C(18)-H(18)	119.9
C(14)-C(45)	1.395(5)	C(22)-C(29)-C(37)	121.5(3)
C(14)-H(14)	0.9500	C(48)-C(30)-C(23)	123.3(3)
C(15)-C(27)	1.509(5)	C(48)-C(30)-N(3)	118.3(4)
C(15)-H(15A)	0.9900	C(23)-C(30)-N(3)	118.4(4)
C(15)-H(15B)	0.9900	C(4)-C(31)-C(47)	119.9(4)
C(16)-C(62)	1.382(5)	C(4)-C(31)-H(31)	120.0
C(16)-H(16)	0.9500	C(47)-C(31)-H(31)	120.0
C(17)-C(25)	1.533(5)	C(35)-C(32)-C(11)	121.0(3)
C(17)-H(17A)	0.9900	C(35)-C(32)-H(32)	119.5
C(17)-H(17B)	0.9900	C(11)-C(32)-H(32)	119.5
C(18)-C(71)	1.389(6)	C(54)-C(33)-C(20)	120.3(4)

C(18)-H(18)	0.9500	C(54)-C(33)-H(33)	119.9
C(19)-C(46)	1.383(5)	C(20)-C(33)-H(33)	119.9
C(19)-H(19)	0.9500	C(41)-C(34)-C(5)	120.6(4)
C(20)-C(33)	1.391(5)	C(41)-C(34)-H(34)	119.7
C(20)-H(20)	0.9500	C(5)-C(34)-H(34)	119.7
C(21)-C(49)	1.396(5)	C(32)-C(35)-C(50)	120.3(4)
C(21)-H(21)	0.9500	C(32)-C(35)-H(35)	119.8
N(2)-C(38)	1.386(5)	C(50)-C(35)-H(35)	119.8
C(22)-C(29)	1.406(5)	C(66)-C(36)-C(10)	120.5(4)
C(22)-C(28)	1.411(5)	C(66)-C(36)-H(36)	119.8
C(23)-C(30)	1.390(6)	C(10)-C(36)-H(36)	119.8
C(23)-C(29)	1.391(5)	C(29)-C(37)-H(37A)	109.5
C(23)-C(69)	1.507(5)	C(29)-C(37)-H(37B)	109.5
C(24)-C(26)	1.386(5)	H(37A)-C(37)-H(37B)	109.5
C(24)-H(24)	0.9500	C(29)-C(37)-H(37C)	109.5
C(25)-H(25A)	0.9900	H(37A)-C(37)-H(37C)	109.5
C(25)-H(25B)	0.9900	H(37B)-C(37)-H(37C)	109.5
C(26)-C(57)	1.389(6)	C(77)-N(3)-C(30)	178.9(5)
C(26)-H(26)	0.9500	N(2)-C(38)-C(52)	118.9(4)
C(27)-H(27A)	0.9900	N(2)-C(38)-C(44)	119.8(3)
C(27)-H(27B)	0.9900	C(52)-C(38)-C(44)	121.3(3)
C(28)-C(48)	1.389(5)	C(40)-C(39)-C(13)	120.0(4)
C(28)-C(60)	1.519(5)	C(40)-C(39)-H(39)	120.0

C(29)-C(37)	1.498(5)	C(13)-C(39)-H(39)	120.0
C(30)-C(48)	1.386(6)	C(39)-C(40)-C(61)	119.4(4)
C(30)-N(3)	1.407(5)	C(39)-C(40)-H(40)	120.3
C(31)-C(47)	1.400(5)	C(61)-C(40)-H(40)	120.3
C(31)-H(31)	0.9500	C(55)-C(41)-C(34)	120.1(4)
C(32)-C(35)	1.384(5)	C(55)-C(41)-H(41)	119.9
C(32)-H(32)	0.9500	C(34)-C(41)-H(41)	119.9
C(33)-C(54)	1.379(6)	C(70)-C(42)-C(3)	120.8(4)
C(33)-H(33)	0.9500	C(70)-C(42)-H(42)	119.6
C(34)-C(41)	1.387(6)	C(3)-C(42)-H(42)	119.6
C(34)-H(34)	0.9500	C(61)-C(43)-C(6)	121.5(4)
C(35)-C(50)	1.386(6)	C(61)-C(43)-H(43)	119.3
C(35)-H(35)	0.9500	C(6)-C(43)-H(43)	119.3
C(36)-C(66)	1.390(6)	C(51)-C(44)-C(38)	119.1(4)
C(36)-H(36)	0.9500	C(51)-C(44)-C(65)	121.8(4)
C(37)-H(37A)	0.9800	C(38)-C(44)-C(65)	119.1(3)
C(37)-H(37B)	0.9800	C(57)-C(45)-C(14)	120.3(4)
C(37)-H(37C)	0.9800	C(57)-C(45)-H(45)	119.8
N(3)-C(77)	1.142(6)	C(14)-C(45)-H(45)	119.8
C(38)-C(52)	1.405(5)	C(19)-C(46)-C(68)	120.0(4)
C(38)-C(44)	1.407(6)	C(19)-C(46)-H(46)	120.0
C(39)-C(40)	1.373(6)	C(68)-C(46)-H(46)	120.0
C(39)-H(39)	0.9500	C(54)-C(47)-C(31)	120.7(4)

C(40)-C(61)	1.394(6)	C(54)-C(47)-H(47)	119.7
C(40)-H(40)	0.9500	C(31)-C(47)-H(47)	119.7
C(41)-C(55)	1.381(6)	C(30)-C(48)-C(28)	118.6(3)
C(41)-H(41)	0.9500	C(30)-C(48)-C(76)	120.3(4)
C(42)-C(70)	1.380(6)	C(28)-C(48)-C(76)	121.1(4)
C(42)-H(42)	0.9500	C(50)-C(49)-C(21)	119.9(4)
C(43)-C(61)	1.381(5)	C(50)-C(49)-H(49)	120.0
C(43)-H(43)	0.9500	C(21)-C(49)-H(49)	120.0
C(44)-C(51)	1.396(5)	C(49)-C(50)-C(35)	119.8(4)
C(44)-C(65)	1.510(5)	C(49)-C(50)-H(50)	120.1
C(45)-C(57)	1.389(6)	C(35)-C(50)-H(50)	120.1
C(45)-H(45)	0.9500	C(53)-C(51)-C(44)	118.1(4)
C(46)-C(68)	1.391(6)	C(53)-C(51)-C(59)	120.7(4)
C(46)-H(46)	0.9500	C(44)-C(51)-C(59)	121.3(4)
C(47)-C(54)	1.379(6)	C(58)-C(52)-C(38)	118.5(4)
C(47)-H(47)	0.9500	C(58)-C(52)-C(64)	121.4(4)
C(48)-C(76)	1.510(6)	C(38)-C(52)-C(64)	120.1(3)
C(49)-C(50)	1.377(6)	C(72)-N(4)-C(53)	179.4(5)
C(49)-H(49)	0.9500	C(58)-C(53)-C(51)	123.3(3)
C(50)-H(50)	0.9500	C(58)-C(53)-N(4)	118.4(4)
C(51)-C(53)	1.392(6)	C(51)-C(53)-N(4)	118.3(4)
C(51)-C(59)	1.498(6)	C(33)-C(54)-C(47)	119.6(4)
C(52)-C(58)	1.402(5)	C(33)-C(54)-H(54)	120.2

C(52)-C(64)	1.496(6)	C(47)-C(54)-H(54)	120.2
N(4)-C(72)	1.141(5)	C(41)-C(55)-C(62)	120.0(4)
N(4)-C(53)	1.405(5)	C(41)-C(55)-H(55)	120.0
C(53)-C(58)	1.384(6)	C(62)-C(55)-H(55)	120.0
C(54)-H(54)	0.9500	C(7)-C(56)-C(75)	120.9(4)
C(55)-C(62)	1.382(6)	C(7)-C(56)-H(56)	119.6
C(55)-H(55)	0.9500	C(75)-C(56)-H(56)	119.6
C(56)-C(75)	1.389(6)	C(26)-C(57)-C(45)	119.2(4)
C(56)-H(56)	0.9500	C(26)-C(57)-H(57)	120.4
C(57)-H(57)	0.9500	C(45)-C(57)-H(57)	120.4
C(58)-C(63)	1.507(6)	C(53)-C(58)-C(52)	118.8(4)
C(59)-H(59A)	0.9800	C(53)-C(58)-C(63)	120.6(4)
C(59)-H(59B)	0.9800	C(52)-C(58)-C(63)	120.6(4)
C(59)-H(59C)	0.9800	C(51)-C(59)-H(59A)	109.5
C(60)-H(60A)	0.9800	C(51)-C(59)-H(59B)	109.5
C(60)-H(60B)	0.9800	H(59A)-C(59)-H(59B)	109.5
C(60)-H(60C)	0.9800	C(51)-C(59)-H(59C)	109.5
C(61)-H(61)	0.9500	H(59A)-C(59)-H(59C)	109.5
C(62)-H(62)	0.9500	H(59B)-C(59)-H(59C)	109.5
C(63)-H(63A)	0.9800	C(28)-C(60)-H(60A)	109.5
C(63)-H(63B)	0.9800	C(28)-C(60)-H(60B)	109.5
C(63)-H(63C)	0.9800	H(60A)-C(60)-H(60B)	109.5
C(64)-H(64A)	0.9800	C(28)-C(60)-H(60C)	109.5

C(64)-H(64B)	0.9800	H(60A)-C(60)-H(60C)	109.5
C(64)-H(64C)	0.9800	H(60B)-C(60)-H(60C)	109.5
C(65)-H(65A)	0.9800	C(43)-C(61)-C(40)	120.0(4)
C(65)-H(65B)	0.9800	C(43)-C(61)-H(61)	120.0
C(65)-H(65C)	0.9800	C(40)-C(61)-H(61)	120.0
C(66)-C(68)	1.369(6)	C(16)-C(62)-C(55)	119.7(4)
C(66)-H(66)	0.9500	C(16)-C(62)-H(62)	120.2
C(67)-C(73)	1.377(6)	C(55)-C(62)-H(62)	120.2
C(67)-H(67)	0.9500	C(58)-C(63)-H(63A)	109.5
C(68)-H(68)	0.9500	C(58)-C(63)-H(63B)	109.5
C(69)-H(69A)	0.9800	H(63A)-C(63)-H(63B)	109.5
C(69)-H(69B)	0.9800	C(58)-C(63)-H(63C)	109.5
C(69)-H(69C)	0.9800	H(63A)-C(63)-H(63C)	109.5
C(70)-C(73)	1.383(7)	H(63B)-C(63)-H(63C)	109.5
C(70)-H(70)	0.9500	C(52)-C(64)-H(64A)	109.5
C(71)-C(74)	1.375(7)	C(52)-C(64)-H(64B)	109.5
C(71)-H(71)	0.9500	H(64A)-C(64)-H(64B)	109.5
C(72)-H(72)	0.9500	C(52)-C(64)-H(64C)	109.5
C(73)-H(73)	0.9500	H(64A)-C(64)-H(64C)	109.5
C(74)-C(75)	1.374(7)	H(64B)-C(64)-H(64C)	109.5
C(74)-H(74)	0.9500	C(44)-C(65)-H(65A)	109.5
C(75)-H(75)	0.9500	C(44)-C(65)-H(65B)	109.5
C(76)-H(76A)	0.9800	H(65A)-C(65)-H(65B)	109.5

C(76)-H(76B)	0.9800	C(44)-C(65)-H(65C)	109.5
C(76)-H(76C)	0.9800	H(65A)-C(65)-H(65C)	109.5
C(77)-H(77)	0.9500	H(65B)-C(65)-H(65C)	109.5
O(1)-C(81)	1.436(8)	C(68)-C(66)-C(36)	120.4(4)
O(1)-C(78)	1.445(6)	C(68)-C(66)-H(66)	119.8
C(78)-C(79)	1.515(7)	C(36)-C(66)-H(66)	119.8
C(78)-H(78A)	0.9900	C(12)-C(67)-C(73)	120.3(4)
C(78)-H(78B)	0.9900	C(12)-C(67)-H(67)	119.8
C(79)-C(80)	1.496(8)	C(73)-C(67)-H(67)	119.8
C(79)-H(79A)	0.9900	C(66)-C(68)-C(46)	119.9(4)
C(79)-H(79B)	0.9900	C(66)-C(68)-H(68)	120.1
C(80)-C(81)	1.442(10)	C(46)-C(68)-H(68)	120.1
C(80)-H(80A)	0.9900	C(23)-C(69)-H(69A)	109.5
C(80)-H(80B)	0.9900	C(23)-C(69)-H(69B)	109.5
C(81)-H(81A)	0.9900	H(69A)-C(69)-H(69B)	109.5
C(81)-H(81B)	0.9900	C(23)-C(69)-H(69C)	109.5
C(85)-C(86)	1.556(18)	H(69A)-C(69)-H(69C)	109.5
C(85)-C(84)	1.76(2)	H(69B)-C(69)-H(69C)	109.5
C(85)-H(85A)	0.9900	C(42)-C(70)-C(73)	120.6(4)
C(85)-H(85B)	0.9900	C(42)-C(70)-H(70)	119.7
C(84)-C(84)#1	1.48(2)	C(73)-C(70)-H(70)	119.7
C(84)-H(84A)	0.9900	C(74)-C(71)-C(18)	120.9(4)
C(84)-H(84B)	0.9900	C(74)-C(71)-H(71)	119.6

C(86)-H(86A)	0.9800	C(18)-C(71)-H(71)	119.6
C(86)-H(86B)	0.9800	N(4)-C(72)-H(72)	180.0
C(86)-H(86C)	0.9800	C(67)-C(73)-C(70)	119.3(4)
O(2)-C(91)#2	0.19(3)	C(67)-C(73)-H(73)	120.3
O(2)-C(92)#2	1.35(2)	C(70)-C(73)-H(73)	120.3
O(2)-C(93)	1.440(16)	C(75)-C(74)-C(71)	119.4(4)
O(2)-C(90)	1.441(16)	C(75)-C(74)-H(74)	120.3
O(2)-C(90)#2	1.55(2)	C(71)-C(74)-H(74)	120.3
C(90)-C(93)#2	0.758(14)	C(74)-C(75)-C(56)	120.3(4)
C(90)-C(92)#2	0.784(13)	C(74)-C(75)-H(75)	119.9
C(90)-O(2)#2	1.55(2)	C(56)-C(75)-H(75)	119.9
C(90)-C(91)	1.565(13)	C(48)-C(76)-H(76A)	109.5
C(90)-C(91)#2	1.617(17)	C(48)-C(76)-H(76B)	109.5
C(90)-C(90)#2	2.02(2)	H(76A)-C(76)-H(76B)	109.5
C(91)-O(2)#2	0.19(3)	C(48)-C(76)-H(76C)	109.5
C(91)-C(93)#2	1.361(19)	H(76A)-C(76)-H(76C)	109.5
C(91)-C(92)	1.490(13)	H(76B)-C(76)-H(76C)	109.5
C(91)-C(90)#2	1.617(17)	N(3)-C(77)-H(77)	180.0
C(92)-C(90)#2	0.784(13)	C(81)-O(1)-C(78)	107.1(5)
C(92)-O(2)#2	1.35(2)	O(1)-C(78)-C(79)	106.0(4)
C(92)-C(93)	1.449(13)	O(1)-C(78)-H(78A)	110.5
C(93)-C(90)#2	0.758(14)	C(79)-C(78)-H(78A)	110.5
C(93)-C(91)#2	1.361(19)	O(1)-C(78)-H(78B)	110.5

C(1)-W(1)-C(8)	89.57(14)	C(79)-C(78)-H(78B)	110.5
C(1)-W(1)-P(2)	78.92(10)	H(78A)-C(78)-H(78B)	108.7
C(8)-W(1)-P(2)	94.05(10)	C(80)-C(79)-C(78)	101.4(5)
C(1)-W(1)-P(4)	96.18(10)	C(80)-C(79)-H(79A)	111.5
C(8)-W(1)-P(4)	84.05(10)	C(78)-C(79)-H(79A)	111.5
P(2)-W(1)-P(4)	174.78(3)	C(80)-C(79)-H(79B)	111.5
C(1)-W(1)-P(3)	95.41(11)	C(78)-C(79)-H(79B)	111.5
C(8)-W(1)-P(3)	162.65(10)	H(79A)-C(79)-H(79B)	109.3
P(2)-W(1)-P(3)	103.21(3)	C(81)-C(80)-C(79)	105.1(5)
P(4)-W(1)-P(3)	78.90(3)	C(81)-C(80)-H(80A)	110.7
C(1)-W(1)-P(1)	156.84(10)	C(79)-C(80)-H(80A)	110.7
C(8)-W(1)-P(1)	92.75(10)	C(81)-C(80)-H(80B)	110.7
P(2)-W(1)-P(1)	77.94(3)	C(79)-C(80)-H(80B)	110.7
P(4)-W(1)-P(1)	106.97(3)	H(80A)-C(80)-H(80B)	108.8
P(3)-W(1)-P(1)	89.18(3)	O(1)-C(81)-C(80)	108.9(5)
C(25)-P(2)-C(5)	103.22(17)	O(1)-C(81)-H(81A)	109.9
C(25)-P(2)-C(7)	102.85(16)	C(80)-C(81)-H(81A)	109.9
C(5)-P(2)-C(7)	101.30(16)	O(1)-C(81)-H(81B)	109.9
C(25)-P(2)-W(1)	111.21(11)	C(80)-C(81)-H(81B)	109.9
C(5)-P(2)-W(1)	119.39(12)	H(81A)-C(81)-H(81B)	108.3
C(7)-P(2)-W(1)	116.76(12)	C(86)-C(85)-C(84)	91.4(11)
C(11)-P(4)-C(27)	103.02(16)	C(86)-C(85)-H(85A)	113.4
C(11)-P(4)-C(6)	99.26(16)	C(84)-C(85)-H(85A)	113.4

C(27)-P(4)-C(6)	98.43(16)	C(86)-C(85)-H(85B)	113.4
C(11)-P(4)-W(1)	121.21(11)	C(84)-C(85)-H(85B)	113.4
C(27)-P(4)-W(1)	111.38(12)	H(85A)-C(85)-H(85B)	110.7
C(6)-P(4)-W(1)	120.02(12)	C(84)#1-C(84)-C(85)	102.1(17)
C(3)-P(1)-C(17)	101.44(16)	C(84)#1-C(84)-H(84A)	111.4
C(3)-P(1)-C(4)	98.82(15)	C(85)-C(84)-H(84A)	111.4
C(17)-P(1)-C(4)	101.92(16)	C(84)#1-C(84)-H(84B)	111.4
C(3)-P(1)-W(1)	119.65(11)	C(85)-C(84)-H(84B)	111.4
C(17)-P(1)-W(1)	107.71(11)	H(84A)-C(84)-H(84B)	109.2
C(4)-P(1)-W(1)	123.98(11)	C(85)-C(86)-H(86A)	109.5
C(10)-P(3)-C(9)	99.72(16)	C(85)-C(86)-H(86B)	109.5
C(10)-P(3)-C(15)	100.39(16)	H(86A)-C(86)-H(86B)	109.5
C(9)-P(3)-C(15)	99.55(16)	C(85)-C(86)-H(86C)	109.5
C(10)-P(3)-W(1)	125.84(11)	H(86A)-C(86)-H(86C)	109.5
C(9)-P(3)-W(1)	118.86(12)	H(86B)-C(86)-H(86C)	109.5
C(15)-P(3)-W(1)	108.20(12)	C(91)#2-O(2)-C(92)#2	132(10)
C(42)-C(3)-C(12)	117.5(3)	C(91)#2-O(2)-C(93)	63(7)
C(42)-C(3)-P(1)	124.4(3)	C(92)#2-O(2)-C(93)	131.3(19)
C(12)-C(3)-P(1)	118.1(3)	C(91)#2-O(2)-C(90)	153(10)
N(2)-C(1)-W(1)	168.4(3)	C(92)#2-O(2)-C(90)	32.4(7)
C(31)-C(4)-C(20)	119.0(3)	C(93)-O(2)-C(90)	109.5(12)
C(31)-C(4)-P(1)	124.4(3)	C(91)#2-O(2)-C(90)#2	92(8)
C(20)-C(4)-P(1)	116.6(3)	C(92)#2-O(2)-C(90)#2	114.1(15)

C(16)-C(5)-C(34)	118.3(3)	C(93)-O(2)-C(90)#2	29.1(7)
C(16)-C(5)-P(2)	118.5(3)	C(90)-O(2)-C(90)#2	85.0(11)
C(34)-C(5)-P(2)	123.1(3)	C(93)#2-C(90)-C(92)#2	140(2)
C(43)-C(6)-C(13)	117.4(3)	C(93)#2-C(90)-O(2)	144(2)
C(43)-C(6)-P(4)	123.4(3)	C(92)#2-C(90)-O(2)	67.6(15)
C(13)-C(6)-P(4)	119.1(3)	C(93)#2-C(90)-O(2)#2	67.6(14)
C(56)-C(7)-C(18)	118.4(4)	C(92)#2-C(90)-O(2)#2	150(2)
C(56)-C(7)-P(2)	118.3(3)	O(2)-C(90)-O(2)#2	95.0(11)
C(18)-C(7)-P(2)	123.3(3)	C(93)#2-C(90)-C(91)	60.4(14)
C(8)-N(1)-C(22)	159.4(4)	C(92)#2-C(90)-C(91)	156(2)
C(14)-C(9)-C(24)	118.1(3)	O(2)-C(90)-C(91)	101.3(10)
C(14)-C(9)-P(3)	123.8(3)	O(2)#2-C(90)-C(91)	7.1(11)
C(24)-C(9)-P(3)	118.1(3)	C(93)#2-C(90)-C(91)#2	146.6(19)
C(19)-C(10)-C(36)	118.2(3)	C(92)#2-C(90)-C(91)#2	66.6(11)
C(19)-C(10)-P(3)	118.8(3)	O(2)-C(90)-C(91)#2	3.2(19)
C(36)-C(10)-P(3)	122.9(3)	O(2)#2-C(90)-C(91)#2	94.6(11)
C(21)-C(11)-C(32)	117.9(3)	C(91)-C(90)-C(91)#2	101.1(8)
C(21)-C(11)-P(4)	122.8(3)	C(93)#2-C(90)-C(90)#2	106.6(16)
C(32)-C(11)-P(4)	119.3(3)	C(92)#2-C(90)-C(90)#2	112.9(15)
C(67)-C(12)-C(3)	121.4(4)	O(2)-C(90)-C(90)#2	49.7(8)
C(67)-C(12)-H(12)	119.3	O(2)#2-C(90)-C(90)#2	45.3(7)
C(3)-C(12)-H(12)	119.3	C(91)-C(90)-C(90)#2	51.7(6)
C(39)-C(13)-C(6)	121.7(4)	C(91)#2-C(90)-C(90)#2	49.4(6)

C(39)-C(13)-H(13)	119.1	O(2)#2-C(91)-C(93)#2	110(8)
C(6)-C(13)-H(13)	119.1	O(2)#2-C(91)-C(92)	43(10)
C(9)-C(14)-C(45)	121.0(4)	C(93)#2-C(91)-C(92)	126.3(12)
C(9)-C(14)-H(14)	119.5	O(2)#2-C(91)-C(90)	81(8)
C(45)-C(14)-H(14)	119.5	C(93)#2-C(91)-C(90)	29.0(6)
C(27)-C(15)-P(3)	110.3(2)	C(92)-C(91)-C(90)	105.7(9)
C(27)-C(15)-H(15A)	109.6	O(2)#2-C(91)-C(90)#2	24(10)
P(3)-C(15)-H(15A)	109.6	C(93)#2-C(91)-C(90)#2	104.1(10)
C(27)-C(15)-H(15B)	109.6	C(92)-C(91)-C(90)#2	28.9(5)
C(7)-C(18)-H(18)	119.9	C(90)-C(91)-C(90)#2	78.9(8)
C(46)-C(19)-C(10)	121.0(4)	C(90)#2-C(92)-O(2)#2	80.0(15)
C(46)-C(19)-H(19)	119.5	C(90)#2-C(92)-C(93)	19.6(11)
C(10)-C(19)-H(19)	119.5	O(2)#2-C(92)-C(93)	97.2(13)
C(33)-C(20)-C(4)	120.5(4)	C(90)#2-C(92)-C(91)	84.5(13)
C(33)-C(20)-H(20)	119.7	O(2)#2-C(92)-C(91)	5.6(18)
C(4)-C(20)-H(20)	119.7	C(93)-C(92)-C(91)	102.2(9)
C(11)-C(21)-C(49)	121.1(4)	C(90)#2-C(93)-C(91)#2	90.6(16)
C(11)-C(21)-H(21)	119.4	C(90)#2-C(93)-O(2)	83.3(16)
C(49)-C(21)-H(21)	119.4	C(91)#2-C(93)-O(2)	7.3(12)
C(1)-N(2)-C(38)	143.9(4)	C(90)#2-C(93)-C(92)	20.3(11)
N(1)-C(22)-C(29)	119.8(3)	C(91)#2-C(93)-C(92)	110.0(11)
N(1)-C(22)-C(28)	118.7(3)	O(2)-C(93)-C(92)	102.9(12)